Process design for production of lipid rich microalgae in a bubble column photobioreactor equipped with membrane-sparger and internal mixer

A Thesis

Submitted for the Degree of

DOCTOR OF PHILOSOPHY

By

VENKATESWARA RAO NAIRA
(146106012)

Under supervision of

Dr. Soumen Kumar Maiti
&
Prof. Debasish Das

October 2020

Department of Biosciences and Bioengineering
Indian Institute of Technology Guwahati
Guwahati 781 039, Assam, India

INDIAN INSTITUTE OF TECHNOLOGY GUWAHATI

Department of Biosciences & Bioengineering

STATEMENT

I do hereby declare that the content embodied in this thesis is the result of investigations carried out by me in the Department of Biosciences & Bioengineering, Indian Institute of Technology Guwahati, Guwahati, Assam, India under the supervision of Dr. Soumen Kumar Maiti and Prof. Debasish Das.

In keeping with the general practice of reporting scientific observations, due acknowledgements have been made wherever the work described is based on the findings of other investigators.

Date: 14-10-2020 **Venkateswara Rao Naira**

INDIAN INSTITUTE OF TECHNOLOGY GUWAHATI
Department of Biosciences and Bioengineering

CERTIFICATE

It is certified that the work described in this thesis entitled, "**Process design for production of lipid rich microalgae in a bubble column photobioreactor equipped with membrane-sparger and internal mixer**" by Mr. Venkateswara Rao Naira for the partial fulfillment of degree of Doctor of Philosophy is an authentic record of the results obtained from the research work carried out under our supervision in the Department of Biosciences and Bioengineering, Indian Institute of Technology Guwahati, Guwahati, India. The work embodied in this thesis has not been submitted elsewhere for a degree.

Soumen Kr Maiti 11/11/2020

Dr. Soumen Kumar Maiti
Associate Professor
Supervisor
Department of Biosciences & Bioengineering
Indian Institute of Technology Guwahati
Guwahati 781 039, India

Debasish Das 11/11/20

Prof. Debasish Das
Professor
Co-supervisor
Department of Biosciences & Bioengineering
Indian Institute of Technology Guwahati
Guwahati 781 039, India

Acknowledgements

I wish to express my sincere gratitude to my research supervisor, ***Dr. Soumen Kumar Maiti and Prof. Debasish Das,*** Department of Biosciences and Bioengineering, for given me an opportunity to pursue this research work, precious advice, guidance, encouragement, and supervision of the research. I must acknowledge the freedom to think, plan, execute and express, that I was given in every step of my research work, while keeping faith and confidence on my capabilities.

My gratitude goes to my doctoral committee members, ***Prof. Kannan Pakshirajan, Dr. Senthil kumar Sivaprakasam, Dr. Lalit Mohan Pandey*** and ***Dr. Priyadarshi Satpati*** for their constructive criticism and suggestions, which helped me to improve my work pertaining to Ph.D. thesis.

I owe my thanks to the ***Department of Biosciences and Bioengineering***, ***mechanical workshop*** and ***Central Instrumentation Facility***, IIT Guwahati for providing me the necessary facilities to fulfill my Ph.D. thesis objectives.

My heartfelt thanks are due to ***lab in charges*** Mr. Nurul, Mrs. Prarthana, Mr. Dipankar, Mr. Chandan and Mr. Niranajan during the course of my research.

I would also like to thank ***IIT Guwahati*** and ***MHRD*** for providing financial assistance and funding my Ph.D. project, which made this study possible.

It was pleasure to work with ***Navodit, Mahesh, Yashawant, Suraj, Meenakshi, Chhavi, and Maibam***. Thanks to them for their suggestions, time, help in practical things and kindness throughout my Ph.D., this is an unforgettable experience.

I thank specially to my seniors, ***Muthuraj, Basawaraj, Vijayan*** and my friends ***Peeyushi, Siran*** and ***Vinay*** for being supportive and providing a welcome diversion from the critical situations during my Ph.D., whenever I needed.

My special thanks and appreciation also goes to ***my parents***, as well as my ***brother*** for their blessings, love, patience, support and understanding throughout my studies and most of all to the ***Almighty God*** who made everything possible.

Abstract

Technology for optimization of biodiesel from microalgae has been facing major production challenges such as low biomass yielding open pond practices, inappropriate CO_2 feed under sunlight, and ineffective photobioreactor (PBR) design. Major influence factors of microalgae cultivation under natural sunlight are reactor design, availability of sunlight intensity and CO_2 supply. Therefore, the algae-biodiesel research should focus on PBR design coupled with process engineering for efficient CO_2 capture/feed and sunlight penetration. Arising from the above, the objectives of the study were set to construct mass transfer efficient bubble column PBR (BC-PBR) along with unidirectional lighting and to perform small-scale experiments under constant lighting for understanding the combined effect of light and CO_2 rather than simple optimization. Consequently, the small-scale studies were used to develop effective CO_2 feed strategies for both small-scale and medium-scale BC-PBRs under diurnal simulated and natural sunlight conditions. Followed by that, a novel mixer design was proposed to integrate in BC-PBR for maximizing light capture, thereby enhanced biomass and biodiesel productivity under natural sunlight.

An indigenous microalgae species and proved biodiesel candidate, *Chlorella sp.* FC2 IITG (FC2) was used in the study. LED lighting and natural sunlight conditions were used for indoor and outdoor experiments respectively. Using an OPTO22 process control unit, light intensity, pH, dissolved CO_2 (dCO_2) or CO_2 levels (% in air), and temperature were recorded/controlled for evaluating the process results. The biomass concentration, chlorophyll content, dissolved oxygen (DO), phosphate, urea, and fatty acid methyl esters (FAME, biodiesel) were also measured/quantified offline. Two scales of bubble column PBRs (BC-PBR) having volumes of 500 ml and 10 L were constructed by integrating newly

designed membrane-sparger. Two unidirectional LED panels, each for small-scale and medium-scale PBRs were customized for generating simulated sunlight conditions in laboratory. The membrane-sparger exhibited high CO_2 mass transfer coefficient of 0.017 s^{-1}, four times higher than conventional L-sparger. Also, it has offered lower cell settling and better scalability in comparison with perforated tubing sparger. Upon evaluating the pumping effect on FC2 strain, the recirculation of cells was not suitable and therefore, batch operation was followed in all the experiments.

In small-scale BC-PBR setup, photosynthesis in the strain was saturated between 700 – 1500 µmol m^{-2} s^{-1} of light intensity. At constant CO_2 feed under constant lighting, the optimum conditions were found to be 2% CO_2 level and 1130 µmol m^{-2} s^{-1} of light intensity. Based on the analysis of combined effect of light and CO_2 at the optimum conditions, strategy of 'maintaining 100 mg L^{-1} dCO_2 throughout the culture' was found desirable for FC2 growth under diurnal simulated sunlight. Using the strategy, growth was recorded up to 5.8 g L^{-1} with an overall biomass productivity of 1.3 g L^{-1} day^{-1}, similar to optimum light and CO_2 conditions. Subsequently in lipid induction phase, the biodiesel was produced with highest productivity of 265 mg L^{-1} day^{-1} and qualified in accordance to ASTM/EU standards. Nevertheless, the desirable strategy or constant CO_2 feeding under diurnal lighting cannot be scalable to medium-scale BC-PBR due to presumable CO_2 limitation along the height of PBR. Consequent to small-scale experimental results and reported photosynthetic observations in cotton leaf, a real time light intensity based CO_2 feeding strategy was proposed and investigated to compare with known biomass-density and pH-control based strategies in medium-scale BC-PBR. The light intensity based strategy under simulated sunlight yielded maximum biomass concentration of 5.12 g L^{-1}, far higher than the known

strategies. In outdoor culturing experiment, the proposed strategy produced final biomass density in the 6.8 and 9.0 g L^{-1} range in growth phases of two-stage and single-stage lipid induction processes respectively. Subsequently, two-stage lipid induction process of 6.8 g L^{-1} titer yielded biodiesel productivity of 120 g L^{-1} day^{-1}, whereas single-stage process of 9.0 g L^{-1} titer was unable to induce lipid. Also, a parallel two-stage lipid induction experiment in small-scale BC-PBR revealed that specific light availability coupled with nitrogen stress enhances lipid induction.

To enhance the specific light availability, a self-rotating bubble-driven mixer was designed and integrated in the BC-PBR. Small-scale experiments in mixer integrated BC-PBR under optimum light and CO_2 conditions exhibited higher biomass productivity, chlorophyll content, and DO when compared with BC-PBR without mixer. Under diurnal simulated sunlight conditions, the productivities of biomass and biodiesel in medium-scale BC-PBR with mixer were enhanced by 1.4 fold and 6.25 fold, respectively compared to the PBR without the mixer. Under natural sunlight conditions, maximum biomass productivity of 1.42 g L^{-1} day^{-1} and overall biodiesel productivity of 521 g L^{-1} day^{-1} were achieved in mixer integrated 10 L BC-PBR.

To the best of the author's knowledge, this is first study to report a PBR with the self-rotating internal mixer that rotates due to bubble-driven force. Also, the process was developed without temperature control for economic viability. The experimental strain in this study does not require conventional pH control, grows in dark cycles, and possesses irreversible photoinhibition at peak sunlight intensity of 2000 µmol m^{-2} s^{-1}. Thus, the designed reactor and process technology in this study can provide leads to commercial feasibility of algae cultivation in photobioreactors as well.

CONTENTS

.

Abbreviations / Notations

Term	Description
IEA	International Energy Agency
BP	British Petroleum
S/V	Surface area / Volume
PBR	Photobioreactor
BC-PBR	Bubble Column Photobioreactor
FC2	*Chlorella* sp. FC2 IITG, model microalgal strain of current study.
LED	Light Emitting Diode
CFL	Cool Fluorescent Lamp
CPU	Central Processing Unit
DC	Direct Current
PWM	Pulse Width Modulation
MFC	Mass Flow Controller
PID	Proportional-Integral-Derivative for control
L-sparger	"L" shaped sparger
dCO_2	Dissolved CO_2
DO	Dissolved Oxygen
Mtoe	Million tonne equivalent
Gt	Giga tonnes
PV	Photovoltaic
FAME	Fatty acid methyl esters
IV	Iodine value
SV	Saponification Value
CN	Cetane Number
DU	Degree of Unsaturation
HHV	Higher Heating Value
ν	Kinematic viscosity
ρ	Density
FP	Flash Point

CP	Cloud Point
PP	Pour Point
CFPP	Cold Filter Plugging Point
ASTM	American Society of Testing and Materials
EN	European Norms
ND	Not Defined
PAR	Photosynthetic Active Radiation
PSI	Photosystem I
PSII	Photosystem II
RuBisCO	Ribulose-1,5-bisphosphate-carboxylase/oxygenase
ATP	Adenosine Tri-Phosphate
ADP	Adenosine Di-Phosphate
NADPH	Nicotinamide Adenine Dinucleotide Phosphate Hydrogen
CoA	Coenzyme A
TCA	Tri-Carboxylic acid
ACP	Acyl Carrier Protein
TAG	Triacylglycerol
ACCase	Acetyl-CoA Carboxylase
DGAT	Diacyl Glycerol Acyl Transferase
ENR	Enoyl-ACP Reductase
FAT	Fatty acyl-ACP Thioesterase
GPAT	Glycerol-3-Phosphate Acyl Transferase
HD	3-Hydroxyacyl-ACP Dehydratase
KAR	3-Ketoacyl-ACP Reductase
KAS	3-Ketoacyl-ACP Synthase
LPAAT	Lyso-Phosphatidic Acid Acyl Transferase
LPAT	Lyso-Phosphatidylcholine Acyl Transferase
MAT	Malonyl-CoA ACP Transacylase
3PGA	3-Phosphoglycerate
G3P	Glyceraldehyde-3-Phosphate
G6P	Glucose-6-Phosphate

PDH	Pyruvate Dehydrogenase
DCW	Dry Cell Weight
$K_L\, a_{,CO_2}$	Overall volumetric CO_2 mass transfer coefficient
$K_L\, a_{,O_2}$	Overall volumetric O_2 mass transfer coefficient
OD	Optical Density
RPM	Rotations per minute
Chl-a	Chlorophyll – a
Chl-b	Chlorophyll – b
GC	Gas Chromatograph
FID	Flame Ionization Detector

List of figures

List of tables

CHAPTER 1

Introduction

1.1 Background and rationale of the study

Energy is one of the major driving forces for world's science and technological advancements that meet various demands of humankind. Most of the energy supplies have been drawn from non-renewable and conventional fossil-based sources like oil, natural gas and coal, which are being utilized largely for transportation, manufacturing industries and residential purposes (Shafiei & Salim, 2014). However, the fuel analysts and consumers have already been understood that the world's energy consumption could easily surpass the energy supply in the very near future, unless the alternative renewable energy sources are found (Owen et al., 2010). In 2018 alone, the world's total energy consumption increased by 2.3%, which is double the average growth rate since 2010 (IEA, 2019). The BP plc has estimated that the global energy demand by 2040 will be increased by a third of current demands (BP, 2019a). At the current consumption rates, even the current reserves of oil, natural gas and coal would be depleted within a 50, 50.9 and 132 years respectively (BP, 2019b).

Due to the rising global energy demands and fast depletion of fossil fuels, the prices have also increasing very sharply (Herrera et al., 2019; Monyem et al., 2001; Sakarika & Kornaros, 2019; Slegers et al., 2011). Also, the devastating CO_2 (major greenhouse gas) emissions from fossil-based fuel combustion has also been increasing year by year, e.g., the CO_2 emissions in 2016 were raised by 57% in comparison with 1990' emissions (IEA, 2018a). By the year of 2018, the global annual average concentration of atmospheric CO_2

was reached to 407.4 ppm (2.4 ppm higher than in 2017). The increase in CO_2 emissions has been linked to global warming as CO_2 is the major greenhouse gas (GHG) in the atmosphere. Therefore, the whole world is currently stepping towards the dual challenge / solution of "More energy and less carbon" (BP, 2019a).

In the recent years, the growth of energy demand and supply of renewables have been increasing very rapidly. For example in 2018, the renewables share was almost a quarter of the world's energy supplies (IEA, 2018b; IEA, 2018c). Though hydroelectricity and solid biomass fuel (firewood) were traditional renewables, other renewables like solar (photo voltaic and thermal), wind, geothermal, tidal, biomass (other than traditional, e.g., lignocelluloses, food crops, etc.), and wastes have already emerged as alternative and 'new' renewables sources of energy since 1990s (IEA, 2019; IEA, 2018c). Among the new renewables, liquid biofuels like bioethanol and biodiesel from biomass feedstock have gained popularity as transportation fuels. The annual average growth of liquid biofuels production in 2018 was 9.7%, which was the highest growth since 2010 (BP, 2019b). In this increased growth, bioethanol and biodiesel were accounted for 56% and 37% of the overall production respectively. In spite of the emergence and increasing use of liquid biofuels in every upcoming year,, the current growth rate of liquid biofuels cannot meet projected future energy consumption rates (IEA, 2019). Hence, the present research study is focused on production enhancement strategies / technologies of liquid biofuels, especially the biodiesel production. Biodiesel is generally produced from various oil/lipid accumulating biomass feedstock via extraction of lipids and transesterifying those lipids using methanol in the presence of acid/base/biological catalyst (Li et al., 2018; Pizarro & Park, 2003). Historically, the biodiesel producible biomass feedstock were divided into three groups namely, first, second and third generations (Issariyakul & Dalai, 2014; Shafiei & Salim, 2014; Williams & Laurens, 2010).

As the first generation feedstock, edible oil sources like vegetable oils (e.g., palm, sunflower, soybean, canola, etc.) and animal oils have been studied (Alptekin et al., 2014; Dias et al., 2008; Issariyakul & Dalai, 2014). Currently, the most of the world's biodiesel has mainly derived the edible oil sources only (IEA, 2018c). However, the future scenario of the liquid biofuels production has been changing due to the associated food vs fuel debates, future food crisis, and invasion of arable/agricultural lands with the use of edible food crops and their lands. Therefore, the feasibility of non-food crops like Jatropha, pongamia, and even waste cooking oils as second generation biodiesel feedstock have been explored (Ahmad et al., 2009; Gao et al., 2019; Ong et al., 2013). Nevertheless, these non-food crops also require agricultural lands for their production. Hence, similar tension arises as for first generation feedstock (Demirbas & Demirbas, 2010; Sun et al., 2019; Williams & Laurens, 2010). Recently, algae (photosynthetic microorganisms) has emerged as third generation biodiesel feedstock and known to be superior to any other feedstock (Chisti, 2008; Demirbas & Demirbas, 2010). Unlike crop plants, algae are peculiar photosynthetic microorganisms that do not require arable lands for their biomass production and offers very high growth rates with top-notch photosynthetic efficiencies. However, the biodiesel production technology from algae is still non-viable due to lags in the developmental stages of biomass growing technology, downstream processing, and biodiesel extraction (Scott et al., 2010; Vasistha et al., 2019). Due to these lags, the edible oils are still being grown and used for biodiesel production. Therefore, the present study was focused on developing an efficient algae biomass production technology, which is the techno-economic decisive part of algae-diesel industrial pant.

1.2 Problem statements

For algae (particularly microalgae) biomass production, there are a wide variety of mass culturing systems. Among them, artificial open ponds are the most economical and

easier systems (Costa et al., 2019; Norsker et al., 2011). However, these open ponds require very large land areas for cultivation and criticized for their poor biomass productivities due to lesser S/V (surface area/volume) ratios, frequent contamination problems and water losses due to high rates of evaporation. Due to the above issues, closed photobioreactors (PBRs) like vertical tubular, horizontal tubular, and flat panels have been studied prominently (Genin et al., 2016; Kumar et al., 2017; Slegers, 2014). The cultivation of microalgae in the PBRs is mainly governed by PBR design and process optimization / engineering of the designed system to produce high biomass densities while utilizing the sunlight efficiently.

1.2.1 Photobioreactor design factors

Photobioreactors (PBR) could offer better S/V ratios and higher biomass productivities compared to the open pond systems However, the current achievable biomass densities in any of the existing PBR designs cannot make algae-biodiesel industry viable. Moreover, the net energy ratios for running and maintenance of these PBRs are negative due to high installation/capital costs and energy requirements. This ultimately imposes burden on the extraction and downstream processing cost of biodiesel from microalgae (Arcigni et al., 2019; Hulatt & Thomas, 2011). This is why, cost-effective engineering design of the PBR in conjunction with capability of producing high cell-density algae cultures is imperative to satisfy the future world's fuel energy demands. An efficient PBR design deals with many aspects such as selection of suitable PBR, land area foot-print, effective CO_2 mass transfer, hydrodynamics, mixing of algae cells to minimize dark zones, and scale-up viability.

Regardless their highest areal productivities compared to any other PBR, the flat panels could not offer good hydrodynamics and they require many compartments for scale-up (Ugwu et al., 2008; Wang et al., 2012). In case of vertical tubular PBRs, they consume

lesser land area footprint compared to the horizontal tubular and flat panels. Moreover, the areal biomass productivities in vertical tubular PBRs were reported up to 20–70% higher than in horizontal tubular PBRs when both kind of tubular PBRs were tested at pilot-scale, (Slegers et al., 2013). Nevertheless, vertical PBRs require special attention in improving mass transfer and mixing in a cost-effective manner to achieve high cell densities and biomass productivities of microalgae. Based on photosynthetic efficiency, high areal productivities, mass transfer, and mixing, column PBRs like bubble column and airlift technologies were demonstrable to be very efficient at laboratory scale experiments (Hulatt & Thomas, 2011; Sánchez Mirón et al., 2000). For effective mass transfer of CO_2 from gaseous phase to algae cells, the design and selection of sparger is the fore-most important step in the construction of a suitable PBR. The attachment / arrangement of the existed spargers such as pipe sparger, ring sparger, ceramic sparger, sieve plate, etc. in airlift / bubble column reactors are limited to the laboratory due to scale-up issues and high installation costs (Gupta et al., 2015; Posten, 2009). Moreover, the operation of these spargers require high pressures, leading to high energy consumption (Posten, 2009). Therefore, the cost-effective integration of the column PBR technologies into vertical tubular PBR with scalable and mass transfer efficient sparger could open the door for commercialization of algae biofuels.

Mixing is another crucial parameter that aids in increasing specific light availability (average light exposure per cell) inside the tubular PBRs. This mixing can increase the frequency of algal cells to move from light to dark zones of the PBR that generates higher biomass productivities compared to the PBRs with less efficient mixing. Moreover, it was widely reported that the combination of higher specific light availability and N-stress can improve the lipid content of some algal species more than the N-stress alone (Cuellar-Bermudez et al., 2015; Munkel et al., 2013; Wang et al., 2018a). Hence, the arrangement

of special internal mixers/baffles inside the PBR would be an innovative solution for increasing the specific light availability to improve both biomass and biodiesel productivities. In the current literature, a very few reports are available on the design of special internal mixers inside the tubular or flat panel PBRs and this technology is still in very early stage of development.

1.2.2 Process optimization criteria

In addition to the effective PBR design, process design and optimization for achieving high cell density and biomass productivity is mainly governed by two critical growth parameters, i.e., light and CO_2 (prime requirements of photosynthetic organisms). Numerous studies on the effect of light and CO_2 were reported based on the 'one at a time optimization' technique implemented by using various statistical methodologies (Kim et al., 2012; Muthuraj et al., 2015). Those reports generally evaluate single optimum values of light intensity and/or CO_2 level that are followed in the outdoor culturing as well. And the applicability of these optimum values could be limited to a very small range of light intensities only. However, the sunlight is diurnal (continuous light intensity variations from dawn to dusk) by nature and it has a broad range (0 – 2000 µmol m^{-2} s^{-1}) of light intensities. Apart from diurnal nature it can also fluctuates due to weather and climatic conditions. Thus, the lower range and very high range of light intensities under diurnal sunlight may have other optimum values of CO_2 levels. For example, a report on *Nannochloropsis Salina* suggested that monthly/seasonally CO_2 variation was required for optimal growth in outdoor open ponds cultivated throughout the year (Malek et al., 2016). The strategy was designed based on the monthly varied average sunlight irradiation due to climate. Hence, real time optimization of CO_2 would be required for the all the ranges of light intensities during the diurnally changing sunlight of every day. Prior to the real time optimization under diurnal light, the determination of inhibiting, optimal, and limiting effects of both

light and CO_2 under constant light intensities (in the range of 0 – 2000 µmol m^{-2} s^{-1}) is vital (Pierobon et al., 2016). This would be highly beneficial in understanding the combinatorial effect of light and CO_2 during the critical phases of photolimitation and photoinhibition.

1.3 Objectives of the study

Based on the outlined problem statements, current challenges and prospective requirements for commercial microalgal biomass and biodiesel production, following objectives were designated for improving the status of research towards a sustainable future of liquid biofuels. The core intention of the present study is to develop a cost-effective process design to cultivate lipid rich microalgae for high biomass and biodiesel production in a customized bubble column photobioreactor with efficient CO_2 mass transfer and mixing. Throughout the study, the temperature was not controlled purposefully to decrease the process economics.

Objectives of the study were:

I. Design and construction of unidirectional LED lighting and bubble column photobioreactor (BC-PBR) with efficient sparging system.

II. Effect of light intensity and CO_2 on the growth of *Chlorella* sp. FC2 IITG in small-scale BC-PBR under LED lighting.

III. Development of a novel real time light intensity based CO_2 feed strategy for enhanced *Chlorella* sp. FC2 IITG biomass production in medium-scale BC-PBR under natural sunlight.

IV. Design of a novel bubble-driven and self-rotating mixer in BC-PBR for enhanced biomass and biodiesel productivities of *Chlorella* sp. FC2 IITG under natural sunlight conditions.

1.4 Uniqueness of the study

The study highlights the optimization of microalgae cultivation for biodiesel production under diurnal natural sunlight (rather than artificial lighting conditions), uniquely by reactor design coupled with process engineering strategies that enhance availability of light and CO_2 for algae cells.

- In the reactor design, conventional bubble column technology is improved by installation of custom-made membrane-sparger. The resource material used for membrane-sparger is abundant, cost-effective, and efficient in CO_2 mass transfer compared to available spargers.
- The methodology of process optimization for algae biomass production is prioritized in finding combined effects of light intensity and CO_2 instead of convetional 'one-variable-at-a-time' optimization. As a result, a new dissolved CO_2 based supply strategy is suggested under simulated diurnal sunlight for optimal algae biomass production in small-scale PBR systems.
- For scaled-up PBR, a novel light intensity based CO_2 feed is developed and implemented under natural sunlight, which yielded unprecedented biomass densities.
- In addition to membrane sparging in reactor design, a self-rotating bubble-driven mixer is customized and installed in the PBR for enhnaced light capturing by algae cells. This type of bubble-driven mixer in algae cultivation has never been reported in the literature.
- Other findings of the study suggests reversible photoinhbition, dark-phase growth, and excellent growth-performance without pH control, altogether exists as unique features in the experimental microalgae species.

1.5 Organization of thesis

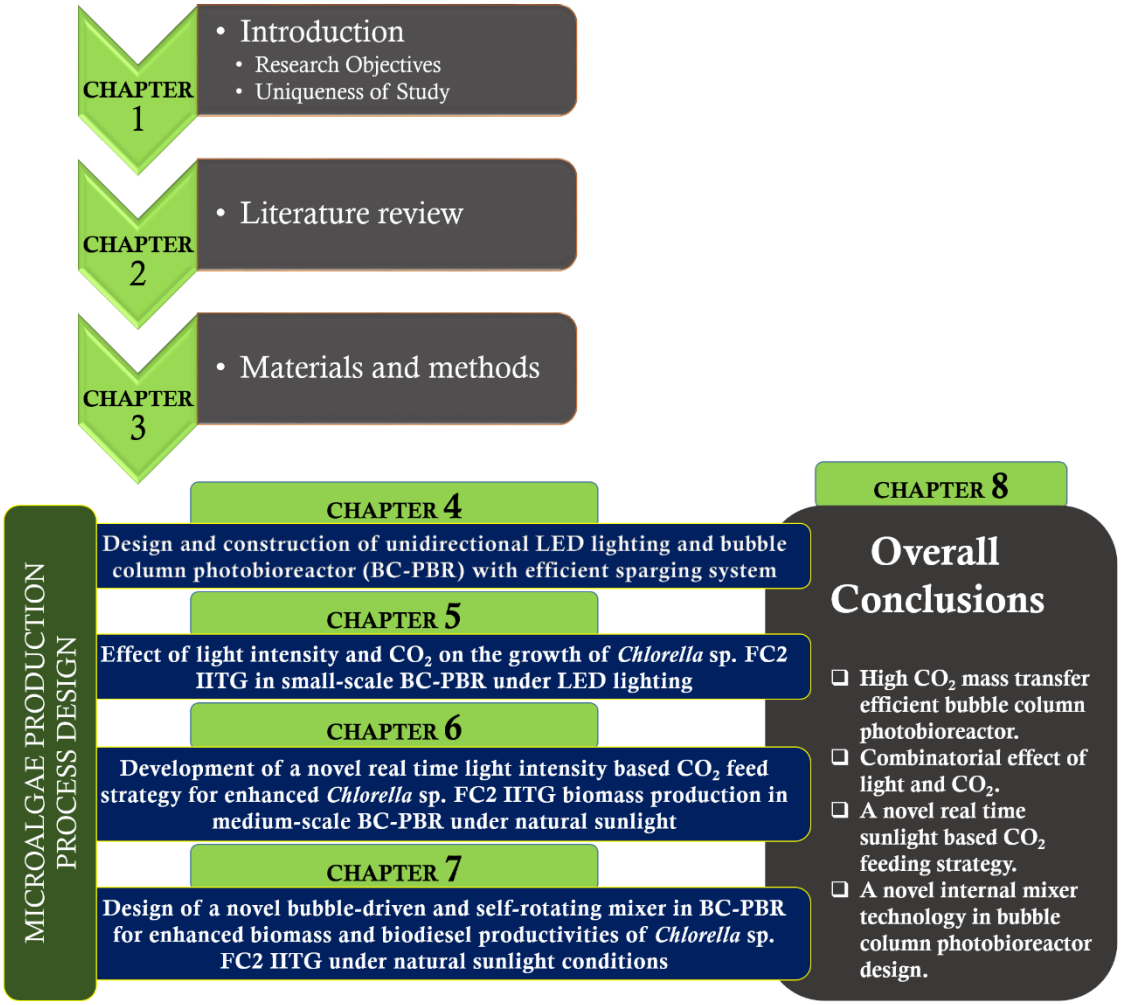

Fig. 1.1 Outline of thesis

Chapter 1 summarizes the background and motivation along with the highlighting of problem statement (bottlenecks of current algae technologies), objectives of the study, outline of thesis (Fig. 1.1) and experimental approaches followed to accomplish the project.

Chapter 2 reviews the recent scientific literature to contextualize the study against the global energy perspectives, emergence of renewable fuels, importance of liquid biofuels (i.e., biodiesel), resources for biodiesel, microalgae as biodiesel feedstock, biology of microalgae, critical growth factors (e.g., sunlight, CO_2, mixing, etc.), mass culturing systems and the techniques for biodiesel production.

Chapter 3 outlines materials and methodologies used for equipment prototype design, experimental setup, and experimental procedures to accomplish the specified research objectives.

Chapter 4 deals with design and construction of unidirectional LED lighting and bubble column photobioreactor (BC-PBR) with efficient sparging system for *Chlorella* sp. FC2 IITG (referred as FC2 hereafter) growth.

Chapter 5 details the effect of light intensity and CO_2 on the growth of *Chlorella* sp. FC2 IITG in small-scale BC-PBR setup using the customized unidirectional LED lighting.

Chapter 6 details the development of a novel real time sunlight based CO_2 feed strategy for enhanced *Chlorella* sp. FC2 IITG biomass production in medium-scale BC-PBR under natural sunlight.

Chapter 7 outlines the design of a novel bubble-driven and self-rotating internal mixer in bubble column photobioreactor for enhanced biomass and biodiesel productivities under natural sunlight conditions.

Chapter 8 provides the **overall conclusions** drawn from all the studies conducted towards accomplishing the designated objectives.

CHAPTER 2

Review of Literature

2.1 Global energy scenario – Emerging renewable energy sources

The combined effects of rising global population and industrial revolution since the 19th century, have led to more intensive exploitation of energy sources, primarily obtained from non-renewable and conventional fossil-based sources like oil, natural gas, and coal. They utilized largely for transportation, manufacturing industries, and residential energy demands (IEA, 2019; IEA, 2018b; Shafiei & Salim, 2014). Hence, the energy became an integral measure/index of a nation's potential prosperity and economic growth. However, the fuel analysts have already been warned that the world's energy consumption could easily surpass the energy supply in the very near future, unless they are replaced by alternative renewable energy sources (Owen et al., 2010). From 1973 to 2016, total primary energy supply was increased from 6,101 to 13,761 Mtoe (IEA, 2018b). When it comes to 2017 and 2018 years, the energy consumption was unprecedentedly higher than the previous years (Fig. 2.1) (IEA, 2019). In 2018 alone, the world's total energy consumption was increased by 2.3%, which is double to average growth rate since 2010. This was mainly due to robust global economies and increased energy requirements for heating and cooling in various parts of the world as average winter and summer temperatures were beyond the historical limits (BP, 2019a; BP, 2019b). The regional increase in the energy consumptions show that China, USA, India, Europe, and Japan were in first, second, third, fourth, and fifth places, respectively (IEA, 2019). The contribution of different fuel resources to the total global energy consumption in 2018 is shown in Fig. 2.2. The fossil fuels accounted for up to 70% of the global demand, and the demand for natural gas was highest (43.6%).

The renewables including solar, wind, hydro, nuclear, biomass, and wastes also increased by double-digit figures, however this rate cannot meet the projected future energy consumption rates.

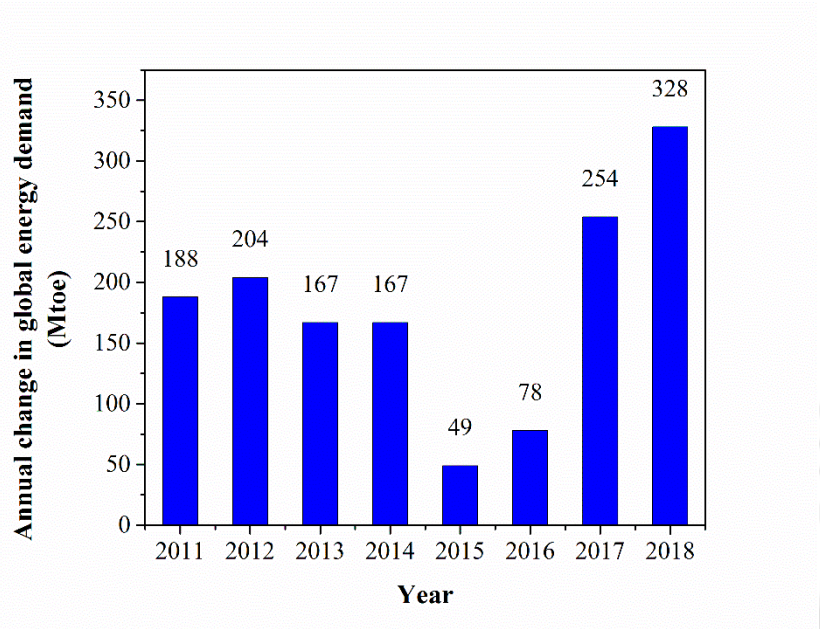

Fig. 2.1 Annual change of global energy demand or consumption from 2011 to 2018. Source: Adapted from (IEA, 2019)

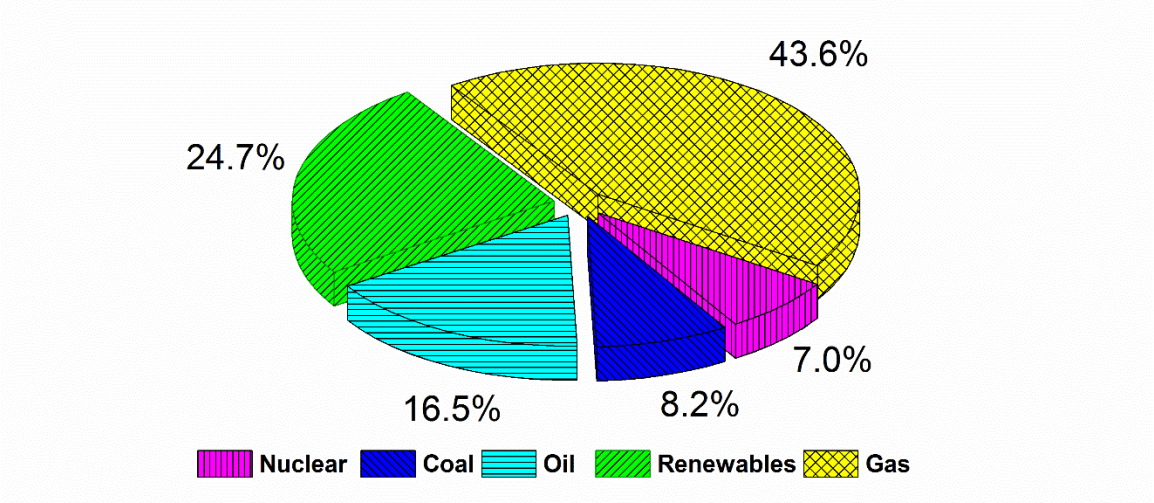

Fig. 2.2 Contribution of various fuel energy resources for total energy consumption in 2018. Source: Adapted from (IEA, 2019)

According to the BP energy outlook 2019, it is estimated that the global energy demand by 2040 will be increased by a third of current demands. In spite of this increase in energy demand, the fossil fuel reserves such as oil, natural gas, and coal were depleting with very faster rates. Based on the current global reserve to production ratios of oil, natural

gas, and coal in 2018, it is predicted that the reserves of oil, natural gas, and coal will be depleted within a very few years (Fig. 2.3) (BP, 2019b). Due to these rising global energy demands and fast depletion of fossil fuels, the prices were also increasing very sharply (Monyem et al., 2001; Sakarika & Kornaros, 2019; Slegers et al., 2011). With reference to global oil prices, the annual average price in 2018 was US \$71.31 barrel^{-1}, increased from \$54.19 barrel^{-1} in 2017 (BP, 2019b).

Apart from prices, CO_2 emissions from fuel combustion has also been increasing year by year, i.e., 57% increment in 2016 compared to 1990' CO_2 emissions (IEA, 2018a). The CO_2 emissions due to high energy demand in 2018 rose by 1.7% (33.1 Gt), which was 70% higher than the average rate since 2010 and highest since 2013 (IEA, 2019). Globally, the annual average concentration of atmospheric CO_2 was 407.4 ppm in 2018, greater by 2.4 ppm compared to 2017 figures. Two-thirds of the emissions was attributed to the power sector (mainly coal-fired power plants), while combustion of other fossil fuels also increased significantly (IEA, 2018a; IEA, 2019). The increase in CO_2 emissions has led to global warming due to greenhouse effect, thereby higher energy supply for more cooling requirements in major cities on the earth.

The outlined energy demands and negative environmental consequences have led to increased exploitation of viable renewable energy sources that could meet the future energy demands as well as decreasing the CO_2 emissions. Nevertheless, the solid biofuel/charcoal for residential heating and cooking remains the largest renewable source, accounting up to 62.4% of all the renewables (IEA, 2018c).

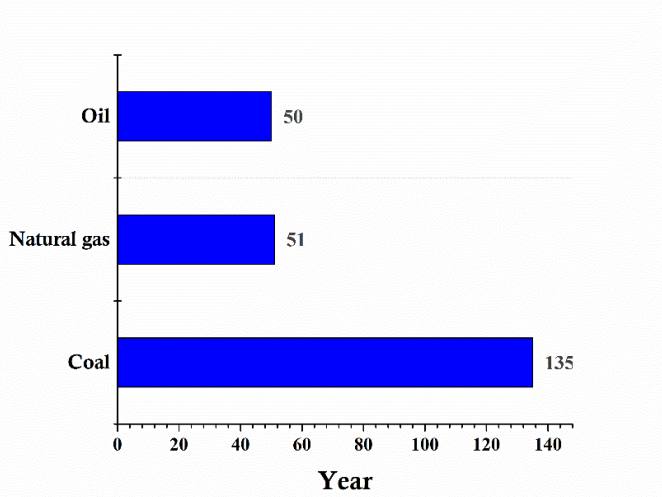

Fig. 2.3 Expected time for complete utilization of fossil reserves. Source: Adapted from (BP, 2019b)

According to IEA, renewable energy includes solar photovoltaic (PV), solar thermal, wind, hydroelectricity, geothermal, wave, tide, ocean, and bioenergy (solid biofuels, liquid biofuels, biogas, and renewable municipal wastes). There has been a global focus on developing the renewables since 1990. In the period of 1990 – 2000, most of the renewables were solid biofuels and hydroelectricity. Whereas the solar, wind, tide, biogas, liquid biofuels, and municipal waste resources have developed as new renewables since 2001. Currently, the supply and demand of new renewables have been growing very rapidly. For example in 2018, the renewable energy demand was increased by 4% compared to the previous year and accounted for nearly a quarter of the total global energy demand (IEA, 2019), of which electricity generation by renewables contributed to up to 45% of total increase in electricity generation solar PV, wind and hydropower of one-third and bioenergy of two-thirds. Apart from electricity generation, the bioenergy utilization in transport was increased by 6% in 2018, mainly from liquid biofuels including bioethanol and biodiesel. The annual average growth of liquid biofuels production in 2018 was 9.7%, highest growth since 2010. In the increased growth, bioethanol and biodiesel were accounted for 56% and 37% of the overall production (Source: BP Statistical Review of World Energy 2019).

Currently, renewable energy is the fastest growing energy source that is projected to contribute over a half of the world's energy demands by 2040 (Source: BP Energy Outlook 2019). Based on specific sustainable development scenario, the use of renewables will have to be increased in all sectors including industry, buildings, and transport in order to meet the future goals of climate-change, clean air, and modern energy source for "more energy and less carbon" challenge (IEA, 2019). By 2040, the contribution of renewables in electricity generation should increase from one quarter to two thirds of the total electricity generation. In heating and transport sectors also, the renewables should be increased from 10% (2018) to 25% and 3.5% (2018) to 19% by 2040 respectively.

2.2 Biodiesel

The world's technological advancement has been actively moved towards the production and development of alternative fuel energy sources for replacing the all the fossil-based fuels since 1970s (Williams & Laurens, 2010). In search of alternative to fossil derived petro-diesel, biochemists found a renewable resource like oleaginous (oil-containing) biomass feedstock that can be used for the production a liquid biofuel called 'biodiesel' (Ma & Hanna, 1999; Mittelbach, 1996). The biodiesel is highly beneficial over petro-diesel in terms of renewability, less toxicity, sulphur-free, and lesser greenhouse gases production (Aransiola et al., 2014; Coh et al., 2019). The produced biodiesel is tested according to the ASTM D6751 or EN 14214 standards, such that it can be used directly in diesel engines by blending with conventional diesel in 5% (B5) or 20% (B20) ratios (Demirbas & Demirbas, 2010).

2.2.1 Feedstock for biodiesel production

Traditionally, oils/fats derived from edible food sources like vegetable oils and animal oils have been used for biodiesel production. The sources of vegetable oil mainly

include food crops like rapeseed, canola, palm, soybean, and sunflower, whereas the animal oils include beef tallow, sheep tallow, and poultry oils (Antolin et al., 2002; Araujo et al., 2010; Dias et al., 2008; dos Santos et al., 2019; Hira & Das, 2016; Nunes et al., 2019; Rashid & Anwar, 2008). These edible food resources were termed as first generation biodiesel feedstock. Since both the oil feedstock were derived from edible food resources, the challenge of food crisis may arise in the near future. As a result, second generation biodiesel feedstock, i.e., non-food crops and waste oils were explored for the production of biodiesel. In the reported literature, majorly studied second generation feedstock were jatropha, pongamia, waste cooking, and waste animal oils (Ahmad et al., 2009; Saleh, 2018; Wang et al., 2018b). However, the production of non-food oil crops poses another future threat by utilizing arable agricultural lands in large amounts. By this way, the emergence of non-food crops for biodiesel production could compete with food-crop lands and ultimately leads the problem of food security for future generations. Hence, both of the 1st and 2nd generation biodiesel feedstock could not be the sustainable sources of renewable biodiesel.

Simultaneous to the development of first and second generation biodiesel feedstock, scientists found that some species in algae (a photosynthetic microorganism) are capable of accumulating lipids/oil in their biomass. Gradually, this algae biomass feedstock has now emerged as a third generation biodiesel feedstock and marked as a promising alternative to first and second generation biodiesel feedstock. . They can accumulate lipids up to 50 – 60 % of the biomass weight (dry weight basis), depending on the growing conditions. Most importantly, the cultivation of algae does not need arable land areas and their growth rates are far higher than food or non-food oil crops. They are also highly efficient in performing photosynthesis and are capable of producing more biodiesel per land area compared to the any other biodiesel feedstock available till date (Fig. 2.4).

Though algae-biodiesel feasibility was debatable (discussed in later section), algae is the superior source of biodiesel without any question.

Table 2.1 An overview of merits and demerits of three generation biodiesel feedstock. Source: (Banerjee et al., 2019; Williams & Laurens, 2010)

Generation	Biomass feedstock	Merits	Demerits
First	Food based oil crops and animal oils, e.g., soybean, sunflower, palm, beef and sheep tallow, etc.	• Very well established technology • Biodiesel produces lesser pollutants than petro-diesel • Production facility can be easily managed with regular farming knowledge	• Compete with regular agricultural lands, leading increase in food prices and food crisis. • Long periods of yield and low growth rates. • Seasonal variations in production outputs • Not sustainable for future generations
Second	Non-food oil crops and waste oils, e.g., pongamia, jatropha, waste cooking oils, etc.	• Produced biodiesel may affect engine life • Requires lesser water and nutrition than food crops • Able to grow in less fertile soils also • Waste valorization • Production facility can be easily managed by farmers	• Can compete with arable lands and cause food crisis • Long (years) periods of productivity/yields • Seasonally varied outputs • Technology is still need to be developed to maximize yields. • Not sustainable for future generations
Third	Algae	• Produces lesser pollutants than petro-diesel • Highest yields and productivities • Higher growth rates • Very high photosynthetic efficiency than oil crops. • Voracious appetite of CO_2 • Able to grow on non-arable lands or even in marine, brackish and waste waters • Best available feedstock for 'More energy', 'less carbon' scenario. • Highly sustainable source. • Immense scope for biorefinery development.	• Comparatively, high cost of production technology • Feasibility is yet to be achieved • Efficient biomass cultivation systems are yet to be developed • Biomass to biodiesel extraction, conversion, and production technologies are still in establishing stage. • Technical labor is required to manage the production facilities.

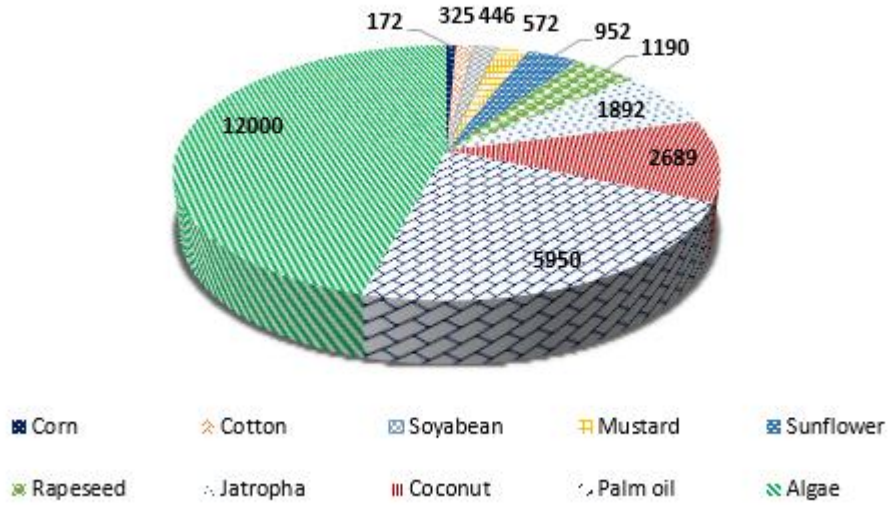

Fig. 2.4 Annual areal biodiesel productivities (L ha^{-1} $year^{-1}$) of various biodiesel feedstock. Source: (Chisti, 2007)

2.2.2 Conversion chemistry and associated technologies

Oleaginous biomass (either of plant or algae) possesses most of the oil in the form of lipids / triglycerides, which are the precursors of the biodiesel (Demirbas, 2002; Issariyakul & Dalai, 2014). After the systematic extraction of lipids from the biomass (discussed in section 2.12.2), the triglycerides are converted into fatty acid methyl/ethyl esters using methanol/ethanol solvent in the presence of chemical or biological catalysts like NaOH, H_2SO_4 and/or lipase enzyme, known as transesterification reaction. The mixture of fatty acid methyl/ethyl esters (biodiesel) having lower viscosity than mixture of triglycerides can serve as alternative fuel to conventional diesel engine. The reaction requires 3 moles of methanol or ethanol to 1 mole of triglyceride (oil) to yield 3 moles of methyl esters and 1 mol of glycerol (Fig. 2.5) (Demirbas, 2003; Li et al., 2018). The conversion efficiency of the biodiesel yield depends on reaction temperature, pressure, molar ratio of alcohol to triglyceride, water content, and free fatty acid content (Demirbas, 2008). In the industries, 6 moles of excess methanol is used to ensure the reaction equilibrium towards the formation of biodiesel (Fukuda et al., 2001). There are mainly four

methods of transesterification reaction has been followed for the production of biodiesel, i.e., catalytic, non-catalytic, microwave-assisted, and ultrasound assisted technologies.

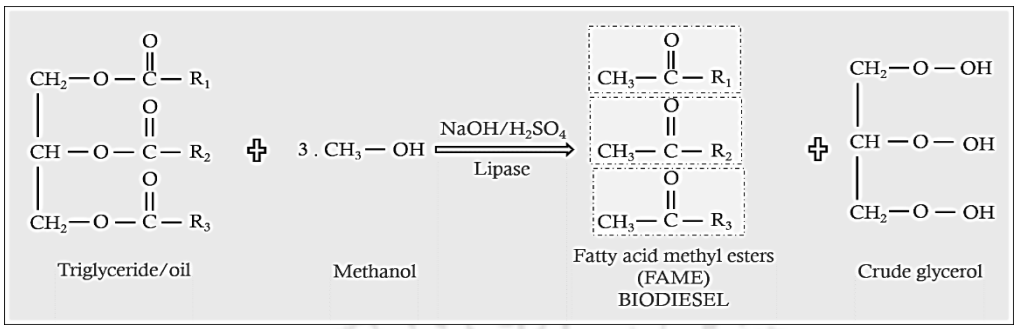

Fig. 2.5 Transesterification reaction for the synthesis of biodiesel from triglycerides extracted from any oleaginous biomass feedstock.

2.2.2.1 Catalytic transesterification

In catalytic transesterification method, homogeneous catalysts like H_2SO_4, NaOH, and KOH and heterogeneous catalysts like enzymes, CaO, and MgO have been widely studied (Bhuiya et al., 2016; Demirbas, 2008). Homogeneous catalysts include acids like methanolic HCl, $Fe_2(SO_4)_3$, sulfonic acid, and methanolic H_2SO_4 and alkali like metal (e.g., Na or K) alkoxides, hydroxides, and even carbonates. Though acid-catalysed method offers better conversion while there is a presence of high water or free fatty acids contents, base-catalysed method is advantageous due to their faster reaction times, i.e., 4000 times more than the acid-catalysis (Cavonius et al., 2014; Juan et al., 2011). However, several challenges like unwanted soap formation due to higher free fatty acid content, high separation costs, and large amounts of waste water generation are associated with both of the homogeneous catalysts. Hence, the oils/lipids containing >1% of free fatty acid content are transesterified using heterogeneous catalysts (Macedo et al., 2006). The heterogeneous catalysts are less corrosive, environmental-friendly, operable with continuous processes, and viable to reuse and regenerate. Specifically the enzyme, lipase-catalysed transesterification would not affected by high water content or high free fatty acid content. Nevertheless, the enzyme-catalysis has not yet been commercialized due to their slower

reaction times, alcohol inhibition, and high lipase costs. Currently, NaOH or KOH are the most preferred catalysts for transesterification of lipids/oil to produce biodiesel due to their low-cost, lesser reaction times, and high reaction rates compared to other catalysts.

2.2.2.2 Non-catalytic transesterification

Non-catalytic methods like supercritical alcohol and BIOX co-solvent processes have been studied to overcome the separation costs and energy requirements associated with the catalytic transesterification methods (Chauhan et al., 2020; Demirbas, 2002). As a supercritical alcohol, methanol, ethanol, propanol, and butanol were widely reported for biodiesel production from various sources ranging from 1st to 3rd generation biodiesel feedstock (Demirbas, 2002; Farobie et al., 2016; Sun et al., 2014; Tobar & Núñez, 2018). In this supercritical alcohol transesterification process, the solvent is exposed to high pressure and temperature above its critical point such that single-phase of oil/alcohol mixture reacts with each other to form biodiesel that can be purified very easily unlike the conventional (catalytic) transesterification process. Moreover, the process facilitates the solubility of oil/alcohol mixtures by decreasing the mass transfer limitations thereby increases reaction rates and lowers the reaction time. The process is generally carried out at pressure of 35 – 60 MPa and temperature of 525 – 675 K that brings the conversion efficiency up to 50 – 95% for the first 10 min of reaction time (Abbaszadeh Mayvan et al., 2012; Demirbas, 2003; Kusdiana & Saka, 2001). In order to lower the demand of alcohol, temperature and pressure in the process, some additional co-solvents such as CO_2, hexane, propane, CaO, and subcritical alcohols were also used several reports (Borugadda & Goud, 2012; Vyas et al., 2010). However, the supercritical alcohol transesterification is currently not viable to scale-up because of the cost of apparatus, operations, and very high alcohol/oil ratios (~ 42) (Bhuiya et al., 2016). Another non-catalytic method known as BIOX co-solvent process (patented technology) involves esterification of free fatty acids followed

by transesterification of triglycerides in single-phase reaction due to addition special co-solvents i.e., tetrahydrofuran or methyl tertiary butyl ether. The process is capable of running continuously at near-ambient temperature and atmospheric pressure along with the recycle and reuse of co-solvent.

2.2.2.3 Microwave-assisted and ultrasound-assisted transesterification

The application of microwave and ultrasound techniques were explored as alternative energy to overcome the problems with conventional transesterification process (Patil et al., 2011; Tan et al., 2019). The use of microwaves offers heat energy by oscillating polar ends of molecules of bi-phasic solvents (alcohol/oil mixture) that results in the increase of biodiesel yield. However, the safety issues and scale-up are the major challenges of microwave-assisted transesterification. On the other hand, ultrasonic irradiation improves the mass transfer between the two-phase heterogeneous systems and thereby facilitates the reaction to occur at lower temperature with lesser amounts of oil and alcohol. It also offers good mixing of bi-phasic system and helps in attaining activation energy sooner than the conventional methods. Thus, the reaction rates and yield of biodiesel can be greatly improved by using ultrasound-assisted transesterification.

2.2.3 Key properties of biodiesel defining fuel quality

Based on the composition of the fatty acids present in the biodiesel, the quality of the oil/fuel varies and it can be assessed in terms of iodine value (IV), saponification value (SV), cetane number (CN), degree of unsaturation (DU), higher heating value (HHV), kinematic viscosity (ν), density (ρ), flash point (FP), cloud point (CP), pour point (PP), and cold filter plugging point (CFPP). The biodiesel produced from any biomass feedstock should comply with the standard values given by American Society of Testing and Materials (ASTM) or European Norms (EN) (Table 2.2).

Table 2.2 Physico-chemical properties of plant and algae biodiesel in comparison with conventional diesel and biodiesel standards based on American standards (ASTM D-6751), European standards (EN 14214/13) and Indian standards (IS 15607)

Property	**ASTM D6751-12**	**EN 14214: 2012**	**IS 15607: 2005**	**Petroleum Diesel ***	**Plant biodiesel ****	**Algal biodiesel *****
IV [g I_2 (100 g oil)$^{-1}$]	ND	≤ 120	ND	ND	ND	ND
SV [mg KOH (g oil)$^{-1}$]	ND	ND	ND	ND	ND	ND
CN	≥ 47	≥ 51	≥ 51	51	45 – 70	41 – 61.4
DU	ND	ND	ND	ND	ND	0.6 – 1.6
HHV (MJ kg^{-1})	ND	≥ 35 (EN 14213)	-	45.9	31.8 – 43.2	38 – 41.5
ν (mm^2 s^{-1}, 40 °C)	1.9 – 6	3.5 – 5	2.5 – 6	1.2 – 3.5	3.6 – 4.9	4.18 – 5.07
ρ (g cm^{-3}, 15 °C)	ND	0.86 – 0.90	0.86 – 0.90	0.83 – 0.84	0.85 – 0.88	0.85 – 0.89
FP (°C)	≥ 93	≥ 101	≥ 120	ND	ND	ND
CP (°C)	Report	Depend on region	ND	-15 – +5	+1 – +13	-2.3 – +17
PP (°C)	ND	ND	ND	-35 – -15	-16 – +9	ND
CFPP (°C)	ND	< +5 (summer) < -15 (winter)	ND	ND	ND	ND

IV-iodine value, SV-saponification value, CN-cetane number, DU-degree of unsaturation, HHV-higher heating value, ν-kinematic viscosity, ρ-density, FP-flash point, CP-cloud point, PP-pour point and CFPP-cold filter plugging point.
*(Brennan & Owende, 2010)
**(Paul & Adewale, 2018; Singh et al., 2010)
***Data was given from 10 algal strains, (Song et al., 2013).

Iodine value (IV) is an indirect measurement of unsaturated bonds in the biodiesel, which expressed as grams of iodine required for iodizing all the double bonds present. The higher the degree of unsaturation, the higher is the NO_x emissions in combustion (Knothe et al., 2006).

Cetane number (CN) is a measure of combustion quality of biodiesel fuel, which signifies the ignition time delay after the fuel is injected into combustion chamber. For shorter time of ignition, the cetane number should be higher. Based on the composition of

fatty acids, the CN increases with the increase in saturation and decreases with the decrease of total carbon atoms in the biodiesel (Bharti et al., 2019).

Saponification value (SV) is determined by reacting the alcoholic KOH with the biodiesel sample in order to saponify the biodiesel and expressed as mg of KOH required for saponify 1 g of biodiesel oil. The SV signifies the average molecular weight of the produced biodiesel as KOH reacts with every acyl group in the biodiesel sample.

Higher heating value (HHV) is another measure and comparison of produced biodiesel with standard biodiesel (EN 14213). It is the total heat energy released after the full combustion of the biodiesel, include the cool down of products to the room temperature.

Density of biodiesel is very important biodiesel property that must be within the limits suggested by the ASTM and EN standards. The diesel engines were designed in such a way that the fuel is injected in a certain volumetric ratio of air/fuel, but not by mass ratio. If the density of biodiesel or its blend is inappropriate, the particulate matter emissions are released as white smoke due to incomplete combustion (Ismail & Ali, 2015). The kinematic viscosity of biodiesel mainly depends on the source of biodiesel production, whose value must be low for better engine operations. If the viscosity is higher than the standard limits, engine deposits can occur. Ideally, lower viscosity along with the higher degree of unsaturation is favourable for better performance of engine. The FP is the temperature at which the biodiesel gets ignited after the impulse of a spark/flame. This value should be high enough to reduce the risks of fire accidents.

Finally, the quality of biodiesel can be can be characterized its flow properties at colder temperatures i.e., applicability in winters and colder regions. The cold flow properties can be expressed as CP, PP and CFPP. The CP is the temperature at which the

biodiesel started to form crystals and looks like cloudy for first time. At the CP, the engine pipelines and combustion chamber start clogging. After the CP, the biodiesel can still flow through certain standardized filters up to a specific colder temperature called CFPP. CFPP is the lowest possible temperature at which the biodiesel or its blend can be used operate the diesel engine. Below the CFPP, the biodiesel get totally freezes at a temperature known as PP, where the engine cannot be run at all. High degree of saturation in the biodiesel can increase the cloud points as saturated ones have higher melting points compared to the unsaturated fatty acids.

2.3 Overview of microalgae as biofuel resource

2.3.1 History, algae biology and classification

Billions of years ago, there was no life on the planet Earth due to high CO_2 levels in the atmosphere. Hence, it was believed that the life was started with cyanobacteria and algae, the primitive photosynthetic organisms that are able to perform all of their cellular functions independently (Barsanti & Gualtieri, 2014; Demirbas & Demirbas, 2010). These fast growing photosynthetic organisms absorbed all the high levels of CO_2 and released O_2 into the atmosphere, resulting the continuous evolution of life on the Earth. In fact, most of the fossil fuels were formed from ancient dead remains of oleaginous algae, bacteria, and plants that performed photosynthesis several million years ago (Bilanovic et al., 2009).

The term, ‘algae’ was coined by Carolous Linnaeus (1753) and the recognition of algae as different from the plants was given by A. L. de Jussieu (1789). He classified the plants and separated the algae from the plants (Sahoo & Seckbach, 2015). Algae are referred as thallophytes since they lack in true roots, stem, leaves, and vasculature and does not contain differentiated tissues unlike plants. The typical structure of algae cell and its organelles is illustrated in the Fig. 2.6. Algae include both microalgae (unicellular) and

macroalgae/seaweeds (multicellular and more complex forms). The size of microalgae ranges between 0.2 – 50 µm of diameter and macroalgae grows up to 60 m of length (McHugh, 2003). They exist in both terrestrial as well as aquatic environments very commonly. According to a recent estimation, 72,500 species of algae exist on the earth (Li-Beisson et al., 2019). Similar to the plants, algae also primarily require sunlight, water and CO_2 for their survival. In order to regenerate their population, algae follow asexual or sexual or both the ways.

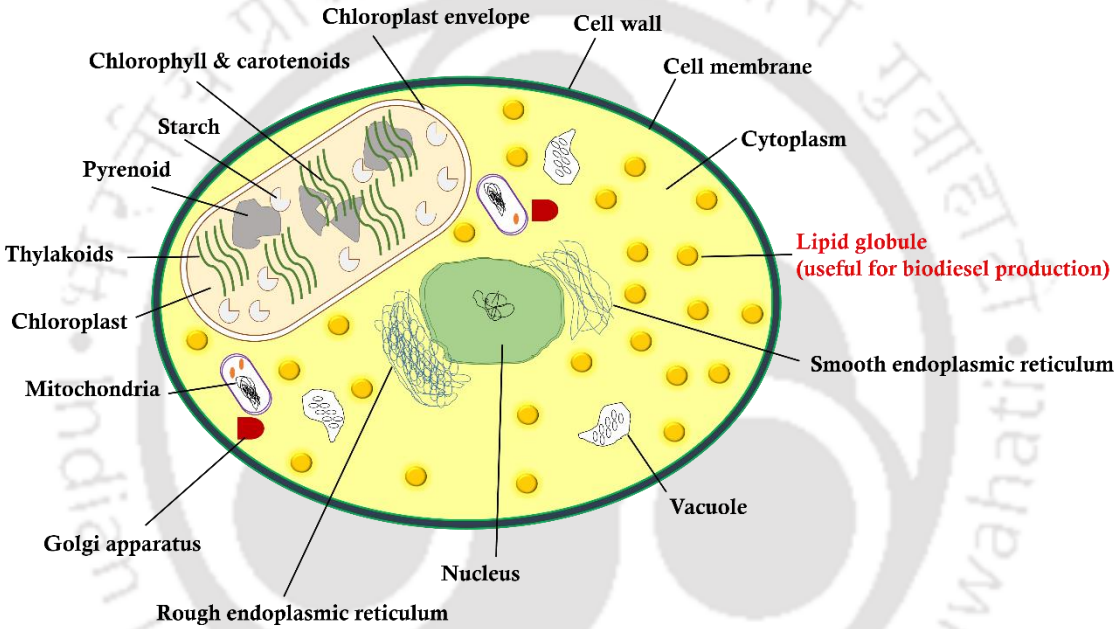

Fig. 2.6. Structure of an algae cell.

Carolous Linnaeus, the first person who classified plants based on their sexual system, proposed 14 genera of algae. However, four of those genera are now considered as algae i.e., *Conferva, Ulva , Fucus, and Chara* (Dahl, 1974). W.H Harvey (1836) was the first algologist who gave first descriptive classification of algae. He divided the algae into four groups on the basis of the thallus colour. Since then, many classifications have been proposed based on a number of characteristics like photosynthetic pigments (chlorophylls, carotenoids, phycobilins), biochemical nature of food reserve, cell wall composition, and flagella. A. W. Eichler (1883) classified plants and formed a new division of thallophyta

for algae and fungi (Baweja & Sahoo, 2015). Engler and Prantle also grouped the algae and fungi together into Euthallophyta (Engler et al., 1897). West classified algae into four groups depending upon the reproductive structures and the presence or absence of flagella (West, 1916). Furthermore, A. Pascher also divided algae into eight divisions on the basis of phylogeny and interrelationships among various groups (Pascher, 1931). Besides, J. E. Tilden classified algae into five classes based on reserve food material, pigmentation and flagellation (Baweja & Sahoo, 2015).

Table 2.3 Classification of algae. Source: (Baweja & Sahoo, 2015; Fritsch, 1935)

Common name	Class	Order
Green algae	Chlorophyceae	Volvocales, chlorococcales, ulotrichales, cladophorales, chaetophorales, charales oedogoniales, conjugales, sipohonales,
Yellow-green algae	Xanthophyceae	Heterochloridales, heterococcales, heterotrichales, heterosiphonales
Orange algae	Chrysophyceae	Chrysomonadales, chrysophaerales, chrysotrichales
Diatoms / yellow or golden brown algae	Bacillariophyceae	Centrales, pennales
Nearly brown algae	Cryptophyceae	Cryptomonadales, cryptococcales
Dark- yellow or brown algae	Dinophyceae	Desmomonadales, thecatales, dinophysiales, dinofl- agellata, dinococcales, dinotrichales
Bright green algae	Chloromonadineae	Chloromonadales
Euglenophyceae	Euglenophyceae	Divided into families- Euglenaceae, astasiaceae, peranemaceae
Brown algae	Phaeophyceae	Ectocarpales, tilopteridales, cutariales,sporochnales, desmarestiales, laminariales, sphacelariales, dictyotales, fucales
Red algae	Rhodophyceae	Bangiales, nemalionales, gelidiales, cryptonemiales Gigartinales, rhodymeniales, ceramiales
Cyanophyceae, blue green algae	Myxophyceae	Chroococcales, chamaesiphonales, pleurocapsales nostocales, stigonemales

Finally, F. E. Fritsch (1935), known as father of phycology gifted a widely acceptable and comprehensive algal classification into 11 classes (Table 2.3). This classification was based on algal pigmentation, chemical nature of the reserve food

material, arrangement of flagella, presence or absence of organized nucleus and mode of reproduction (Fritsch, 1935). He gave importance to living forms of algae rather than the fossil forms. For biodiesel production from algae, several species belonging to various genera have been studied and reported by researchers (Abou-Shanab et al., 2011; Mutanda et al., 2011)

2.3.2 Biochemistry of photosynthesis and lipid biosynthesis

The bio-manufacturing of biodiesel precursor (lipids/triacyglycerols) by algae can be explained by occurrence of synergistic phenomena, i.e., CO_2 fixation via photosynthesis followed by lipid biosynthesis inside the algae cell. Photosynthesis is the process that occurs in plants and algae, helps in preparing their own food molecules using water, CO_2 and light energy. In plant or algae cells, photosynthesis is performed in a special photosynthetic structure known as chloroplast (Fig. 2.6). A typical photosynthesis mechanism is illustrated in Fig. 2.7. Inside this chloroplast, thylakoid membrane sacs containing light-harvesting pigments like chlorophyll, carotenoids, and phycobiliproteins are the actual members that initiates the whole process of photosynthesis, preparing food molecules and growth. In order to perform their respective functions, each pigment absorbs a different set of wavelengths that are available in photosynthetic active radiation (PAR, 400 – 700 nm) of sunlight irradiation. Chlorophyll pigment mainly absorbs red and blue colours and thus appears in green colour (typical colour of green algae and green plants). Primarily two types of chlorophylls known as photosystem I (PSI) and photosystem II (PSII) participate in absorbing the sunlight energy (Fig. 2.7). The maximum absorption wavelengths of PSI and PSII are 700 and 680 nm respectively.

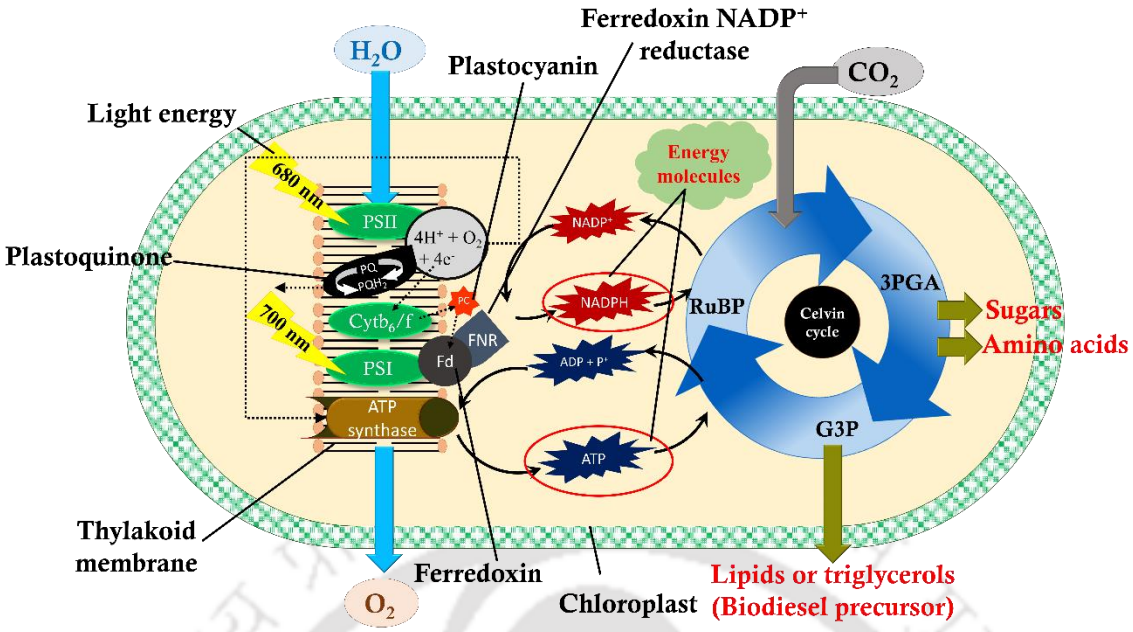

Fig. 2.7 Illustration of a typical C3 photosynthetic process in algae or higher plants prior to biosynthesis of sugars, amino acids, and lipids. Dotted arrows represent electron/proton transport chain.

The process of photosynthesis can be divided into two reactions called light-dependent reaction and light-independent reaction (dark reaction or Calvin cycle). During the light-dependent reaction, the PSII reaction centre catalyses splitting of water molecule into O_2 and proton gradient (H^+ ions) with the help of photon energy from light, an exothermic reaction ($2H_2O \rightarrow 4H^+ + O_2 + 4e^-$) that generates electrons and protons leading to the synthesis of ATP and NADPH for carbohydrate synthesis during the dark reaction (Fig. 2.7). The electron transport chain donates half of the electrons to plastoquinone and transfers another half via cytochrome b_6/f complex to the site of PSI (a redox enzyme), where $NADP^+$ is reduced to NADPH with the help of ferredoxin/ferredoxin $NADP^+$ reductase complex and creates an extra proton gradient in thylakoid membrane that drives ATP synthase to synthesize ATP from ADP. The newly formed NADPH and ATP is utilized as energy source for the fixation of CO_2 into 3-phosphoglycerate, precursor of acetyl CoA that leads to TCA cycle and fatty acid biosynthesis (Fig. 2.7 and 2.8). Since the 3-phosphoglycerate is a 3-carbon compound, algae was known to follow C3 photosynthesis. However, some marine algae species were shown existence of C4

photosynthetic pathway in their systems. For example, *Ulva prolifera*, *Udotea flabellum*, *Macrocystis integrifolia* and many species of brown algae were known to fix CO_2 via C4 photosynthetic pathways (Kremer Bruno, 1981; Reiskind & Bowes, 1991; Xu et al., 2012).

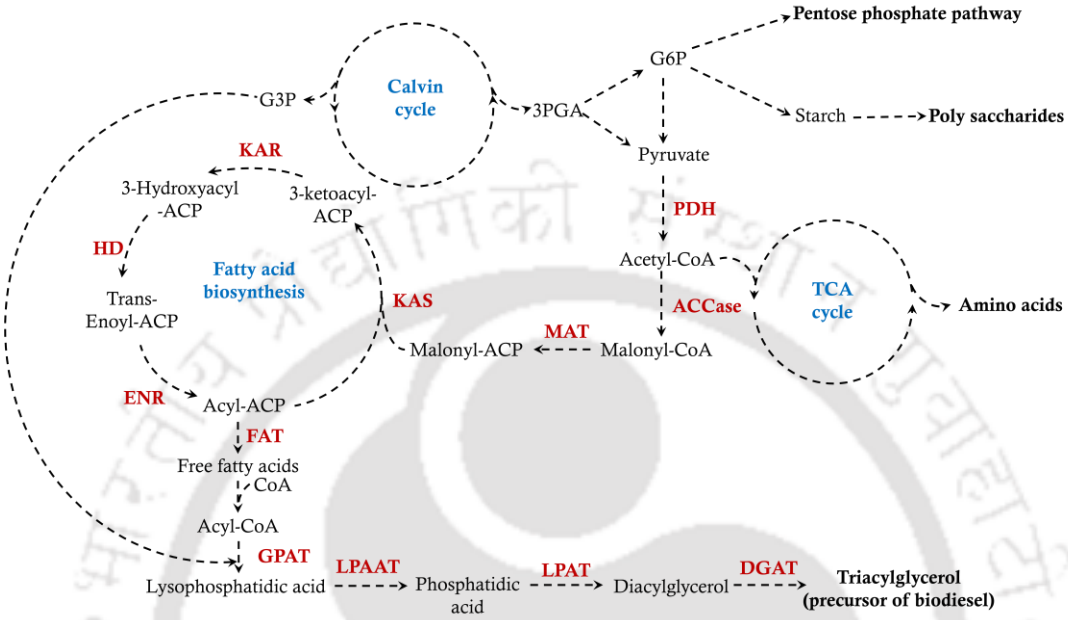

Fig. 2.8 An overview of fatty acid biosynthesis pathway coupled with tri-carboxylic acid cycle and Calvin cycle. **ACCase** acetyl-CoA carboxylase; **ACP** acyl carrier protein; **CoA** coenzyme A; **DGAT** diacylglycerol acyltransferase; **ENR** enoyl-ACP reductase; **FAT** fatty acyl-ACP thioesterase; **GPAT** glycerol-3-phosphate acyltransferase; **HD** 3-hydroxyacyl-ACP dehydratase; **KAR** 3-ketoacyl-ACP reductase; **KAS** 3-ketoacyl-ACP synthase; **LPAAT** lyso-phosphatidic acid acyltransferase; **LPAT** lyso-phosphatidylcholine acyltransferase; **MAT** malonyl-CoA ACP transacylase; **3PGA** 3-phosphoglycerate; **G3P** glyceraldehyde-3-phosphate; **G6P** glucose-6-phosphate; **PDH** pyruvate dehydrogenase.

In lipid accumulating algae species, the biosynthesis of lipids or tricayglycerols follows almost similar pathway that exists in higher plant cells (Hu et al., 2008; Maraschin et al., 2019). The formation of malonyl-CoA from acetyl-CoA via acetyl CoA carboxylase enzyme is the rate determining step towards the free fatty acid synthesis in chloroplasts or plastids, thereby lipid synthesis in cytosol as well (Fig. 2.8). Acetyl(C2)-CoA can be available from various metabolic pathways and it is metabolized into malonyl(C3)-acyl carrier protein (ACP) by the action of malonyl-CoA:ACP transacylase on malonyl-CoA.

Subsequently, acetyl-CoA and malonyl-ACP act as primary substrates and acetyl donor units for the initiation of fatty acid synthesis.

Table 2.4 Lipid contents (% of dry weight) of various microalgal strains (Mutanda et al., 2011; Um & Kim, 2009).

Algae species	**Lipid content (% of biomass weight)**
Anabaena cylindrical	11
B. braunii	25–75
C. vulgaris	14–22
Chlorella pyrenoidosa	2
Chlorella sp.	28–32
Chlamydomonas rheinhardii	21
Dunaliella bioculata	8
Dunaliella salina	6
E. gracilis	14–20
Prymnesium parvum	22–39
Tetraselmis maculata	3
Scenedesmus obliquus	12–14
Scenedesmus quadricauda	1.9
Scenedesmus dimorphus	16–40
Spirogyra sp.	11–21
Spirulina maxima	6–7
Schizochytrium sp.	50–77
Isochrysis sp.	25–33
Spirulina platensis	4–9
Synechoccus sp.	11
Tetraselmis sueica	15–23
Chaetoceros muelleri F&M-M43	33.6
Chaetoceros calcitrans CS178	39.8
Monallanthus salina	>20
Monodus subterraneus UTEX151	16.1
Nannochloropsis sp.	31–68
Neochloris oleoabundans	35–54
Nitzschia sp.	45–47
Pavlova salina CS49	30.9
Pavlova lutheri CS182	35.5

Firstly, acetyl-CoA and malonyl-ACP are metabolized into butyryl (C4)-ACP through a series of reactions e.g., condensation, decarboxylation, and reduction to produce a fatty acid chain. The fatty acid chain is elongated by adding C2 saturating carbon units via addition of malonyl-ACP to form saturated acyl-ACP up to acyl(C_{16} – C_{18})-ACP.

Secondly, free fatty acids are synthesized by removing ACP from the acyl(C_{16} – C_{18})-ACP. For this reason, fatty acids of C_{2n} exist in high amounts in the organisms though the fatty acids of C_{2n-1} are also synthesized from fatty acids of C_{2n} by losing a carbon. The free fatty acids synthesized in the chloroplast are then excreted into cytoplasm for further synthesis of very long fatty acids or formation of glycolipids, phospholipids, glycerolipids and triacylglycerols (TAGs). The elongation of fatty acid chain beyond the C_{18} carbon number takes place in endoplasmic reticulum that follows almost similar pathway in the chloroplast, however the excreted acyl-CoA and malonyl-CoA are act as substrates for synthesizing very long fatty acid chains of C_{20} – C_{24} (Baba & Shiraiwa, 2013; Kunst & Samuels, 2009). For example, fatty acids like eicosapentaenoic acid (C20:5ω3), docosahexaenoic acid (C22:6ω3) and arachidonic acid (C20:4ω6) are the long fatty acids that have huge importance in food and drug industries. The popularity of algae for biodiesel was actually due to the accumulation of TAGs (storage lipids), having majority of C_{16} –C_{18} fatty acids. Typically, microalgae have the capability of accumulating total lipid contents from 1 – 85% of dry weight depending on the nutritional status and stress conditions (Chernova & Kiseleua, 2017). The lipid contents of various species of algae are shown in Table 2.4.

2.4 Nutritional modes of algae growth

The characteristics of algae growth, lipid induction and fatty acid profile of biodiesel highly depends on the growing conditions or mode of cultivation it experiences. Four modes of cultivation may be followed based on the sources of energy and carbon. They are namely photoautotrophic, heterotrophic, mixotrophic and photoheterotrophic propagation modes (Benavente-Valdés et al., 2016; Josetespardellier et al., 1978). In photoautotrophic propagation, light (e.g., sunlight, artificial lighting) and inorganic carbon source (e.g., CO_2) are used (Gouveia et al., 2009; Guo & Tong, 2014; Illman et al., 2000). In heterotrophic mode, organic carbon sources (e.g., sugars and organic acids) are used as

sole energy as well as carbon source in the absence of light (Rattanapoltee et al., 2008; Tian-Yuan et al., 2019). Generally, heterotrophic cultivation is carried out in closed environments, e.g., stirred-tank bioreactors. In mixotrophic cultivation, the algae utilizes both CO_2 and organic carbon with light as the sole energy source.

2.5 Salient growth factors of algae in photoautotrophic cultivation

2.5.1 Nutritional medium

Microalgae require a range of growth nutrients for their growth in addition to the light energy and CO_2 involved in the photosynthesis process. Nitrogen and phosphorus sources are the two key nutrients that can be manipulated for achieving high growth rates of algae as they are the main sources of protein and nucleic acid biosynthesis. Other essential nutrients include S, Ca, Mg, Na, K and Cl. These are responsible for cell-signalling mechanisms and act as cofactor of some enzymes involved in cell-division, replication and photosynthesis (Pruvost et al., 2011). Some minor nutrients like Fe, B, Mn, Cu, Mo, Co, Ni, Si and Se are also vital for specific enzymatic functions required for maintenance of the cells. Depending on the natural occurrence or source of isolation, the requirements in the nutritional medium varies. For example, marine algae are maintained under salinity conditions by providing NaCl, diatoms require Si as it is the major constituent of cell wall and most of the fresh water algae does not require the above nutrients at all. Therefore, the selection and optimization of nutritional medium for cultivation has been reported as foremost and basic step in the process engineering of newly isolated microalgae. Statistical techniques have made the optimization of nutritional medium very easy (Muthuraj et al., 2015).

For lipid induction for biodiesel production from a potential oleaginous microalgal strain, the lipid content (% of DCW) can be increased by limiting some of the nutrients like

N or P. Basically, three modes of nutrient supply, i.e., nutrient-sufficient, nutrient-limited and nutrient-deficient have been proposed for achieving higher production of lipids in the algal biomass (Rodolfi et al., 2009). In nutrient-limited supply, the algae cells are provided with a constant but insufficient supply of a nutrient such that the cells get adapted to it. This nutrient-limited supply is also used to evaluate the yield coefficients of crucial nutrients while designing chemostat operational modes. Whereas in the nutrient-deficient supply, an essential nutrient/s are not provided for creating stress environment inside the cell metabolism for shifting all the metabolism towards the production of interested compounds.

2.5.2 Effect of light intensity

Light intensity is one of the most crucial growth factors that drive the whole photosynthetic process of microalgae growth and is responsible for the overall cellular metabolism, cell cycles and growth. For a commercially feasible biomass production, microalgae cultured under natural sunlight is desirable (Wang et al., 2014). The growth of microalgae increases with the increase in light intensity irradiation as there would be a proportional generation of electron transport chain that drives the preliminary light reaction of photosynthetic process. However, depending on strain, the algal cells experience light saturation beyond a certain limit of light intensity range (Mussgnug et al., 2007). The evaluation of this saturation range of light intensity is vital for growth process design. The photoinhibition refers to the inhibition of the PSII activity when photosynthetic organisms are exposed to high light intensities. In classical terms, high light intensities induce the production of reactive oxygen species, which are highly unstable and thus damages the photochemical reaction centre at PS II, the preliminary step of photosynthesis becomes the primary target of photoinhibition (Murata et al., 2007).

Another evidence from molecular biology studies confirms that it can be directly related to the damage and recovery of D1 protein in PS II (Han, 2002). Recovery of D1 protein is directly proportional to its damage. When the rate of damage of D1 protein exceeds the rate of recovery, then PS II is said to be in inhibitory state, but at the same time, the inhibition of net photosynthesis cannot be attributed to high light intensities alone (Pope, 1975).

In other way, the concentrations of dissolved oxygen (DO) and/or dissolved CO_2 (dCO_2) could shift the saturated light intensity (depends on strain), thereby decides the occurrence of photoinhibition. For example, increment of dissolved oxygen (DO) due to photosynthesis can decrease saturating light intensity lower than typical range (Pope, 1975). Other report on *Lolium perenne* L. (perennial ryegrass, plant species) suggested that the range of saturated light intensity was significantly increased with increasing CO_2 partial pressure (Wilson & Cooper, 1969). Therefore, the interplay between these process parameters should be well understood in the indoor/laboratory experiments before taking the process directly to the outdoor sunlight. For determining the saturated light intensity for a specific microalgae species, indoor experimental studies under mimicked/simulated outdoor sunlight conditions is necessary for avoiding the unexpected weather (short-term fluctuations in atmosphere) and climatic (long-term variations of weather) conditions. Also, the experiments under simulated sunlight are repeatable. Simulation of sunlight in the lab environment can be achieved by using light emitting diodes (LED) technology, which have already been proven for green houses and horticulture experiments (Darko et al., 2014; Ergil, 2014).

2.5.3 Carbondioxide supply and feed strategies

Carbondioxide is the major carbon source for photoautotrophic growth of microalgae. As photoautotrophic cultivation is the only feasible method for large-scale

production of microalgae, the supply, availability and influence of CO_2 is crucial for understanding and developing an efficient CO_2 feed strategy. The dissolved CO_2 (dCO_2) is an important parameter to be considered during the growth of microalgae for obtaining the CO_2 uptake rates by the cells. The CO_2 uptake rates in turn depends on the overall mass transfer coefficient ($K_L\, a_{,CO_2}$) and supply rate of CO_2. The supply rate of CO_2 should be increased upon growth of microalgae due to increasing CO_2 uptake rates. However, the CO_2 should not reach levels such as to inhibit photosynthesis, hence, growth of microalgae (Kunjapur & Eldridge, 2010).

The CO_2 level (% in air) at which the inhibition occurs can vary with microalgae strain. For example, the strains of *Chlorella* sp. KR-1 and *Scenedesmus obliquus* showed their highest biomass titers at 10% and 15% CO_2 levels (% in air) respectively (Kaewkannetra et al., 2012; Sung et al., 1999). Therefore, the CO_2 levels in the range of inhibition or tolerance should be determined at early stage in process development. The minimum CO_2 required for specific biomass concentration referred to as critical dCO_2 concentration. It depends on the CO_2 supply and its mass transfer rate, CO_2 affinity of the species, growth rate, cell size and shape of organism. When the microalgal strain is specified, CO_2 supply and CO_2 mass transfer are the two areas of technology improvement. Several CO_2 supply strategies such as constant feed of predetermined optima, biomass density based feed, and pH control based feed have been studied for microalgae cultivation (Chen et al., 2016; Duarte-Santos et al., 2016; Guo et al., 2015; Singh & Singh, 2014; Sung et al., 1999; Tang et al., 2011).

Although the above strategies are well-studied and widely reported for outdoor culturing of algae, the process economics for achieving commercial success of algae is still a major challenge. In constant feed, the maintenance of optimum CO_2 level (generally determined under constant lighting) cannot be applicable to the wide range of light

intensities observed in sunlight. The biomass density based feed where the CO_2 levels are increased upon growth would not be sustainable after reaching certain biomass density due to inevitable light limitation. In pH control based feed, usually performed at constant pH set point, CO_2 feed strategy do not account the CO_2 uptake rates. Therefore, some novel CO_2 feed strategies coupled with cost-effective photobioreactor technology is necessary towards achieving high cell density and high biomass productivity required for scale-up to commercial viability. Current literature does not include the coupling of CO_2 supply, DO and light intensity for better understanding of the interplay between them. However, the reports related to the effect of light intensity, partial pressures of CO_2 and O_2 on plant physiology provide leads to better understanding of the green algae physiology as both systems follow the C3 photosynthetic pathway. On this basis and the sunlight's diurnal nature (variation of light intensities from dawn to noon and noon to dusk), a CO_2 feed strategy for high photosynthetic rates can be developed by decreasing CO_2 levels during the low light conditions instead of maintaining CO_2 level throughout the day. At the same time, the CO_2 levels higher than the CO_2 level at low light should be followed at high light conditions for better photosynthetic performance compared to the constant CO_2 feed.

2.5.4 Design of microalgae cultivation system

For a successful design of process and technology for algae biomass production, the mass culturing system should be cost-effective and suitable to capture the sunlight efficiently. It is the techno-economic decisive leg in life-cycle assessment of Algae – Diesel plant for commercial production scale. First attempts for production of liquid fuel from Diatomeae were made in Germany during World War 2, which led to the production of *Scenedesmus* and *Chlorella* biomass from the waste CO_2 of industrial zones (Chisti, 2007). Since light energy is the major growth factor for microalgae, the ideal cultivation system should have more surface area for sunlight absorption and distribution. Therefore, an algae

cultivation technology should maximize the surface area to volume ratio (S/V). This is the reason why the geometry of algae cultivation systems looks very different from the conventional bioreactors where light does not play any role. In the present scenario of large-scale algae cultivation, open ponds and enclosed photobioreactors like vertical tubular, horizontal tubular and flat panels are scalable systems that have been extensively studied. Depending on the biomass requirements and to enhance growth rates, these cultivation systems can be operated in various operational modes, e.g., batch, fed-batch, semi-continuous and continuous modes of operation.

2.5.4.1 Artificial open ponds

The most practiced cultivation systems are artificial open ponds due to their economic feasibility, easy installation and maintenance. They include shallow big ponds, tanks, circular ponds and raceway ponds. Open ponds are mostly equipped with baffles and paddle-wheels for better mixing (Xu et al., 2009). The depth of pond is one of the most important consideration while manufacturing artificial open ponds. The pond should be shallow enough such that it can absorb sufficient amount of light for the growing culture as well as it should be deep enough to promote the mixing and minimizing the evaporation. Open raceway ponds operated at water depths of 15 – 30 cm using paddle wheels for mixing. The schematic of a basic open pond cultivation system is shown below (Fig. 2.9). The major disadvantage is the susceptibility to contamination, i.e., monoalgal culturing becomes highly difficult as other competitive microorganisms or predators often contaminates the ponds. In addition to that, poor biomass productivity and inability to

control the process parameters has necessitated the consideration of alternative algae cultivation technologies such as photobioreactors.

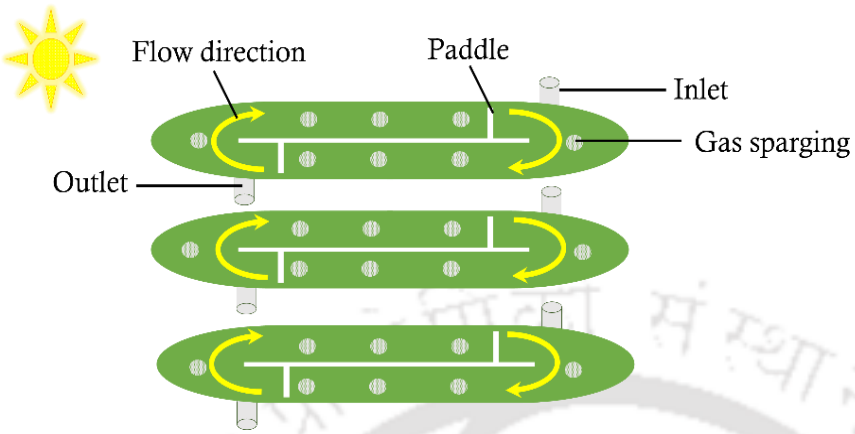

Fig. 2.9. A schematic of an artificial open pond for microalgae cultivation

2.5.4.2 Scalable photobioreactor technologies

Due to the low biomass productivities and contamination issues of pond systems, photobioreactor systems were developed to obtain high biomass productivities by allowing better control over culture conditions (Ugwu et al., 2008). Photobioreactor is a closed culturing system made up of transparent tubes or panels for growth of microalgae using CO_2 and essential nutrients under the illumination/exposure of light energy. Scalable enclosed photobioreactor technologies include three main categories, namely, tubular/horizontal, column/vertical tubular and flat-plate or flat panel reactors (Fig. 2.10, 2.11 and 2.12) (Saad et al., 2019; Yen et al., 2019).

For achieving higher biomass productivities, engineering of these production systems is necessary (Chisti, 2013; Nwoba et al., 2019). Tubular PBRs offer desirable amounts of surface to volume ratios. Though flat panel PBRs have highest S/V ratios, they do not offer good hydrodynamics and their scale-up is not easy. Moreover, the flat panels pose heating issues to algae cultures when the temperatures rises due to high sunlight intensity (Sánchez Mirón et al., 1999). Average photosynthetic efficiency is higher in tubular photobioreactor than in flat panel (Tredici & Zittelli, 1998). Notably, curved surface

area of tubular reactor diffuse radiation and decreased the photoinhibition on algal culture as they experienced lower light saturation effect. Based on photosynthetic efficiency and high areal productivities, column PBRs including bubble-column and airlift technologies are better performers in laboratory scale experiments (Miron et al., 2000; Pulz & Scheibenbogen, 1998). They are scalable but have high costs of installation (Kunjapur & Eldridge, 2010; Sánchez Mirón et al., 1999). From the pros and cons of the cultivation systems, vertical tubular/column PBRs with improved mass transfer technology could achieve high biomass densities. Also, vertical PBRs require lesser land requirements compared to the flat panels and horizontal tubular PBRs. In vertical PBRs, the DO build-up can be easily controlled by limiting the height of PBR up to non-lethal DO accumulation. Apart from that, vertical PBRs can be up-scaled by incorporating the technologies of airlift or bubble-column for effective aeration, leading to sufficient mass transfer of CO_2 that also aids in lower DO build-up as the CO_2 can strip out the O_2 effectively from the vent provided at the top of vertical PBRs. Another attractive feature of vertical PBRs is that there is scope for arranging special internal mixers to enhance sunlight capture efficiency (see chapter 7, later).

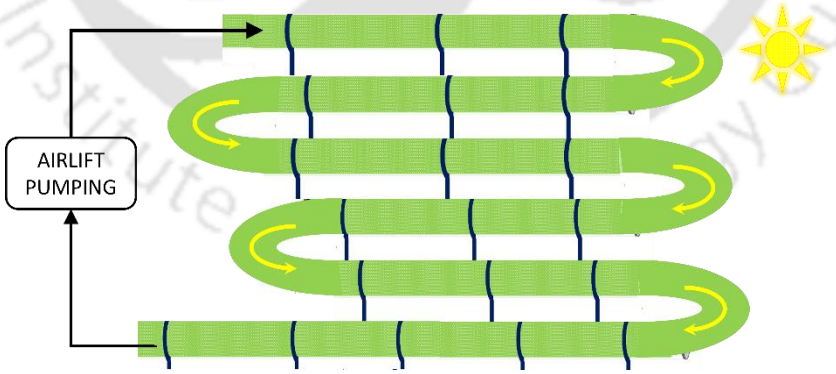

Fig. 2.10. A schematic of horizontal tubular photobioreactor for microalgae cultivation

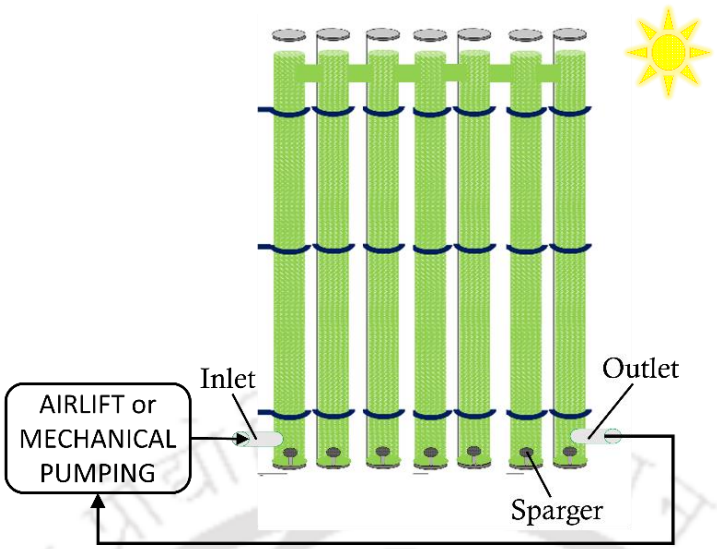

Fig. 2.11. A schematic of vertical tubular photobioreactor for microalgae cultivation.

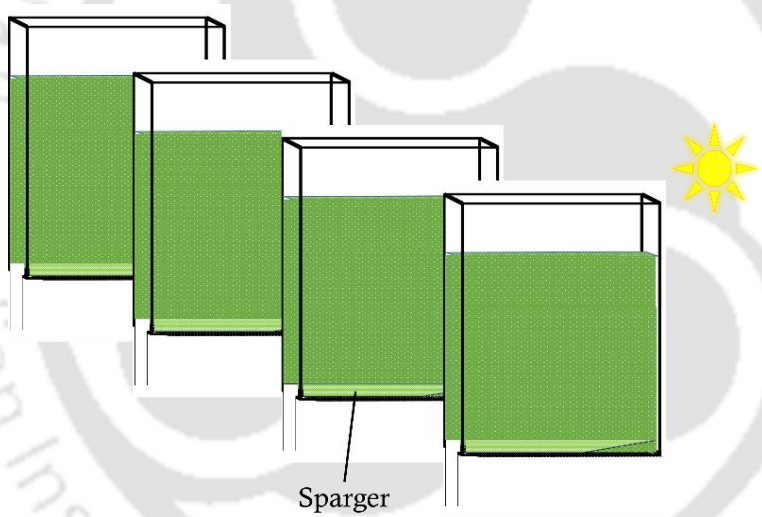

Fig. 2.12. A schematic of flat panel photobioreactor for microalgae cultivation.

2.5.5 CO_2 mass transfer and sparging equipment

The absorption of CO_2 and other basic essential nutrients mainly depends on the mass transfer efficiency of the algae cultivation system. The nutrients other than CO_2 can be easily by distributed by mixing the algae culture broth in homogeneously. The transportation of CO_2 for efficient absorption by the cells requires a sparger (a gas sparging apparatus) having high CO_2 mass transfer coefficient. The sparger's mass transfer

efficiency is usually measured in terms of overall CO_2 or O_2 mass transfer coefficients ($K_L\, a_{,CO_2}$ or $K_L\, a_{,O_2}$).

In the conventional bench-top bioreactors, O_2 is sparged through a metallic L-shaped sparger that actually generates very big bubbles. However, the agitation and contact created by electricity-driven impellers break the bubble into small-size for an efficient mass transfer. But this extra electrical energy would add more cost to the already existing cost of a mass algae cultivation technology. Thus, the algae researchers adopted the sparging technologies from well-studied bubble column or airlift type of reactors where the mass transfer and agitation are driven by the smaller or medium size bubbles (Miron et al., 2000; Ugwu et al., 2008). In the reported studies of algae cultivation systems, different type of sparger designs have been used e.g., L-shaped, ring-shaped, perforated tubing, ceramic, compressed stainless steel and sintered disc, etc. (Contreras et al., 1998; Merchuk et al., 2000; Ugwu et al., 2002; Vega-Estrada et al., 2005). Apart from having high CO_2 mass transfer coefficient, an ideal sparger should also be energy-efficient, i.e., be able to minimize electricity requirement for the aeration. This can be directly correlated with the aeration rates used in the cultivation systems. Usually, the aeration rates in the range of 0.025 – 0.1 VVM are feasible for the scale-up of algae cultivation process (Kunjapur & Eldridge, 2010).

2.5.6 Importance of efficient mixing and mixing equipment

During the culturing of microalgae under sunlight, efficient mixing prevents the settling of cells, minimizes the diffusion gradients (CO_2 + growth medium components), strips out accumulated DO and most importantly aids the algal cells movement from light to dark zones more frequently (Kunjapur & Eldridge, 2010). In this way, the mixing can improve biomass productivity by maximizing the solar energy capture leading to increase in specific light availability, i.e., average light exposure per algal cell (Wang et al., 2012).

It also aids in the improvement of lipid contents in some oleaginous species that enhances biodiesel production. For example, in a study on *Chlorella vulgaris*, the combination of N-deficiency and increment in specific light availability by decreasing the biomass density induced more lipid compared to the cells grown only in N-deficient nutritional medium (Munkel et al., 2013). Although aeration via bubbling or mechanical agitation results in some level of mixing in the photobioreactors, installation of baffles or special internal mixing equipment improves effectiveness, hence, such have been tested in recent developments in photobioreactor design (Huang et al., 2017; Munkel et al., 2013; Wang et al., 2012).

The typical use of draft tube or baffles in concentric tube or split cylinder also aids in internal mixing, but these cannot generate the frequent movement of cells from light to dark zones that is vital for microalgae culturing to improve biomass or lipid productivity. The bubble-driven mixing caused by aeration in bubble column does provide efficient mixing as the scale of PBR increases. Other side, mechanical agitation systems incur capital as well as maintenance cost to the PBRs while scale-up is both challenging and energy intensive. Therefore, adaptation of specially designed internal static mixers have been studied for flat panel and tubular PBRs (Huang et al., 2015; Ugwu et al., 2003; Ugwu et al., 2002).

In general, the static mixers act as baffles that generate local turbulences due to the motion of bubbles and fluid flow. The turbulence agitate the algal cells exposing them to light/dark zones inside the PBR. However, the mobile mixers are more effective than static mixers as they can directly cause motion of fluid through their rotations. It is also desirable that such agitation mechanisms do not require external energy input. To date, there is only one study that reported on installation of mobile mixers inside the tubular PBR (Yan et al., 2018). In the study, a single and long helical rotor was used, which was self-rotating by the

virtue of continuous fluid (algae culture) flow, therefore incurring no extra energy demand. This study recognized the scope for the design of self-rotating bubble-driven mixer in vertical/bubble column.

2.5.7 Effect of temperature and pH

In the outdoor cultivation of microalgae under sunlight, the cells can experience a wide range of temperatures, e.g., ranging from 20 – 40 °C in the summer and 10 – 35 °C in the winter. Depending on the natural habitat from where the species is isolated, the optimum range of temperature may vary from species to species. Therefore, the temperature is controlled by spraying cold water or by thermostat controller in outdoor photobioreactors for improving biomass production (Richmond et al., 1993; Ugwu et al., 2008). However, some reports under natural sunlight conditions suggest that the temperature control is not mandate for some microalgal strains as it saves the cost of overall process (Fuentes-Grunewald et al., 2013; Guo et al., 2015). For this reason, the process design of microalgal biomass production on commercial-scale would be more feasible if the selected strain is tolerant to a wide range of temperatures.

Unlike temperature, the pH maintenance in algae culture is vital for efficient CO_2 uptake by the cells. In water, CO_2 exists in three forms, namely, dissolved CO_2 (dCO_2) species at acidic pH, bicarbonate (HCO_3^-) species at neutral pH and carbonate (CO_3^{2-}) at alkaline pH levels and dissolved CO_2 at acidic/neutral pH levels in the water (Imamura et al., 1983; Scherholz & Curtis, 2013). However, most of the microalgal cells prefer dCO_2 or HCO_3^- over the CO_3^{2-} species (Scherholz & Curtis, 2013). For this reason, the pH of culture medium should be maintained in acidic or neutral pH conditions. Exceptionally, some strains of microalgae species are capable of growing at higher pH. For example, *Chlorella vulgaris* (FACHB-1227) can still grow at 10 pH even though its initial optimum pH was 7.0 (Gong et al., 2014). For such species, the pH control in the night times (dark-

phases of culturing period) may not be required as the CO_2 supply is usually stopped in the dark-phase. Therefore, it is imperative to study both the selection of pH control set point and control for better understanding of the process design. It is arguable that optimization studies for ranges of CO_2 levels or concentrations should be carried out after setting same pH for all the variations.

2.5.8 Effect of dissolved oxygen

Generally, excessive oxygen accumulation can inhibit algae cells in two ways, i.e., photoinhibition and/or photorespiration. Photoinhibition occurs due to generation of reactive oxygen species induced by high light intensities, which is already discussed in section 2.5.2. In the latter phenomenon, unwanted respirational events occur in microalgae cells where CO_2 is generated in tandem with regular consumption for photosynthesis. This phenomenon is explained as photorespiration where the crucial enzyme of photosynthesis, RuBisCO (Ribulose-1,5-bisphosphate-carboxylase/oxygenase) shares both oxygenase and carboxylase activities (Lloyd et al., 1977; Zelitch, 1971). According to the very well-known Warburg's effect, photosynthetic rate decreases at high O_2 concentrations due to competitive inhibition of carboxylase (CO_2 fixation by RuBisCO) activity. Due to this, at least 25% of fixed CO_2 would be efflux back to the environment. However high temperature also favours more CO_2 to get released. In order to understand and tackle both the challenges of photoinhibition and/or photorespiration, the effect of DO accumulation should be accounted specifically for purposes of process scale-up.

The DO accumulation resulting from photosynthesis process can cause serious problems in the enclosed photobioreactors compared to the open ponds. The DO build-up cannot be seen in small-scale cultivation as the sufficient supply of air/CO_2 and the efficiency gas sparging apparatus aids in removing the DO build-up instantaneously. However, the microalgae cells do experience inhibition due to DO build-up in large-scale

or industrial-scale culturing systems (Lee & Yeh, 2015). The DO accumulation should not be allowed to increase beyond 400% air saturation, which sets limitation for the length of horizontal or even vertical tubular PBRs design (Kunjapur & Eldridge, 2010).

2.6 Methods of induction for enhanced lipid biosynthesis

2.6.1 Engineering of nutritional medium

Microalgae production as feedstock for biodiesel production requires investigation of production factors that could help in maximization of lipid production. Basic stressors, particularly the limitation of phosphorus and nitrogen in culture medium helps to induce the lipid contents of several microalgae such as, *Scenedesmus subspicatus*, *Scenedesmus* sp. *Spirulina platensis, Dunaliella tertiolecta, Neochloris oleoabundans, Chlorella vulgaris* and others (Brennan & Owende, 2010; Chernova & Kiseleua, 2017; Pal et al., 2011; Rodolfi et al., 2009; Sharma et al., 2012; Singh & Singh, 2015; Widjaja et al., 2009). The stressor for diatoms microalgae (for example, *Cyclotella cryptica*) is the limitation of silicon source. In many algae, lipid growth is observed when one of the biogens is absent in culture medium or during their joint action (such as absence of nitrogen or iron or phosphorus in *Chlorella* sp.). Phenomenon is well explained by "snow-algae", which grows on snowfields and glaciers as they possess considerable amount of lipid content due to the unavailability of biogenic elements in the habitats.

The effect of illuminance condition on lipid induction has also been widely reported. For example, the microalgae species like *Chlorella vulgaris*, *Nannochloropsis* sp, *Pavlova lutheri, Monodus subterraneus,* have shown higher TAG/lipid accumulation when they were exposed to high light intensities (Munkel et al., 2013). In some species, low light intensities of 2 µmol m^{-2} s^{-1} can also induce lipid accumulation in the biomass (Chernova & Kiseleua, 2017). Ultraviolet irradiation also acts as a stress factor for induction of high

lipid content in microalgal cells like *N. oculata* and *N. salina*, however, the method is not economically viable. The changes in ambient temperatures also induces lipid accumulation (Zhu et al., 2016).

The combined effect of high illuminance and N-absence in the media is known to enhance the lipid contents of *C. vulgaris* and *M. subterraneus* compared to the stress created by N-absence alone (Munkel et al., 2013). From the above literature, it is clear that the stress factors for the lipid induction are strain specific, therefore identification of potential stress factor is crucial for biodiesel directed algal biomass production.

2.6.2 Lipid induction processes

Upon identification of specific stress factor nutrient in growth medium that enhances lipid induction, the growth of algae is allowed to complete that nutrient and to grow more for lipid induction by maintaining other nutrients in excess. This process is called single-stage lipid induction (Yeh & Chang, 2011). In two-stage lipid induction process, the microalgae cultivation is carried out until the end of growth-phase and the culture is harvested (usually by means of centrifugation at very low speeds) and re-suspended in fresh growth medium without the stress factor component (usually N and/or P sources in most cases) (Muthuraj et al., 2015; Nagappan et al., 2019). Although the single-stage process saves centrifugation costs, most of the reports suggested that the amount of lipid contents (% of DCW) were observed more in the latter strategy (San Pedro et al., 2014; Su et al., 2011; Xia et al., 2013). For example, the two-stage lipid induction process for *Nannochloropsis oculata* ha produced 3 times more lipid yield compared to the single-stage batch process (Su et al., 2011). Another study on *Chlorella vulgaris* ESP-31 shown that single-stage process with lower initial N can yield lipid content up to 55% (of DCW) with 78 mg L^{-1} day^{-1} of lipid productivity (Yeh & Chang, 2011). Therefore, the applicability of single-stage lipid

induction method for an oleaginous strain is worth considering for process economy reasons. Apart from the single-stage or two-stage lipid induction via nutrient-stress, more light exposure through induced mixing can also enhance lipid induction (see previous section 2.6.1). Since PBR receives limited light intensity in the natural sunlight conditions, an efficient internal mixer installation inside the PBR can also enhance the lipid contents and lipid productivity.

2.7 Processing of microalgae for biodiesel production

2.7.1 Harvesting and dewatering technologies

In succession to the cultivation and lipid induction, the microalgal broth culture is subjected to harvesting via various techniques, such as filtration (vacuum, pressure, cross-flow, and tangential-flow), centrifugation (disc stack, decanter), sedimentation, flotation (dissolved air, dispersed air, electrolytic), flocculation (chemical – organic / inorganic, biological, magnetic, electrolytic, auto-flocculation), and electrolytic coagulation (Al-Hattab et al., 2015; Chatsungnoen & Chisti, 2016; Dassey & Theegala, 2013; Landels et al., 2019). These above techniques could separate algal biomass, extracellular products (if any) and water.

During the mass culturing of algae (microalgae or seaweeds), an effective harvesting technique is decided by several critical factors like reusability of water/media, efficiency, scalability, species specificity, toxicity, cost, time and maintenance. Based on the above criteria, an evaluation study on industrially feasible / scalable harvesting techniques for biodiesel production revealed that disc stack centrifugation, decanter centrifugation, cross-flow filtration, and organic flocculation are the only suitable methods for large-scale harvesting (Al-Hattab et al., 2015). However, the associated energy-intensive problems with centrifugation / filtration at industrial-scale suggested that organic

flocculation followed by cross-flow filtration or centrifugation could reduce the energy consumption to a greater extent (Al-Hattab et al., 2015; Dassey & Theegala, 2013). Consequent to the harvesting and dewatering steps, the direct use of wet microalgae for the production of biodiesel is very promising due to reduction of drying time and extra-energy cost associated with the drying processes. Nevertheless, the biodiesel extraction / production using the wet algal biomass is still limited to research and development because of the high costs and environmental safety issues associated with wet-extraction solvents (Ghasemi Naghdi et al., 2016). Conversely, the wet algal biomass could also be processed through various large-scale drying methods include rotary drying, spray drying, solar drying, flash drying, vacuum shelf drying, incinerator drying, and cross-flow air drying to obtain dry biomass (Show et al., 2015).

For small-scale research and laboratory studies, lyophilisation or freeze drying is the most commonly used method for drying the microalgae as it can handle small-volume samples. Moreover, it avoids degradation or inter-conversion of lipids before the extraction process and aids in evaluating the exact quantity and quality of biodiesel (Ryckebosch et al., 2011). The biodiesel quantity and quality derived from the freeze-dried algal biomass can be used as a benchmark for developing the suitable large-scale drying method. The wet / dried algal biomass after harvesting is generally fractionated into platform molecules of lipids, carbohydrates and proteins via various extraction and conversion processes (discussed in the next section).

2.7.2 Biodiesel production: Cell disruption, extraction, and conversion

The lipid extraction from algal biomass is an energy demanding process. Therefore, economics of downstream processing is critical step in the algae-biodiesel production cycle. Depending on the cell wall rigidity of specific microalgal species and products of

interest, selection of cell disruption technology is important (Günerken et al., 2015; Lee et al., 2017). Broadly, the cell disruption methods are mainly divided into two types, namely, mechanical and non-mechanical. The mechanical type of cell disruption requires energy input in the forms of shear force, wave energy, electric energy and heat. The methods like bead milling, high pressure homogenization etc., can be categorized under shear-force based cell disruption. The wave-energy based cell disruption techniques include ultra-sonication, microwaves and pulsed electric-field treatment (Günerken et al., 2015).

The non-mechanical cell disruption methods include chemical and biological techniques. In the former, chemicals like antibiotics, ionic liquids, special nanoparticles, chelating agents, chaotropes, detergents, solvents, supercritical liquids, hypochlorites, acids and alkali are used (Parmar et al., 2011).

The use of ultra-sonication, microwaves and supercritical transesterification methods are very efficient in extracting lipids from algal biomass, but they cannot be used for large-scale applications due to their very high energy demands (Hidalgo et al., 2013). Hence, low-cost chemical methods are used for large-scale conversion of algal biomass to biodiesel. Most commonly used methods are conventional lipid extraction followed by transesterification or direct transesterification. Both the methods were developed for mainly biodiesel production from lipids, however the by-products crude glycerol and residual algal biomass may be used for other applications like fermentation, biogas production, etc.

In the conventional method, firstly the lipids are extracted by lysing the cell wall chemically followed by solvent extraction of lipids. In algal lipid research, Bligh and Dyer method was reported as most applicable method for any kind of microalgal strain (Bligh & Dyer, 1959; Hidalgo et al., 2013). Subsequent to the lipid extraction, the lipids are

transesterified at higher temperatures using methanol or ethanol as acyl acceptors in the presence acid or base or heterogeneous catalysts (discussed in section 2.2.2). In direct transesterification, both the lipid extraction as well as transesterification are carried out in a single-step by using a single solvent that can acts as both lipid extracting solvent and acyl acceptor for transesterification in the presence of catalyst only (Hidalgo et al., 2013; Kumar et al., 2014). The direct transesterification decreases the downstream cost as well as cut down the time scales as compared to the conventional one. The direct transesterification process is carried out using methanol and acid/base catalysts (e.g., H_2SO_4, NaOH). Hence, the use of direct transesterification method is imperative for large-scale production of biodiesel from oleaginous microalgae.

CHAPTER 3

Materials and methods

3.1 Experimental microalgae species

An indigenous microalgae species, *Chlorella* sp. FC2 IITG (hereafter referred as FC2) was isolated from local fresh water ponds inside the campus of Indian Institute of Technology (IIT) Guwahati, Assam, India (Muthuraj et al., 2014). It has already been characterized as a novel biodiesel candidate in the previous works (Kumar et al., 2014; Muthuraj et al., 2015; Muthuraj et al., 2014). This lipid rich microalgae species is capable of producing 65 – 85 % fatty acids (up to 56% w/w in stirred tank reactor), contributing palmitic acid (C16:0), oleic acid (C18:1) and linoleic acid (C18:2), which are key elements of good quality biodiesel based on ASTM and EN standards (Table 2.2). The microscopic image of the model organism taken in an inverted microscope (specifications: appendices, Table A2) is shown below (Fig. 3.1).

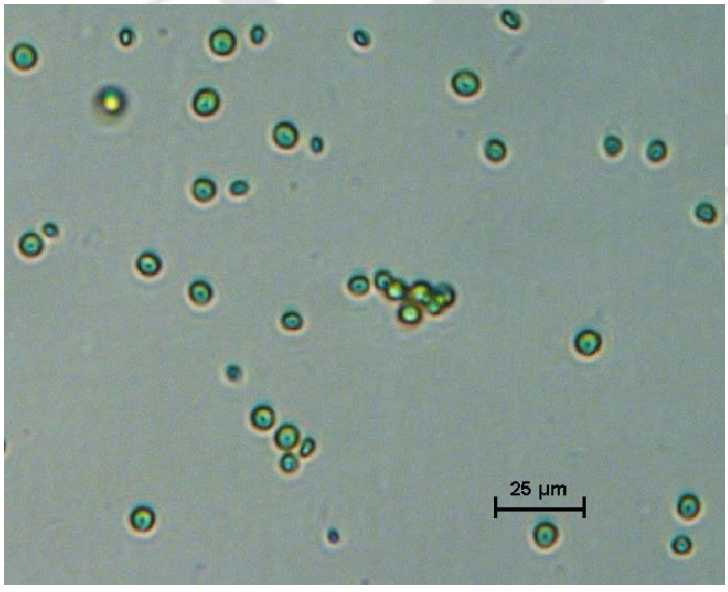

Fig. 3.1. Microscopic image of *Chlorella* sp. FC2 IITG.

3.2 Culture medium and maintenance

In all experiments, the experimental strain was cultured in sterile BG11 medium that was previously modified and optimized for FC2 growth in shake-flask conditions (Muthuraj et al., 2015). The composition of the growth medium is shown in Table 3.1. The initial pH of the medium was set at 7.1 ± 0.1. The inoculum preparation for all the experimental studies was carried out using perforated tubing equipped reagent bottle (Fig. 3.2) by providing 800 µmol m^{-2} s^{-1} of constant LED lighting and 1% CO_2 (in air). However, low light of 100 µmol m^{-2} s^{-1} and air (0.035% CO_2) were used in the preliminary studies for evaluating the performance of newly designed PBRs (see chapter 4 later).

Table. 3.1 Composition of FC2 growth medium for all the experiments

Media component	**Composition (g L^{-1})**
Urea	1.8
K_2HPO_4	0.076
$MgSO_4.7H_2O$	0.075
$CaCl_2.2H_2O$	0.036
Na_2CO_3	0.02
Citric acid	0.006
Ferric ammonium citrate	0.006
Na_2EDTA	0.001
A5+Co solution	1 ml L^{-1}

Component	***Concentration (g L^{-1})***
H_3BO_3	2.86
$MnCl_2.H_2O$	1.81
$ZnSO_4.7H_2O$	0.222
$CuSO_4.5H_2O$	0.079
$Na_2MoO_4.2H_2O$	0.390
$Co(NO_3)_2.6H_2O$	0.049

*pH was adjusted to 7.1±0.1 after sterilization.

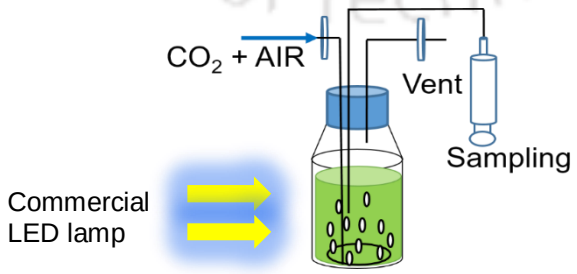

Fig. 3.2 Perforated tubing equipped transparent bottle for inoculum preparation

3.3 Description of light sources used for microalgae growth

3.3.1 Conditions for indoor studies

The experimental studies on algae conducted directly under sunlight cannot be analysed systematically due to uncontrollable variations in weather (short-term atmospheric fluctuations in sunlight intensity and temperatures) and climate (long-term weather conditions). For repeatability, experiments should be carried out under constant incident light intensities or mimicked sunlight to optimize other growth parameters like process pH, CO_2 feed etc. For these reasons, an artificial lighting system that can mimic sunlight irradiation was developed. Since most of the reported laboratory research have been carried out under cool fluorescent lamps (CFL) to understand the growth characteristics of microalgae, the CFL lighting system was applied to mimic natural lighting. However, their light intensity cannot be controlled by varying either input voltage or current to produce light intensity of "0 – 2000 – 0" µmol m^{-2} s^{-1}, such as to mimic the variation in sunlight intensity from dawn to dusk (Fig. 3.3).

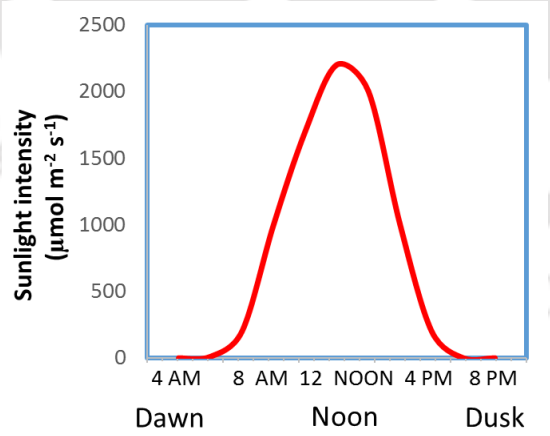

Fig. 3.3 Sunlight irradiation of typical clear daylight in natural sunlight conditions

In contrast to the CFL bulbs, light emitting diodes (LED) offer controllable light intensity with variations in input voltage. In this study, the variation of input voltage was controlled manually by DC regulated power supply and automatically by pulse width modulation (PWM) adapter (specifications: appendices, Table A2). Unlike other artificial light sources, the emission spectrum of cool white LEDs (specifications: appendices, Table A2) is close comparison to the sunlight's emission spectrum (Fig. 3.4). The LED lighting also offers lower working temperatures and high efficiency (80 – 100%) of photosynthetic active radiation (PAR) compared to the other artificial systems (Darko et al., 2014). Therefore, LEDs have recently emerged as most preferred artificial light sources conducting experiments in green houses or horticulture systems for plant as well as algae growth (Darko et al., 2014; Nwoba et al., 2019; Ouzounis et al., 2015).

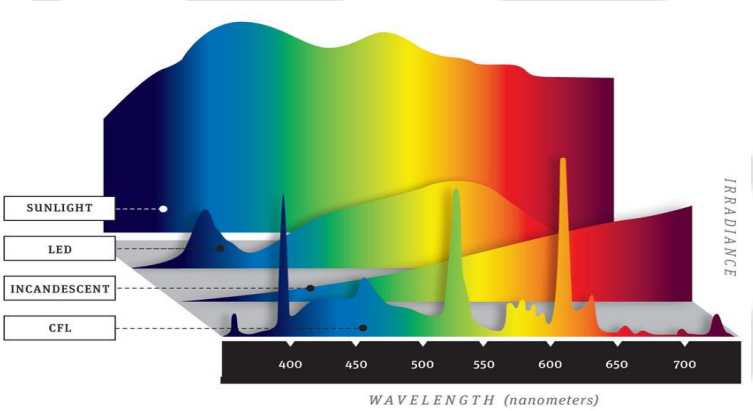

Fig. 3.4 Comparison of wavelength emission spectrum of various artificial light sources with sunlight emission spectrum. Source: (Ergil, 2014)

3.3.2 Conditions for outdoor studies

All the experimental studies in the outdoor conditions were performed under natural sunlight in the period of September 2018 to April 2019 at the geographical coordinates of 26° 10′ 20″ N and 91° 44′ 45″ E (Guwahati, Assam, India). The outdoor sunlight intensity was measured timely using a lux meter (specifications: appendices, Table A2).

3.4 Supplementation of CO_2

Carbon dioxide serves as carbon source for the photoautotrophic culturing of algae similar to the plants (see section, 2.4, chapter 2). However, high levels or pure CO_2 can inhibit the growth of algae (see section 2.5.3, chapter 2). Therefore, CO_2 level for algae broth culture was managed by mixing appropriate CO_2 from high pressure CO_2 cylinder with the continuous flow of compressed air. This mixing was achieved by manual or automatic (specifications: appendices, Table A2) flow meters of air and CO_2 according to the requirements. Using the setup shown in Fig. 3.5, mass flow controllers (MFC) for both and air and CO_2 injection were controlled by OPTO22 control system (below) for automation.

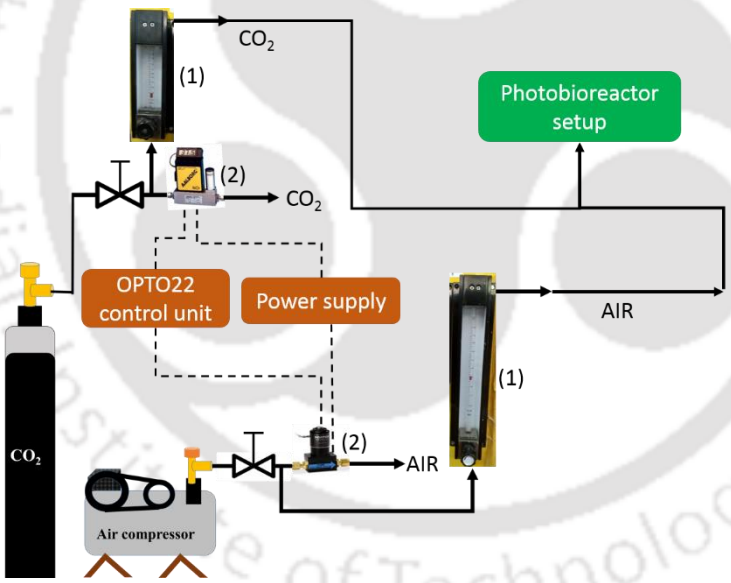

Fig. 3.5 Manual rotameters (1) and mass flow controllers (2) for air and CO_2 supplementation along with sources of air and CO_2.

3.5 Process control system

The process control unit (OPTO22 control system, USA, additional information given in appendices, Table A2) was additional sensor control system to the bioreactor or photobioreactor operation. It was used to control, monitor and gather data information related to various process parameters with simple input/output (I/O) modules driven by

current or voltage signals (analog). It was connected to the computer and ran with the PAC control basic software (version: 9.4) to collect the data and to control the process variables per experimental setup.

Basically the OPTO22 control consists of five parts, namely (Fig. 3.6): circuit board; power supply for circuit board; I/O modules; main controller, and; PAC software. The I/O modules receives and sends analog input and output signals respectively. In this study, 4 I/O modules (refer appendices, Table A2 for model specification) including '-20 to +20 mA, analog input', '-10 to +10 VDC, analog input', '+4 to +20 mA, analog output', and '0 to +10 VDC, analog output' were used with the control system. A computer with PAC software installed was connected to the main controller using Ethernet crossover cable. This computer was used for creating flow chart-based or OPTOscript-based commands that were executed by the main controller to accomplish the tasks (see schematic in Fig. 3.7).

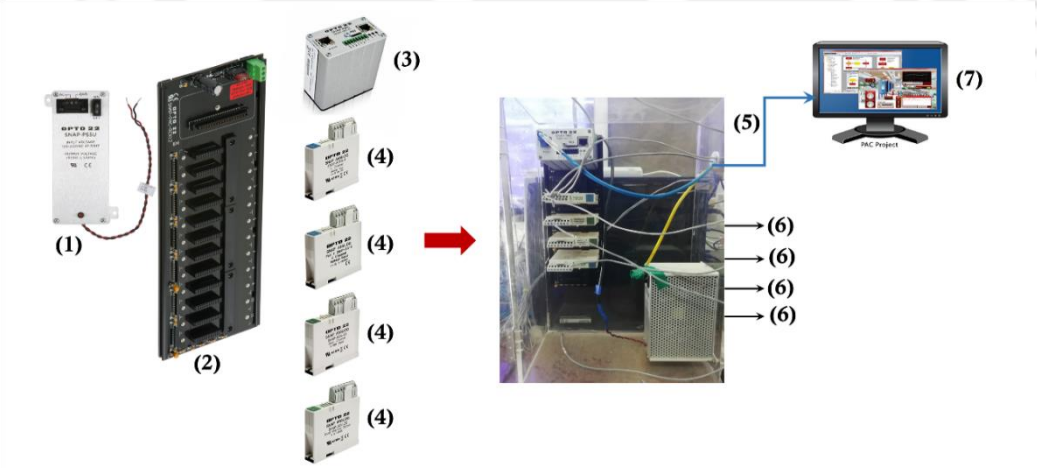

Fig. 3.6 Assembly of OPTO22 control system. Power supply to circuit board (1), circuit board (2), main controller (3), I/O modules (4), Ethernet crossover cable connection (5) and connections for input/output current or voltage (DC) signals.

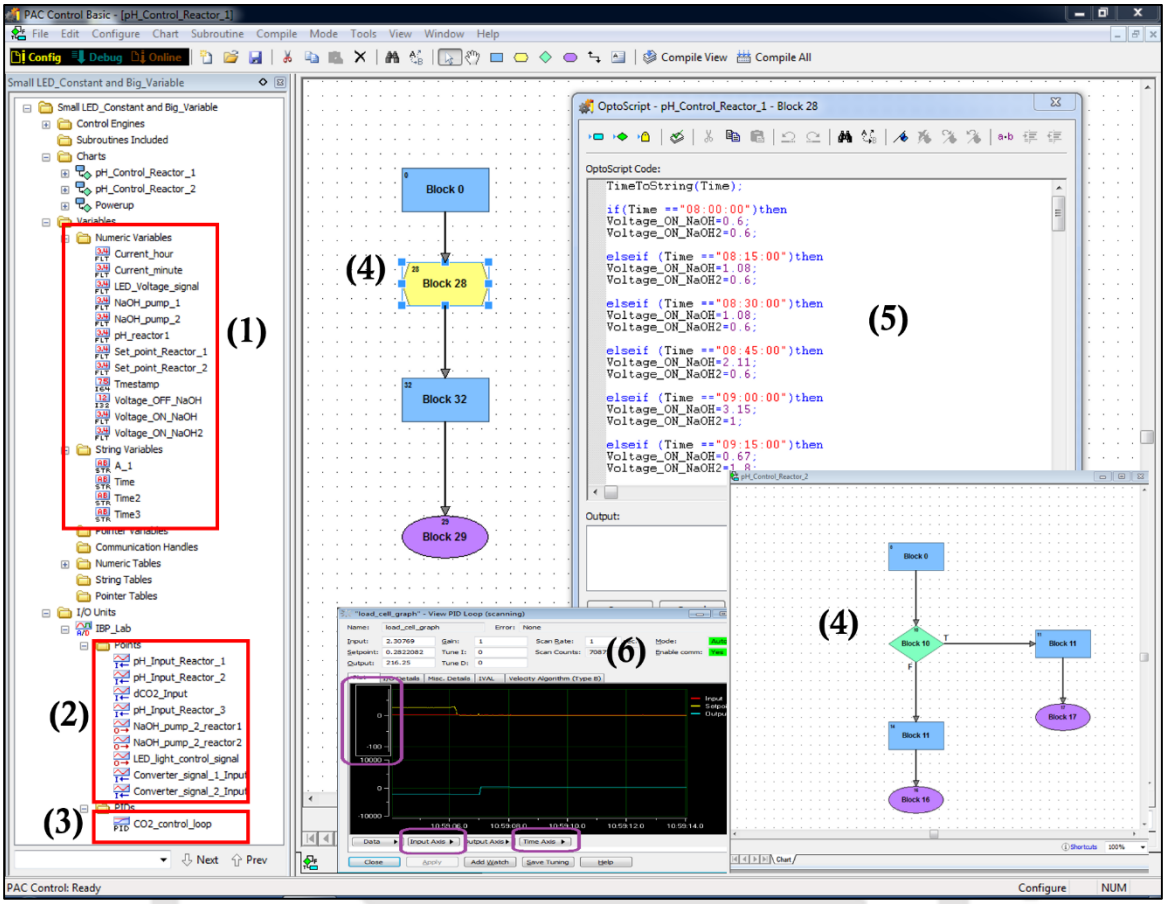

Fig. 3.7 An overview of PAC software (v9.4) implementation. User-defined variable area (1), variables generated from I/O modules (2), User-defined PID control loops area (3), flow chart based algorithms (4), OPTOscript based algorithms (5) and PID mechanism and results area (6).

3.6 Materials for bubble-column PBR and spargers

Flanged acrylic tubes (specifications: appendices, Table A2) (Fig. 3.8A) were used for the construction of three small-scale (500 ml) and medium-scale (10 L) bubble column photobioreactors for growing the FC2. The membrane sparging system in BC-PBRs was customized for the setup using a neoprene rubber sheet (Fig. 3.8B). Before the actual implementation, the performance of membrane-sparger was tested and compared with known spargers like L-sparger (Fig 3.8C) and perforated silicone tubing (Fig. 3.8D). The L-sparger component was cannibalized from the conventional bench-top fermenter/bioreactor (specifications: Appendices Table A2).

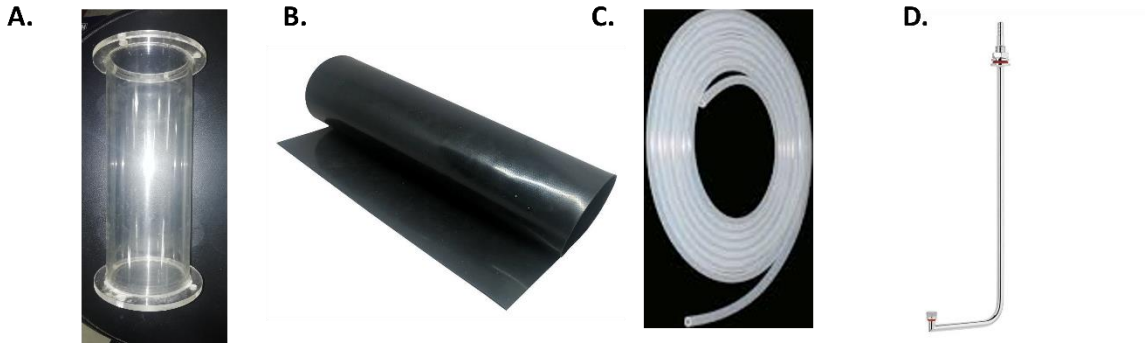

Fig 3.8 Materials used for design of BC-PBR and different spargers. A. Flanged acrylic tube, B. Neoprene rubber sheet, C. Silicone tubing, and D. L-sparger.

3.7 Measurement and control of dCO_2, DO, pH, and temperature

In the experimental setup for both the small-scale and medium-scale BC-PBRs, all the probes were inserted from the top of the PBRs. The meters/controllers (specifications: appendices, Table A2) for dCO_2, pH and temperature probes having 4 – 20 mA analog output signal were connected to '-20 to +20 mA, analog input' module of the control unit. Whereas the DO (see appendices, Table A2 for specifications) data was collected at set intervals offline. The respective probe assemblies as used are illustrated in Fig. 3.9. Occasionally, the control of dCO_2 concentration was executed by PID control loop such that the resulting output voltage signal was transferred to CO_2 mass flow controller via '0 to +10 VDC, analog output' module. Similarly, the pH of algal cultures was also controlled either by relay based (for acid/base control) or PID loop based (for CO_2 feed based control) using the same '0 to +10 VDC, analog output' module.

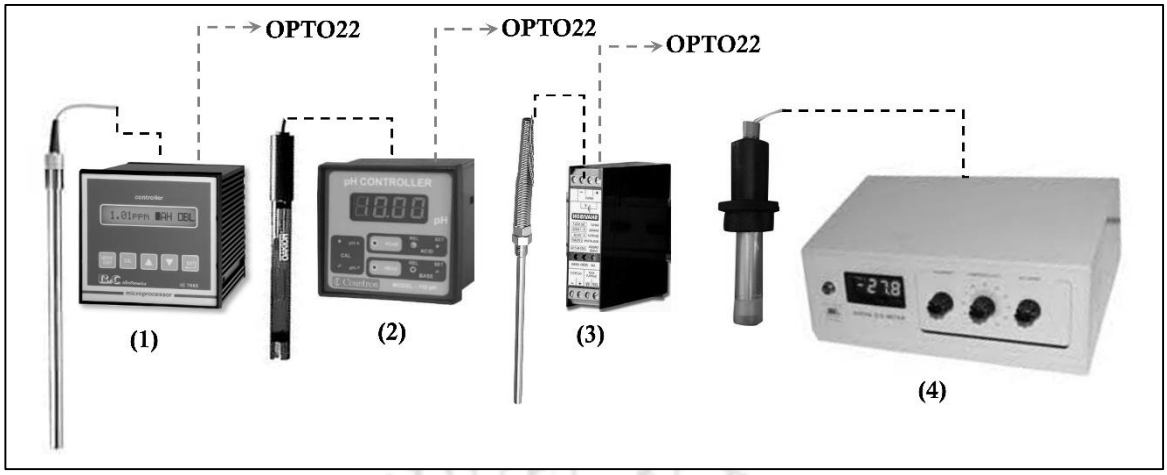

Fig. 3.9 Illustration of probe assemblies for measurement and control of various process parameters in algae cultures. The dCO_2 probe assembly (1), pH probe assembly (2), temperature probe assembly (3) and DO probe assembly (4).

3.8 Lipid induction strategy for biodiesel production from FC2 biomass

It is known that the starvation of nitrogen source and/or phosphate source of the growth medium triggers the induction of neutral lipids and thereby increasing the overall biodiesel production in starvation-phase rather than the growth phase (Kokabi et al., 2019; Li et al., 2010; Rodolfi et al., 2009). The experimental microalgae species, *Chlorella* sp. FC2 IITG has already been tested for its lipid induction capability with nitrogen starvation, e.g., urea deprivation (Muthuraj et al., 2015; Muthuraj et al., 2014). However, the previous studies were performed with two-stage lipid induction strategy for production of biodiesel from FC2. In this study, the lipid induction of FC2 biomass using urea starvation was investigated in two different processes, namely: single-stage and; two-stage lipid induction processes. In the two-stage process, the FC2 biomass was harvested after growth-phase via centrifugation at 3000 RPM for 5 min. Subsequently, the biomass harvested was washed with 0.9% NaCl and re-suspended in freshly prepared urea-free BG11 medium for inducing the lipids from nitrogen deprivation. In the single-stage process, the FC2 culture was allowed to consume all the urea to reach stationary-phase followed by the lipid-induction phase. This single-stage process was considered to be highly beneficial as it has potential to save time as well as removes the costly centrifugation operation.

3.9 Analytical procedures

3.9.1 Determination of biomass growth and biomass productivity

The cell biomass density of *Chlorella* sp. FC2 IITG was quantified by measuring the optical density (OD) at 690 nm in a visible spectrophotometer (specifications: appendices, Table A2). These absorbance values were converted into dry cell weight using the calibration equation derived from Fig. 3.10, one cell optical density = 0.4537 g dry cells L^{-1} (R^2 = 0.99). The calibration was performed with the FC2 biomass grown in modified BG11 medium under photoautotrophic conditions only.

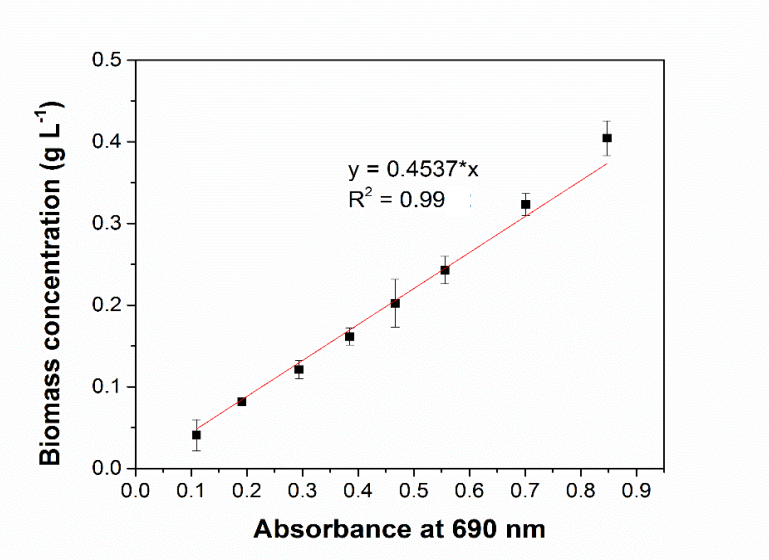

Fig. 3.10 Calibration curve for biomass estimation

The specific growth rate in day $^{-1}$ (every 24 h) and overall biomass productivity in g L^{-1} day^{-1} were calculated Eq. 3.1 and Eq. 3.2 respectively.

Specific growth rate, $\mu = (\ln X_2/X_1)/(t_2 - t_1)$ …….. (3.1)

Where, X_2 and X_1 are biomass concentration at time t_2 and t_1 respectively.

Biomass productivity, $P_B = \frac{X_{fg} - X_0\ (g\ L^{-1})}{t_{fg} - t_0\ (day)}$ …….. (3.2)

Where X_{fg} is final biomass titer at the end of growth phase at time, t_{fg} and X_0 is initial biomass concentration at time, t_0.

3.9.2 Determination of chlorophyll concentration

The level of photosynthetic activity was measured by quantification of chlorophyll 'a' (Chl-a) and chlorophyll 'b' (Chl-b) in methanol (Pruvost et al., 2011; Ritchie, 2006). Firstly, FC2 cell culture of 0.1 – 0.7 OD (A_{690}) was centrifuged at 13,500 RPM for 5 min in a 2 ml centrifuge tube and the supernatant collected for further analysis of major nutrient utilization, i.e., urea and phosphate. The pellet was extracted with 1.5 ml of 99.9% methanol by incubating in the dark at 45 ºC for 30 min followed by centrifugation at 13,500 RPM for 5 min. The absorbance spectra were measured at 652, 665 and 690 nm using the visible spectrophotometer. The following calculations (Eq. 3.3 and 3.4) were used to determine chlorophyll content (in mg L^{-1}).

$$[\text{Chl-a}]=16.5169*A_{665}-8.0962*A_{652} \quad \text{(3.3)}$$

$$[\text{Chl-b}]=27.4405*A_{652}-12.1688*A_{665} \quad \text{(3.4)}$$

Where A_{652} and A_{665} are the absorbance values at 652 and 665 nm respectively. For turbidity correction, A_{652} and A_{665} values were taken relative to the A_{690} value and represented as $*A_{652}$ and $*A_{665}$ respectively.

3.9.3 Quantification of extracellular urea concentration

The supernatants of appropriate culture samples after centrifugation were used to determine urea concentration. The concentration was estimated using diacetyl monoxime method using standard urea in double-distilled H_2O (Momose et al., 1965). Under strong acidic conditions, urea reacts with diacetyl monoxime to form a yellow condensed product, which is intensified to red colour in the presence of ferric ions and thiosemicarbazide. The colored product is measured spectrophotometrically at 540 nm and the absorbance values were converted into urea concentration from the following calibration curve (Fig. 3.11)

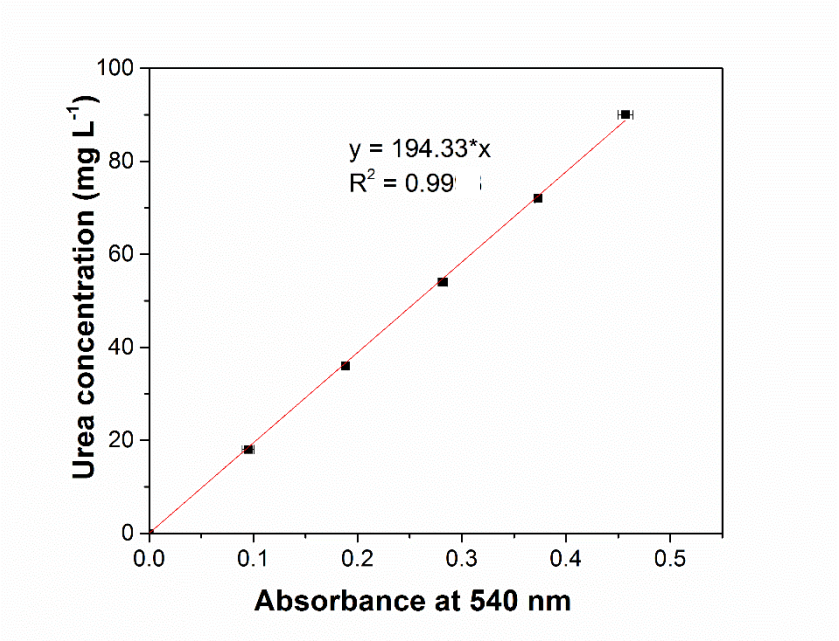

Fig. 3.11 Calibration curve for urea estimation

3.9.4 Quantification of extracellular phosphate concentration

The remaining supernatant after analysis of urea concentration was used for phosphate estimation by ascorbic acid method using K_2HPO_4 as standard (John, 1970). In the method, ammonium molybdate and antimony potassium tartarate in acidic medium react with phosphate to form heteropoly acid – phosphomolybdic acid, which is reduced to molybdenum blue colour in the presence of ascorbic acid. The intense blue colour can be quantified at 880 nm spectrophotometrically. Based on the derived equation in calibration curve (Fig. 3.12), the absorbance values at 880 nm were converted into respective phosphate concentration.

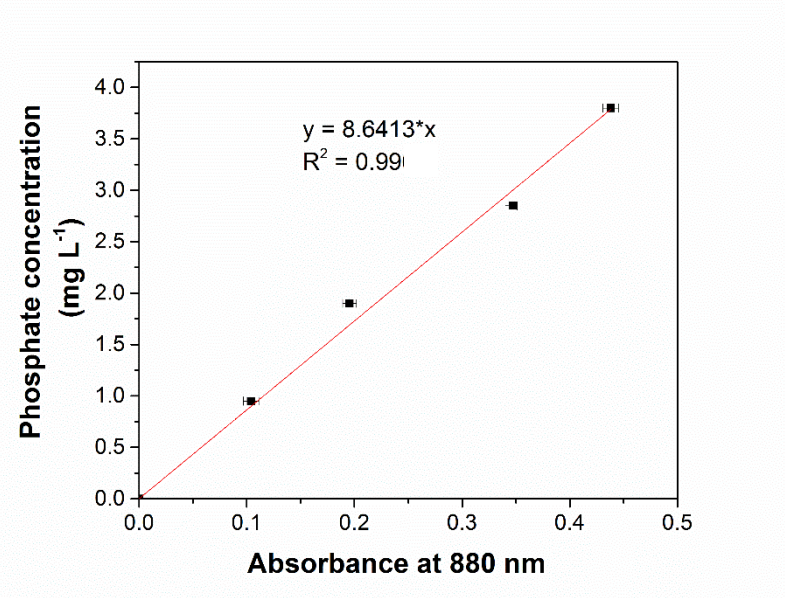

Fig. 3.12 Calibration curve for phosphate (K_2HPO_4) estimation

3.9.5 Direct transesterification of biomass for biodiesel production

The biodiesel from FC2 was characterized with respect to FAMEs. The lipids were extracted from 30 mg of biomass and converted to FAMEs via direct transesterification as described in previous studies (Kumar et al., 2014; Muthuraj et al., 2015). The FAMEs were analysed in CP-Sil 8 CB column (specifications: appendices, Table A2) by gas chromatography with FID detector (specifications: appendices, Table A2). Supelco® 37 component FAME mix (Sigma Aldrich chemicals) was used as standard for the analyses. A volume of 1 µl sample was injected into the GC while injector temperature was maintained at 250 °C. Helium was used as a carrier gas by keeping a splitting ratio of 20:1. Temperature of the column was programmed as 60 °C (hold time, 5 min) followed by a ramping rate of 5 °C min^{-1} until 280 °C (hold time, 15 min). The total FAME productivity at the end of induction-phase of each experimental study was calculated using Eq. 3.5

FAME productivity, $P_{FAME} = \frac{FAME_f - FAME_i}{t_{fi} - t_{fg}}$ ..... (3.5)

Where $FAME_f$ is the maximum FAME concentration and $FAME_i$ is the FAME concentration at start of induction phase. The t_{fi} is time taken to achieve maximum FAME concentration and t_{fg} is the time of start of induction phase, which is same as the end of growth phase.

3.9.6 Biodiesel characterization

The quality of produced biodiesel was characterized using the factors namely: saponification value (SV); iodine value (IV); cetane number (CN); degree of unsaturation (DU); higher heating value (HHV); kinematic viscosity (ν); density (ρ) ; flash point (FP); cloud point (CP); pour point (PP); and cold filter plugging point (CFPP). These were calculated using equations (3.6) to (3.16) (Francisco et al., 2010; Gülüm & Bilgin, 2017; Mandotra et al., 2016; Saxena et al., 2013). A sample calculation procedure is given in additional information (refer section 1 and Table A1, appendices).

$$SV = \sum[(560 \times F_i) / M_i] \quad \text{(3.6)}$$

Where 'F_i' and 'M_i' are percentage and molecular weight of individual FAME respectively. SV is in mg KOH (g oil)$^{-1}$

$$IV = \sum[(254 \times F_i \times D_i) / M_i] \quad \text{(3.7)}$$

Where 'D_i' is number of double bonds in individual FAME. IV is in g I_2 (100 g oil)$^{-1}$

$$CN = \left(46.3 + \frac{5458}{SV}\right) - (0.225 \times IV) \quad \text{(3.8)}$$

$$DU = MUFA + (2 \times PUFA) \quad \text{(3.9)}$$

Where '*MUFA*' is monounsaturated FAME (% of Wt.), and '*PUFA*' is polyunsaturated FAME (% of Wt.).

$$HHV = \sum[(F_i \times \delta_i)/100 \quad \text{..... (3.10)}$$

Where '*HHV*' is in MJ kg^{-1} and $\delta_i = 46.19 - \frac{1794}{M_i} - 0.21 \times D_i$

$$\nu = e^{\sum[F_i \times \ln(\nu_i)]/100} \quad \text{..... (3.11)}$$

Where 'ν' is in mm^2 s^{-1} and $\ln(\nu_i) = -12.503 - 0.178 * D_i + 2.496 \times \ln(M_i)$

$$\rho = \sum[(\rho_i \times F_i)/100] \quad \text{..... (3.12)}$$

Where 'ρ' is g cm^{-3} and $\rho_i = 0.8463 + \frac{4.9}{M_i} + 0.0118 \times D_i$

$$FP = 23.362 \times \sum[(N_i \times F_i)/100] + 4.854 \times \sum[(D_i \times F_i)/100] \quad \text{..... (3.13)}$$

Where N_i is number of carbon atoms in individual FAME.

$$CP = (0.526 \times F_{C16:0}) - 4.992 \quad \text{..... (3.14)}$$

$$PP = (0.571 \times F_{C16:0}) - 12.24 \quad \text{..... (3.15)}$$

$$CFPP = (0.511 \times F_{C16:0}) - 7.823 \quad \text{..... (3.16)}$$

CHAPTER 4

Design and construction of unidirectional LED lighting and bubble column photobioreactor (BC-PBR) with efficient sparging system

4.1 Background and uniqueness of the study

On the basis of photosynthetic efficiency in outdoor sunlight conditions, the vertical tubular PBRs were proved to be more productive (per land area) than other large-scale PBRs. On the other hand, column PBRs like bubble columns and airlift systems were highly efficient but mostly limited to laboratory studies due to cost and scalability issues. Therefore, the scope of incorporating bubble column or airlift technologies into vertical PBRs is very beneficial for a feasible microalgal biodiesel production. However, they require a cost-effective and highly efficient mass transfer component, i.e., sparging system. Conventional spargers in stirred-tank bioreactors are efficient enough only when the agitators/impellers are running. Those spargers usually produce big air bubbles and later they break up into smaller bubbles due to contact with the impeller blades. Moreover, baffles provided in the stirred tank reactors also helps in better mixing and bubble break-up. However, the biggest issue in stirred-tank reactor is energy/electricity consumption for the mechanically driven agitation. Therefore, the large-scale cultivation of microalgae using stirred tank bioreactor is not economically feasible due high energy inputs requirement. Moreover, the mechanical agitation created by the impeller blades can cause shear stress to the growing algae cells thereby cell death occurs.

As alternative to the stirred tanks, airlift and bubble columns have been developed for enhanced mixing and efficient mass transfer without the requirement for mechanical

agitation (Miron et al., 2000; Miron et al., 2004). In both kinds of technologies, air bubbles are introduced from the bottom side of the reactor via special spargers (e.g., ring type, ceramic type, perforated tubing, etc.). The bubble force acts as a driving force for the mixing and agitation in these airlift and bubble-column reactors. For airlift type of PBR, the installation of draft tube is more challenging due to diameter limitation and longer lengths required for scale-up of the reactor design. Therefore, bubble-columns are more suitable for their efficient non-mechanical mixing, saving on agitation cost, and ease of scale-up. In this study, a low-cost, scalable, and efficient bubble-column photobioreactor (BC-PBR) was customized with membrane-sparger equipped at the bottom of the reactor. The designed membrane-sparger was compared with well-known L-sparger of conventional stirred-tank bioreactor and perforated tubing for its mass transfer efficiency and FC2 growth performance. In line with design of PBR, a special unidirectional LED system was customized in the laboratory to supply light energy to the microalgae grown in the designed PBR.

4.2 Construction of PBR and lighting system

4.2.1 Setup for bubble column photobioreactors

Two scales of bubble column photobioreactors (BC-PBR), i.e., 500 ml and 10 L for small-scale and medium-scale studies respectively, were constructed by using transparent flanged acrylic tubes (Fig. 4.1). For both the scales, same path length of 0.075 m was maintained (i.e., inner diameter = 0.069 m and outer diameter = 0.075 m). And the heights of small-scale and medium-scale BC-PBRs are 0.175 m and 2.75 m respectively. The closures of top and bottom of the PBRs were also made of acrylic lids that were fastened with wing nuts by placing the rubber sheet-made gaskets (ensures no-air-leak). On the top lid of the reactor, appropriate holes were drilled for installation of analytic probes (i.e., DO, dCO_2, pH, and temperature) and an air vent.

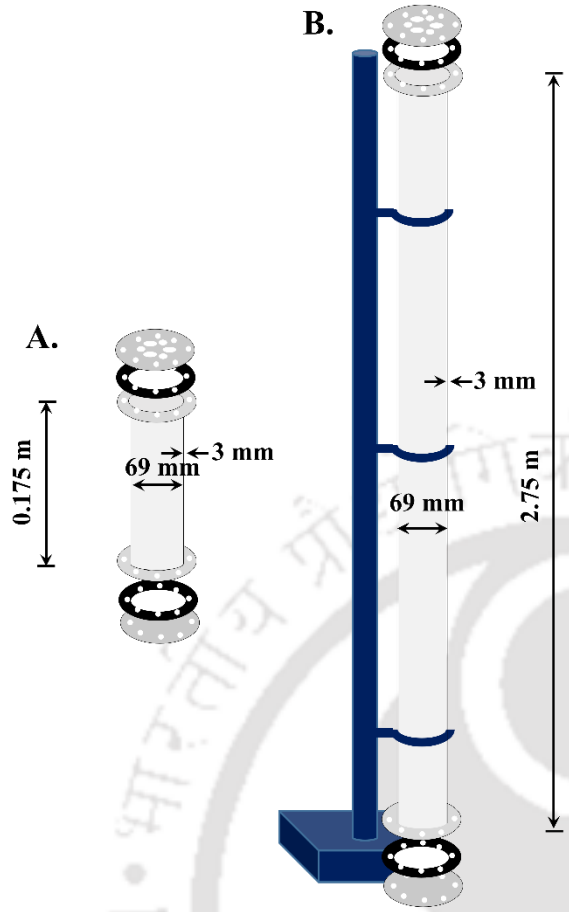

Fig. 4.1 Schematic of a bubble column photobioreactor setups showing dimensions for small-scale (500 ml) (A) and medium-scale (10 L) (B).

4.2.2 Construction of LED lighting to simulate sunlight conditions for indoor experiments

In this study, two unidirectional LED lighting systems were customized by using 50 W cool white LED cobs). These LED cobs had colour temperature of 6500 K equivalent to the clear daylight of an outdoor sunny day. As these LED cobs could generate high levels of heat while lights up, CPU fans (generally found in desktop computer setup) were installed as heat sink on the backside of LED cobs. For both the scales of BC-PBRs, a smaller and larger LED lighting systems were personalized in the laboratory. The smaller LED lighting system could simultaneously accommodate three small-scale BC-PBRs, such that three parallel experimental studies could be performed. It had 6 fans (3 columns) accommodated with 9 LEDs. The larger LED nest was constructed by arranging 32 fans

and 63 LEDs in a single column, 2.75 m height of medium-scale BC-PBR. For experiments requiring constant light intensity, the lighting systems were powered by constant DC voltage regulated power supply. For simulation of sunlight under indoor conditions, the lighting systems were controlled by using pulse width modulation (PWM) controller connected through OPTO22 control unit, the setup is outlined in Fig. 4.2.

Using the setup in Fig. 4.2, an algorithm was written in OPTOscript coding language to affect a variable voltage output signal to the input of pulse width modulation (PWM) controller, for regulation of the LED light intensity. The light intensity of LED was manipulated to increase or decrease the light intensity in a step-wise manner, thereby simulating sunlight variations for the laboratory (indoor) environment. For all experiments under simulated sunlight, the same diurnal lighting was followed, i.e., based on the sunlight intensity data taken on a typical clear day in May 2017 (Guwahati region, India; 26° 10′ 20″ N and 91° 44′ 45″ E).

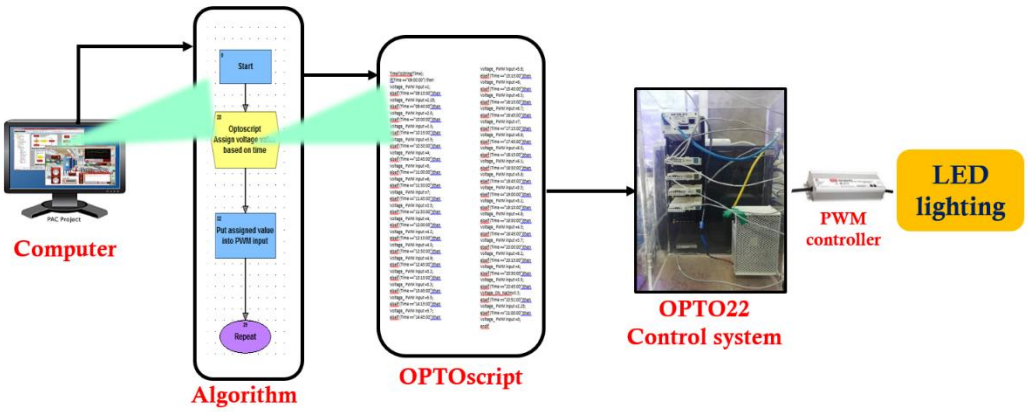

Fig. 4.2 Schematic of experimental setup used to simulate typical sunlight conditions with LED lighting.

4.2.3 Design of membrane-sparger

A flexible neoprene rubber sheet having 2 – 3 mm of thickness was used to customize the low-cost membrane sparger (see section 3.6). The flexible sheet was perforated using 0.5 mm needle maintaining 10 mm spacing between the holes. The

designed membrane-sparger was installed at the bottom of flanged acrylic tube and tightened with wing nuts along with the gaskets made of same rubber sheet (Fig. 4.3). Conversely, the well-known L-sparger and perforated tubing sparger were installed by inserting from the top of PBR. The L-sparger was obtained from commercial bench-top bioreactor (specifications: appendix) and the perforated tubing was made of silicone rubber tubing (commonly used for peristaltic pumps). The porosity of silicone tubing (Himedia Laboratories, India) was also generated similar to the membrane sparger. .

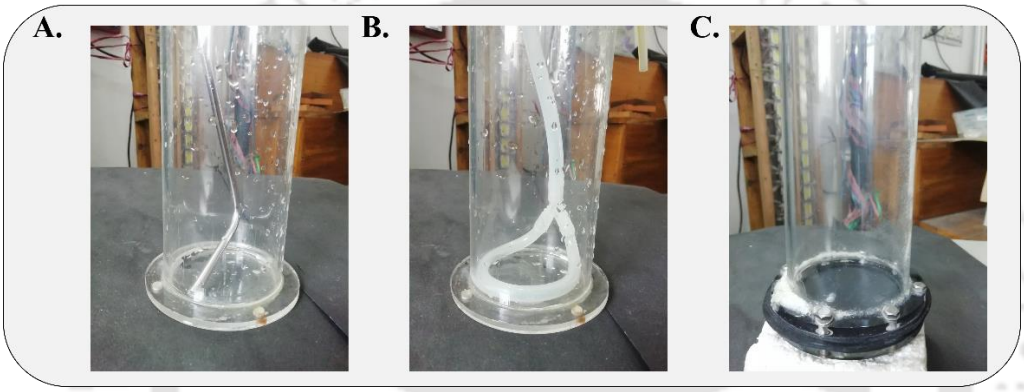

Fig. 4.3 Small-scale BC-PBRs with different spargers. A. Conventional L-sparger, B. Perforated tubing, and C. Membrane sparger.

4.3 Experimental studies

4.3.1 Estimation of volumetric CO_2 mass transfer coefficient for spargers

Prior to the estimation of volumetric CO_2 mass transfer coefficient ($K_L\, a_{,CO_2}$), the probe time constant (τ_p) of dCO_2 probe was calculated by considering the transportation of CO_2 from bulk liquid to membrane of probe as a first-order process (described in following equations) (Geankoplis, 2003; Philichi & Stenstrom, 1989).

$$\frac{dC_p}{dt} = k_p * \left(C_L - C_p\right) \qquad \ldots\ldots\ldots\ldots\ldots\ldots\ldots\ldots\ldots\ldots\ldots\ldots \qquad (4.1)$$

Where C_p is measured dCO_2 concentration by probe at any time t, C_L is actual dCO_2 concentration in bulk liquid and k_p is inverse of the probe time constant (τ_p).

To measureτ_p, two equilibrium dCO_2 concentrations of 92.52 mg L^{-1} (lower) and 294 mg L^{-1} (higher) were saturated in two different small-scale BC-PBRs that filled with equal amounts of distilled water (500 ml). The desired variation of dCO_2 concentrations were maintained by increasing percentage of CO_2 in air, supplied by sparging CO_2 enriched air (1 bar pressure)- at aeration rate of 1 VVM for 30 min. After reaching the saturation, the CO_2 enriched air supply was stopped and the system was kept completely closed without any headspace to ensure the zero transportation rate of CO_2 from liquid to gas phase (headspace). The dCO_2 probe was firstly placed in the reactor with lower saturation value, 92.52 mg L^{-1} followed by shifting the probe into reactor with higher saturation value immediately for a step-change. In this whole procedure, the dynamic change in the probe measured values, C_p were recorded and stored in the computer.

Upon solving the Eq. 4.1, following linear equation was resulted.

$$\ln\frac{(C_L - C_{po})}{(C_L - C_p)} = k_p * t \qquad \text{(4.2)}$$

Where C_{po} is measured dCO_2 concentration by probe at $t = 0$. After plotting the Eq. 4.2 in Microsoft excel, the slope was used for determination of probe time constant.

For $K_L\, a_{,CO_2}$ estimation, the well-known simple dynamic method was used with following assumptions: the change in CO_2 concentration of gas phase is negligible; the gas holdup in the reactor does not change with time; the concentrations of CO_2 are in equilibrium at the gas-liquid interface; the liquid is well mixed; and there are no algae cells in the liquid phase. Based on these assumptions, mass balances, and convective mass transfer theories, the rate of change of CO_2 concentration at any time can be written as follows.

$$\frac{dC_L}{dt} = (K_L a_{,CO_2}) * (C_L^* - C_L) \quad \ldots\ldots\ldots\ldots\ldots\ldots\ldots\ldots\ldots\ldots\ldots\ldots\ldots\ldots\ldots\ldots \quad (4.3)$$

After substituting the integrated form of Eq. 4.3 in Eq. 4.1, Eq. 4.1 was solved with initial and final conditions of C_p as C_{po} and C_L^* respectively. The solution was resulted as follows.

$$C_p = (C_L^*) * \left\{\frac{K_L a_{,CO_2} * e^{-k_p * t}}{k_p - K_L a_{CO_2}} - \frac{k_p * e^{-K_L a_{,CO_2} * t}}{k_p - K_L a_{,CO_2}}\right\}$$

$$-(C_{po}) * \left\{\frac{K_L a_{,CO_2} * e^{-k_p * t}}{k_p - K_L a_{,CO_2}} - \frac{k_p * e^{-K_L a_{,CO_2} * t}}{k_p - K_L a_{,CO_2}}\right\} \quad \ldots\ldots\ldots\ldots\ldots\ldots\ldots\ldots\ldots\ldots\ldots\ldots\ldots\ldots\ldots\ldots (4.4)$$

The experimental setup for the estimation of $K_L\, a_{,CO_2}$ was consisting of a small-scale BC-PBR saturated with an equilibrium dCO_2 concentration of 60 ± 5 mg L^{-1} sparged at 1 VVM of aeration rate. To satisfy the assumptions, water was used as a liquid phase without algal cells. Initially, the probe was maintained in lower CO_2 concentration that has already been saturated. Followed by that, the CO_2flow rate was increased to attain a significantly higher CO_2 concentration in the PBR immediately for a step change. The measured values by the probe (C_p) were stored in the computer for every second interval to evaluate $K_L\, a_{,CO_2}$ of all the three spargers (Fig. 4.3) installed in the small-scale BC-PBRs.

4.3.2 Evaluation of *Chlorella* sp. FC2 IITG growth performance using membrane sparger and perforated tubing

To compare the performance of membrane sparger with perforated tubing, FC2 was grown at a constant light intensity of 120 µmol m^{-2} s^{-1} in small-scale BC-PBRs using atmospheric air (0.035% CO_2) as carbon source. As the bubbling of L-sparger was not comparable with the membrane-sparger and perforated tubing, L-sparger was not used in this study. By keeping the initial biomass density (inoculum density) as 0.03 g L^{-1}, the culture was grown in batch up to 5 days for ensuring no limitation of nutrients thereafter.

4.3.3 Investigation of pumping effect on FC2 growth for prospective recirculation

Photoinhibition in algal cultures during the high light conditions (noon times in outdoor sunlight) is a very common problem that have been faced by many algae researchers since the beginning of algae bioresource exploitation. In order to minimize photoinhibition, average light exposure per individual cell should not exceed the saturating light intensity, beyond which photoinhibition occurs in the algae cultures (Li et al., 2009; Sforza et al., 2012). Hence, recirculation of algal cells from an external dark chamber to the illumination area of the PBR could be one of the effective solutions to control photoinhibition. By tuning the speed of recirculation, the frequency of light exposure per individual cell can be decreased. It all needs a perfectly optimized 'pumping speed' to recirculate the algae cultures between dark chamber and illumination surface area of the PBRs. Moreover, the recirculation of cells offers better mixing and aids in performing continuous reactor operation along with the increase of total culture volumes beyond the capacity of the PBRs. Thus a peristaltic pump and a centrifugal pump have been used to investigate the effect of pumping against *Chlorella* sp. FC2 IITG growth. An additional experiment 'without pumping' was also carried out as control study. All the three studies were performed at light intensity of 700 µmol m^{-2} s^{-1} with atmospheric CO_2 (air) as carbon source. The initial biomass density was kept at 0.15 g L^{-1} of biomass concentration.

4.4 Results and discussion

4.4.1 LED lighting for indoor studies

Two types (smaller and larger) of unidirectional LED lighting systems having LED cobs coupled with CPU fans are shown in Fig. 4.4. The resulting light intensity outputs from the light systems were satisfied with the expected range of 0 – 2000 µmol m^{-2} s^{-1} for conducting experiments in the indoor environment. Using the DC-regulated power supply and

computer-controlled PWM technology, the lighting systems could able to generate constant (Fig. 4.5A) and diurnal (Fig. 4.5B) patterns of light intensity respectively, similar to typical clear daylight.

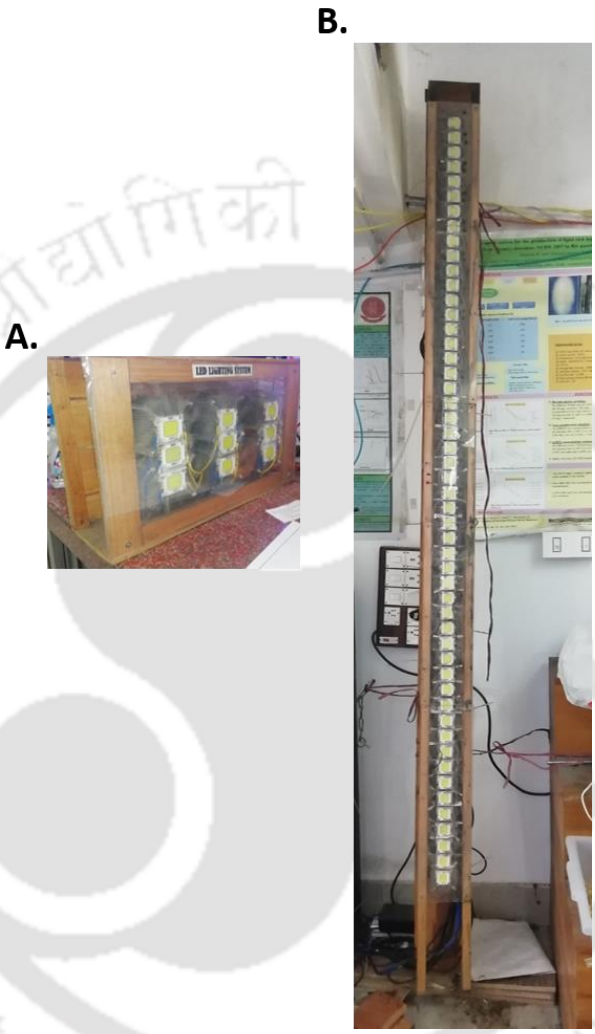

Fig. 4.4 Unidirectional LED lighting systems. A. For small-scale BC-PBRs and B. For medium-scale BC-PBR

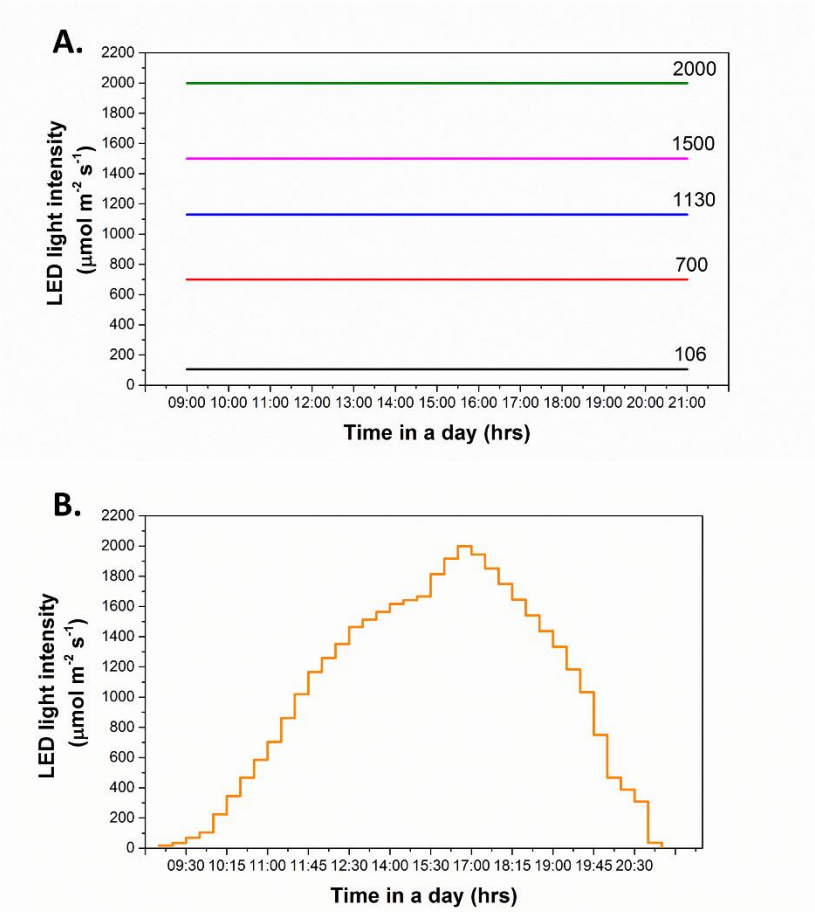

Fig. 4.5 Patterns of light intensities generated by unidirectional LED lighting systems. A. Constant light and B. Diurnal light

4.4.2 Determination of volumetric CO_2 mass transfer coefficients for perforated tubing, membrane sparger and conventional L-sparger

The dCO_2 probe time constant was evaluated as 38 s (τ_p) from the plot of Eq. 2 (Fig. 4.6A). Using the τ_p value and recorded online measured dCO_2 concentrations from $K_L\, a_{,CO_2}$ experiment, Eq. 4.4 was solved by nonlinear regression to estimate the $K_L\, a_{,CO_2}$ values of membrane sparger and the other known spargers. Same BC-PBR (small-scale) with interchange of each sparger was used for the entire procedure of estimation. Based on the $K_L\, a_{,CO_2}$ values, the mass transfer efficiency of membrane sparger was found superior than the perforated tubing and conventional L-sparger. The time required to reach the higher equilibrium saturation value for membrane-sparger, perforated tubing, and L-sparger were 250 s, 450 s, and 1200 s respectively (Fig. 4.6B, 4.6C, and 4.6D). It should

be noted that the results were evaluated without mechanical agitation. Also, it has been clearly observed that the bubble size produced by the perforated tubing were smaller than the L-sparger resulting the higher $K_L\, a_{,CO_2}$ value due to improper mixing in case of L-sparger. However, the bubbles generated by membrane-sparger were much smaller and the mass transfer efficiency was greater than the perforated tubing. The $K_L\, a_{,CO_2}$ value of membrane sparger was observed to be 4.1 and 1.3 times to the conventional L-sparger and perforated tubing, respectively (Table 4.1).

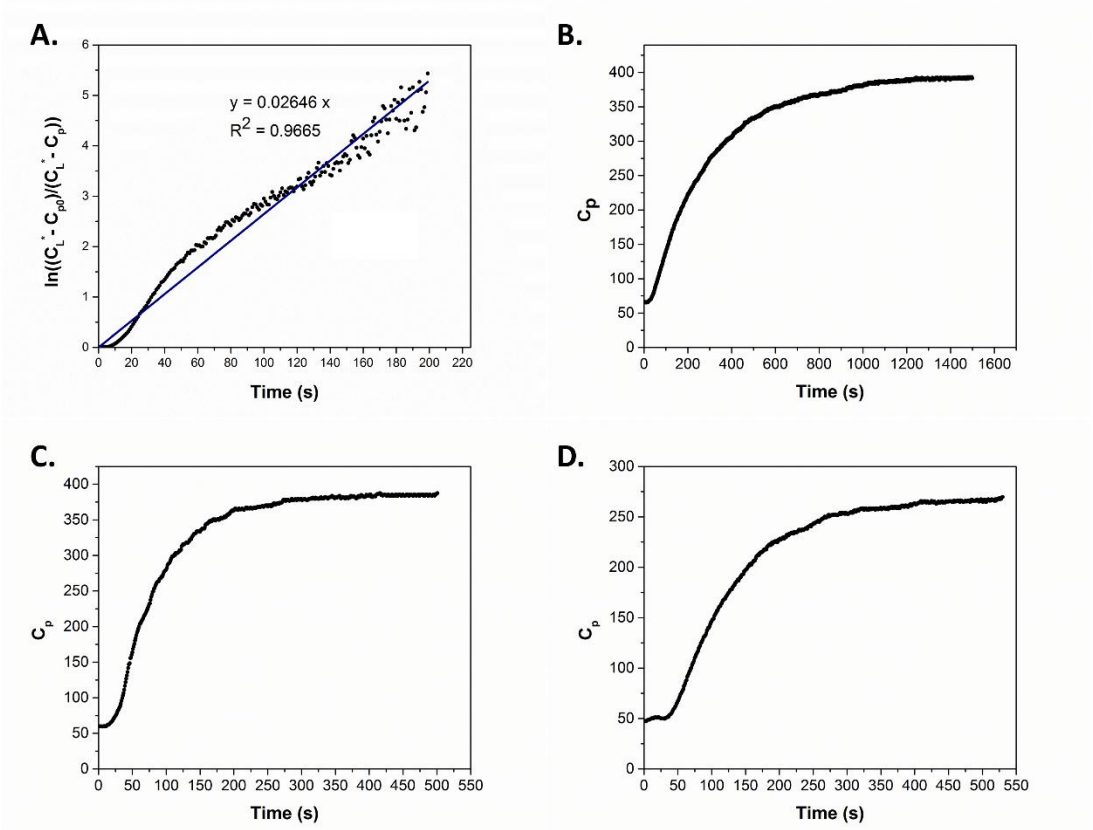

Fig. 4.6 Representation of measured dCO_2 concentration by dCO_2 probe (C_p) for A. calculation of dCO_2 probe time constant (τ_p) by plotting Eq. 4.2 and estimation of volumetric CO_2 mass transfer coefficients ($K_L\, a_{,CO_2}$) for B. L-sparger, C. membrane-sparger, and D. perforated silicone tubing.

Table 4.1 Comparison of CO_2 gas-liquid mass transfer coefficients of various spargers

Type of sparger	$K_L\, a_{,CO_2}$ **(s^{-1})**
Conventional	0.0042±0.0004
Perforated tubing	0.0135±0.003
Membrane	0.0174±0.006

4.4.3 Comparison of membrane-sparger and perforated tubing for FC2 growth

As the membrane sparger and perforated tubing were exhibited near $K_L\, a_{,CO_2}$ values, the performance of both spargers were compared by investigating the growth of microalgae. In this experimental study, the small-scale BC-PBRs were installed with membrane-sparger and perforated tubing to grow FC2 at specific conditions described in section 4.3.2. Interestingly, theFC2 was grown up to biomass density of 0.8 g L^{-1} with similar growth rates for5 days of culturing in both the cases of spargers (Fig. 4.7). However, the BC-PBR with perforated tubing was exhibited more cell-settling than PBR with membrane-sparger. This was confirmed while the sampling for biomass estimation was carried out by rigorous mixing of culture with the 10 ml pipette that was not performed in case of PBR with membrane-sparger. The cell-settling in the case of perforated tubing can be attributed to the absence of gas sparging in the overall cross-sectional area at the bottom of reactor. This can lead to more settling in case of medium-scale BC-PBR as it adds additional pressure due to up-scaling the height. Moreover, the length of insertion tubing for perforated tubing sparger increases with height of the PBR and it adds to higher capital costs than the membrane sparger. Nevertheless, the membrane sparger designed for small-scale BC-PBR can be directly applied to medium-scale BC-PBR without any modifications due to same cross sectional area of both scales, saving the cost of scale-up. Based on the cost-effectiveness and easy scale-up, the membrane-sparger was selected and used for final construction of both small and medium-scale BC-PBRs.

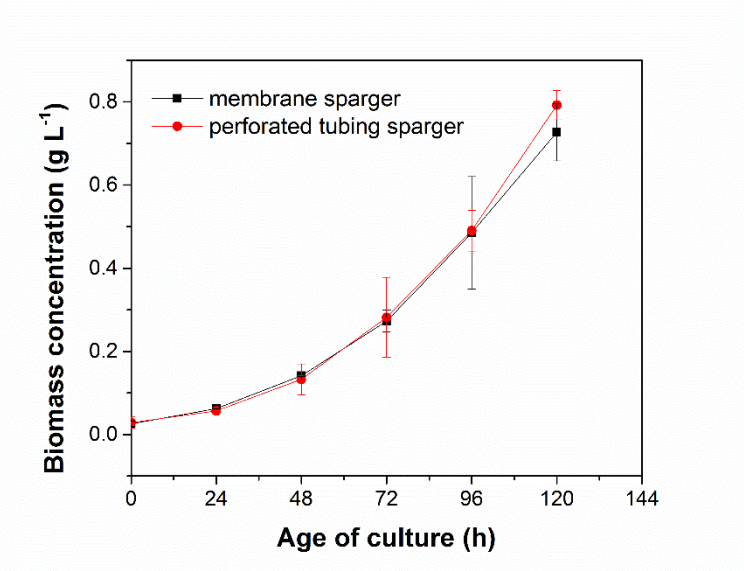

Fig. 4.7 Comparison of *Chlorella* sp. FC2 IITG growth in BC-PBRs equipped with membrane-sparger (square) and perforated tubing (circle).

4.4.4 BC-PBRs equipped with membrane sparger

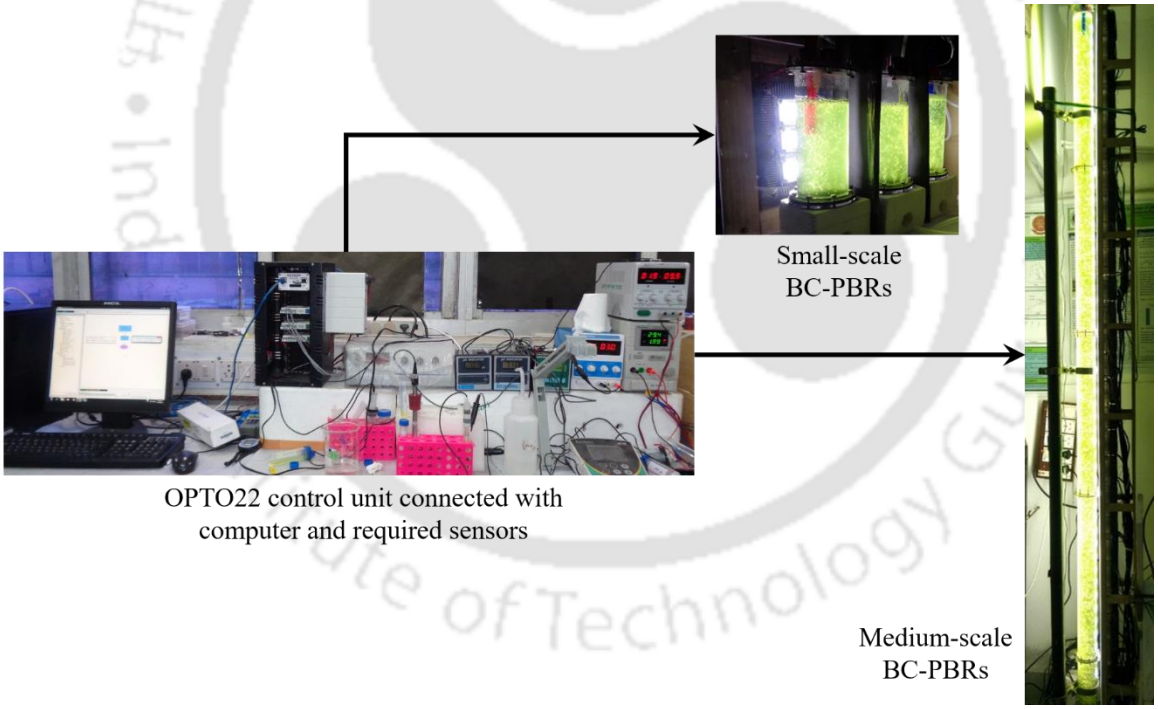

Fig. 4.8 Membrane sparger equipped small-scale and medium scale BC-PBRs with FC2 culture, connected to OPTO22 control unit and sensors.

Both the scales of BC-PBRs were finally equipped with membrane sparger due to its superiority over perforated tubing and L-sparger, without any external agitation requirements (Fig. 4.8). Their respective unidirectional lighting systems were also shown

besides the PBRs. Online monitoring of culture parameters were accomplished by the OPTO22 control system (left side of Fig. 4.8).

4.4.5 Effect of recirculation on FC2 growth

The recirculation of algal culture between illumination surface and dark chamber could adjust the light/dark cycles exposure and thus, serves as a potent solution for expected photoinhibition under high light intensities (Sforza et al., 2012). Therefore, the effects of peristaltic pump and centrifugal pump (booster pump) were tested on the growth of FC2 under low light and low CO_2 conditions as there was no idea of optimum conditions. Unfortunately, both the pumps resulted in lowered biomass densities of FC2 compared with the non-circulated FC2 culture (control) (Fig. 4.9). FC2 could grow up to some extent while pumping by peristaltic pump, but the booster pump killed the algal cells totally. Therefore, further process design and optimization studies with the designed BC-PBRs were performed in batch operational modes.

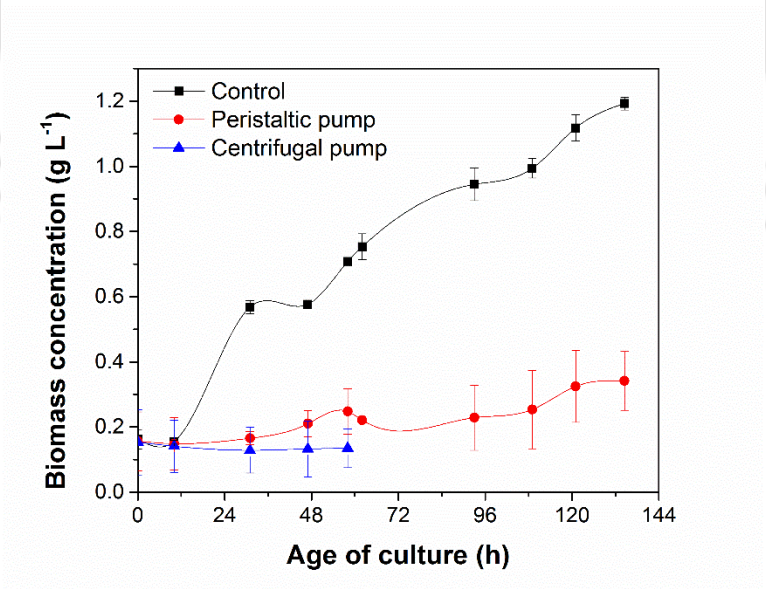

Fig. 4.9 Effect of recirculation mechanism (via pumping) on the growth of *Chlorella* sp. FC2 IITG. Control study without recirculation (square), peristaltic pump (circle) and centrifugal pump (upper triangle)

4.5 Conclusions

For cultivation of experimental microalgae species, *Chlorella* sp. FC2 IITG, bubble column PBR (BC-PBR) technology was selected and constructed with prospect to integrate in vertical PBRs. As sunlight is the superior light source from the perspective of economics, an artificial lighting system was firstly self-designed to mimic sunlight irradiation for conducting comparative studies inside the laboratory. The foremost engineering and design of BC-PBR involves the selection of a mass-transfer efficient and cost-effective gas-sparging device that lies at bottom of the reactor. Therefore, a high mass-transfer efficient membrane sparger was also designed to incorporate in the BC-PBR. In comparing the membrane-sparger equipped BC-PBR with the same BC-PBR equipped with known spargers, its mass transfer efficiency was found superior than the both and offered overall CO_2 mass transfer coefficient of 0.017 s^{-1}. Also, the membrane-sparger was found scalable and exhibited lesser cell-settling of model microalgae species (*Chlorella* sp. FC2 IITG) when compared to the perforated tubing. For the prospective photoinhibition control and continuous operation, the recirculation of FC2 cells was also investigated. Nevertheless, recirculation of the current strain might not be suitable as there was a significant negative effect on its growth due to pumping.

CHAPTER 5

Effect of light intensity and CO_2 on the growth of *Chlorella* sp. FC2 IITG in small-scale BC-PBR under LED lighting

5.1 Background and uniqueness of the study

The main technology constraint in microalgae production for biodiesel is in biomass growth and productivity. In algal culturing, reactor design and process technology are governed by two critical parameters namely, availability of light and CO_2 supplementation. Process technology involves the evaluation of possible inhibiting and limiting combined effects of both light and CO_2 (Pierobon et al., 2016). Some studies have indicated that the inhibition of net photosynthesis could not be attributed to high light intensities alone (Iñiguez et al., 2017; Pope, 1975; Powles, 1984). At high light intensities, damage of photochemical reaction centre at photosystem II (PS II) is increased due to the production of reactive oxygen species (Murata et al., 2007). On the other hand, concentration of CO_2 as dCO_2 in the culture medium another crucial growth factor that could be regulated via modulating the rates of CO_2 supply and CO_2 uptake by cells. At desired/optimum dCO_2 concentration, CO_2 uptake is maximum and hence growth will be maximum. Therefore, it is imperative to monitor the dCO_2 concentration throughout entire cultivation cycles.

Overall, the CO_2 gas-liquid mass transfer coefficient ($K_L\, a_{,CO_2}$) is the primary factor that helps in maintaining desired dCO_2 concentration in the medium. The demand for CO_2 in turn depends on the light energy availability photosynthesis Therefore, the combined effects of both light and CO_2 is the primary consideration for design and optimization. High concentration of dCO_2 could inhibit the growth of algae, due to two possible factors

namely: lowered pH levels and usual CO_2-substrate inhibition. Therefore, it is also important to locate the optimum pH levels before the evaluation of CO_2 effect.

Before the actual experiments on evaluating the effect of light or CO_2, selection of an appropriate inoculum size is the foremost step towards developing a large-scale cultivation system for microalgal growth. Apart from prolonged lag phases, lower inoculum sizes can contribute in maximizing photoinhibition by increasing average light intensity per individual cell (Bunt, 1968). Higher inoculum sizes can also decrease initial specific growth rates and even decreases the lipid contents (Bohutskyi et al., 2016; Lu et al., 2012).

Since the microalgae cultivation under diurnal sunlight is the only feasible method towards economic biodiesel production (Wang et al., 2014), studies under diurnal pattern of lighting similar to natural sunlight conditions are most relevant. However, we cannot perform comparative/reproducible studies directly under sunlight due to highly unstable climatic conditions. Studies under constant lighting are also useful for evaluating photoinhibition and photolimitation characteristics and the combined effects of light and CO_2. Therefore LED lighting system with computer-dimmable technology was designed to mimic diurnal sunlight. This part of the study is focused on the objectives namely: the effect of inoculum size, light, pH control and CO_2 on growth of microalgae in small-scale BC-PBR. The combined effects of variations in light and CO_2 levels was studied to determine the optimal CO_2 supply strategy with the aim of maximizing the biomass and lipid productivity under diurnal LED lighting conditions.

5.2 Experimental design

In this study, all the experiments were carried out in batch mode using the small-scale membrane-sparger equipped BC-PBR in a setup depicted in Fig. 5.1. For constant

light and simulated sunlight OPTO22 control system was used. The pH was measured online, whereas the dissolved CO_2 (dCO_2) was measured offline at every 2 h for each of the three BC-PBRs.

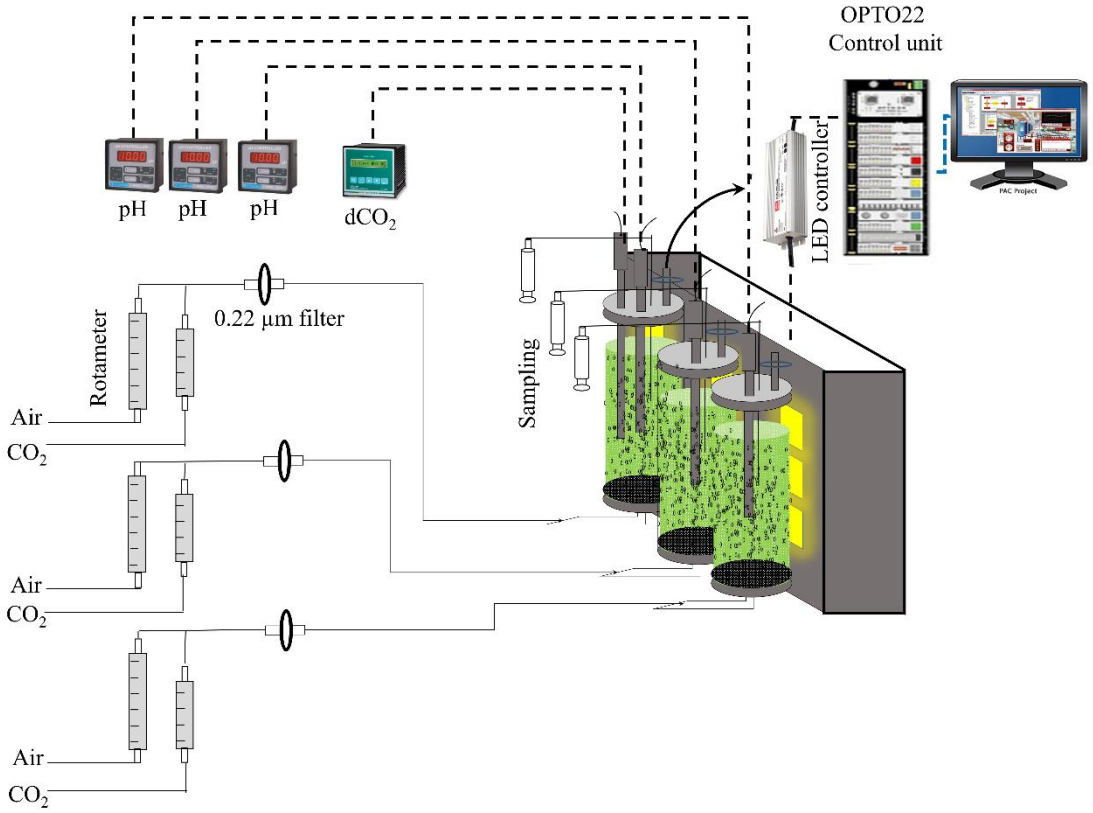

Fig. 5.1 Schematic of three parallel small-scale BC-PBRs equipped with membrane sparger, connected to OPTO22 control unit.

Estimation of cell density, phosphate and urea were carried out at start and end of each light cycle. As mentioned in chapter 1, the temperature was not controlled deliberately to make the process economic and to perform real-time (near-natural) studies.

The growth of FC2 was investigated at various inoculum densities ranging from 0.007 – 0.49 g L^{-1}. The studies were conducted at a constant light intensity of 1200 µmol m^{-2} s^{-1} with atmospheric CO_2 as carbon source. Light:dark cycle was maintained at 10:14 h. The obtained optimum inoculum density was maintained in all the subsequent studies.

Since, outdoor sunlight intensity in Guwahati (India) region ranges from 0 – 2000 µmol m^{-2} s^{-1}, effect of constant light intensity on FC2 growth was evaluated at 106, 700, 1130, 1500 and 2000 µmol m^{-2} s^{-1} at a constant CO_2 supply of 1% (1 VVM, CO_2 in air). The light:dark cycle was maintained at 10:14 h. During the dark periods, supply of pure CO_2 was stopped and only atmospheric air was provided to keep the culture mixing. At the same time, O_2 would be available for respiration.

Various pH control strategies namely 'full control', 'day control' and 'no control' were applied in FC2 culturing by providing constant CO_2 supply of 10 % (1 VVM, CO_2 in air) and constant light intensity of 1130 µmol m^{-2} s^{-1}. The pH control set point was maintained at 7.2. In 'full control' NaOH and CO_2 were used as controlling agents for day and night respectively. In 'day control', NaOH was used as controlling agent only during the daytime. The pH was not controlled in 'no control' experiment. Except in 'full control' experiment, supply of pure CO_2 was stopped during the dark hours of culturing and only air was provided to keep the culture mixing. Secondly, effect of pH control set point on the growth of FC2 was evaluated at 5.9, 7.2 and 8.8 using HCl, CO_2 and NaOH according to the requirements of respective experiments.

At a constant light intensity, 1130 µmol m^{-2} s^{-1}, dynamic growth and dCO_2 concentration profiles of FC2 were studied under various CO_2 levels (% in air, v/v) of 0.035%(atmospheric air), 1%, 2%, 5%, 10% and 15% that can produce different equilibrium dCO_2 concentrations in liquid phase ($C^*_{CO_2}$). This $C^*_{CO_2}$ values are the starting dCO_2 concentrations in the respective experiments. In all the experiments, light:dark cycle was maintained at 10:14 h by stopping pure CO_2 during the dark hours. The pH was not controlled in any of the studies.

Diurnal lighting was mimicked similar to outdoor sunlight intensities using the LEDs via OPTO22-PWM control system. This could produce light intensities ranging from

17 – 2000 – 17 μmol m^{-2} s^{-1} during the light period. Under this lighting pattern, FC2 was cultured by maintaining constant dCO_2 concentration of 100 ± 10 mg L^{-1} based on previous experimental results. In order to maintain desired dCO_2 concentration in the culture, CO_2 levels (% in air) were adjusted in a discrete manner. This light:dark cycle of 12:12 h was chosen on the basis of average sunlight cycle in Guwahati region (India). After achieving sufficient biomass density in growth phase, the centrifuged cells were transferred to urea-free BG11 medium for lipid induction. High lipid containing biomass was transesterified to analyse fatty acids in terms of fatty acid methyl esters (FAME).

5.3 Results and discussion

5.3.1 Effect of inoculum density on the growth of FC2

In this study, a higher light period-specific growth rate on day 1 (μ_{day1}) was chosen as screening criteria for optimal inoculum density. The inoculum densities of 0.025, 0.07 and 0.12 g L^{-1} exhibited almost similar μ_{day1} of 1.50 ± 0.11, 1.69 ± 0.03 and 1.59 ± 0.06 day^{-1} respectively (Fig. 5.2). Whereas at higher inoculum densities, 0.25 and 0.49 g L^{-1}, μ_{day1} of 1.25 ± 0.10 and 0.79 ± 0.09 day^{-1} were observed respectively. Since, we could choose any inoculum density from the range of 0.025 – 0.12 g L^{-1}, inoculum density of 0.07 g L^{-1} was adapted for all further studies. And the inoculum densities below 0.025 g L^{-1} were considered as limiting and above 0.12 g L^{-1} were treated as inhibitive for FC2 culturing (Fig. 5.2).

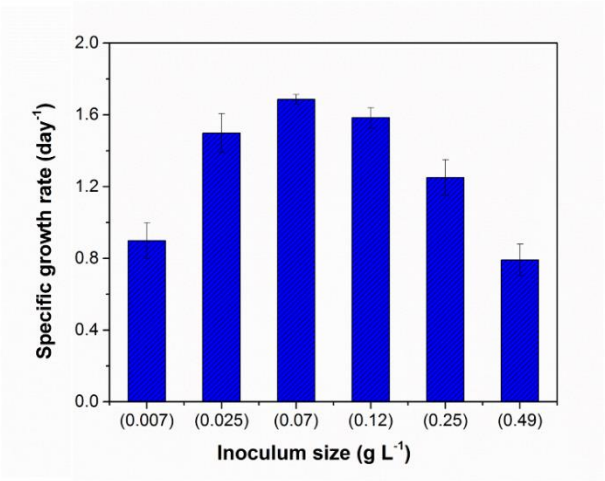

Fig. 5.2 Initial period specific growth rates of *Chlorella* sp. FC2 IITG (FC2) at various inoculum densities. Light intensity was maintained at 1200 µE m^{-2} s^{-1} with atmospheric CO_2 (from air) as carbon source and light:dark cycle was maintained at 10:14 h.

5.3.2 Effect of light intensity on the growth of FC2

Based on the light period specific growth rates of all the culturing light periods, the saturated light intensity for growth of *Chlorella* sp. FC2 IITG was observed in a broad range of 700 – 1500 µmol m^{-2} s^{-1} (Fig. 5.3B). This indicates that the strain could perform photosynthesis up to 1500 µmol m^{-2} s^{-1} without any photoinhibition. At 2000 µmol m^{-2} s^{-1} light intensity (highest of outdoor sunlight tested), the specific growth rate of 1st day (μ_{day1}) was clearly showing photoinhibition phenomenon that would have occurred due to a very high average light exposure per cell. Strangely, the phenomenon was noticed as a reversible process for the strain from 2nd day onwards (Fig. 5.3B). The reason behind this reversible phenomenon can be depicted from an unusually observed highest specific growth rate of '3.69 ± 0.009 day^{-1}' on 2nd day (μ_{day2}) of culturing under 2000 µmol m^{-2} s^{-1}. Since light was provided from single side of PBR, it was strongly suggesting that the average light availability across the diameter of PBR would have reached near to optimum value. Consequently, highest specific growth rate was seen on the 2nd day of culturing under 2000 µmol m^{-2} s^{-1}. In addition to the above reason, a special photo-protective mechanism could also be responsible for sudden appearance of high and an abnormal specific growth rate in

photoinhibited FC2 cells compared to the other light intensities. The specific growth rates in none of the studies (including others) exceeded 3 day^{-1}. This photo-protective mechanism was well cited as photorecovery phenomena (Han, 2002; Tikkanen et al., 2014). According to this phenomenon, damage of a crucial D1 protein in photosystem II (PS II) is responsible for photoinhibition and this damage itself acts as an inducer for new D1 protein synthesis to carry out usual photosynthesis. Moreover, it has reported as protective mechanism takes place in overall culture even though few number of cells undergo photoinhibition (Fernandez et al., 1998). This could also be another reason why the highest specific growth rate was observed on 2nd day in the case of 2000 µmol m^{-2} s^{-1}. Since μ_{day1} was lesser than μ_{day2} of 2000 µmol m^{-2} s^{-1} grown cells, the rate of D1 protein recovery on day 2 might have dominated over the rate of damage of D1 protein.

Thus, the photoinhibition was assumed to be reversible and recoverable in FC2 cells even at the high diurnal light intensity of 2000 µmol m^{-2} s^{-1}. In order to confirm chlorophyll damage due to photoinhibition, total chlorophyll content (Chl-a + Chl-b) was also measured on each day morning of 4 days culturing (Fig. 5.3A). No significant decrease in chlorophyll content was noticed at all the higher light intensities. And in fact this data was also indicating that photosynthesis could get saturated after 700 µmol m^{-2} s^{-1}. Since there was no evidence of photoinhibition at 1130 µmol m^{-2} s^{-1}, this light intensity was chosen as optimum for further studies. Moreover, highest final biomass titer (Fig. 5.3C) of 4.06 ± 0.06 g L^{-1} was achieved at 1130 µmol m^{-2} s^{-1}. Note that this light intensity is close to the average day-light intensity range and much higher than typical optimum value, 200–300 µmol m^{-2} s^{-1} that is generally evaluated by illuminating from all the sides of reactor unlike the current study (Dechatiwongse et al., 2014; Singh & Singh, 2015).

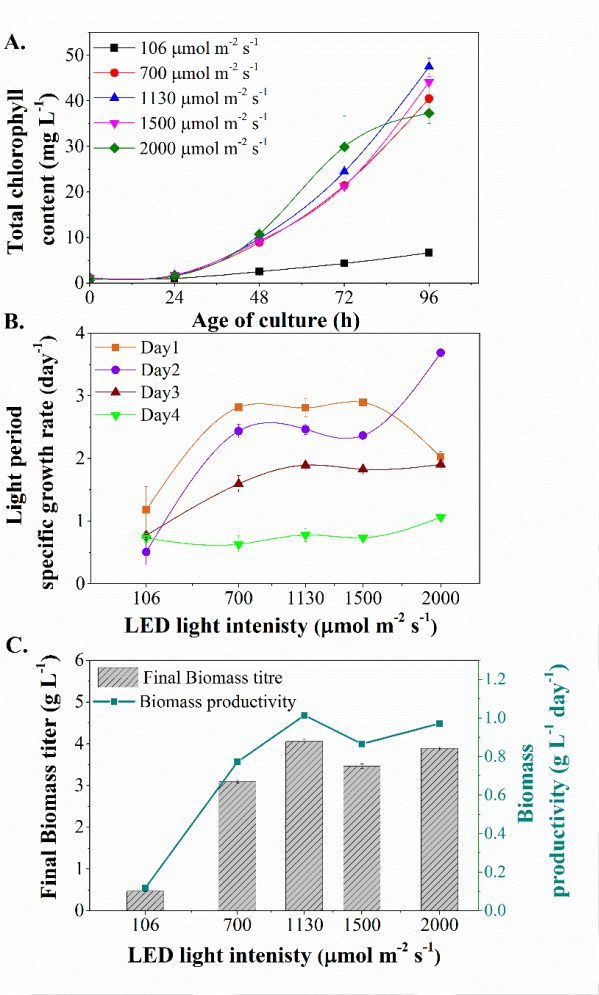

Fig. 5.3 Growth analysis of FC2 under various LED light intensities (constant supply). **A.** Total chlorophyll content (sum of chlorophyll 'a' and 'b'), **B.** day wise (10 h light period) specific growth rates, **C.** final biomass titers (bar graph) and overall biomass productivities of FC2. 1% CO_2 was used as carbon source in all the experiments with a light:dark cycle of 10:14 h. This experimental study was carried out in triplicate.

5.3.3 Analysis of pH control requirement for cultivation of FC2

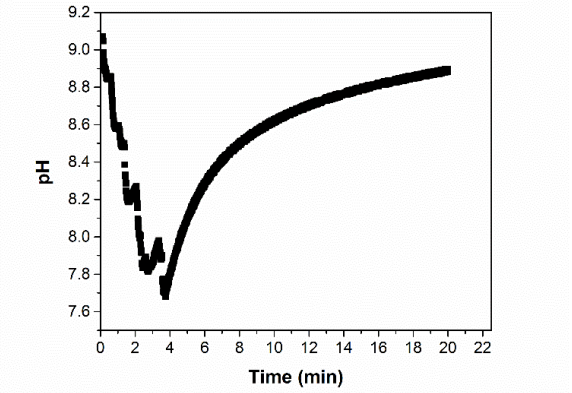

Fig. 5.4 Change in the pH after the addition of 600 µl of concentrated HCl while controlling the pH at 7.2 by NaOH in day time (CO_2 sparged with air) and HCl in night time (only air sparging) for pH control. The experimental condition was constant light of 1130 µE m^{-2} s^{-1} and 10% CO_2.

As CO_2 is supplied only during daytime, FC2 requires base (usually NaOH) in day times and acid (usually CO_2 or HCl) in night times for pH maintenance. HCl was unable to control alkaline pH in the night periods of culturing (Fig. 5.4). It was observed that pH was raised within 20 minutes' addition of 600 µl of concentrated HCl. This implied that H^+ ions would be utilized for cell's metabolism.

The HCl was reported to serve as a source of H^+ ion during heterotrophic cultivation of FC2 (Palabhanvi et al., 2016) as it plays a key role in assimilation of nitrate. Therefore, the dark phase (no carbon source) of photoautotrophic cultivation may also following similar kind of H^+ ion absorption.

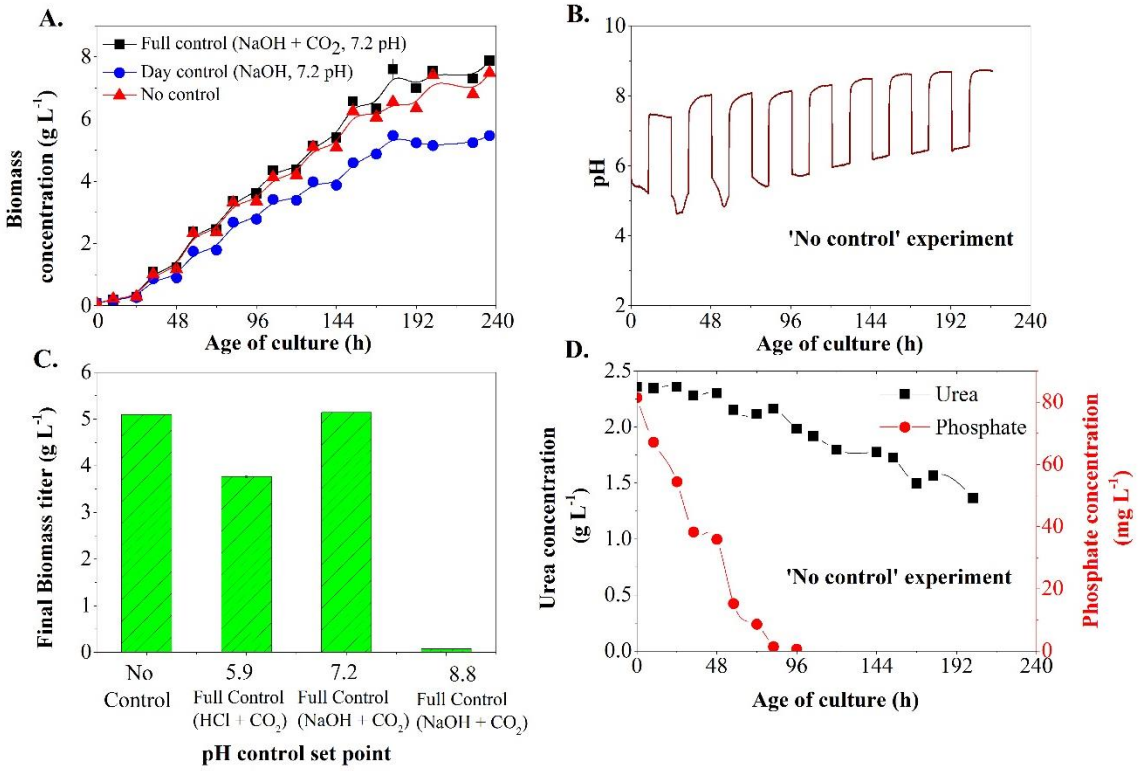

Fig.5.5 Growth analysis of FC2 at various pH control studies along with major substrate analysis. **A.** Biomass growth analysis for various pH control strategies. **B.** pH profile of 'no control' experimental study. **C.** Variation of pH set-points for optimization of FC2 growth (represented till 130 h) using full control strategy. **D.** Dynamic urea and phosphate profiles in the culture medium. All the experiments were carried out at constant lighting of 1130 µE m^{-2} s^{-1} and 10% CO_2 feed.

Using CO_2 as photoautotrophic carbon source as well as alkaline pH controlling agent, three pH control strategies namely 'full control' ($NaOH+CO_2$), 'day control' (NaOH) and 'no control' (without pH control) were tested for growth of FC2 at 10% CO_2 level. The pH in full control and day control was maintained at 7.2 ± 0.1. In comparison to day control, full control strategy exhibited higher biomass titer of 7.5 ± 0.01 g L^{-1}. However, the growth patterns of FC2 were the same in both full control and no control strategies (Fig. 5.5A). This suggested that FC2 may be capable of growing well in wide pH range, 4.6 – 8.6 pH (Fig. 5.5B and Fig. 5.5A).

For further elaboration on this observation, the study hypothesized that there could be a different set point for controlling pH instead of 7.2. The pH of 7.2 was chosen based on previous reports on FC2 where pH control was carried out on the basis of optimum initial pH values, 6 – 8, i.e., the optimization experiment was carried out at different initial pH values. However, the optimum process pH control set point, which is maintained throughout the study experiment can be different from optimum initial pH value. For instance, *Chlorella vulgaris* shown optimum initial pH values ranging from 7 – 10, but its growth was observed highest while process pH was controlled at 10 (Gong et al., 2014). Thus, FC2 was also tested against three pH control set points, 5.9, 7.2 and 8.8 using full control strategy, and pH of 7.2 was evaluated as optimum (Fig. 5.5B). The FC2 displayed impressive growth even at no pH control, which could decrease the cost of process technology for scale-up.

The 'no control' experiment was continued until the stationary phase (Fig. 5.5A) in order to evaluate yield coefficients of phosphate (96.54 g cells g $phosphate^{-1}$) and urea (7.41 g cells g $urea^{-1}$) in order to confirm their interference in other's limitation effects. According to the data, the stationary phase occurs at 7.41 g L^{-1} primarily due to the phosphate limitation.

5.3.4 Evaluation of the combined effect of lighting and CO_2 feed at various CO_2 levels (%)

In all the tested CO_2 levels ranging from air (0.035% CO_2) to 15% (v/v), cells grown at 2% CO_2 level ($C^*_{CO_2} = 100\ mg\ L^{-1}$) exhibited highest biomass titer and overall biomass productivity of 4.33 ± 0.12 g L^{-1} (Fig. 5.6A) and 1.08 g L^{-1} day^{-1} respectively. Maximum specific growth rate (μ_{max}) of 2.95 ± 0.24 day^{-1} was observed on 1st day of culturing, which was highest among all the individual μ_{max}' of other cultures. On day 2, specific growth rates of 5% ($C^*_{CO_2} = 190\ mg\ L^{-1}$) and 10% ($C^*_{CO_2} = 275\ mg\ L^{-1}$) CO_2 levels, were observed higher than 2% CO_2 level (Fig. 5.6C). This could be attributed to either light limitation in 2% CO_2 grown cells, due to higher biomass, or limitation of dCO_2 concentration. Based on Beer-Lambert's light attenuation coefficient (K_a = 200 m^2 kg^{-1}) of *Chlorella* sp. (Ogbonna et al., 1995), light becomes almost zero (< 1% of incident light intensity) at the center of small-scale BC-PBR when cell concentration reaches about 0.67 g L^{-1} with single-sided incident light of 1130 µE m^{-2} s^{-1}. At the same time, continuously increasing cell density can also demand more CO_2 and therefore, high supply rates to meet CO_2 uptake. For this reason, CO_2 levels (% in air, v/v) should be elevated to maintain dCO_2 concentration as per increasing demand. Since, it is not practicable to overcome light limitation under realistic diurnal sunlight conditions (main goal of this study); maintenance of desired dCO_2 concentration by manipulating the CO_2 levels may be the only option for enhancing biomass productivity in process design.

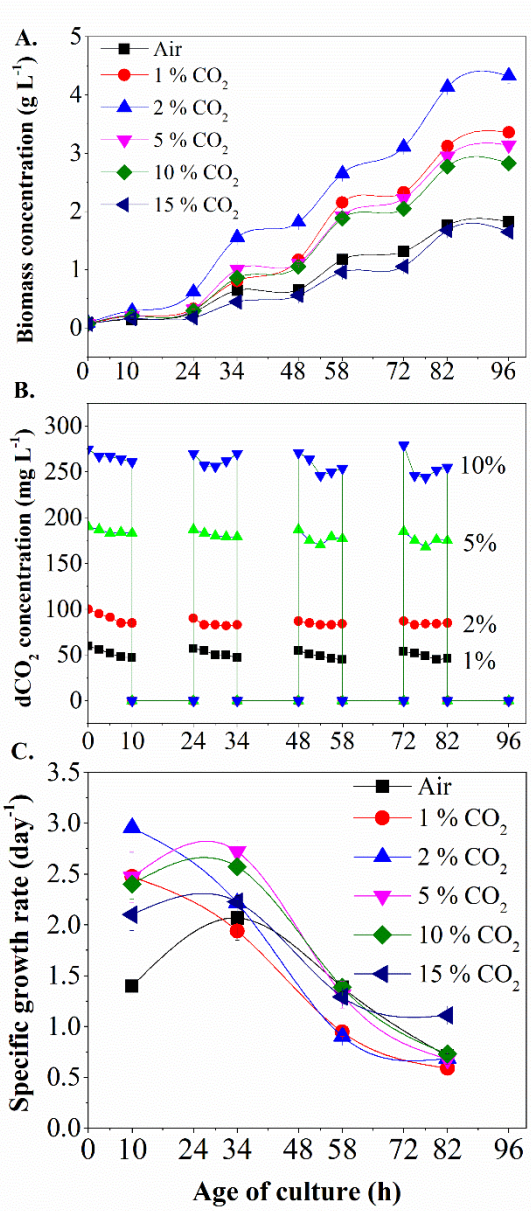

Fig. 5.6 Effect of different CO_2 levels (% in air) on the growth of FC2. **A.** Dynamic growth analysis of FC2 under various CO_2 levels in the range of 0.035% (atmospheric air) to 15% ($C^*_{CO_2} = 340\ mg\ L^{-1}$). **B.** Dynamic dCO_2 concentrations profiles of FC2 cells cultured at CO_2 levels of 1% ($C^*_{CO_2} = 60\ mg\ L^{-1}$), 2% ($C^*_{CO_2} = 100\ mg\ L^{-1}$), 5% ($C^*_{CO_2} = 190\ mg\ L^{-1}$) and 10% ($C^*_{CO_2} = 275\ mg\ L^{-1}$). **C.** Dynamic specific growth rates of FC2 calculated at the end of each light period (based on 10 h). For all experiments, light intensity of 1130 µE m^{-2} s^{-1} was maintained constantly with 10:14 h light:dark cycle. Since, FC2 was capable of growing without pH control; pH of the culture medium was not maintained/controlled.

For the evaluation of desired/optimum dCO_2 concentration, dCO_2 concentrations of FC2 cultures at different CO_2 levels were measured with the dCO_2 probe at every 2.5 h intervals. At 1% CO_2, dCO_2 concentration was decreased with time during the lighting

periods, which implied that CO_2 uptake rate for photosynthesis was higher than the CO_2 supply rate. In the case of 2% CO_2, the dCO_2 concentration reached to steady state after certain hours of culturing (Fig. 5.6B). The steady-state dCO_2 concentration suggested that both the CO_2 uptake rate and supply rate were at equilibrium. Hence, the photosynthetic rate in FC2 sustained at 2% CO_2 feed.

In case of 5 and 10% CO_2 levels, dCO_2 concentration decreased during first 2 days and 1 day of culturing respectively. In the later stages of cultivation, an increased dCO_2 concentration was observed mainly due to the domination of CO_2 supply over decreasing total CO_2 uptake rates due to the light limitation by increasing cells. Overall, the CO_2 supply plays a critical role in maintaining the dCO_2 concentration in such a way that it should meet the demand of increasing cells as well as required CO_2 uptake.

Cells grown at air and 15% CO_2 were clearly exhibiting limiting and inhibitive CO_2 levels for FC2 respectively, possibly due to their low biomass yields. In 2% CO_2 conditions, steady state dCO_2 concentration was maintained at 83 ± 1 mg L^{-1} consistently until biomass concentration of 4.33 ± 0.12 g L^{-1} was attained after 96 hours. This suggested that photosynthetic rates were also sustained despite the incremental light limitation. The 2% CO_2 was determined as optimum for FC2 growth under the specified conditions.

The specific CO_2 uptake rate in 2% CO_2 grown cells was measured as 19.8 mg (g cells)$^{-1}$ h^{-1}. The value of steady state dCO_2 concentration of 2% CO_2 grown cells, 83 ± 1 mg L^{-1} (500 ml culture) indicate that it could drop to much lesser value in large-scale cultivation where the cell number will be high. Also, the steady state concentration should not drop below 60 mg L^{-1} as 1% CO_2 ($C^*_{CO_2} = 60\ mg\ L^{-1}$) level was limiting for FC2 growth. Hence, the maintenance of constant dCO_2 concentration (via modulation of CO_2 level) was chosen as desirable CO_2 feed strategy for sustainable cultivation of FC2. For this reason, 100 ± 10

mg L^{-1} ($C^*_{CO_2}$ of 2% CO_2 level) was used throughout the culturing of FC2 under simulated diurnal lighting using the designed smaller LED system.

5.3.5 Growth and FAME analysis of FC2 culture under diurnal lighting pattern

In this part of study, FC2 was cultured in simulated diurnal lighting (Fig. 5.7C) by maintaining constant dCO_2 concentration of 100 ± 10 mg L^{-1} using OPTO22 controller system. As the temperature was not controlled, the resulted temperature was due to light intensity variation and algae metabolism (Fig. 5.7C). Though there was a biomass loss on 2nd night of culturing, FC2 shown impressive growth performance under diurnal light regime by exhibiting biomass productivity of 1.29 g L^{-1} day^{-1}, equivalent to optimum lighting (1130 µE m^{-2} s^{-1}) and CO_2 (2% in air) conditions (section 5.4.4).. Through the light periods, the CO_2 levels corresponding to maintenance of the desired dCO_2 concentration (100 mg L^{-1}) were observed to increase or decrease in proportion to supplied diurnal light intensity (Fig. 5.7A and Fig. 5.7C). The reason would be an obvious demand of CO_2 by photosynthesis cycle due to increase/decrease in light intensity. The elevated CO_2 levels at high light intensities were also depicting effective photosynthesis and thus no photoinhibition. The range of saturated light intensity for the FC2 strain might have increased with increasing CO_2 concentration as occurred in *Lolium perenne* L. (perennial ryegrass, plant species) can (Wilson & Cooper, 1969). Although the outcome in Fig. 5.7A suggested the importance of elevated CO_2 levels up to 3%, the reduced CO_2 levels below 2% from 2nd day morning was abnormal (Fig. 5.7A). The CO_2 levels were fallen up to 0.8%, which occurred especially during the exposure of low light intensities. Recalling the section 5.4.4, the equilibrium dCO_2 concentration ($C^*_{CO_2}$) of 100 mg L^{-1} corresponds to the 2% (in air) CO_2 level in growth medium without cells, i.e., a minimum of 2% CO_2 level is required to maintain $C^*_{CO_2}$ of 100 mg L^{-1}. Hence, the phenomenon of reduced CO_2 levels could be possible only when CO_2 was generated in tandem with the regular consumption.

Therefore, it was assumed that CO_2 would be releasing into medium due to a well-known phenomenon called photorespiration (Lloyd et al., 1977; Maurino & Peterhansel, 2010).

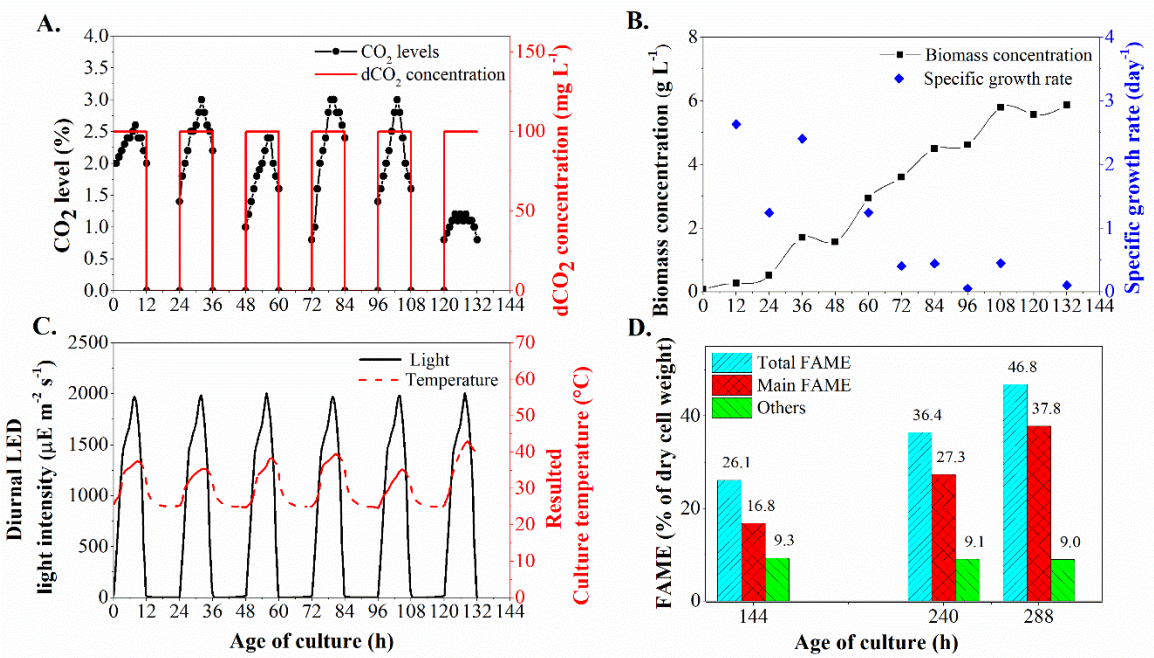

Fig. 5.7 Characteristics of growth and FAME profiles of FC2 grown under diurnal lighting pattern using the optimal CO_2 feed strategy. **A.** Dynamic profiles of discretely adjusted CO_2 levels (% in air) along with dCO_2 concentration maintenance. **B.** Biomass growth and specific growth rates of FC2 under diurnal lighting pattern. **C.** Variation of diurnal light intensity on the surface of BC-PBR over the growth phase of total culturing period and dynamic resulted temperatures of FC2 culture medium. **D.** FAME analysis of *Chlorella* sp. FC2 IITG under nitrogen (urea) starvation condition for 6 days of lipid induction period. During the induction phase also, same diurnal lighting pattern was followed. Urea-free BG11 medium was used during this phase. Diurnal light variations were achieved by OPTO22 – PWM controller and the light:dark cycle was maintained at 12:12h (average of Guwahati region, India). The pH and temperature of the culture were not controlled.

In photosynthesis, Ribulose-1,5-bisphosphate-carboxylase/oxygenase (RuBisCO) shares both oxygenase and carboxylase activities. Hence, photosynthetic rate decreases at high O_2 concentrations due to competitive inhibition of carboxylase (CO_2 fixation by RuBisCO) activity, known as Warburg's effect (Zelitch, 1971). Due to photorespiration, a minimum of 25% fixed CO_2 could effluxes back to environment (Maurino & Peterhansel, 2010). Besides this, high temperatures can also favor Warburg's effect to release more CO_2 into the environment. However, the elevation of CO_2 levels beyond the 2% level at high light intensities and high culture temperatures indicate the photosynthesis domination over

the photorespiration (Fig. 5.7A and 5.7C). The photorespiration phenomenon was pronounced more during the low light intensities when light limitation is maximum. The FC2 cells reached stationary phase at biomass concentration of 5.79 ± 0.08 g L^{-1} (Fig. 5.7B), after with the CO_2 levels were fallen below 1% (Fig. 5.7A). As the light limitation was increasing after 120 hours, the combination of both dark respiration and photorespiration might have dominated the photosynthesis. . Based on the phosphate yield and biomass growth obtained in 'no control' experiment of previous section 5.4.3, the growth of FC2 in this study could not be limited by phosphate as it stopped at 5.79 g L^{-1}.

FC2 culture of cell density 5.79 ± 0.08 g L^{-1} was transferred to urea-free optimized BG11 medium for lipid induction followed by biodiesel production. After 6 days of induction phase growth, the FC2 produced a total FAME content (TFC) of 46.8% (of cell dry weight) with an overall FAME productivity of 145 mg L^{-1} day^{-1} (Fig. 5.7D). The FAME productivities of 85 mg L^{-1} day^{-1} (first 4 days) and 265 mg L^{-1} day^{-1} (last 2 days) at the end of 4^{th} and 6^{th} day respectively indicating that the induction phase was continuing. After 6 days of total induction phase, the total FAME production was 2.38 g L^{-1}. The cetane number (*CN*) of the FAME mixture (biodiesel) was maintained in the range of 57 – 62 that are far higher than required limits (> 47 by ASTM D6751 and >51 by EN 14214)), indicating the fuel is applicable for operation of high speed diesel engines.

Apart from this, Table 5.1 suggested that main fatty acids (C16 – C18) accumulation was increased from 74% to 89.41% (% of TFC) through the induction phase, suggesting the nitrogen starvation improved quantity of biodiesel along with the maintenance of quality.

Table 5.1 Individual FAMEs profile of biodiesel produced from *Chlorella* sp. FC2 IITG during the induction phase of culturing under diurnal lighting pattern.

FAME/Property name	Sample (144 h)	Sample (240 h)	Sample (288 h)
C12:0	0.024	0	0.08
C13:0	0.255	0	0.076
C14:0	0	0	0
C15:0	0	0	0
C15:1	0.23	0.254	0.21
C15:2	0.232	0.196	0.18
C15:3	0.27	0.306	0.478
C16:0	1.32	1.07	1.85
C16:1	0.518	1.298	1.488
C16:2	0.2	0.32	0.28
C16:3	0	0.4	0.28
C17:0	0	0	0.52
C17:1	0.36	0.48	0.32
C17:2	0.348	0.58	0.37
C18:0	1.32	2.56	3.6
C18:1 Cis	0.972	1.74	2.62
C18:2 Cis	0.38	0.816	1.226
C20:0	0	0	0
Others	0.893	0.896	0.463
SAT FAME (% of TFC)	39.87	33.25	43.63
MUFA (% of TFC)	28.41	34.55	33.03
PUFA (% of TFC)	19.53	23.98	20.04
TFC (% DCW)	**26.15**	**36.42**	**46.8**

5.3.6 Biomass growth analysis in dark-phase of culturing

In all the conduct experiments of this study, a strange dark-phase growth was occurred instead of usual night biomass loss. Generally, the biomass loss occurs as a result of dark respiration that remained as another unavoidable problem affecting the productivity of algae cultures (Edmundson & Huesemann, 2015; Ogbonna & Tanaka, 1996). The fascinating growth of FC2 strain during night times was recorded and tabulated (Table 5.2). Please note that dark periods (night) were maintained by covering the reactors with black paper from all the sides. It was observed that 80-90% of dark-phase growth was occurred in the first 5h of the 14h dark period (data is not shown). This was suggesting that the absorbed energy from light periods would have promoted the growth in night periods. Except at light intensity of 2000 µE m^{-2} s^{-1} (section 5.4.2), FC2 cells shown positive net

biomass gain in all the studies. Sometimes, biomass losses were also occurred along with gains in the same experiments. However, higher night biomass gains were observed at suboptimal/optimal light and CO_2 levels in comparison with low or high levels. In an experiment conducted under natural sunlight conditions (data was not shown), night growth was observed around 0.82 g L^{-1} within 3 days of culturing (Table. 5.2). Also, the biomass grown under diurnal simulated sunlight (with LEDs) was shown to exhibit 0.88 g L^{-1} of net biomass gain. Hence, the strain was proved to exhibit dark-phase growth irrespective of light conditions.

Table 5.2 Dark phase growth of *Chlorella* sp. FC2 IITG in various studies.

Experimental study	**Net biomass gain in dark-phase (g L^{-1})**
Variation of light intensities (µmol m^{-2} s^{-1}), 1 % CO_2, 4 days.	
106	0.14
700	0.80
1130	0.93
1500	0.70
2000	0.00
Variation of CO_2 levels (% in air) at constant light 1130 µmol m^{-2} s^{-1}, 4 days.	
AIR	0.34
1	0.89
2	1.23
5	0.70
10	0.50
15	0.19
Diurnal LED lighting (100 ppm CO_2, 0.8 to 3 %), 4.5 days.	0.88
Natural sunlight, 1% CO_2 (3 days, September 2016, mixture of clear, cloudy and rainy daylights)	0.82

Similar to this study, earlier reports on night cell divisions suggest that the dark-phase growth is mainly linked to energy supply in the light regime, temperature, and cell-cycle events (Chisholm, 1981; Harding & Heinbokel, 1984). Harding and Heinbokel showed that cell divisions of a marine diatom, *Ditylum brightwellii* could take place at any point of light or dark periods of culturing. . The occurrence of asynchronous cell divisions causing night growth is mainly forced by environmental factors especially night temperatures rather than the light regime experienced by the cells during light cycle (Chisholm, 1981). As the temperature was not controlled in the current study to minimize process costs, the natural temperature profiles might have promoted the dark-phase growth. Therefore, the observation of dark-phase growth in the FC2 strain was considered beneficial as it enhances overall biomass productivity.

5.4 Conclusions

This study was conducted in small-scale BC-PBR to evaluate appropriate inoculum size, behavior of *Chlorella* sp. FC2 IITG at different simulated sunlight intensities, optimum pH control set point, and combined effect of light and CO_2 at different CO_2 levels. Consequently, an optimal CO_2 supply strategy under diurnal simulated sunlight was proposed and investigated for FC2 growth and biodiesel production. . Based on specific growth rates at different inoculum sizes, the optimum inoculum biomass density was observed as 0.07 g L^{-1}. In this BC-PBR setup with unidirectional simulated sunlight conditions, the strain's saturated light intensities were observed in the wide range of 700 – 1500 µmol m^{-2} s^{-1}. The strain has also been proved that it can overcome photoinhibition at peak light intensities (2000 µmol m^{-2} s^{-1}) possibly by means of its intrinsic photoprotective mechanism. In addition to this mechanism, 2000 µmol m^{-2} s^{-1} light intensity appears only for few hours in diurnal lighting conditions. Hence, the photoinhibition was not noticed at high light levels in the study conducted under simulated sunlight variation. Also, this strain

of *Chlorella* is peculiar in exhibiting similar growth profile with (at pH 7.2) and without pH control by mineral acid/base addition strategy. When the FC2 was tested against different CO_2 levels (without pH control) under optimum light intensity of 1130 µmol m^{-2} s^{-1}, 2% (in air) CO_2 level was determined as optimum due to maximum biomass growth of 4.33 g L^{-1}. Considering the dCO_2 concentration profiles during equilibrium and light limiting conditions, 'constant maintenance of 100 mg L^{-1} dCO_2 concentration in light periods' was evaluated as optimal CO_2 feed strategy in small-scale BC-PBR under diurnal light e.g., simulated sunlight by LEDs. . The strategy achieved sustained specific growth rates and final biomass concentration of 5.79 g L^{-1} with biomass productivity equivalent to optimum light and CO_2 conditions. Apart from no temperature control from the perspective of saving costs, the *Chlorella* strain in this study shown its unique abilities by growing without pH control and exhibiting dark-phase growth, making the process of algae-biodiesel production more economical.

CHAPTER 6

Development of a novel real time light intensity based CO_2 feed strategy for enhanced *Chlorella* sp. FC2 IITG biomass production in medium-scale BC-PBR under natural sunlight

6.1 Background and uniqueness of the study

The high downstream costs caused by lower biomass densities/productivities in open ponds and closed photobioreactor technologies is the main commercial constraint for establishment of commercial-scale algae derived biorefinery/biodiesel plant (Chisti, 2013). High density cultivation is necessary to maximize multiple product generation and for minimizing the cost of dewatering. (Chisti, 2013). Apart from optimization of photobioreactor design (discussed in chapters 4 and 5), the role of process system engineering is crucial for biomass production in large-scale bubble column/vertical photobioreactors (Chen et al., 2011). In respect to process engineering, CO_2 feed is important parameter for propagation under sunlight conditions, and several strategies for high biomass production have been proposed (Singh & Singh, 2014). For example, the maintenance of an optimum CO_2 level (% in air) throughout the culturing has been reported extensively (Sung et al., 1999; Tang et al., 2011). Such optima CO_2 levels have been determined for constant light intensity. However under continuously varying outdoor sunlight conditions, the optimum CO_2 level is applicable only for a specific range of light intensities and biomass concentrations. With growth, the rate of CO_2 uptake increases, while increasing biomass concentration can lead to CO_2 limitation. Therefore, corresponding increase in CO_2 levels with the increase of biomass density is critical.

There are many ways to increase CO_2 supply during the culturing period. The easier option is to increase CO_2 levels (% in air) or daily supply frequency based on the increasing cell-density (Guo et al., 2015). This type of CO_2 supply regime is termed biomass density based CO_2 feed strategy. Otherwise, the CO_2 feed can also be regulated by controlling the pH of culture at optimum set point referred to as 'pH-stat CO_2 feed' (Chen et al., 2016; Duarte-Santos et al., 2016). When CO_2 is the sole carbon source, the pH change in the culture can be directly attributed to the CO_2 availability (Goldman et al., 1982). In general at fixed CO_2 feed, the pH during the growth of microalgae culture, increases therefore, elevation of CO_2 supply would counter the pH increase. The CO_2 can co-exist in three forms depending on the pH level: as bicarbonate at neutral pH; dissolved CO_2 at acidic pH and; carbonate at alkaline pH. Algae thrive better in bicarbonate and dissolved CO_2. Therefore, efficient carbon assimilation occurs at neutral or acidic pH compared to the alkaline pH (Imamura et al., 1983; Scherholz & Curtis, 2013). Consequently, an effective pH-control system based CO_2 feed strategy will depend on the pH set point selection.

Currently, economic production of algae biomass for any cultivation system is only feasible under natural sunlight conditions. In this study, the artificial lighting for simulation of sunlight was used purely for experimental purposes. Since the natural sunlight is diurnal with fluctuation of light intensities, the algal cells inevitably experience light limitation during morning and evening times of a day. Seasonal changes also result in variation of sunlight irradiation throughout the year. Hence, a study on *Nannochloropsis Salina* culture in outdoor open ponds reported monthly varied CO_2 feed based on average sunlight irradiation during a particular month (Malek et al., 2016). Also, observation of report on cotton plant leaf (a C3 photosynthetic system similar to green algae) suggested CO_2 assimilation rates under low light conditions were observed to be increased at lower CO_2 partial pressures in comparison with high CO_2 partial pressures (Woo & Wong, 1983). Whereas under high light conditions in the same study, the CO_2 assimilation rates were

increased at higher CO_2 partial pressures compared to the lower CO_2. Therefore by inference, light conditions will require commensurate CO_2 feed; this study hypothesized requisite CO_2 levels throughout the daylight period should be based on the real time sunlight intensity for optimum CO_2 assimilation and growth of microalgae.

In this chapter, a novel real time light based CO_2 feed strategy for growing *Chlorella* sp. FC2 IITG towards biodiesel production is proposed in medium-scale BC-PBR. To determine whether the proposed strategy could enhance the cell density of FC2, following sequence of experiments were conducted.

a. Other known strategies namely: constant CO_2 (% in air) feed; biomass-density based feed and; pH-control based CO_2 feed were investigated to compare with the proposed strategy under simulated sunlight. While comparing the above strategies, the effects of high CO_2, pH and DO accumulation on growth inhibition were mainly accounted.
b. To understand DO inhibition on FC2, the proposed strategy was tested at low DO accumulation levels.
c. Consequently, the proposed CO_2 feed strategy was applied under natural sunlight to perform two separate experiments on single-stage and two-stage lipid induction processes for biodiesel production.
d. Additionally, the effects of scale-up and specific light availability on lipid induction process were also investigated in small-scale BC-PBRs along with medium-scale BC-PBR. Note that the small-scale experiments were performed purely for obtaining additional information on scale-up losses (if any) and light-dependent lipid induction (refer chapter 7), related to the biodiesel production.

6.2 Experimental setup

All the experimental studies of indoor (diurnal simulated sunlight) and outdoor sunlight were carried out in the medium-scale BC-PBR (Fig. 6.1), shown below. Probes for measuring dissolved oxygen (DO), temperature and pH were located at the top end of the PBR. Monitoring and control of pH, CO_2 flow rates, and the LED light intensity were accomplished by the OPTO22 control unit.

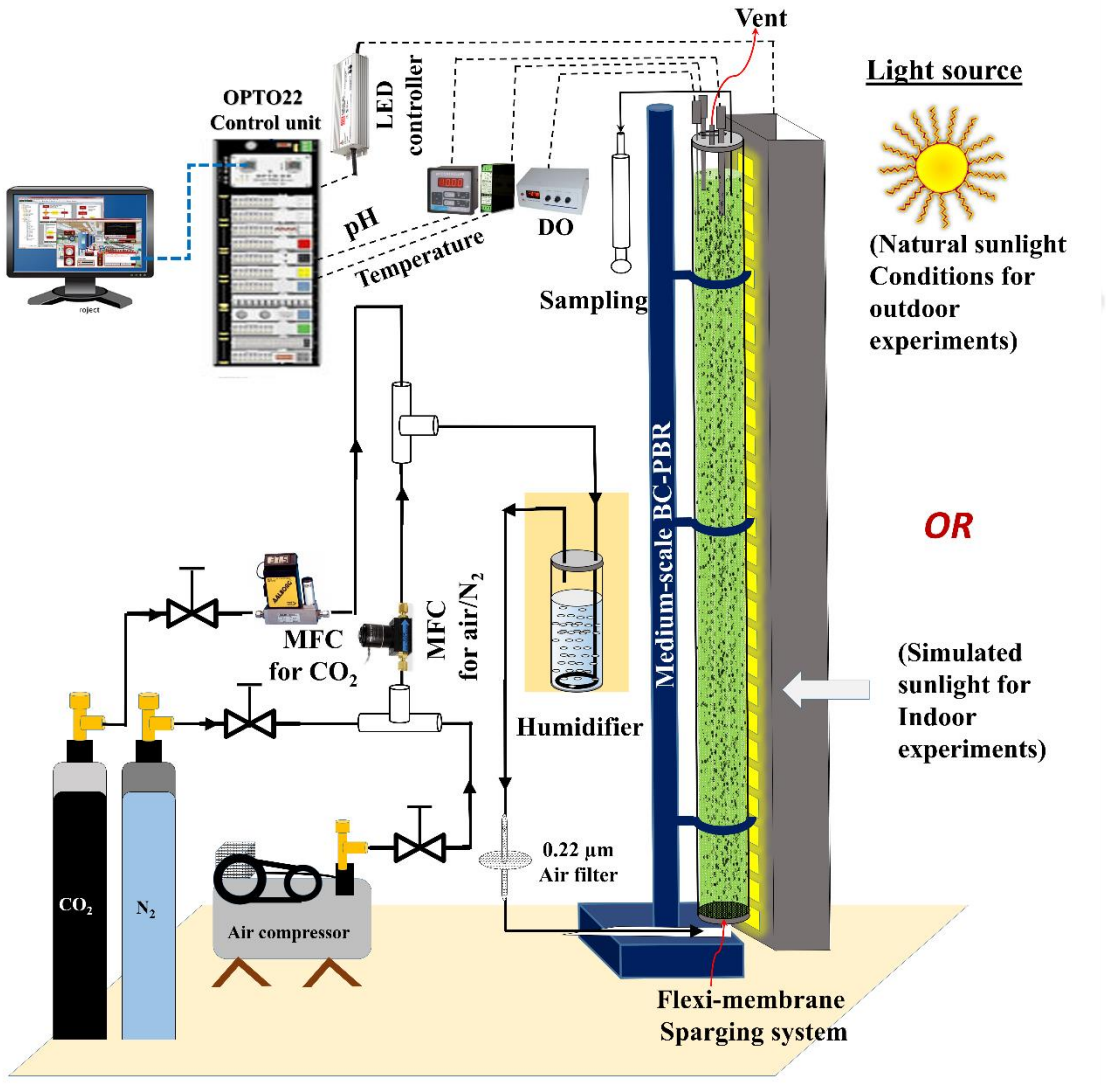

Fig. 6.1 Schematic of medium-scale BC-PBR showing the essential components.

6.2.1 Performance under indoor growing conditions

FC2 growth studies were firstly investigated in indoor using different CO_2 feed strategies. For constant lighting conditions, 10:14 h (similar to small-scale BC-PBR

studies)_ of light:dark cycle was followed under 1130 µmol m^{-2} s^{-1} of light intensity (optimum of constant light intensities). For simulated diurnal sunlight conditions, 12:12 h of light:dark cycle was followed based on a day of May month (Guwahati, India) (Fig. 4.5). The CO_2 enriched air flow rate was kept as 0.75 L min^{-1} (0.08 VVM) for medium-scale (10 L) BC-PBR in all the experimental studies. The CO_2 feed was shut during dark cycles representing absence of photoreaction, though the air flow was undisturbed to avoid settling and to facilitate respiration.

6.2.1.1 Constant 2% CO_2 feed

As mentioned in the chapter 5, constant 2% CO_2 in air (3.34 cm s^{-1} superficial velocity) was determined as optimum CO_2 level for FC2 growth in small-scale BC-PBR (H:175 mm, OD: 75 mm, ID: 69 mm and working volume 500 ml) under constant light intensity of 1130 µmol m^{-2} s^{-1} (typical average sunlight intensity throughout the day at experimental area) with 10:14 light/dark period. Therefore, the performance of medium-scale (10 L) BC-PBR was firstly evaluated by using same CO_2 feed condition under diurnal simulated sunlight (12:12 h as light/dark period) to investigate the effect of diurnal lighting on FC2 growth in comparison with constant lighting. To analyze the results more precisely, another growth study was conducted to compare scale-up effect on the FC2 growth, i.e. small-scale study (refer Chapter 5) vs medium-scale study with same CO_2 condition under constant light intensity of 1130 µmol m^{-2} s^{-1}.

6.2.1.2 Biomass-density based CO_2 feed under diurnal simulated sunlight

The variation of CO_2 levels with biomass density was investigated in medium-scale BC-PBR by maintaining at 2% on first day, 2.5% on second day and 3% for the rest of culturing time. Based on the 48 h growth profiles of FC2 at 0.04, 1, 2, 3, 5, 10 and 15%

constant CO_2 levels (extracted and modified from chapter 5), 2 and 3% CO_2 levels were selected as lower and upper limits.

6.2.1.3 pH-control based CO_2 feed under diurnal simulated sunlight

Two types of pH-control based CO_2 feed strategies were examined in medium-scale BC-PBR. In Type-I, CO_2 was fed continuously to control the pH at 5.8 only during light periods, whereas the CO_2 feed was stopped during the dark periods. The pH 5.8 was chosen based on the pH observed in small scale experiment (refer chapter 5) with optimum CO_2 level (2% in air) for FC2 growth and this acidic pH was believed to be more favourable for algae growth than alkaline pH (Scherholz & Curtis, 2013). It should be noted that control of pH by NaOH/HCl is not required for FC2 growth, studied previously in chapter 5. Based on the performance of Type-I strategy, an alternative Type-II strategy was proposed to increase pH set points dynamically during the course of growth, wherever applicable. In Type-II strategy, the pH set points were kept at 5.8 for first 2 days, 6.3 for next 3 days and 6.7 for the rest of culturing time. Note that the CO_2 feed for pH-control was carried out only during simulated daylight condition.

6.2.1.4 Real time light based CO_2 feed under diurnal simulated sunlight condition

In this strategy, the CO_2 supply was regulated proportionately to the incident light intensity for growing the FC2 in medium-scale scale BC-PBR. As a preliminary real time light based strategy, CO_2 levels in air were maintained as 2% at low light (< 800 µmol m^{-2} s^{-1}), 2.5% at moderate light (800 – 1700 µmol m^{-2} s^{-1}) and 3% at high light (1700 – 2100 µmol m^{-2} s^{-1}) intensities throughout the daylight equivalent period (Table 6.1). Subsequent to the growth-phase, the lipid induction was carried out by two-stage lipid induction strategy. For lipid induction, the biomass was harvested by centrifuging at 3000 RPM for 5 min followed by washing and re-suspended in 9.6 L of fresh N-free BG11 medium. The

FC2 biomass with N-free BG11 medium was transferred to same 10 L BC-PBR under same diurnal LED lighting and CO_2 feed conditions.

Table 6.1 Real time light based CO_2 feed strategies followed in the indoor and outdoor experiments.

Light intensity (I) (µmol m^{-2} s^{-1})	**CO_2 flow rate (% in air/N_2)**
Prototype of novel real time light based CO_2 feed (indoor using LED)	
$0 \leq I < 800$	2.0
$800 \leq I < 1700$	2.5
$1700 \leq I < 2100$	3.0
Fine-tuned real time light based CO_2 feed (outdoor)	
$0 \leq I < 100$	0.5
$100 \leq I < 450$	1.0
$450 \leq I < 800$	1.5
$800 \leq I < 1300$	2.0
$1300 \leq I < 1700$	2.5
$1700 \leq I$	3.0

6.2.1.5 Real time light based CO_2 feed at low DO levels under diurnal simulated sunlight condition

There was a significant amount of DO accumulation in all the above strategies, which is comparable with inhibitive values of some particular species. For example, the specific growth rate was linearly decreased when *Nannochloropsis* sp. was cultured beyond the DO level of 75% air saturation at 100 µmol m^{-2} s^{-1} (Raso et al., 2012). Hence, it was imperative to check the effect of DO accumulation on the FC2 growth. As the DO accumulation in the real time light based strategy with air as aeration medium, was resulted up to 135% air saturation (almost near to the 150% air saturation, that observed in the cases of biomass-density and single point pH-control based strategies) (Fig. 6.4D, 6.6C and 6.7D), the growth of FC2 was investigated at very low DO condition under diurnal LED light to check the effect of DO accumulation in the culture**.** In this study, the DO accumulation was minimized by sparging CO_2 enriched N_2 instead of CO_2 enriched air during light periods only in the 10 L BC-PBR. However, in the night periods, the air only was used as aeration

medium. The CO_2 feed strategy (% CO_2 in N_2) was kept same as light based CO_2 feed strategy where CO_2 enriched air was used (Table 6.1). For further enhancement of FC2 biomass production, the DO accumulation was taken into consideration by decreasing the DO levels in the experiment of real time light based strategy. Therefore, in this study, the strategy was re-examined by using N_2 as aeration medium instead of air. The CO_2 enrichment in N_2 was followed same as in section 6.2.1.4, i.e., preliminary real time light based CO_2 supply.

6.2.2 Outdoor studies under natural sunlight using real time light based CO_2 feed

Under natural sunlight, FC2 culture was firstly grown in medium-scale BC-PBR with the preliminary light based CO_2 feed strategy that was used in the indoor study. However, later experiments in the outdoor were conducted using a fine-tuned strategy (Table 6.1) due to the failure of first outdoor study (discussed later). Two sets of 'growth' experiments were conducted in September 2018 and October 2018 where two-stage and single-stage lipid induction processes were followed respectively for biodiesel production. In the single-stage induction process, the FC2 culture was allowed to consume all the N-source (i.e., urea) for its growth and therefore automatic lipid induction stage begins due to zero/low nitrogen substrate in the medium-scale BC-PBR. In the two-stage process, the biomass from medium-scale PBR was harvested at the end of growth phase (i.e., early stationary phase) by centrifugation at 3000 RPM for 5 min followed by washing. The harvested biomass was re-suspended in 9.6 L (working volume of medium-scale BC-PBR) of fresh N-free BG11 medium (without urea).

For checking the effect of scale-up and specific light availability on lipid production, three experiments of two-stage lipid induction process were conducted. From the 9.6 L of re-suspended FC2 culture after harvesting, 8.85 L was transferred to medium-scale BC-PBR. The remaining amount of 0.75 L was transferred to two small-scale BC-

PBRs each one having 0.5 L (for scale-up effect) and 0.25 L. To the small-scale BC-PBR having 0.25 L culture, 0.25 L of N-free BG11 medium was added for decreasing light distribution per cell (specific light availability) to half of the PBR having 0.5 L culture. The air/CO_2 conditions in dark cycles and the aeration rates (VVM) in the outdoor studies were followed same as indoor studies.

6.3 Results and discussion

6.3.1 Influence of various CO_2 feed strategies under simulated sunlight condition

6.3.1.1 FC2 growth at constant 2% CO_2 feed

In this experiment, the FC2 could grow up to maximum biomass concentration of 4.26±0.09 g L^{-1} with biomass productivity of 0.27± 0.01 g L^{-1} day^{-1}. However to reach such biomass density, the strain took a long culturing time of 16 days (Fig. 6.2C). The CO_2 feed and lighting conditions were shown in Fig. 6.2A. The pH was decreased from 5.8 to 5.0 initially in light period (Fig. 6.2B) and later it was increased up to 7.5 by the end of growth phase. Thus the delayed biomass growth in medium-scale BC-PBR could definitely not due to low pH as the strain was able to grow at same rate in a wide pH range of 4.5 - 7.5, reported previously in chapter 5.The urea was also not limiting and phosphate was fed when its concentration dropped below half of initial concentration (Fig. 6.2D). For checking the reason of lowered biomass productivity in this study, another experimental study in medium-scale PBR was conducted under constant lighting and 2% CO_2 feed conditions that were followed in the previous small-scale study (refer chapter 5). In small-scale (0.175 m height) and medium-scale (2.75 m height) PBRs, the 4-day biomass titers were 4.33 and 3.15 g L^{-1} respectively (Fig. 6.3). The corresponding biomass productivity was observed lower in the medium-scale PBR as a result of scale-up effect. This could be due to the height of 10 L scale PBR that possibly triggered CO_2 limitation and/or DO build-up at

upper portion of the reactor. The biomass titer in medium-scale PBR under diurnal light resulted 2.1 g L^{-1} on 4^{th} day, which was lesser than the growth in both small-scale and medium-scale scale PBRs under constant light (Fig. 6.2C and Fig. 6.3). This could be attributed to the continued light limitation effect caused by diurnal lighting conditions and the scale-up effect. Overall, the reason for lowered biomass growth and productivity in the medium-scale BC-PBR could be caused by light limitation, CO_2 limitation and/or oxygen build up (due to scale-up effect), but not due to nutrient limitation or pH effects. Since the diurnal nature of the sunlight is a natural phenomenon, only the impacts of CO_2 limitation and oxygen inhibition were addressed further through various CO_2 feed strategies.

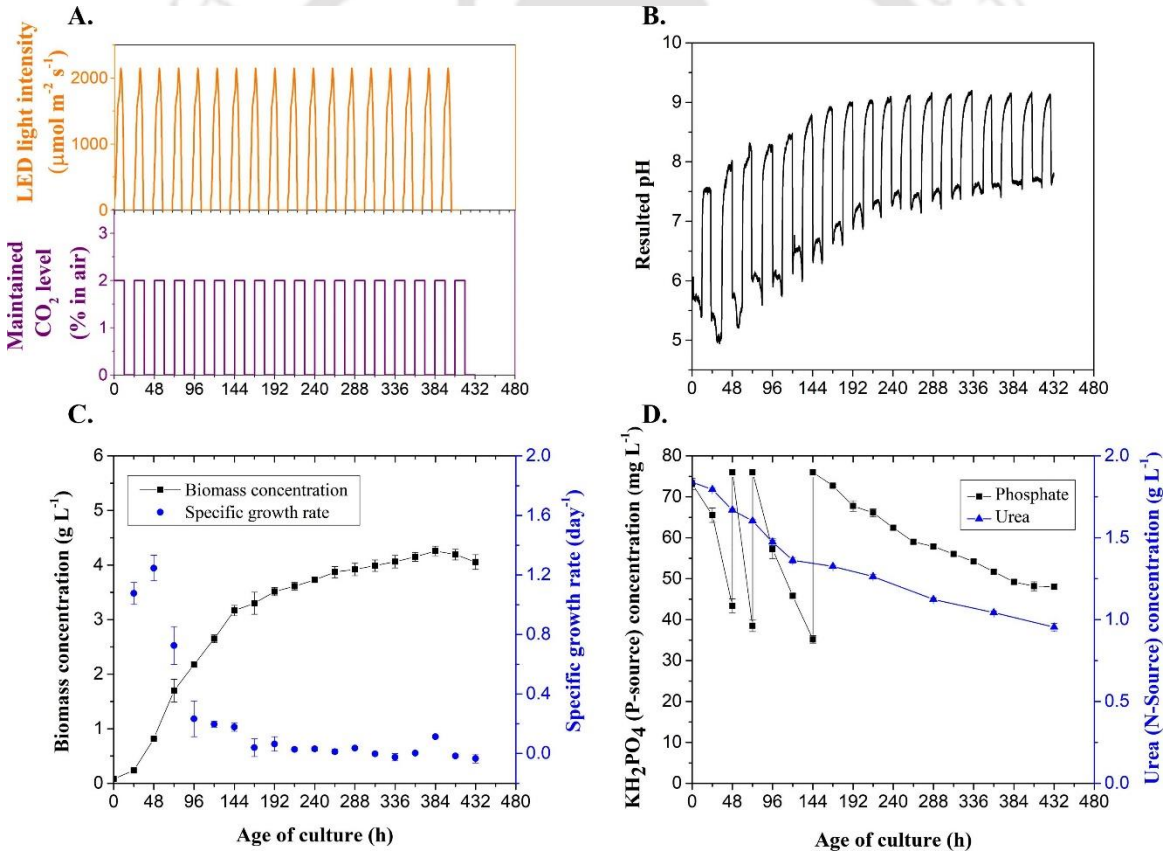

Fig. 6.2 FC2 growth at constant 2% CO_2 (in air) under simulated diurnal sunlight (indoor). A) Simulated supply light intensity at source (top) and CO_2 feed (bottom) during artificial diurnal light cycles (12:12 h of light:dark cycle), B) pH of culture medium during the growth of FC2, C) Biomass growth (square) and specific growth rates (circle) of FC2 during the culturing time and D) Dynamic phosphate (square) and urea (triangle) consumption along with the addition of phosphate intermittently.

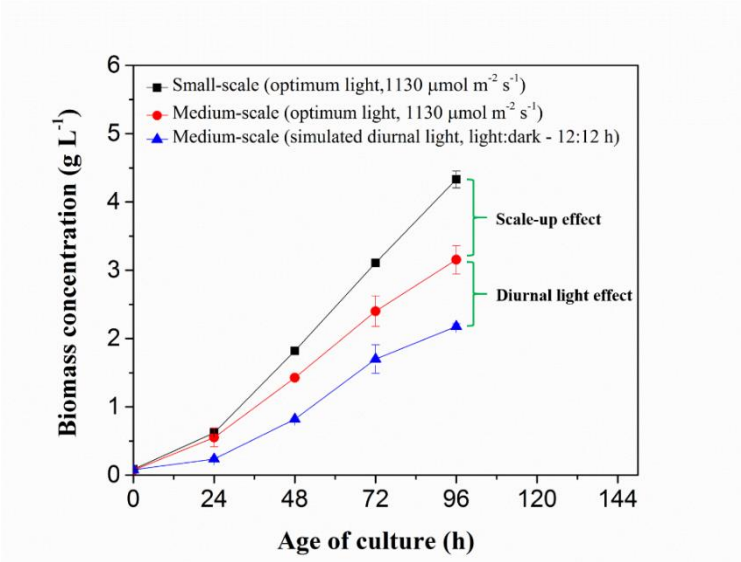

Fig.6.3 Effect of PBR scale up and diurnal light on FC2 growth at constant 2% CO_2 level.

6.3.1.2 FC2 growth using biomass-density based CO_2 feed strategy

During growth period, the CO_2 uptake rate is expected to increase with time due to the increment in biomass-density day by day. Therefore, it is desirable to increase the CO_2 supply as a simple strategy for addressing potential CO_2 limitation. In the strategy employed in this experiment, CO_2 levels (% in air) were elevated day wise as 2% for 1st day, 2.5% for 2nd day and 3% for 3rd day to the end of culture (Fig. 6.5A). The lower and upper limits of CO_2 were chosen based on the optimum and inhibition levels observed in the 500 mL scale cultures of the same strain, studied in chapter 5 (Fig. 6.4).

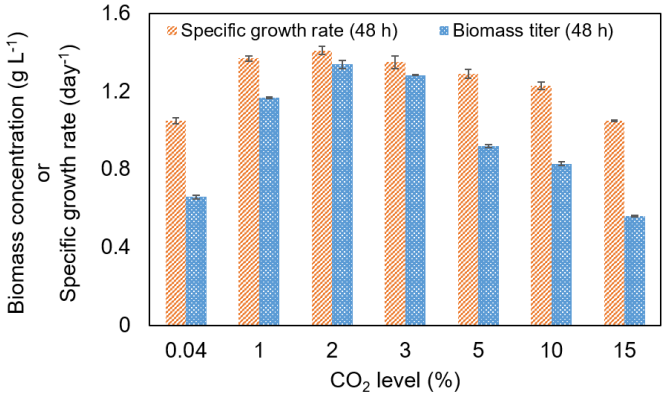

Fig. 6.4 FC2 growth (at 48 h) at different constant CO_2 level (% in air) under constant LED light at 1130 µmol m^{-2} s^{-1} (10:14 h of light:dark cycle) in small-scale BC-PBR. Data is extracted from chapter 5.

In the strategy, the measured biomass yield was 2.27±0.14 g L^{-1}, which was lower than for the constant 2% CO_2 level (Fig. 6.2C and 6.5C). When the cell growth was same up to 3 days of culturing (1.7 g L^{-1}) in both the cases of biomass-density based CO_2 feed (2→2.5→3%) and constant 2% CO_2, the specific growth rate in the case of biomass-density based strategy (0.2 day^{-1}) was less than for the constant 2% CO_2 level (0.3 day^{-1}) (Fig. 6.2C and 6.5C). The recorded pH values due to combined effects of metabolism and CO_2 supply were observed in the range of 5-6, which is tolerable for FC2 growth (Fig. 6.5B). Strangely, a maximum dissolved oxygen (DO) of 150% air saturation was recorded consistently from third day to the end of culturing period (Fig. 6.5D). This phenomenon was not observed with the other CO_2 feed strategies investigated in this study. One possible reason is that the constant maintenance of 3% CO_2 level might have induced the FC2 cells to release constantly high DO into the growth medium. Another reason could be that the ratio of CO_2 to light intensity also increased with the day-wise step increment of CO_2 levels during the lower lighting periods of the diurnal cycle (i.e., morning and evening times). Also, the light intensity at a point inside the reactor decreases with the increased in biomass density in the exponential phase of growth cycle. High CO_2 to light intensity ratio and high DO conditions have been observed to cause growth inhibition in the case of cotton leaf photosynthetic process (Woo & Wong, 1983). From the outlined observations and reported study, a novel real time light based CO_2 feed strategy was proposed, developed, and demonstrated from this study and is covered later in chapter 7.

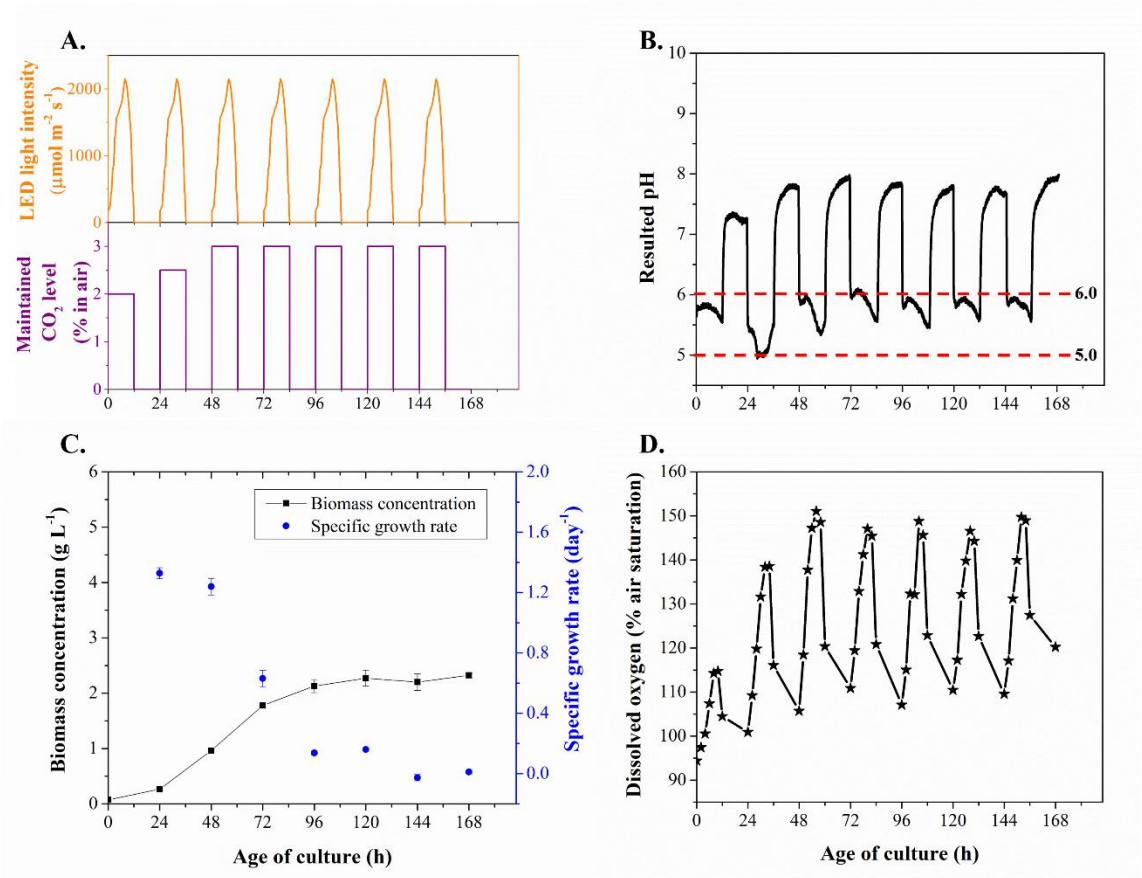

Fig. 6.5 FC2 growth using biomass-density based CO_2 feed strategy under simulated diurnal sunlight (indoor). A) Simulated supply light intensity at source (top) and CO_2 feed (bottom) during artificial diurnal light cycles (12:12 h of light:dark cycle), B) pH of culture medium during the growth of FC2, C) Biomass growth (square) and specific growth rates (circle) of FC2 during the culturing time and D) DO concentration during the culturing time. The experiment was conducted in duplicate to confirm the results.

6.3.1.3 FC2 growth using constant (Type-I) and dynamic (Type-II) set point pH-control based CO_2 feed strategies

In Type-I pH-control based CO_2 feed strategy, the growth of FC2 could reach only up to 2.63±0.05 g L^{-1} by the end of 6 days (Fig. 6.6B). The reason for this lower biomass concentration could be due to increased CO_2 levels beyond the inhibition range after 72 h (Fig. 6.6A). To maintain the desired pH of 5.8 in the FC2 culture, the pH-control unit raised CO_2 levels to more than 5% (in air) after 72 h and thereafter reached up to 14% (Fig. 6.6A and 6.6B). Note that the CO_2 levels of 5%, 10% and 15% (in air) are inhibitive to the FC2 (refer chapter 5 and Fig. 6.4). Apart from the CO_2 inhibition, a highest DO of 150% air

saturation was observed only on fourth day and thereafter it was decreased and dropped till 115% air saturation (Fig. 6.6C). The decrease in DO from 150% to 115% air saturation could be attributed to lowered photosynthetic rates due to raised CO_2 levels (> 5% in air) beyond the inhibition range (Fig. 6.6A).

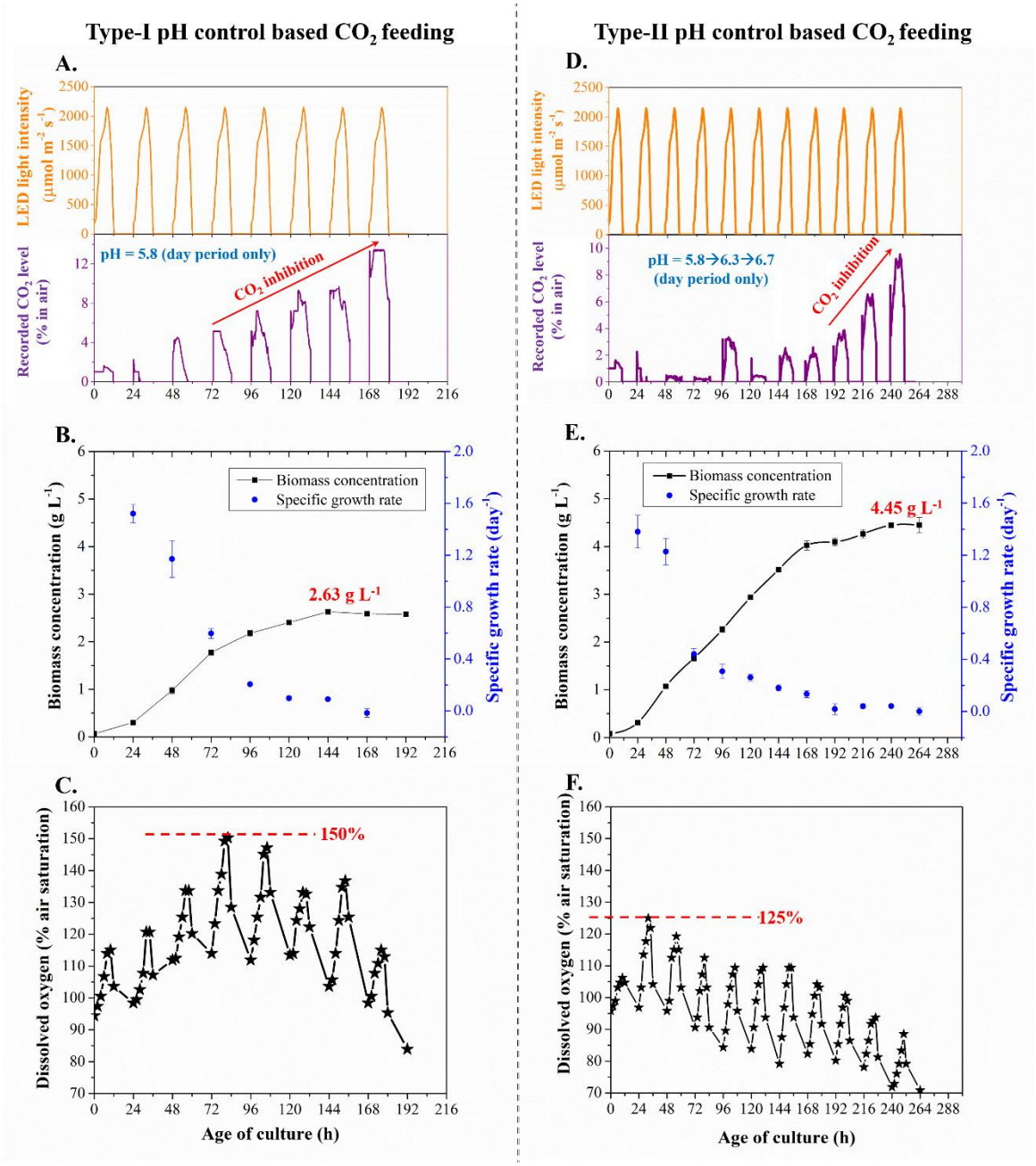

Fig. 6.6 FC2 growth using pH-control based CO_2 feed strategy under simulated diurnal sunlight (indoor). A and D) Simulated light intensity (top) and resulted CO_2 feed due to maintenance of pH (bottom) during artificial diurnal light cycles (12:12 h of light:dark cycle), B and E) Biomass growth (square) and specific growth rates (circle) of FC2 during the culturing time and C and F) Dissolved oxygen concentration with respect to age of culture. A, B and C for Type-1 pH control based CO_2 feed strategy and D, E and F for Type-II pH control based CO_2 feed strategy.

Since the single set point pH-control based CO_2 feed strategy caused the CO_2 levels to rise beyond the inhibition range, the set point had to be increased to decrease the supply of CO_2 for minimizing typical CO_2 inhibition. Experimental pH set points were therefore kept at 5.8 for first 2 days, 6.3 for next 3 days and 6.7 thereafter in the dynamic pH-control based CO_2 feed strategy. The final biomass titer was 4.45±0.05 g L^{-1} with a little improvement in comparison with above two strategies (Fig.6.6E). However, the CO_2 levels overshot the inhibition range (> 5% in air) even when the pH was controlled at 6.7 (Fig. 6.6E). Compared to the single set point pH-control strategy, the rise in CO_2 levels in the dynamic pH-control strategy started late after 8 days of culturing (Fig. 6.6D). These raised CO_2 levels were reached up to 10% by the end of 10 days, where the stationary phase was occurred thereafter. Similar to the Type-I strategy, the DO in Type-II strategy was 125% air saturation on 2nd day but it was decreased further due to rise in CO_2 levels only. It could be interpreted that the alkalinity of this particular strain's culture medium would be increasing during the 'control of pH by CO_2 supply'. In this case, both the pH-control based CO_2 feed strategies were unsuitable for achieving high cell densities under diurnal light, primarily due to rise in CO_2 levels beyond the inhibitory levels. However, under the diurnal light, the Type-II strategy might have scope for improvement if the set points are close enough to avoid CO_2 limitation (especially during 3 – 4 days) and inhibition (during 8 – 10 days) (Fig. 6.6E).

6.3.1.4 FC2 growth using real time light intensity based CO_2 feed strategy

The rationale for developing a real time CO_2 feed strategy based on the diurnally varying light intensities was drawn from outcomes of reported studies on cotton plant leaves and *Nannochloropsis salina* (Malek et al., 2016; Woo & Wong, 1983). Hence, a novel prototype of a real time light based CO_2 feed strategy was required to provide high CO_2 at

high light and vice-versa under typical diurnal light cycle shown in Table 6.1. Experimental results are presented in Fig. 6.7.

Based on varying average light availability, a model-based CO_2 feed was not feasible as the light distribution becomes zero very soon at 0.67 g L^{-1}. Therefore, the CO_2 was purged proportionately to the magnitude of incident light intensity by keeping 2% and 3% CO_2 levels as lower and upper limits respectively (Fig. 6.7A and Table 6.1). The limits for light-based CO_2 feed were selected on the basis of optimum FC2 growth at various CO_2 levels (Fig. 6.4). The results show a final biomass titer of 5.12±0.30 g L^{-1} in growth phase with an overall biomass productivity of 0.57±0.03 g L^{-1} day^{-1} within 9 days of culturing (Fig. 6.7C and Table 6.2), higher than other known strategies investigated in this part of study under diurnal simulated sunlight conditions (shown in additional information, section 3, appendices). The DO accumulation inside the culture reached a maximum value of 135% air saturation during 4^{th} and 5^{th} daylight cycles and decreased from 6^{th} daylight cycle (Fig. 6.7D). The resulting pH values due to CO_2 supply and cell's metabolism were in the range of 4.8 – 6.5 (Fig. 6.7B).

After the growth phase, the cells were transferred to N-free BG11 medium for biodiesel production using two-stage lipid induction strategy under same diurnal lighting (described in materials and methods section). The FAME analysis and results were shown in Table. 6.2, where all the FAME results were compared (discussed in section 6.3.3). After 24 days of induction, highest FAME content of 30.81% was obtained with maximum biodiesel concentration of 2.12 g L^{-1} (productivity, 77.92 mg L^{-1} day^{-1}, based on induction period). Based on the resulted maximum biomass titers in all the above indoor studies under diurnal light, highest biomass titer and biomass productivity were obtained in case of real time light based CO_2 feed strategy (Table 6.2). Hence, low CO_2 at low light and high CO_2 at high

light (the ratio of CO_2/light) is crucial for achieving high cell densities and productivities under diurnal light.

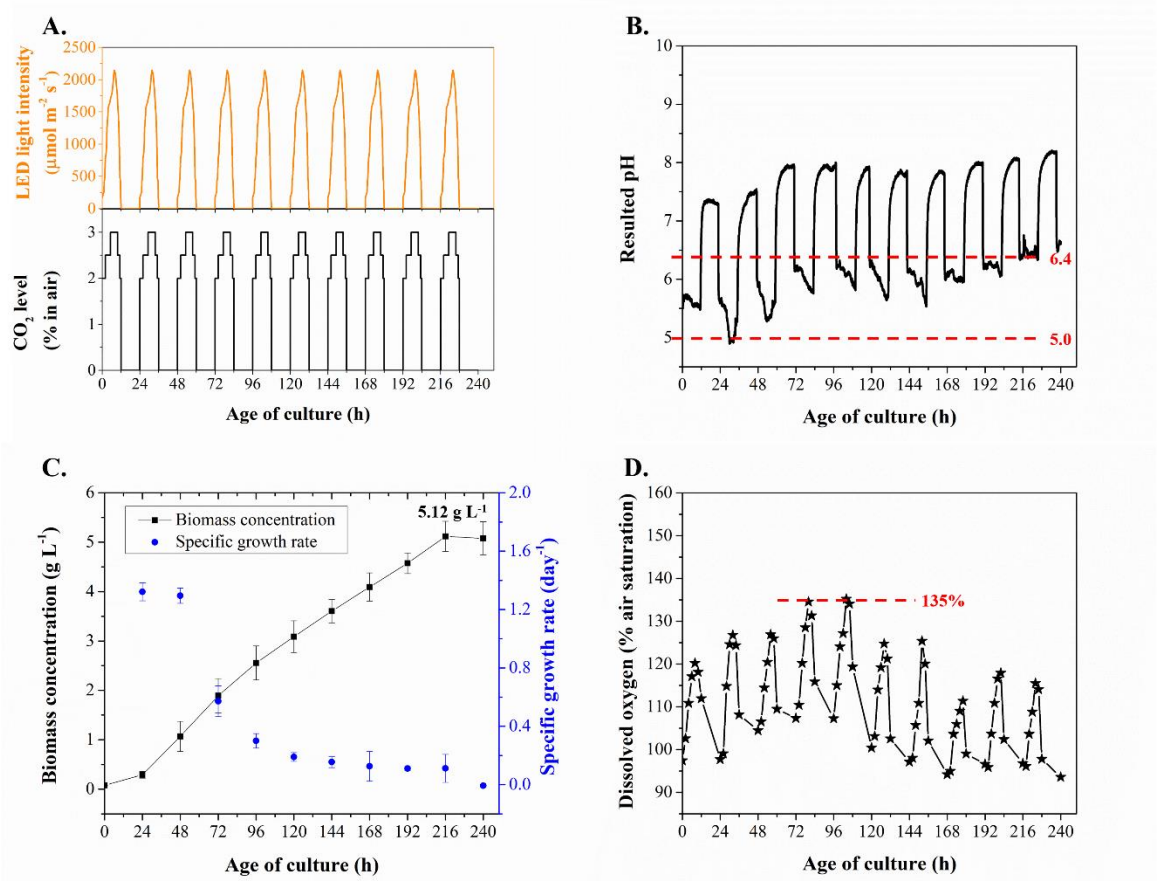

Fig. 6.7 FC2 growth using real time light based CO_2 feed strategy under simulated diurnal sunlight (indoor). A) Simulated light intensity (top) and CO_2 feed (bottom) during artificial diurnal light cycles (12:12 h of light:dark cycle), B) pH of culture medium during the growth of FC2, C) Biomass growth (square) and specific growth rates (circle) of FC2 during the culturing time and D) Dissolved oxygen concentration with respect to age of culture.

6.3.1.5 FC2 growth under low dissolved oxygen (DO) using CO_2 enriched N_2

In this study, the CO_2 feed strategy was followed same as the prototype of real time light based CO_2 feed strategy where N_2 was used instead air as aeration medium (Table 6.1). Under low DO conditions, there was a slight improvement in biomass productivity of 0.64±0.01 g L^{-1} day^{-1} (Fig. 6.8) with the similar maximum biomass titer of 5.10±0.09 g L^{-1} that observed in the previous experiment (section 6.3.1.4).

This study was performed as significant DO accumulation of 125 – 150% air saturation was observed in the above CO_2 feed strategies, which is comparable with inhibition DO values of some particular species. For example in *Nannochloropsis* sp., the specific growth rate was linearly decreased when the DO levels were raised above 75% air saturation at 100 µmol m^{-2} s^{-1} (Raso et al., 2012). Therefore, it was deemed imperative to study the effect of DO accumulation on FC2 growth. Since the low DO condition offered same biomass titer in one-day advance when compared with CO_2 enriched air, N_2 is not an economical option as compared to air as aeration medium. Hence the CO_2 enriched air was followed in the subsequent outdoor cultivation studies. Also, it was understood that DO accumulation up to 150% air saturation cannot affect the growth of FC2 in the medium-scale BC-PBR with the specified conditions.

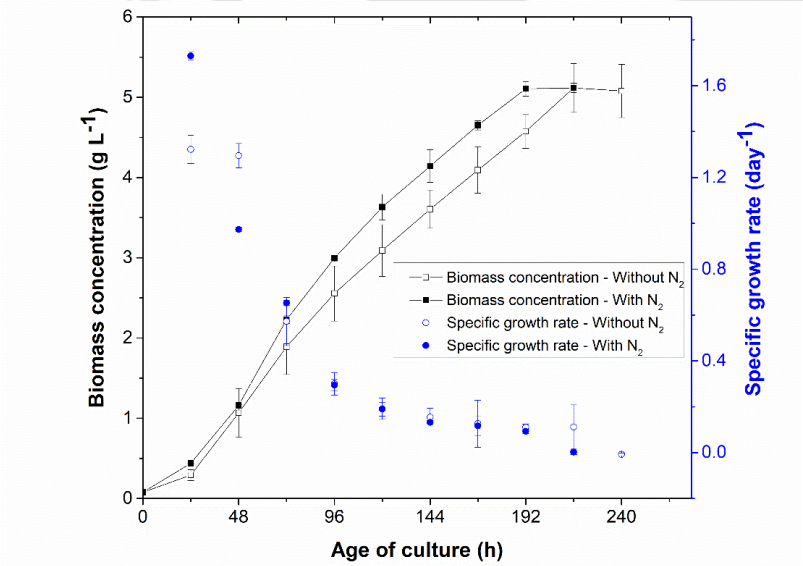

Fig.6.8 Comparison of FC2 growth at low DO and significant DO conditions using real time light based CO_2 feed strategy under simulated sunlight.

6.3.2. Outdoor experiments under natural sunlight

6.3.2.1 Two-stage lipid production using real time sunlight based CO_2 feed strategy

On the basis of outcomes from the studies under simulated sunlight conditions, prototype light based CO_2 feed strategy using air was applied for outdoor studies under natural sunlight. In the initial experiment, FC2 cells died (culture colour was turned from

green to white) unexpectedly possibly due to the sudden drop of culture pH (< 2.5) on second day. This lower pH range had not been observed in controlled lab conditions (lowest pH was 4.8 on day 2). It had been previously established that the FC2 strain could grow well up to a lower pH of 4.5 without requirement for pH control (see chapter 5). The acidification in the outdoor conditions would have occurred due to the release of H^+ ions or organic/inorganic acids. The HPLC analysis of 'growth medium without cells did not reveal formation of acids. Hence, the drop of pH may be attributed to some abnormal cellular activities leading to the acidification of growth medium. However, the reason for this sudden drop in pH was not investigated further.

In the subsequent outdoor studies, the pH was controlled immediately using 4 N of NaOH (one-shot) when the pH was dropped down to 3.5 on day 2 morning (Fig. 6.9). The culture pH was remained above 4.5 (inhibition point) throughout the remaining growth period. Prior to the recorded low pH, FC2 cells had also experienced a maximum DO value of 222% of air saturation on first day, suggesting an exceptionally high photosynthetic rate in the outdoor culture conditions compared to indoor cultures. The maximum DO concentrations were 120% (on day 1) and 135% (overall) of air saturation in the indoor study with prototype of real time light based strategy (Fig. 6.7D). This could have been caused by higher light availability in the outdoor cultures.

Since, high DO was observed in the outdoor culture, the prototype light based CO_2 feed used in the indoor was fined-tuned based on the report on cotton plant leaf at different partial pressure of CO_2 and light intensity conditions under varying partial pressures of O_2 (Woo & Wong, 1983). In the study, the CO_2 assimilation rate under low light condition and O_2 partial pressure of 200 mbar was decreased at CO_2 partial pressure of 900 µbar as compared to the 300 µbar. Conversely, the CO_2 requirements was vice versa under high

light condition and same O_2 partial pressure. And this phenomenon was intensified upon elevated O_2 partial pressures around the leaf.

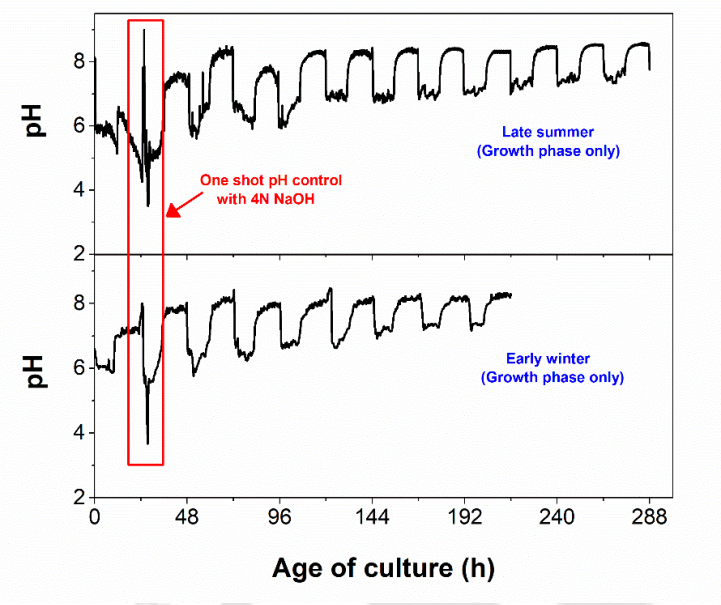

Fig. 6.9 One-shot pH control during the FC2 growth of diurnal-sunlight based CO_2 feed strategy in outdoor experiments conducted in late summer (top) and early winter (bottom).

Based on the above information, the prototype of CO_2 feed was fine-tuned by decreasing CO_2 levels further at low light regimes (morning and afternoon times, < 1300 µmol m^{-2} s^{-1}) under sunlight (Table 6.1) and used to grow FC2 by two-stage lipid induction strategy. Based on the real time fluctuations of natural sunlight intensity (Fig. 6.10A), the CO_2 level was manipulated at every 30 min interval as per bands prescribed in the Table 6.1. The CO_2 flow rates, outdoor temperatures, sunlight intensity, DO and culture temperatures recorded are shown in Fig. 6.10A and 6.10B. It is shown that under the fine-tuned real time light CO_2 feed, the FC2 was grown up to maximum biomass titer of 6.8±0.2 g L^{-1} (8 days) corresponding to biomass productivity of 0.85±0.03 g L^{-1} day^{-1} (only growth phase) (Fig. 6.10C). The phosphate (added intermittently for maintaining at least half of optimum concentration) and urea consumption were shown in Fig. 6.10C. For lipid induction, the culture was transferred to N-free BG11 medium on the eighth day when the biomass concentration was 6.8 g L^{-1} in the medium-scale BC-PBR.

In order to determine the effect of light limitation and scale-up, the culture from the medium-scale BC-PBR was aliquoted into two small-scale PBRs of same diameter. In the first one, N-free original culture was tested without dilution, referred as control experiment for both light limitation and scale-up. In the second PBR, the culture was diluted to 3.4 g L^{-1} (250 ml of N-free original culture and 250 ml of N-free medium) to determine the effect of light limitation on lipid production. By diluting the culture, specific light availability (light per cell) can be increased such that lipid content can also be increased as observed in a recent study (Munkel et al., 2013). The time dependent biodiesel content (% of cell dry weight) and biodiesel concentrations (g L^{-1}) of both indoor and outdoor studies were evaluated (Fig. 6.11). The results revealed that both specific light availability and scale-up affects the lipid content of FC2 biomass (see discussion in later section 6.3.3). In the study of small-scale (diluted), the biodiesel content of 55.47% was observed on 16 day of induction phase, higher than small-scale (original) and medium-scale (original) cultures (Table 6.2). The small-scale (original) and medium-scale FC2 cultures exhibited 42.29% (20 days) and 34.86% (20 days) of biodiesel contents respectively (Table 6.2). This suggested that the scale-up resulted in decreased lipid content (see discussion in later section 6.3.3).

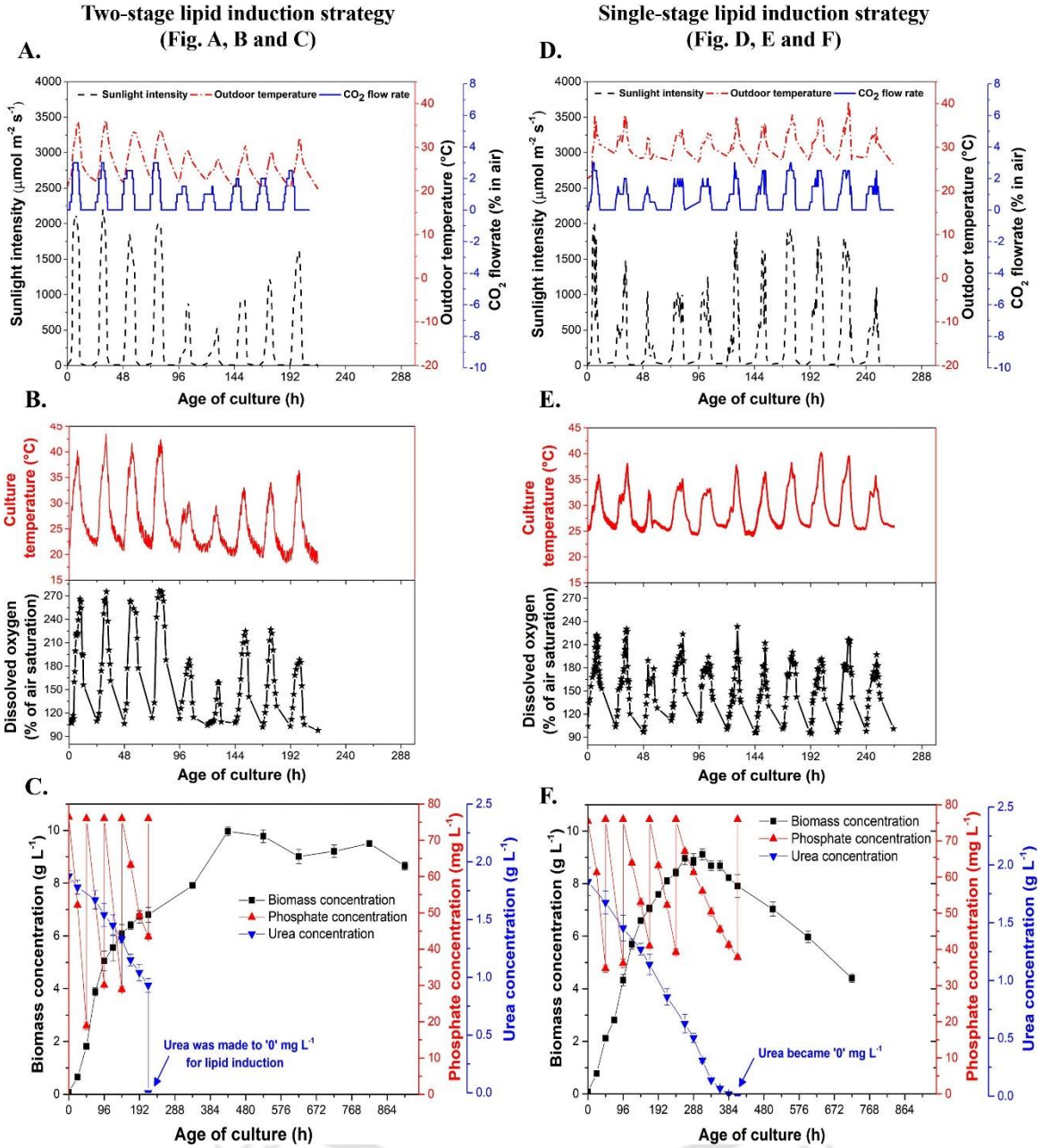

Fig. 6.10 FC2 growth using real time sunlight intensity based CO_2 feed strategy under natural diurnal sunlight conditions (outdoor). A and D) diurnal sunlight intensity, maintained CO_2 flow rates and outdoor temperature, B and E) resulted culture temperature and dissolved oxygen concentrations during the culturing time and C and F) Biomass growth (square), urea (down triangle) and phosphate (up triangle) during the culturing time. A, B and C for two stage experiment conducted in September, 2018 and D, E and F for single stage experiment conducted in October, 2018

6.3.2.2 Single-stage lipid production using real time sunlight based CO_2 feed strategy

The centrifugation step used for transferring the cells into N-free medium for lipid induction is energy intensive. In order to avoid the cost of centrifugation and wastage of growth media water in two-stage process, single-stage lipid induction process was studied. In this process, the culture was allowed to consume all the urea (N-source) after the growth-phase and to enter the lipid induction stage directly. The fine-tuned real time sunlight based CO_2 feed was used for growth as well as lipid induction in the single-stage process under sunlight along with intermittent phosphate supplementation (Fig. 6.10D and 6.10F). Interestingly, the observed FC2 growth resulted a maximum biomass titer of 9.0±0.2 g L^{-1} within 11 days corresponding to biomass productivity of 0.82±0.02 g L^{-1} day^{-1} (Fig. 6.10F). Even though urea was consumed totally by the end of growth-phase, death phase was appeared instead of continuing for lipid induction phase after a prolonged stationary phase (Fig. 6.10C). The culture density decreased to 4.4 g L^{-1} after 13 days of presumed induction phase (Fig. 6.10C). Therefore, single-stage lipid induction process was deemed to have failed to produce biodiesel from the FC2 strain under natural sunlight. However, enhanced cell density of FC2 biomass feedstock could be highly beneficial for thermochemical conversion of biomass feedstock into other biofuels and value added chemicals.

The FC2 cells grown in two-stage process experienced fewer fluctuations in incident sunlight intensity as compared to the single-stage process (Fig. 6.10A and 6.10D). However, poor light intensities from 5^{th} day onwards decreased the final biomass titer in the two-stage process as compared to the single-stage process (Fig. 6.10A, 6.10C, 6.10D and 6.10F). The DO accumulation was also observed higher in case of two-stage process, especially during the early stages of culturing when the lighting conditions were favourable (Fig. 6.10B and 6.10E). Using the fine-tuned CO_2 feed and one-shot pH control, FC2 was

grown successfully up to 6.8 g L^{-1} (growth-phase) in two-stage and 9.0 g L^{-1} in single-stage lipid induction strategies respectively (Fig. 6.10C and 6.10F). As would be expected, the biomass titers of FC2 in outdoor studies were higher than the indoor studies due to more favourable lighting conditions. This outdoor 9.0 g L^{-1} of biomass titer was highest of all the experimental studies. In outdoor photoautotrophic cultivation, such high cell-density is rarely possible in bubble-column PBRs. For example in a 8 L bubble column PBR (height, 1 m and inner diameter, 0.1 m), the outdoor cultivation of *Chlorella vulgaris* yielded a maximum biomass titer of 2.6 g L^{-1} by using CO_2 feed strategies namely: 2% CO_2 level (with intermittent supply) and; 2% + 4% CO_2 levels (alternation supply) (Guo et al., 2015). In another report on microalga *Phaeodactylum tricornutum* grown in a bubble column and two airlift PBRs (working volume, 60 L; height, 2 m and inner diameter, 0.193 m) under outdoor sunlight conditions, 4 g L^{-1} of final biomass titer were observed using constant set point (7.6) pH-control based CO_2 feed strategy (Sánchez Mirón et al., 2002).

6.3.3 FAME analysis of biodiesel from FC2 grown under indoor and outdoor conditions using real time light based CO_2 feed strategy

The lipid-rich FC2 biomass produced under indoor and outdoor conditions, and induced by two-stage lipid induction process were analysed for FAME by gas chromatography dynamically through stage of the lipid induction phase (Fig. 6.11). Data for individual FAME composition and salient physico-chemical properties of biodiesel at highest total FAME content (TFC) (all lipid induction studies) are listed in Table 6.3. In addition to the results shown, the specific FAME content (C16 – C18, biodiesel quality determining FAMEs) at maximum FAME concentration of all the lipid induction studies were represented in terms of percentage of 'total FAME content' (TFC) (Fig. 6.11).

In the two-stage lipid induction process using the medium-scale PBR, it took 24 days to achieve a highest TFC of 30.8% (of DCW) with 33.7, 25.8 and 40.5% (of TFC) of saturated (SAT FAME), monounsaturated (MUFA) and polyunsaturated (PUFA) FAME contents (Table 6.2 and Table 6.3). Whereas in the two-stage lipid induction process of medium-scale outdoor study, a TFC of 34.86% (of DCW) was achieved on 20th day of lipid induction phase (Table 6.2), which was slightly higher in amount as well as reached early in comparison with the indoor study. This could be attributed to the enhanced growth conditions in outdoor sunlight (contains reflected and diffused light in addition to direct incident light). The SAT FAME, MUFA and PUFA (% of TFC) in the medium-scale outdoor study were observed as 31.8, 28.3 and 36.9% respectively. The cetane numbers of both the indoor and outdoor studies were 54.39 and 52.77 respectively, satisfying the quality standards of biodiesel (Table 6.3). In the small-scale PBRs with dilution (250 mL N-free original culture + 250 mL N-free medium) and without dilution, the maximum TFCs were 55.47% (16 days induction) and 42.29% (20 days induction) respectively (Table 6.2). In both cases, the cetane numbers were identical (56), higher than both indoor and outdoor medium-scale PBR experiments. Results from small-scale experiments suggest that the specific light availability affects the lipid production and productivity of FC2 biomass as well. The difference in lipid content of non-diluted FC2 culture in 500 mL and 10 L scale due to scale-up can also be explained in terms of specific light availability. The mixing of microalgal cells (provides an adequate movement of algal cells from dark zone to light zone inside the PBR) in small-scale system (0.175 m) is typically more efficient than higher scale system (2.75 m) of vertical PBRs due to usage of same sparging system in both the scales with similar superficial gas velocities. The final biodiesel production of two-stage lipid induction strategy in outdoor 10 L scale (without dilution), 500 mL scale (without dilution) and 500 mL scale (with dilution) were 3.30, 3.97 and 3.62 g L^{-1} with FAME productivity (induction period) of 120, 154 and 195 mg L^{-1} day^{-1} respectively (Table 6.3).

The results on the effect of specific light availability on FC2 strain were consistent with other reported studies on *Chlorella vulgaris* and *Nannochloropsis aculata* (Munkel et al., 2013; Su et al., 2011).

In the later outdoor study of single-stage lipid induction strategy in 10 L scale PBR, lipid induction did not occur even though the urea (N-source) became zero after prolonged stationary phase (Fig. 6.10F). The TFC of un-induced FC2 was 15.14% of DCW (Table 6.3 and Fig. 6.11). The cetane number of the biodiesel from the control sample was 46.6, which was below the quality standards (Table 6.3).

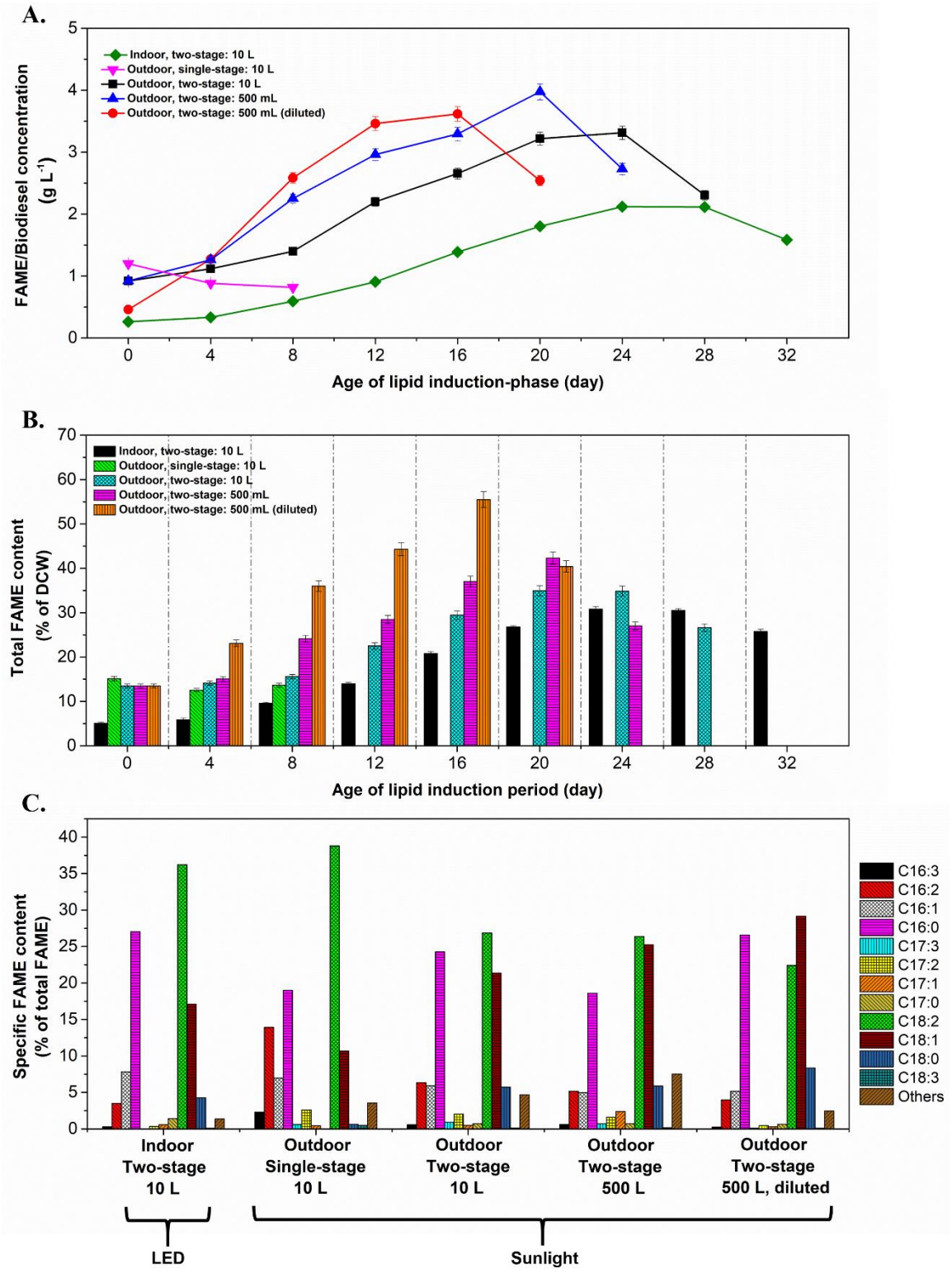

Fig. 6.11 FAME analysis of FC2 biodiesel produced in different experimental studies. A) Dynamic FAME concentration, B) Dynamic FAME content and C) Composition of C16-C18 FAMEs (quality deciding FAME) at maximum FAME concentration/content of each experimental study.

Table 6.2 Comparison of biomass and FAME production by *Chlorella* sp. FC2 IITG in different experimental studies

CO_2 feed strategy	Biomass titer (growth period) (g L^{-1})	Growth period (day)	Biomass productivity (g L^{-1} day^{-1})	FAME content (% of DCW)	FAME titer (g L^{-1})	Lipid induction period (day)	FAME productivity (mg L^{-1} day^{-1})
Indoor under diurnal (simulated sunlight)							
Constant 2%	4.26±0.09	16	0.27±0.01	na	na	na	na
Biomass density based	2.27±0.14	5	0.45±0.03	na	na	na	na
Single set point PH control based	2.63±0.05	6	0.44±0.01	na	na	na	na
Dynamic set point PH control based	4.45±0.05	10	0.44±0.005	na	na	na	na
Diurnal light (simulated sunlight) based (two staged)	5.12±0.30	9	0.57±0.03	30.81	2.12	24	78
Diurnal light (simulated sunlight) based (low DO with N_2 purging)	5.10±0.09	8	0.64±0.01	na	na	na	na
Outdoor under natural sunlight							
Diurnal sunlight based (single stage, 10L)	9.0±0.2	11	0.82±0.02	15.14	1.36	8	No induction
Diurnal sunlight based (two stage, 10L)	6.8±0.2	8	0.85±0.03	34.86	3.30	20	120
Diurnal sunlight based (two stage, 10 L followed by 500 ml)	na	na	na	42.29	3.97	20	154
Diurnal sunlight based (two stage, 10 L followed by 500 ml diluted)	na	na	na	55.47	3.62	16	195

na: not applicable; FAME titer was measured based on the final biomass titer achieved after lipid induction.

Table 6.3 Biodiesel composition. and properties (at maximum % of total FAME content) under various experimental conditions using real time light based CO_2 feed strategy.

FAME/Property name	Outdoor				Indoor
	Two-stage			Single-stage	Two-stage
	10 L scale (20 Days) (%DCW)	500 mL scale (16 Days) (% DCW)	500 mL scale (20 Days) (% DCW)	10 L scale (0 Days) (% DCW)	10 L scale (24 Days) (% DCW)
C12:0	0.02	0.02	0.02	0.02	0.03
C14:0	0.05	0.05	0.04	0.01	0.04
C15:1	0.03	0.03	0.03	-	0.03
C15:0	0.03	0.02	0.03	0.04	0.02
C16:3	0.05	0.04	0.07	0.09	0.03
C16:2	0.60±0.02	0.60±0.01	0.62±0.03	0.57±0.02	0.29
C16:1	0.56±0.01	0.78±0.02	0.60±0.01	0.29	0.64±0.03
C16:0	2.29±0.12	3.98±0.13	2.23±0.15	0.78±0.03	2.22±0.13
C17:3	-	-	0.09	0.02	-
C17:2	0.28	0.09	0.19	0.08	0.03
C17:1	0.05	0.05	0.12	0.02	0.05
C17:0	0.07	0.10	0.08		0.12
C18:2 trans	0.14	0.14	0.24	0.33	0.21
C18:2 cis	2.39±0.14	3.22±0.10	2.92±0.11	1.26±0.13	2.76±0.11
C18:1 trans	1.98±0.11	-	-	-	-
C18:1 cis	0.04	4.37±0.14	3.02±0.17	0.44±0.01	1.40±0.12
C18:0	0.54±0.04	1.25±0.04	0.70±0.04	0.03	0.35
C18:3	0.01	0.01	0.02	0.02	0.01
C20:1	0.02	0.01	0.01	-	-
C20:0	0.02	0.06	0.01	-	-
Others	0.29	0.17	0.93±0.01	0.10	-
Σ C16-C18 (% of TFC))	95.1	97.6	98.6	95.9	98.5
SAT FAME (% of TFC)	31.84	36.58	26.00	21.46	33.72
MUFA (% of TFC)	28.25	34.96	31.59	18.1	25.8
PUFA (% of TFC)	36.89	27.33	34.64	58.13	40.47
TFC (% DCW)	**34.86**	**55.47**	**42.29**	**15.14**	**30.81**
	Biodiesel properties*				
IV [g I_2 (100 g oil)$^{-1}$]	90.62	78.80	90.08	123.07	93.95
SV [mg KOH (g oil)$^{-1}$]	191.67	194.38	181.16	194.81	197.69
CN	54.39	56.65	56.16	46.63	52.77
DU	162.64	89.62	100.88	134.37	106.75
HHV (MJ kg^{-1})	38.28	39.04	36.52	38.60	39.63
ν (mm^2 s^{-1}, 40 °C)	3.88	4.13	3.67	3.64	4.07
ρ (kg m^{-3})	0.85	0.86	0.81	0.86	0.88
FP (°C)	407	407	377	395	406
CP (°C)	7.77	8.97	4.80	5.00	9.22
PP (°C)	1.61	2.93	-1.61	-1.38	3.19
CFPP (°C)	4.57	5.74	1.69	1.88	5.98

*ASTM D6751 (for transportation fuel): CN ≥ 47, 1.9 ≥ ν ≥ 6.0, and FP ≥ 93.

*EN 14213 (for heating oil): HHV≥35, IV≤120, 0.86 ≥ ρ ≥ 0.91, CP–location dependent.

*EN 14214 (for transportation fuel): CN ≥ 51, IV≤120, 0.86 ≥ ρ ≥ 0.91, CP–location dependent, CFPP <+5(summer) or <-15 (winter).

6.4 Conclusions

An efficient CO_2 feed strategy based on real time light intensity was developed for high cell-density cultivation of lipid-rich *Chlorella* sp. under natural sunlight. The strategy was found to be more effective than biomass-density and pH-control based CO_2 feed strategies. It has produced highest cell-density of 9.0 g L^{-1} in outdoor cultivation. When used with two-stage lipid induction, 3.3 g L^{-1} of biodiesel was produced under outdoor sunlight conditions. The biodiesel production was affected by specific light availability. This novel CO_2 feed strategy can also be applied for any kind of outdoor photobioreactor (open/closed) and microalgal strain.

CHAPTER 7

Design of a novel bubble-driven and self-rotating mixer in BC-PBR for enhanced biomass and biodiesel productivities of *Chlorella* sp. FC2 IITG under natural sunlight conditions

7.1 Background and uniqueness of the study

After providing the optimum supplementation of CO_2 and nutrients, mixing is the crucial parameter that should be considered for large scale production of algal biomass in photobioreactors (Kunjapur & Eldridge, 2010; Pires et al., 2017). Appropriate mixing prevents the microalgae cells from settling, minimizes the development of diffusion gradients for nutrient absorption, strips out dissolved oxygen and most importantly, aids the algal cells to move frequently enabling uniform exposure in any lighting period. It is known that mixing enhances biomass productivity by maximizing the capture of solar energy leading to an increase in specific light availability, i.e., light availability per algal cell (Munkel et al., 2013; Wang et al., 2012). In addition, lipid induction (precursor of biodiesel) has also been reported to be increased, coupled with the increase in nitrogen stress. It has been widely reported that many algae strains show increased lipid content with increasing light intensity irradiation (Chernova & Kiseleua, 2017). Therefore, efficient mixing can enhance both biomass and lipid production.

Typically, the mixing in bioreactors or photobioreactors is enabled by aeration/air bubbling, mechanical agitation (e.g., using integrated impellers) or static/non-static mixers (e.g., baffles) (Huang et al., 2017; Wang et al., 2012). The bubble-driven mixing by rigorous

aeration of liquid mixture are limited to small-scale PBRs (e.g., 500 ml scale PBR in the previous experimental studies). The bubble-driven mixing through aeration cannot provide efficient mixing in large-scale column or vertical tubular PBRs. On the other hand, mechanical agitation is energy intensive with scale-up challenges due to limitations in tube diameter as a critical design parameter for PBRs. For outlined reasons, the installation of static/non-static mixers with flat panel and tubular PBRs have been investigated as they do not require external energy inputs (Huang et al., 2015; Ugwu et al., 2003; Ugwu et al., 2002; Yan et al., 2018). In general, static mixers act as baffling system that create local turbulences due to the motion of bubbles and/or fluid flow. From the turbulences, algal cells are agitated and near uniformly exposed to light/dark zones inside the PBR. The mobile or non-static mixers are more effective as they directly cause motion due to their rotations in addition to the localised turbulences. However, these advantages have seldomly been displayed and, to date, only a single publication has described the use of mobile mixer with tubular PBR (Yan et al., 2018). The report highlights the design of a single and long helical rotor that can be self-rotatable by the virtue of continuously recirculating algae culture, making the rotor to run without extra energy inputs.

In this part of study, the objective was to design a novel bubble-driven mixer that would enhance biomass growth of the model microalgae and biodiesel production by increasing specific light availability inside the BC-PBR. The mixer should rotate by the virtue of bubble flow without external energy for mechanical rotation and, should be adaptable in all the scales of algae production. Therefore, the designed mixers were firstly installed and tested in 500 ml small-scale bubble-column PBR. Later, the mixers were scaled-up to 10 L medium-scale bubble-column PBR.

7.2 Bubble-driven mixer design and test

The designed self-rotating bubble-driven mixer is comprised of a rotating body mounted on a stationary shaft (Fig. 7.1). The rotating body with the blades was made of transparent plastic material. The stationary shaft was made of hard plastic pipe to be integrated along the inner diameter of the PBR (Fig. 7.2). The bubble-driven mixers were installed in 10 L medium-scale BC-PBR (Fig. 6.1, see chapter 6). The mixer did not rotate while the reactor was kept straight and perpendicular to the ground during initial testing. This resulted a dynamic equilibrium due to evenly distributed bubbles in the column. Subsequently, this was corrected with positioning setup with 15° – 20° angle to the ground (Fig. 7.2), thereby generating uneven bubble force to enable continuous blade rotations.

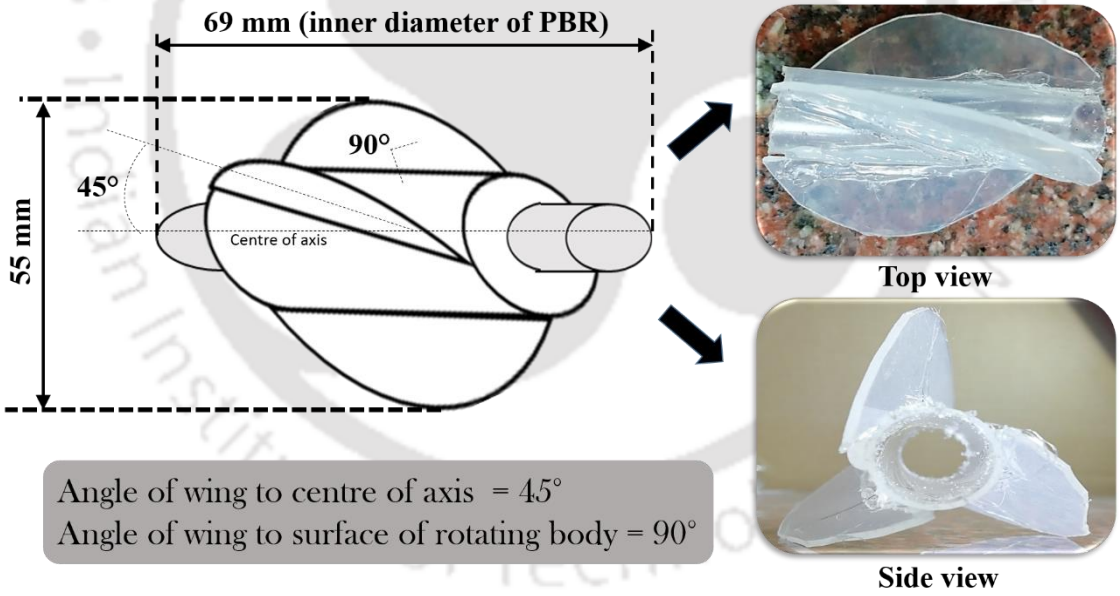

Fig 7.1 Illustration of novel bubble-driven mixer showing key dimensions. The distance between the centre of axis and the tip of wings is 27.5 mm such that it could generate a clearance zone of 7 mm inside the PBR after the rotation. Hence, the radius of imaginary sphere around the rotation could be 27.5 mm that can cause all the cells inside the sphere to expose light/dark zones with higher frequency compared to control (without mixer).

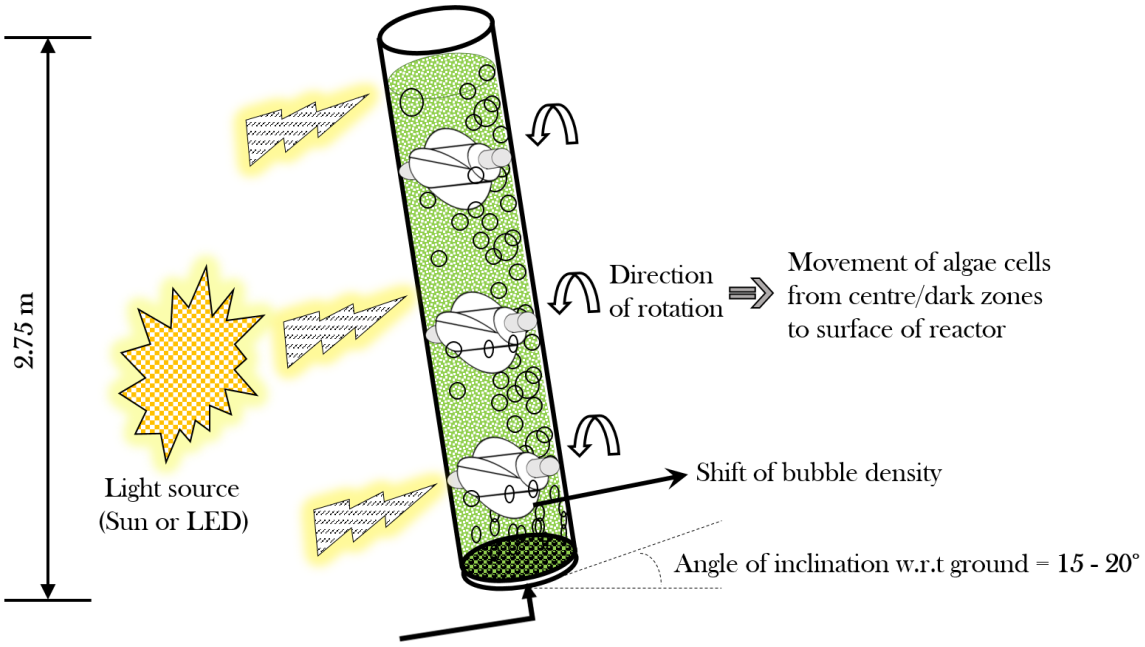

Fig. 7.2 Integration of bubble-driven self-rotating mixer to the BC-PBR

7.3 Experimental setup and methods

The designed mixers were firstly installed in 500 ml small-scale bubble-column PBR to test whether the biomass production of FC2 is enhanced. Subsequently, the mixers were equipped in 10 L medium-scale bubble-column PBR to evaluate the mixer performance on up-scaled growth of microalgae and lipid induction for biodiesel production. The experimental setup of mixer equipped 10 L BC-PBR with essential components is shown in Fig. 7.3.

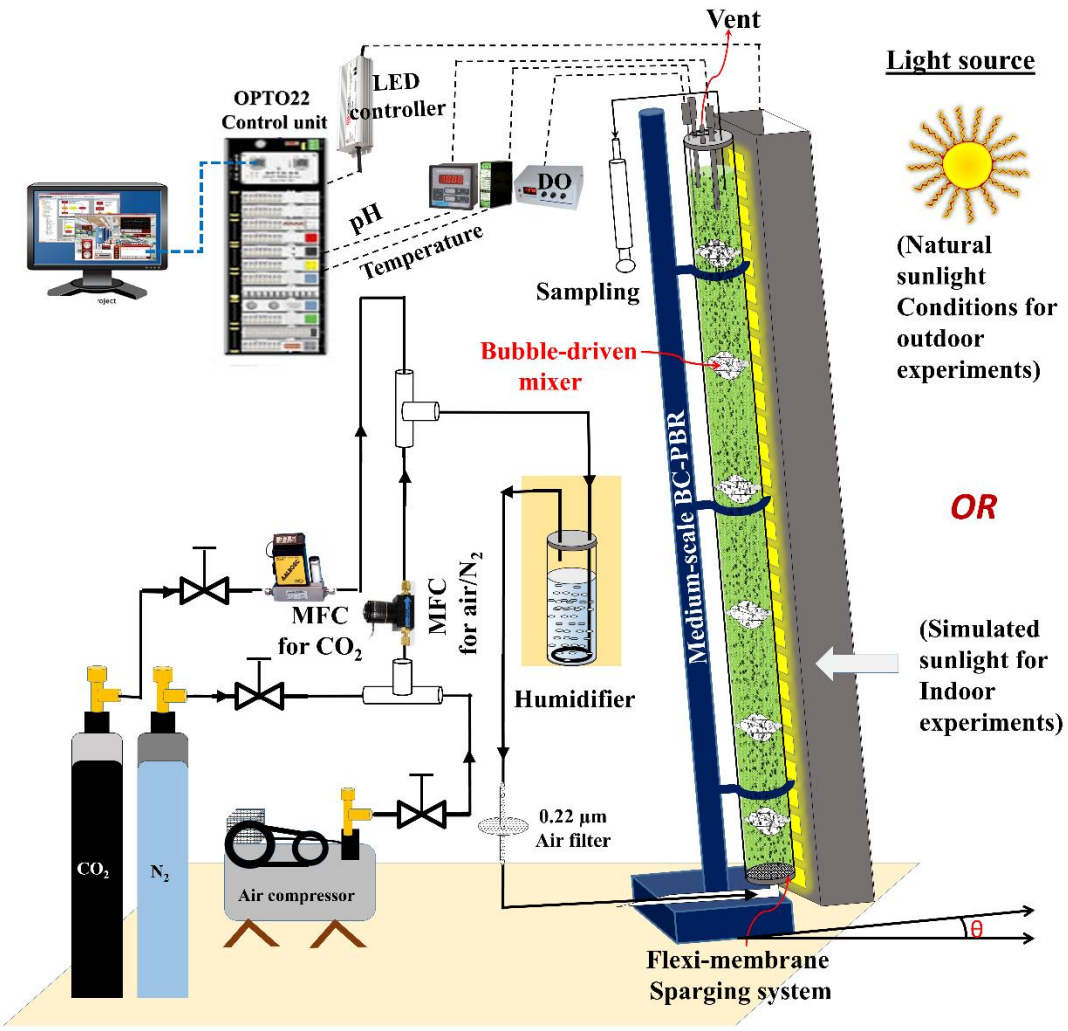

Fig 7.3 Schematic representation of medium-scale BC-PBR with novel bubble-driven mixers.

7.3.1 Investigation of FC2 growth in small-scale BC-PBR with integrated mixers under simulated sunlight conditions

Initially, the mixer's capability to enhance biomass productivity was investigated in small-scale BC-PBR setup (500 ml of working volume). Since small-scale BC-PBR was already proved to be efficient at 2% constant CO_2 feed (see chapter 5), the same strategy was followed for experiments under diurnal simulated sunlight conditions. In this study, FC2 was grown in two sets of experiments sequentially at 1.0 VVM (0.5 L min^{-1}) and 1.5 VVM (0.75 L min^{-1})of

aeration rates, where each set was consisting of one PBR with mixer and another PBR without mixer (as control study). Due to these aeration rates, the bubble-driven mixer could self-rotate with an average speed of 27 and 37 RPM at 1.0 VVM and 1.5 VVM respectively. Generally, impellers/mixers in stirred tank reactors cause shear stress to biological cells. Therefore, the shear sensitivity of the model microalgae was checked under bright field microscope while investigating the performance of newly designed mixer in small-scale PBR experiments.

7.3.2 Investigation of FC2 growth in medium-scale BC-PBR with integrated mixer under simulated sunlight conditions

For these experiments, nine bubble-driven mixers spaced 30 cm apart were installed in 10 L medium-scale BC-PBR. The setup was firstly evaluated under diurnal simulated sunlight to establish performance. As prototype of real time light based CO_2 feed (Table 6.1) was determined as optimum for FC2 growth in medium-scale PBR under indoor conditions, the same CO_2 feed strategy was followed and biodiesel was produced by two-stage lipid induction methodology. In the lipid induction phase, the lipid content of FC2 biomass was analyzed at 4-day interval via FAME extraction and gas chromatography analysis.

7.3.3 Investigation of FC2 growth in medium-scale BC-PBR with integrated mixer under natural sunlight conditions

Performance of the medium-scale PBR with bubble-driven mixers was investigated under natural sunlight conditions using fine-tuned real time sunlight based CO_2 feed strategy (Table 6.1). Under natural sunlight conditions, two experiments were conducted sequentially to test and enhance biodiesel production based on the biomass density at the end of growth-phase. In the first experiment, two-stage lipid induction was started after the cell growth reached

stationary phase. In the second experiment, the FC2 growth was re-investigated by starting the two-stage lipid induction at biomass titer when day-wise biomass productivity was highest. In both first and second experiments, the lipid contents were analyzed at every 4-day and 2-day intervals respectively.

7.4 Results and discussion

7.4.1 FC2 growth in small-scale BC-PBR with integrated mixers under simulated sunlight conditions

Based on the rotational speeds at the aeration rates of 1.0 VVM (corresponding gas flow rate is 0.5 L min^{-1}) and 1.5 VVM (corresponding gas flow rate is 0.75 L min^{-1}), the mixer's Reynolds numbers (calculated by assuming water as medium, formula: Reynolds number = $(n \times D^2 \times \rho) / v$, where 'n' is rotational speed of mixer, 'D' is diameter of imaginary sphere creates by mixer, 'ρ' is density of water and 'v' is viscosity of water) were 9.1×10^4 and 12.5×10^4 at 27 and 37 RPM respectively. At both the gas (CO_2 + air) mixture flow rates, 0.5 and 0.75 L min^{-1} or aeration rates, 1 and 1.5 VVM, the mixer has improved the biomass productivity by achieving the final biomass titer in one-day advance compared to the control study (Fig. 7.4A and 7.4C). Similar to the growth patterns of both the cases, high chlorophyll content was observed in the mixer equipped BC-PBR only (Fig. 7.4B and 7.4D). Moreover, the deviation in cell density was more at the lower gas flow rate of 0.5 L min^{-1} than at the 0.75 L min^{-1}. This was suggesting that mixer may be more effective at lower aeration rates compared to the higher aeration rates. Also, macro-level mixing (causing more frequent exposure of algae cells to local light:dark cycles) at lower aeration rates is less efficient than higher aeration rates. Due to this phenomenon, the biomass productivity was also observed more at higher gas flow rate or

aeration rate (Table 7.1). However, the bubble-driven mixer could improve overall biomass productivity even at that higher gas flow rate of 0.75 L min^{-1}.

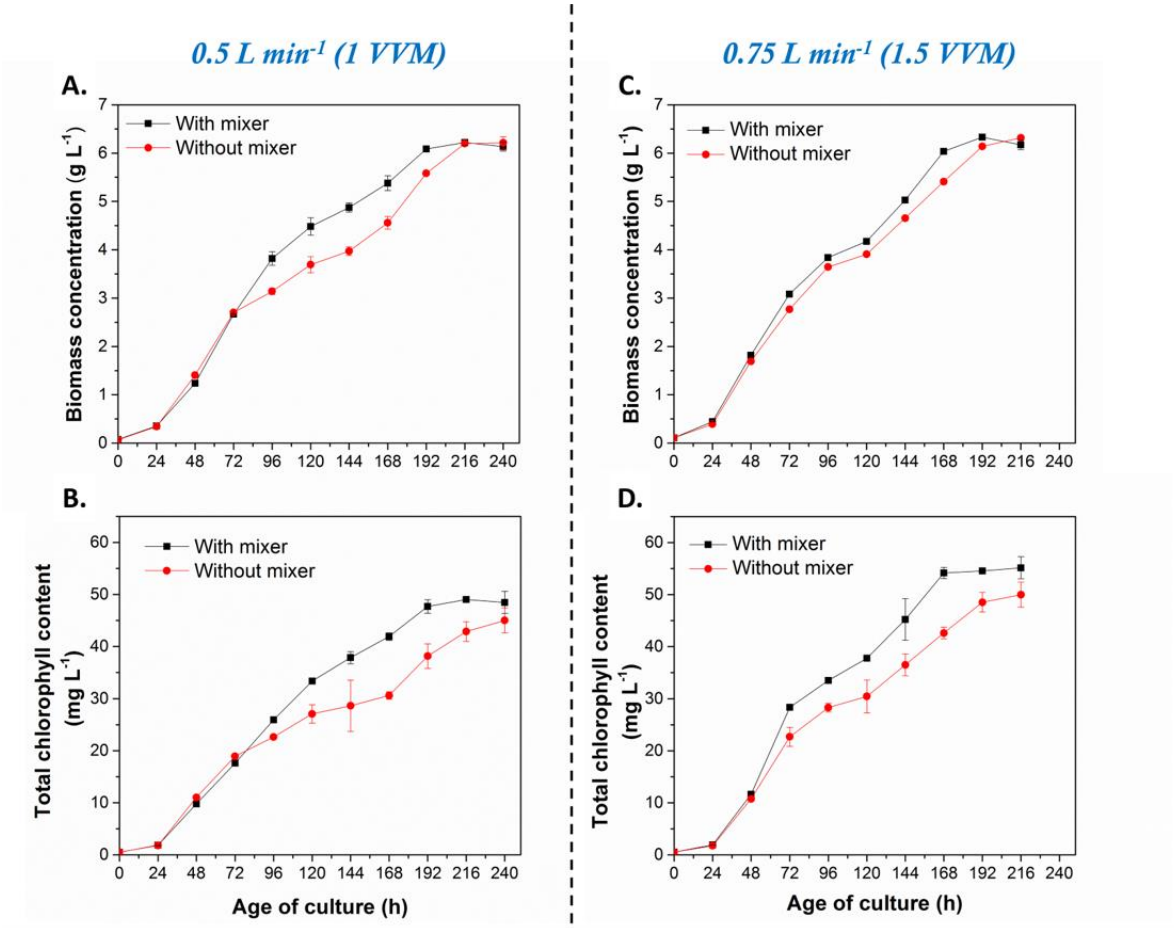

Fig. 7.4 Effect of novel bubble-driven mixer in small-scale BC-PBR (500 mL) at different gas sparging rate with 2% constant CO_2 feed under diurnal simulated sunlight. A. and B. growth and Chlorophyll content of FC2 at 1.0 VVM aeration rate (0.5 LPM gas mixture (air +CO_2) sparging) respectively. C. and D. growth and chlorophyll content of FC2 at 1.5 VVM (0.75 LPM gas mixture (air +CO_2) sparging) respectively.

Table 7.1 Comparison of biomass productivities of FC2 in small-scale BC-PBR (500 ml working volume) equipped with and without bubble-driven mixer.

Aeration rate	**Biomass productivity (g L^{-1} day^{-1})**	
(VVM)	**With mixer**	**Without mixer**
1.0 (0.5 LPM)	0.76 ± 0.03	0.68 ± 0.02
1.5 (0.75 LPM)	0.86 ± 0.04	0.76 ± 0.02

7.4.2 FC2 growth in medium-scale BC-PBR with integrated mixer under simulated sunlight conditions

In this study, the results indicated that the 10 L medium-scale BC-PBR having bubble-driven mixer exhibited the maximum biomass concentration of 5.1 g L^{-1} one-day earlier (8 days) when compared to the medium-scale BC-PBR without mixer (Fig. 7.5A). The total chlorophyll content of FC2 biomass was also observed higher in case of mixer equipped BC-PBR (Fig. 7.5C). The dissolved oxygen accumulation was also increased with the highest value of 190% air saturation recorded in case of mixer equipped BC-PBR compared to the BC-PBR without mixer (Fig. 7.5D). As the objective of installing mixer was to increase the light availability per cell by mixing, the resulted high DO would be due to high photosynthesis caused by higher specific light availability to algae cells. In two-stage lipid induction strategy conducted in mixer equipped BC-PBR, a total FAME content of 25.75±0.49 % DCW was achieved within 8 days of induction with 121.8±5.5 mg L^{-1} day^{-1} of FAME productivity (Fig. 7.5B). Whereas in the BC-PBR without mixer, it took 20 days to achieve FAME content of 26.79±0.27 % DCW with FAME productivity of 74.6±0.3 mg L^{-1} day^{-1}. The observations suggest that the increased specific light availability due to bubble-driven mixer enhanced the lipid production. The study was subsequently extended to investigate the FC2 growth under natural sunlight conditions.

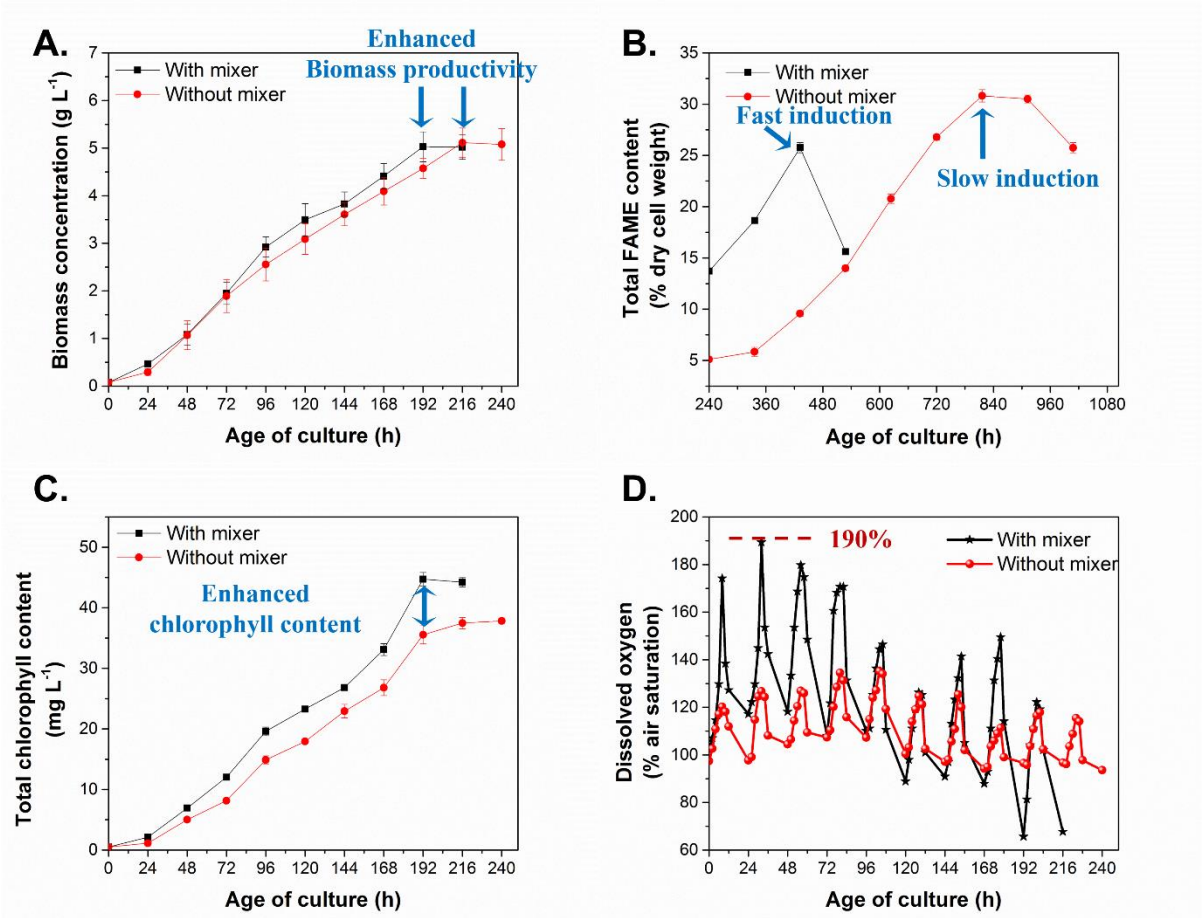

Fig. 7.5 Effect of novel bubble-driven mixer in medium-scale BC-PBR (10L) under diurnal simulated sunlight followed with prototype of real time light based CO_2 feed strategy. **A.** Growth of FC2, **B.** total FAME content and **C.** chlorophyll content of FC2 in BC-PBR with (square) and without (circle) mixer and **D.** Dissolved oxygen accumulation in 10 L BC-PBR with (star) and without (circle) mixer.

7.4.3 FC2 growth in medium-scale BC-PBR with integrated mixer under natural sunlight conditions

In this part of study under natural sunlight conditions, the outdoor temperature and sunlight intensities in the first 3 days of culturing was almost similar in both the experiments (Fig. 7.6), i.e., BC-PBR with and without bubble-driven mixers installation. Sunlight intensity in the experiment with mixer was lesser than the experiment without mixer. Hence, the growth of FC2 in medium-scale BC-PBR with and without integration of mixer under natural sunlight

conditions were compared. After three days of culturing time, the biomass titers in the PBR with and without mixer were observed as 4.4±0.2 and 3.9±0.2 g L^{-1} respectively (Fig. 7.7A). The total chlorophyll content and accumulated DO in the experiments with and without mixers were shown in Fig. 7.7B and 7.7C. As far as the experimental studies conducted, this high DO of 336% air saturation (with mixer) has never been observed elsewhere. The results show enhanced oxygen production in mixer equipped BC-PBR possibly due to more efficient photosynthesis attributed to increased specific light availability in BC-PBR with integrated mixers. However, the final biomass titer of FC2 with mixer achieved up to 8.6 g L^{-1} (stationary phase) with 0.86 g L^{-1} day^{-1}, which was almost similar to the study without mixer. This observation suggests that the enhanced specific light availability due to mixer integration might not be sufficient to overcome the light limitation caused by high biomass densities (e.g., 8.6 g L^{-1}).

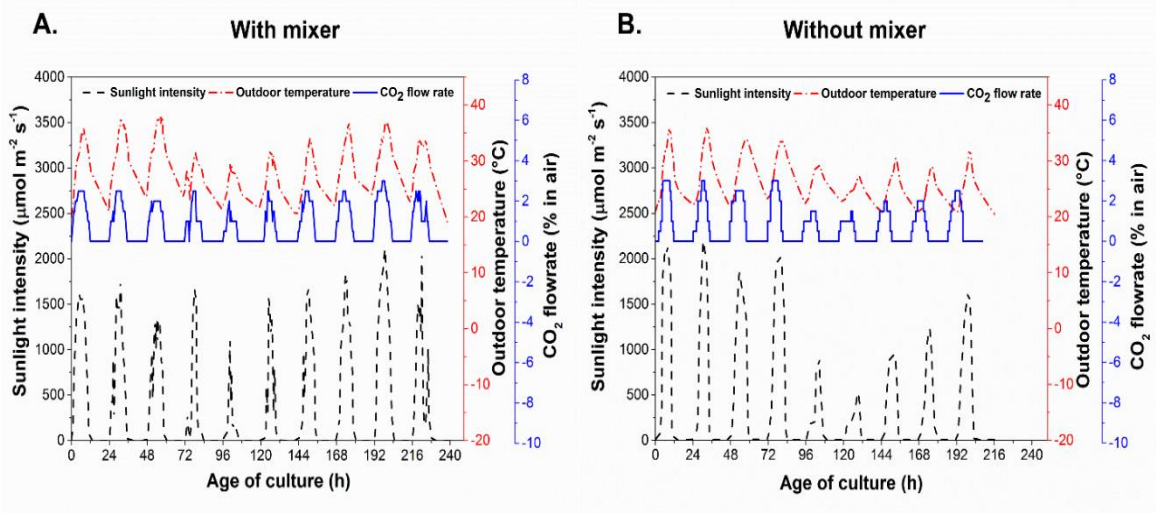

Fig. 7.6 Comparison of natural sunlight conditions, sunlight intensity (dashed line) and temperature (dash dot dash line) and fine-tuned real time CO_2 feed (continuous line). **A.** BC-PBR with bubble-driven mixers and **B.** BC-PBR without bubble-driven mixers.

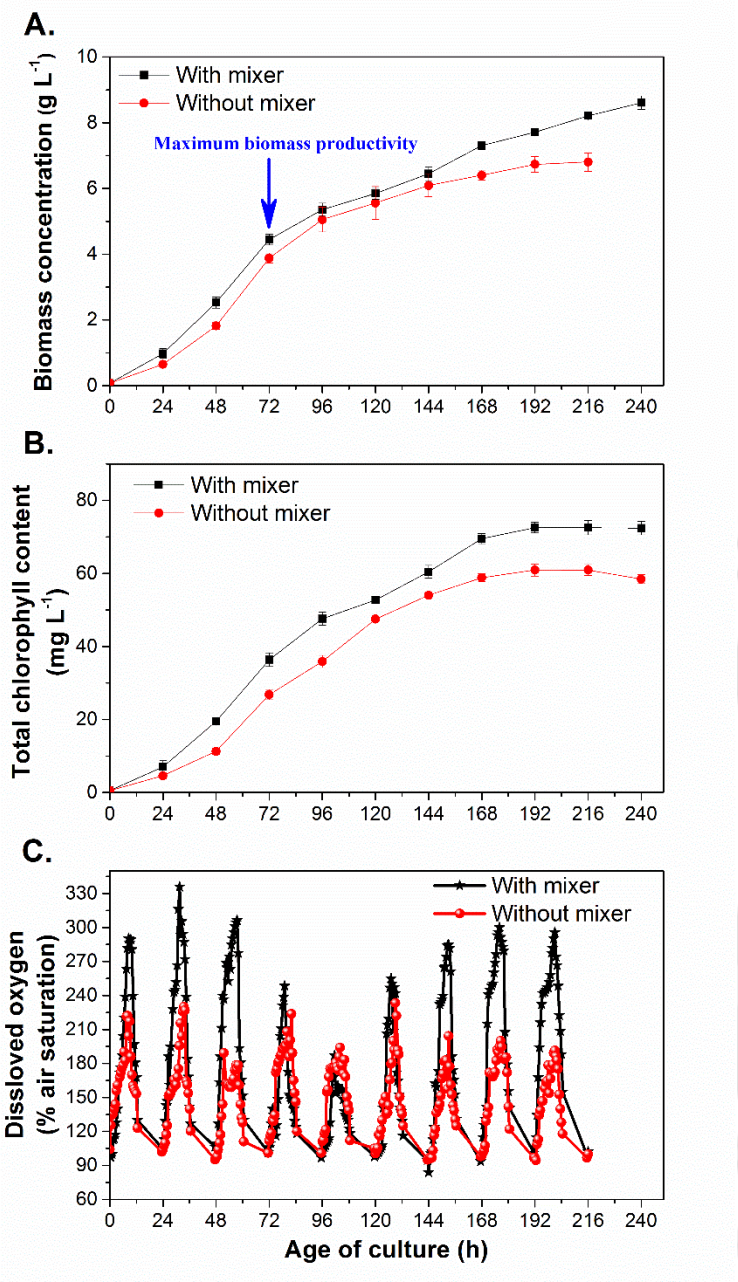

Fig. 7.7 Effect of novel bubble-driven mixer in medium-scale BC-PBR (10L) under diurnal natural sunlight followed with fine-tuned real time sunlight based CO_2 feed strategy. **A.** Growth of FC2 and **B.** chlorophyll content of FC2 in BC-PBR with (square) and without (circle) mixer and **C.** Dissolved oxygen accumulation in 10 L BC-PBR with (star) and without (circle) mixer.

Also, the lipid content in terms of FAME was also accumulated only up to 15.95% DCW in 8 days with a starting FAME content of 4.71% DCW. The quality determining FAME composition i.e., C16 – C18, was 75.13% of total FAME, which should be at least 80% for

producing quality biodiesel from microalgae (Table 7.2). Hence, the properties of biodiesel like higher heating value (HHV) and density were not satisfying the European biodiesel standards (i.e., EN 14213 for heating oil and EN14214 for transportation fuel) (Table 7.2) (Knothe, 2006). Even the biodiesel properties at 15.95% DCW were not satisfying the European and American biodiesel standard values (Table 7.2). The low production of FAME in FC2 strain is attributed to the dependence of lipid induction process on specific light availability (see chapter 6). The light availability at 8.6 g L^{-1} was not favourable for lipid induction even though the mixer was integrated in the PBR. Therefore, the objective of achieving high microalgae biomass production with quality biodiesel would not be feasible at high growth-phase biomass density, i.e., 8.6 g L^{-1}.

On the basis of enhanced lipid contents at higher specific light availability (see chapter 6, section 6.3.2.2), another experiment was performed for high biomass and biodiesel productivities. In this experiment, growth-phase of FC2 was seized at 4.24 g L^{-1} when biomass productivity was maximum, i.e., 1.42 g L^{-1} day^{-1} (Fig. 7.8). This ensured successful lipid induction as well as ability of the mixer to induce lipids with faster rates. The results indicated that the highest total FAME content of 48.85% DCW was achieved only within 4 days of lipid induction (7 days of overall culturing time) (Fig. 7.8). The biodiesel productivity in lipid induction phase was 753 mg L^{-1} day^{-1} (overall biodiesel productivity was 521 mg L^{-1} day^{-1}), which is the highest of all the experiments performed in this thesis study (refer additional information, section 2, appendices).

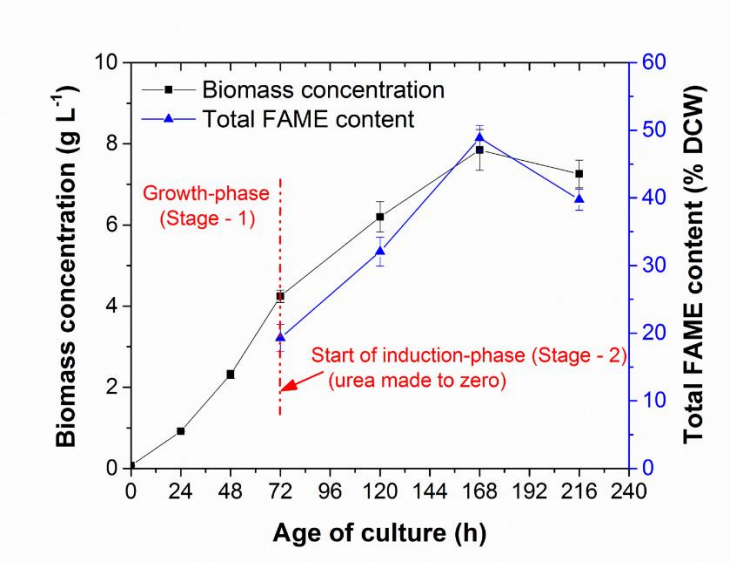

Fig. 7.8 Growth of FC2 and lipid accumulation for high biomass and biodiesel productivities using novel bubble-driven mixer under natural sunlight

The obtained biodiesel productivity due to the mixer integrated BC-PBR (a vertical tubular PBR) in this study is significantly higher than many reported studies on *Chlorella vulgaris* (refer Appendices, section 2 for additional information). For example in a *Chlorella vulgaris* strain grown in 30 L flat panel PBRs (0.03 m of path length) integrated with static mixers, 44.6% of TFC (% DCW) with induction-phase FAME productivity of 390 mg L^{-1} day^{-1} was reported under natural sunlight conditions (Munkel et al., 2013). In that study, the two-stage lipid induction was applied to induce lipid when biomass concentration was 3.8 g L^{-1} (Munkel et al., 2013). In the current BC-PBR setup with mobile mixers, it should be noted that similar TFC (% DCW) with 1.9 times more induction-phase biodiesel productivity was achieved despite the path length of reactor is 2.5 times more than the reported study.

The produced biodiesel in terms of iodine value, saponification value, degree of unsaturation, cetane number, higher heating value, viscosity, density, flash point and cold flow properties was satisfying the standard properties of biodiesel suggested by American Society of Testing and Materials (ASTM D6751) and/or European Norms (EN 14213/14) (Table 2)

(D6751-20, 2020; Knothe, 2006). The iodine value and degree of unsaturation of the 4.2 g L^{-1} derived biodiesel were significantly lower than the 5.1 g L^{-1} study (indoor), indicating the better oxidation stability, shorter ignition delay, decreased emissions of total hydrocarbons and nitrogen oxides (NO_x), and decreased white smoke of final biodiesel (Benjumea et al., 2011; Schober & Mittelbach, 2007). But the biodiesel produced with 8.6 g L^{-1} (initial biomass titer at the start of induction) did not satisfied the standard properties of biodiesel, i.e., lower HHV and density than the specified limits in EN 14213 and 14214, respectively. Thus the biodiesel produced with very high biomass density at the start of induction-phase could be neither used as heating oil nor transportation fuel. The reason for the lower HHV and density of biodiesel derived from 8.6 g L^{-1} biomass concentration was the lowered total FAME content (TFC) in the final biomass due to very low light availability in comparison to the biodiesel derived from the biomass concentrations of 4.2 or 5.1 g L^{-1} as initial biomass titers at the start of lipid induction-phase (Table 2). Even the quality determining FAMEs, C16 – C18 of biodiesel derived from 8.6 g L^{-1} were as low as 75.13% (of TFC) when compared to the 93.59% and 95.27% of the biodiesel derived from 5.1 g L^{-1} (simulated sunlight condition) and 4.2 g L^{-1} (natural sunlight condition), respectively. Hence, the quality biodiesel production from microalgae under N-stress is also governed by initial biomass titer at the start of lipid induction (i.e., the lipid induction is a strongly light-dependent phenomenon) and efficient mixing for increasing the average light exposure (i.e., current mixing arrangement).

Table 7.2 FAME composition and properties of produced biodiesel (at maximum TFC) from FC2 biomass grown under various experimental conditions using diurnal-light based CO_2 feed strategy

FAME/Property name	**Indoor study**	**Outdoor studies**	
		8.6 g L^{-1}	**4.2 g L^{-1}**
C12:0	0.02	0.02	0.03
C14:0	0.02	0.02	0.04
C15:1	0.03	0.02	0.03
C15:0	0.04	0.03	0.05
C16:3	0.09	0.03	0.12
C16:2	0.53±0.04	0.23±0.02	0.84±0.05
C16:1	0.74±0.03	0.02	0.96±0.07
C16:0	1.39±0.09	0.73±0.13	3.05±0.12
C17:2	0.11	0.22±0.01	0.06
C17:1	0.06	0.01	0.05
C17:0	0.03	0.008	0.05
C18:2 trans	0.33±0.02	0.15±0.02	0.29±0.03
C18:2 cis	1.37±0.1	1.06±0.06	3.07±0.14
C18:1 trans	-	0.34±0.02	-
C18:1 cis	1.70±0.12	0.33±0.05	3.28±0.15
C18:0	0.07	0.08	0.74±0.02
C18:3	0.04	0.02	0.05
C20:1	-	0.01	0.02
C20:0	-	-	0.02
Others	0.29	0.63	0.35±0.02
C16 – C18 (% of TFC)	93.59	75.13	95.27
SAT FAME (% of TFC)	22.99	20.33	30.19
MUFA (% of TFC)	36.79	9.2	32.85
PUFA (% of TFC)	28.28	34.40	27.23
TFC (% DCW)	**25.4±1.50**	**15.95±1.70**	**48.85±1.89**
	Biodiesel properties		
IV [g I_2 (100 g oil)$^{-1}$]	97.77	80.18	93.66
SV [mg KOH (g oil)$^{-1}$]	190.16	137.17	190.98
CN	53	68.05	53.80
DU	93.35	78.01	87.32
HHV (MJ kg^{-1})	37.89	30.49	38.19
ν (mm^2 s^{-1}, 40 °C)	3.73	2.88	3.89
ρ (kg m^{-3})	0.84	0.68	0.85
FP (°C)	406	383	405
CP (°C)	5.66	3.96	7.16
PP (°C)	-0.67	-2.52	0.96
CFPP (°C)	2.53	0.87	3.99

*ASTM D6751 (for transportation fuel): CN ≥ 47, 1.9 ≥ ν ≥ 6.0, and FP ≥ 93.

*EN 14213 (for heating oil): HHV≥35, IV≤120, 0.86 ≥ ρ ≥ 0.91, CP–location dependent.

*EN 14214 (for transportation fuel): CN ≥ 51, IV≤120, 0.86 ≥ ρ ≥ 0.91, CP–location dependent, CFPP <+5(summer) or <-15 (winter).

7.5 Conclusions

This study was conducted to design and integrate a novel bubble-driven mixer in membrane-sparger equipped bubble column PBR enabling higher specific light availability, thereby enhanced biomass and biodiesel productivities from model microalgae strain, *Chlorella* sp. FC2 IITG. In 500 ml small-scale and 10 L medium-scale BC-PBRs the mixer was firstly characterized for higher biomass and lipid productivities under simulated sunlight. The minimum mixer's Reynolds number in both 500 ml and 10 L scale BC-PBRs was observed as 9.1×10^4, indicating the occurrence of fully turbulent flow of fluid around the novel bubble-driven mixer. The mixer induced light/dark fluctuations have successfully improved the productivities of both biomass as well as biodiesel from *Chlorella* sp. FC2 IITG in all the conducted experimental studies (additional information, section 3, appendices). The results were also confirmed by analysis of total chlorophyll contents and dissolved oxygen profiles in the studies with and without the use of bubble-driven mixer. Since 8.6 g L^{-1} was unable to induce lipids for quality biodiesel despite of integrating the mixer, the biodiesel production was re-investigated by starting the two-stage lipid induction at 4.2 g L^{-1} of biomass density (a point at which the biomass productivity was highest in the prior experiment in which maximum biomass titer was 8.6 g L^{-1}). In the study, the mixer equipped BC-PBR has achieved 1.4 g L^{-1} day^{-1} (growth-phase) of biomass productivity and 753 mg L^{-1} day^{-1} (induction-phase) of biodiesel productivity. At the end of induction-phase, the final biomass titer and biodiesel production were 7.5 g L^{-1} and 3.7 g L^{-1} respectively.

CHAPTER 8

Overall conclusions

As a third generation biofuel/biodiesel feedstock, microalgae biomass has potential to produce high oil per unit area. However, the economics of biodiesel production from algae has been suffering from low biomass yield, therefore, lower biodiesel productivity, arised from open pond cultivation practices and high investment photobioreactors (PBRs). Therefore, current study is interested in developing a cost-effective photobioreactor with effective process design and engineering to produce high biomass and biodiesel yields under natural sunlight. Based on major influence factors of microalgae cultivation, the study is firstly aimed to design and a low-cost cum mass trasnfer efficient PBR. Subsequently, the effect of light and CO_2 on the model microalgae strain is well understood for growth optimization under diurnally varying light instead of constant light. Followed by that, high biomass yielding CO_2 feed strategy is developed to implement under both simulated and natural sunlight conditions. Finally an additional mixing equipment is integrated inside the PBR to increase light capturing ability in the reactor, therefore, enhanced biomass and biodiesel productivity.

With respect to reactor design, bubble column PBR technology has selected due to its better features of low-land area consumption, higher photosynthetic efficiency and sufficient light dilution for avoiding photoinhibition. The BC-PBR technology has designed by incorporating newly customized membrane-sparger that is cost-effective, scalable, and energy-saving in comparison with known perforated tubing and conventional L-shaped spargers. In

terms of volumetric CO_2 mass transfer coefficient and cell-settling membrane-sparger was proved superior to conventional L-sparger and perforated tubing. Also, a customized LED lighting system and other process sensors were installed to generate simulated sunlight and to monitor/control various process variables related to algae growth analysis. For availing higher sunlight irradiation per algae cell, novel bubble-driven mixer has designed and successfully integrated in BC-PBR to address mixing affected lower productivity. The mixer do not require external electricity and extra aeration energy for exerting rotational force. It simply requires an imbalanced bubble force that can be generated by a slight inclination of 15 - 20° to the ground. The integration of mixer effectively enhanced the productivity of both biomass and biodiesel.

From the process engineering perspective, rather than statistical optimization, the combined effect of light intensity and CO_2 concentration was considered in growth experiments of FC2 under variable light intensities (ranges from 0 – 2000, typical range of natural sunlight) and CO_2 levels. At 2% CO_2 level and 1130 µmol m^{-2} s^{-1} of light intensity, growth of FC2 was maximum with steady-state dCO_2 concentration of 83 mg L^{-1}, at which the photosynthetic rates were sustained even in light limiting conditions. Hence, "maintenance of 100 mg L^{-1} dCO_2 (equilibrium dCO_2 concentration at 2% CO_2 level without algae cells) throughout the culture" has developed as desirable strategy in small-scale BC-PBR setup under diurnal lighting conditions where light limitation is inevitable. As the dCO_2 based strategy depends on dCO_2 probe position, a novel real time light intensity based CO_2 feed strategy was proposed and implemented in medium-scale BC-PBR for FC2 growth under simulated and natural sunlight conditions. The light-based CO_2 feed was proved highly productive than the known biomass density and pH control based strategies. Compared to the known biomass

density based and constant pH control based strategies, the light based CO_2 feed notably produced 120% and 97% higher final biomass concentrations respectively (additional information, appendices). Even in 2% constant CO_2 feed and dynamic pH control strategies, maximum biomass concentration in light-based CO_2 feed strategy were observed to be 20% and 15% lesser. When implemented under natural sunlight conditions, it has produced highest cell-density of 9.0 g L^{-1} with 0.85 g L^{-1} day^{-1} of overall biomass productivity. This high biomass density has not been observed in several reports related to microalage biomass production in tubular (vertical, horizontal, annular, bubble column, and airlift) photobioreactors (additional information, section 2, appendices). Also, the real time light intensity based CO_2 feed strategy can be applicable to any photosynthetic microorganism that required to be grown in any cultivation system.

In this study, the process development from CO_2 feed strategy to integration of mixer in medium-scale BC-PBR has shown continuous improvement in biodiesel productivity (Fig. A3 and A4, appendices). Similar to several reported microalage species., the biodiesel production from *Chlorella* sp. FC2 IITG has also shown that lipid induction is inversely proportional to the biomass density at the start of induction-phase. It has shown enhanced FAME content with N-stress coupled with increased specific light availability. Also, two-stage lipid induction process is favourable for this species rather than single-stage process. Therefore, the integration of bubble-driven mixer in addition to the developed light based CO_2 feed strategy yielded final oleaginous biomass density of 7.5 g L^{-1} with overall biomass productivity of 1.07 g L^{-1} day^{-1}, nearly 25% more than that of FC2 growth in BC-PBR without mixer. It has also yielded total FAME content of 49% (of DCW), which is highest of all indoor and outdoor experiments (Fig. A3, appendices). The final biodiesel production in the 10 L

medium-scale BC-PBR equipped with membrane sparger and internal mixer was found 3.6 g L^{-1} when the real time CO_2. The produced biodiesel was satisfying the required limits of salient properties of typical biodiesel in accordance with ASTM and EU norms. At high biomass densities, e.g., 8.6 or 9.0 g L^{-1}, the lipid is not induced due light limitation. Hence, for quality biodiesel production from microalgae, the selection of time point to start two-stage induction process is crucial.

Other peculiarity of the study include the experimental strain's features in the specified experimental setup. Unlike most of the reported microalgae species, this species can grow in a wide range of pH, i.e., 4.5 – 8.8, and, photosynthesis is saturated between a range of light intensities, 700 – 1500 µmol m^{-2} s^{-1}. Also, the growth of FC2 at 2000 µmol m^{-2} s^{-1} exhibited reversible photoinhbition, thereby offers minimum photo-damage in the noon times. Another interesting charateristic of the strain was growth in dark cycles (night times) instead of biomass losses. Therefore, all the above findings have favored the whole process development in the view of commercial angle. The major acheivements of the study, i.e., reactor design and CO_2 feed strategies can substantially contribute to future developments of algal biomass-biodiesel process technology in photobioreactors.

Future Prospects

- ✓ The designed bubble column photobioreactor with mass transfer efficient membrane sparger, real time light based CO_2 feed strategy and the novel bubble-driven mixer would be applicable for mass culturing of any microalgal strain that suspends homogeneously in liquid culture medium. For non-suspending microalgal strains, the proposed CO_2 feed principle can be applied unless sufficient engineering of CO_2 input method is accomplished in the respective cultivation system.

- ✓ In this study, sterilized synthetic growth medium was used by focusing mainly on reactor design and CO_2 feed engineering. However, from the energetic point of view, the energy balance analysis may be performed further to explore cost-effective and non-sterile growth culture media for achieving positive net energy ratios.

- ✓ This kind of multiple BC- PBR setup with novel characteristics can be interconnected to design a novel vertical tubular PBR of pilot-scale and even industrial-scale. When there would not be any pumping effect due to external pumps (other microalgal strains), current batch operational mode can be transformed into semi-batch or even continuous mode for achieving better results, e.g., final experimental study in the fourth objective, where the FC2 grown up to 4.4 g L^{-1} within 3 days to achieve highest biomass productivity of 1.42 g L^{-1} day^{-1}.

- ✓ The study proved biodiesel production and productivity can be increased by lowering the initial biomass density at the starting time of lipid induction, suggesting that the algal culture can be semi-continuously removed after three days and transferred in another

similar BC-PBR setup to start lipid induction for achieving results faster than the usual.

- ✓ In some cases, other than the biodiesel production, e.g., bio- oil, the production and the extraction cost decreases with the increase in biomass density. For this purpose, the proposed real time sunlight intensity based CO_2 feed strategy was already proved to generate 9 g L^{-1} of final biomass titer within 10.5 days. This novel CO_2 feed strategy can also be applied for any kind of outdoor photobioreactor (open/closed) and microalgal strain.

- ✓ In mixer design, there is a lot of scope for further investigations of engineering the shape of mixer and angle of mixer blades that can enhance specific light availability in the current design of BC-PBR.

- ✓ Some designs of vertical tubular PBRs in industries can have diameters up to 100 mm. In such cases, the installation of bubble-driven mixers are useful to achieve higher biomass productivities

References

Abbaszadeh Mayvan, A., Ghobadian, B., Omidkhah, M., Najafi, G. 2012. Current biodiesel production technologies: A comparative review. *Energy Conversion and Management*, **63**, 138-148.

Abou-Shanab, R.A.I., Matter, I.A., Kim, S.-N., Oh, Y.-K., Choi, J., Jeon, B.-H. 2011. Characterization and identification of lipid-producing microalgae species isolated from a freshwater lake. *Biomass and Bioenergy*, **35**(7), 3079-3085.

Ahmad, M., Zafar, M., Khan, M.A., Sultana, S. 2009. Biodiesel from Pongamia pinnata L. Oil: A Promising Alternative Bioenergy Source. *Energy Sources Part a-Recovery Utilization and Environmental Effects*, **31**(16), 1436-1442.

Al-Hattab, M., Ghaly, A., Hammouda, A. 2015. Microalgae harvesting methods for industrial production of biodiesel: critical review and comparative analysis. *J. Fundam. Renewable Energy Appl.*, **5**.

Alptekin, E., Canakci, M., Sanli, H. 2014. Biodiesel production from vegetable oil and waste animal fats in a pilot plant. *Waste Management*, **34**(11), 2146-2154.

Antolin, G., Tinaut, F.V., Briceno, Y., Castano, V., Perez, C., Ramirez, A.I. 2002. Optimisation of biodiesel production by sunflower oil transesterification. *Bioresource Technology*, **83**(2), 111-114.

Aransiola, E.F., Ojumu, T.V., Oyekola, O.O., Madzimbamuto, T.F., Ikhu-Omoregbe, D.I.O. 2014. A review of current technology for biodiesel production: State of the art. *Biomass & Bioenergy*, **61**, 276-297.

Araujo, B.Q., Nunes, R.C.D., de Moura, C.V.R., de Moura, E.M., Cito, A.M.D.L., dos Santos, J.R. 2010. Synthesis and Characterization of Beef Tallow Biodiesel. *Energy & Fuels*, **24**(8), 4476-4480.

Arcigni, F., Friso, R., Collu, M., Venturini, M. 2019. Harmonized and systematic assessment of microalgae energy potential for biodiesel production. *Renewable & Sustainable Energy Reviews*, **101**, 614-624.

Baba, M., Shiraiwa, Y. 2013. Biosynthesis of lipids and hydrocarbons in algae. *Photosynthesis*, 978-953.

Banerjee, S., Kaushik, S., Tomar, R.S. 2019. Global Scenario of Biofuel Production: Past, Present and Future. in: *Prospects of Renewable Bioprocessing in Future Energy Systems*, (Eds.) A.A. Rastegari, A.N. Yadav, A. Gupta, Springer International Publishing. Cham, pp. 499-518.

Barsanti, L., Gualtieri, P. 2014. *Algae: anatomy, biochemistry, and biotechnology*. CRC press.

Baweja, P., Sahoo, D. 2015. Classification of Algae. in: *The Algae World*, Springer, pp. 31-55.

Benavente-Valdés, J.R., Aguilar, C., Contreras-Esquivel, J.C., Méndez-Zavala, A., Montañez, J. 2016. Strategies to enhance the production of photosynthetic pigments and lipids in chlorophycae species. *Biotechnology Reports*, **10**, 117-125.

Benjumea, P., Agudelo, J.R., Agudelo, A.F. 2011. Effect of the Degree of Unsaturation of Biodiesel Fuels on Engine Performance, Combustion Characteristics, and Emissions. *Energy & Fuels*, **25**(1), 77-85.

Bharti, R.K., Katiyar, R., Dhar, D.W., Prasanna, R., Tyagi, R. 2019. In situ transesterification and prediction of fuel quality parameters of biodiesel produced from Botryococcus sp. MCC31. *Biofuels*, DOI: 10.1080/17597269.2019.1594592.

Bhuiya, M.M.K., Rasul, M.G., Khan, M.M.K., Ashwath, N., Azad, A.K. 2016. Prospects of 2nd generation biodiesel as a sustainable fuel—Part: 1 selection of feedstocks, oil extraction techniques and conversion technologies. *Renewable and Sustainable Energy Reviews*, **55**, 1109-1128.

Bilanovic, D., Andargatchew, A., Kroeger, T., Shelef, G. 2009. Freshwater and marine microalgae sequestering of CO_2 at different C and N concentrations – Response surface methodology analysis. *Energy Conversion and Management*, **50**(2), 262-267.

Bligh, E.G., Dyer, W.J. 1959. A rapid method of total lipid extraction and purification. *Canadian Journal of Biochemistry and Physiology*, **37**(8), 911-917.

Bohutskyi, P., Kligerman, D.C., Byers, N., Nasr, L.K., Cua, C., Chow, S., Su, C.Y., Tang, Y.T., Betenbaugh, M.J., Bouwer, E.J. 2016. Effects of inoculum size, light intensity, and dose of anaerobic digestion centrate on growth and productivity of Chlorella and Scenedesmus microalgae and their poly-culture in primary and secondary wastewater. *Algal Research-Biomass Biofuels and Bioproducts*, **19**, 278-290.

Borugadda, V.B., Goud, V.V. 2012. Biodiesel production from renewable feedstocks: Status and opportunities. *Renewable and Sustainable Energy Reviews*, **16**(7), 4763-4784.

BP. 2019a. Energy Outlook 2019 https://www.bp.com/en/global/corporate/energy-economics/energy-outlook.html.

BP. 2019b. Statistical Review of World Energy 2019 https://www.bp.com/en/global/corporate/energy-economics/statistical-review-of-world-energy.html.

Brennan, L., Owende, P. 2010. Biofuels from microalgae—a review of technologies for production, processing, and extractions of biofuels and co-products. *Renewable and sustainable energy reviews*, **14**(2), 557-577.

Bunt, J.S. 1968. The influence of inoculum, size on the initiation of exponential growth by marine diatom. *Journal of Basic Microbiology*, **8**(4), 289-292.

Cavonius, L.R., Carlsson, N.-G., Undeland, I. 2014. Quantification of total fatty acids in microalgae: comparison of extraction and transesterification methods. *Analytical and Bioanalytical Chemistry*, **406**(28), 7313-7322.

Chatsungnoen, T., Chisti, Y. 2016. Harvesting microalgae by flocculation–sedimentation. *Algal Research*, **13**, 271-283.

Chauhan, D.S., Goswami, G., Dineshbabu, G., Palabhanvi, B., Das, D. 2020. Evaluation and optimization of feedstock quality for direct conversion of microalga Chlorella sp. FC2 IITG into biodiesel via supercritical methanol transesterification. *Biomass Conversion and Biorefinery*, **10**(2), 339-349.

Chen, C.-Y., Kao, P.-C., Tan, C.H., Show, P.L., Cheah, W.Y., Lee, W.-L., Ling, T.C., Chang, J.-S. 2016. Using an innovative pH-stat CO_2 feeding strategy to enhance cell growth and C-phycocyanin production from Spirulina platensis. *Biochemical Engineering Journal*, **112**, 78-85.

Chen, C.Y., Yeh, K.L., Aisyah, R., Lee, D.J., Chang, J.S. 2011. Cultivation, photobioreactor design and harvesting of microalgae for biodiesel production: A critical review. *Bioresource Technology*, **102**(1), 71-81.

Chernova, N.I., Kiseleua, S.V. 2017. Microalgae biofuels: Induction of lipid synthesis for biodiesel production and biomass residues into hydrogen conversion. *International Journal of Hydrogen Energy*, **42**(5), 2861-2867.

Chisholm, S.W. 1981. Temporal Patterns of Cell-Division in Unicellular Algae. *Canadian Bulletin of Fisheries and Aquatic Sciences*(210), 150-181.

Chisti, Y. 2007. Biodiesel from microalgae. *Biotechnology Advances*, **25**(3), 294-306.

Chisti, Y. 2008. Biodiesel from microalgae beats bioethanol. *Trends in Biotechnology*, **26**(3), 126-131.

Chisti, Y. 2013. Constraints to commercialization of algal fuels. *Journal of Biotechnology*, **167**(3), 201-214.

Coh, B.H.H., Ong, H.C., Cheah, M.Y., Chen, W.H., Yu, K.L., Mahlia, T.M.I. 2019. Sustainability of direct biodiesel synthesis from microalgae biomass: A critical review. *Renewable & Sustainable Energy Reviews*, **107**, 59-74.

Contreras, A., Garcia, F., Molina, E., Merchuk, J.C. 1998. Interaction between CO_2-mass transfer, light availability, and hydrodynamic stress in the growth of Phaeodactylurn tricornutum in a concentric tube airlift photobioreactor. *Biotechnology and Bioengineering*, **60**(3), 317-325.

Costa, J.A.V., Freitas, B.C.B., Santos, T.D., Mitchell, B.G., Morais, M.G. 2019. Chapter 9 - Open pond systems for microalgal culture. in: *Biofuels from Algae (Second Edition)*, (Eds.) A. Pandey, J.-S. Chang, C.R. Soccol, D.-J. Lee, Y. Chisti, Elsevier, pp. 199-223.

Cuellar-Bermudez, S.P., Romero-Ogawa, M.A., Vannela, R., Lai, Y.S., Rittmann, B.E., Parra-Saldivar, R. 2015. Effects of light intensity and carbon dioxide on lipids and fatty acids

produced by Synechocystis sp PCC6803 during continuous flow. *Algal Research-Biomass Biofuels and Bioproducts*, **12**, 10-16.

D6751-20, A. 2020. Standard Specification for Biodiesel Fuel Blend Stock (B100) for Middle Distillate Fuels, ASTM International. West Conshohocken, PA.

Dahl, A. 1974. The biology of the Rhodophyta. *Taxon*, **23**, 391-392.

Darko, E., Heydarizadeh, P., Schoefs, B., Sabzalian, M.R. 2014. Photosynthesis under artificial light: the shift in primary and secondary metabolism. *Philosophical Transactions of the Royal Society B-Biological Sciences*, **369**(1640).

Dassey, A.J., Theegala, C.S. 2013. Harvesting economics and strategies using centrifugation for cost effective separation of microalgae cells for biodiesel applications. *Bioresource Technology*, **128**, 241-245.

Dechatiwongse, P., Srisamai, S., Maitland, G., Hellgardt, K. 2014. Effects of light and temperature on the photoautotrophic growth and photoinhibition of nitrogen-fixing cyanobacterium Cyanothece sp ATCC 51142. *Algal Research-Biomass Biofuels and Bioproducts*, **5**, 103-111.

Demirbas, A. 2002. Biodiesel from vegetable oils via transesterification in supercritical methanol. *Energy Conversion and Management*, **43**(17), 2349-2356.

Demirbas, A. 2003. Biodiesel fuels from vegetable oils via catalytic and non-catalytic supercritical alcohol transesterifications and other methods: a survey. *Energy Conversion and Management*, **44**(13), 2093-2109.

Demirbas, A. 2008. Comparison of transesterification methods for production of biodiesel from vegetable oils and fats. *Energy Conversion and Management*, **49**(1), 125-130.

Demirbas, A., Demirbas, M.F. 2010. *Algae energy: algae as a new source of biodiesel*. Springer Science & Business Media.

Dias, J.M., Alvim-Ferraz, M.C.M., Almeida, M.F. 2008. Mixtures of Vegetable Oils and Animal Fat for Biodiesel Production: Influence on Product Composition and Quality. *Energy & Fuels*, **22**(6), 3889-3893.

dos Santos, L.K., Hatanaka, R.R., de Oliveira, J.E., Flumignan, D.L. 2019. Production of biodiesel from crude palm oil by a sequential hydrolysis/esterification process using subcritical water. *Renewable Energy*, **130**, 633-640.

Duarte-Santos, T., Mendoza-Martín, J.L., Acién Fernández, F.G., Molina, E., Vieira-Costa, J.A., Heaven, S. 2016. Optimization of carbon dioxide supply in raceway reactors: Influence of carbon dioxide molar fraction and gas flow rate. *Bioresource Technology*, **212**, 72-81.

Edmundson, S.J., Huesemann, M.H. 2015. The dark side of algae cultivation: Characterizing night biomass loss in three photosynthetic algae, Chlorella sorokiniana, Nannochloropsis salina and Picochlorum sp. *Algal Research-Biomass Biofuels and Bioproducts*, **12**, 470-476.

Engler, A., Prantl, K.A.E., Pilger, R.K.F., Krause, K. 1897. *Die Natürlichen pflanzenfamilien nebst ihren gattungen und wichtigeren arten, insbesondere den nutzpflanzen, unter mitwirkung zahlreicher hervorragender fachgelehrten begründet*. W. Engelmann.

Ergil, V. 2014. Usage of LED lights, details about lighting, Atlas Aquarium. Tekirdag, Turkey https://www.atlasakvaryum.com/index.php?id=2564.

Farobie, O., Leow, Z.Y.M., Samanmulya, T., Matsumura, Y. 2016. New insights in biodiesel production using supercritical 1-propanol. *Energy Conversion and Management*, **124**, 212-218.

Fernandez, F.G.A., Camacho, F.G., Perez, J.A.S., Sevilla, J.M.F., Grima, E.M. 1998. Modeling of biomass productivity in tubular photobioreactors for microalgal cultures: Effects of dilution rate, tube diameter, and solar irradiance. *Biotechnology and Bioengineering*, **58**(6), 605-616.

Francisco, É.C., Neves, D.B., Jacob-Lopes, E., Franco, T.T. 2010. Microalgae as feedstock for biodiesel production: Carbon dioxide sequestration, lipid production and biofuel quality. *Journal of Chemical Technology & Biotechnology*, **85**(3), 395-403.

Fritsch, F.E. 1935. Structure and Reproduction of the Algae.

Fuentes-Grunewald, C., Garces, E., Alacid, E., Rossi, S., Camp, J. 2013. Biomass and Lipid Production of Dinoflagellates and Raphidophytes in Indoor and Outdoor Photobioreactors. *Marine Biotechnology*, **15**(1), 37-47.

Fukuda, H., Kondo, A., Noda, H. 2001. Biodiesel fuel production by transesterification of oils. *J Biosci Bioeng*, **92**(5), 405-16.

Gao, Y.X., Chen, Y.F., Gu, J.H., Xin, Z., Sun, S.Z. 2019. Butyl-biodiesel production from waste cooking oil: Kinetics, fuel properties and emission performance. *Fuel*, **236**, 1489-1495.

Geankoplis, C.J. 2003. *Transport processes and separation process principles:(includes unit operations)*. Prentice Hall Professional Technical Reference.

Genin, S.N., Aitchison, J.S., Allen, D.G. 2016. Photobioreactor-Based Energy Sources. in: *Nano and Biotech Based Materials for Energy Building Efficiency*, (Eds.) F. Pacheco

Torgal, C. Buratti, S. Kalaiselvam, C.-G. Granqvist, V. Ivanov, Springer International Publishing. Cham, pp. 429-455.

Ghasemi Naghdi, F., González González, L.M., Chan, W., Schenk, P.M. 2016. Progress on lipid extraction from wet algal biomass for biodiesel production. *Microbial Biotechnology*, **9**(6), 718-726.

Goldman, J.C., Dennett, M.R., Riley, C.B. 1982. Effect of nitrogen-mediated changes in alkalinity on pH control and CO_2 supply in intensive microalgal cultures. *Biotechnology and Bioengineering*, **24**(3), 619-631.

Gong, Q., Feng, Y., Kang, L., Luo, M., Yang, J. 2014. Effects of Light and pH on Cell Density of Chlorella Vulgaris. *Energy Procedia*, **61**, 2012-2015.

Gouveia, L., Marques, A.E., da Silva, T.L., Reis, A. 2009. Neochloris oleabundans UTEX #1185: a suitable renewable lipid source for biofuel production. *Journal of Industrial Microbiology & Biotechnology*, **36**(6), 821-826.

Gülüm, M., Bilgin, A. 2017. Measurements and empirical correlations in predicting biodiesel-diesel blends' viscosity and density. *Fuel*, **199**, 567-577.

Günerken, E., D'Hondt, E., Eppink, M.H.M., Garcia-Gonzalez, L., Elst, K., Wijffels, R.H. 2015. Cell disruption for microalgae biorefineries. *Biotechnology Advances*, **33**(2), 243-260.

Guo, Z., Phooi, W.B.A., Lim, Z.J., Tong, Y.W. 2015. Control of CO_2 input conditions during outdoor culture of Chlorella vulgaris in bubble column photobioreactors. *Bioresource Technology*, **186**, 238-245.

Guo, Z., Tong, Y.W. 2014. The interactions between Chlorella vulgaris and algal symbiotic bacteria under photoautotrophic and photoheterotrophic conditions. *Journal of Applied Phycology*, **26**(3), 1483-1492.

Gupta, P.L., Lee, S.-M., Choi, H.-J. 2015. A mini review: photobioreactors for large scale algal cultivation. *World Journal of Microbiology and Biotechnology*, **31**(9), 1409-1417.

Han, B.P. 2002. A mechanistic model of algal photoinhibition induced by photodamage to Photosystem-II. *Journal of Theoretical Biology*, **214**(4), 519-527.

Harding, L.W., Heinbokel, J.F. 1984. Periodicities of Photosynthesis and Cell-Division - Behavior of Phase-Lagged Replicate Cultures of Ditylum-Brightwellii in a Diurnally Varying Photic Regime. *Marine Ecology Progress Series*, **15**(3), 225-232.

Herrera, A.M., Karaki, M.B., Rangaraju, S.K. 2019. Oil price shocks and US economic activity. *Energy Policy*, **129**, 89-99.

Hidalgo, P., Toro, C., Ciudad, G., Navia, R. 2013. Advances in direct transesterification of microalgal biomass for biodiesel production. *Reviews in Environmental Science and Bio-Technology*, **12**(2), 179-199.

Hira, A., Das, D. 2016. Performance and emission evaluation of diesel engine fuelled with biodiesel produced from high free fatty acid crude soyabean oil. *Biofuels-Uk*, **7**(4), 413-421.

Hu, Q., Sommerfeld, M., Jarvis, E., Ghirardi, M., Posewitz, M., Seibert, M., Darzins, A. 2008. Microalgal triacylglycerols as feedstocks for biofuel production: perspectives and advances. *Plant Journal*, **54**(4), 621-639.

Huang, J.K., Feng, F., Wan, M.X., Ying, J.G., Li, Y.G., Qu, X.X., Pan, R.H., Shen, G.M., Li, W. 2015. Improving performance of flat-plate photobioreactors by installation of novel

internal mixers optimized with computational fluid dynamics. *Bioresource Technology*, **182**, 151-159.

Huang, Q.S., Jiang, F.H., Wang, L.Z., Yang, C. 2017. Design of Photobioreactors for Mass Cultivation of Photosynthetic Organisms. *Engineering*, **3**(3), 318-329.

Hulatt, C.J., Thomas, D.N. 2011. Productivity, carbon dioxide uptake and net energy return of microalgal bubble column photobioreactors. *Bioresource Technology*, **102**(10), 5775-5787.

IEA. 2018a. CO_2 emission from fuel combustion- Highlights https://www.iea.org/reports/co2-emissions-from-fuel-combustion-overview.

IEA. 2019. Global Energy and CO_2 Status Report https://www.iea.org/reports/global-energy-co2-status-report-2019.

IEA. 2018b. Key world energy statistics - 2018 https://webstore.iea.org/key-world-energy-statistics-2018.

IEA. 2018c. Renewables 2018 https://www.iea.org/reports/renewables-2018.

Illman, A.M., Scragg, A.H., Shales, S.W. 2000. Increase in Chlorella strains calorific values when grown in low nitrogen medium. *Enzyme and Microbial Technology*, **27**(8), 631-635.

Imamura, M., Tsuzuki, M., Shiraiwa, Y., Miyachi, S. 1983. Form of Inorganic Carbon Utilized for Photosynthesis in Chlamydomonas-Reinhardtii. *Plant and Cell Physiology*, **24**(3), 533-540.

Iñiguez, C., Heinrich, S., Harms, L., Gordillo, F.J.L. 2017. Increased temperature and CO_2 alleviate photoinhibition in Desmarestia anceps: from transcriptomics to carbon utilization. *Journal of Experimental Botany*, **68**(14), 3971-3984.

Ismail, S.A.-e.A., Ali, R.F.M. 2015. Physico-chemical properties of biodiesel manufactured from waste frying oil using domestic adsorbents. *Science and technology of advanced materials*, **16**(3), 034602.

Issariyakul, T., Dalai, A.K. 2014. Biodiesel from vegetable oils. *Renewable & Sustainable Energy Reviews*, **31**, 446-471.

John, M.K. 1970. Colorimetric Determination of Phosphorus in Soil and Plant Materials with Ascorbic Acid. *Soil Science*, **109**(4), 214-&.

Josetespardellier, F., Astier, C., Evans, E.H., Carr, N.G. 1978. Cyanobacteria Grown under Photoautotrophic, Photoheterotrophic, and Heterotrophic Regimes - Sugar Metabolism and Carbon-Dioxide Fixation. *Fems Microbiology Letters*, **4**(5), 261-264.

Juan, J.C., Kartika, D.A., Wu, T.Y., Hin, T.-Y.Y. 2011. Biodiesel production from jatropha oil by catalytic and non-catalytic approaches: an overview. *Bioresource technology*, **102**(2), 452-460.

Kaewkannetra, P., Enmak, P., Chiu, T. 2012. The effect of CO_2 and salinity on the cultivation of Scenedesmus obliquus for biodiesel production. *Biotechnology and bioprocess engineering*, **17**(3), 591-597.

Kim, W., Park, J.M., Gim, G.H., Jeong, S.H., Kang, C.M., Kim, D.J., Kim, S.W. 2012. Optimization of culture conditions and comparison of biomass productivity of three green algae. *Bioprocess and Biosystems Engineering*, **35**(1-2), 19-27.

Knothe, G. 2006. Analyzing biodiesel: standards and other methods. *Journal of the American Oil Chemists' Society*, **83**(10), 823-833.

Knothe, G., Sharp, C.A., Ryan, T.W. 2006. Exhaust emissions of biodiesel, petrodiesel, neat methyl esters, and alkanes in a new technology engine. *Energy & Fuels*, **20**(1), 403-408.

Kokabi, K., Gorelova, O., Ismagulova, T., Itkin, M., Malitsky, S., Boussiba, S., Solovchenko, A., Khozin-Goldberg, I. 2019. Metabolomic foundation for differential responses of lipid metabolism to nitrogen and phosphorus deprivation in an arachidonic acid-producing green microalga. *Plant Science*, **283**, 95-115.

Kremer Bruno, P. 1981. C4-Metabolism in Marine Brown Macrophytic Algae. in: *Zeitschrift für Naturforschung C*, Vol. 36, pp. 840.

Kumar, D., Singh, B., Sharma, Y.C. 2017. Challenges and Opportunities in Commercialization of Algal Biofuels. in: *Algal Biofuels: Recent Advances and Future Prospects*, (Eds.) S.K. Gupta, A. Malik, F. Bux, Springer International Publishing. Cham, pp. 421-450.

Kumar, V., Muthuraj, M., Palabhanvi, B., Ghoshal, A.K., Das, D. 2014. Evaluation and optimization of two stage sequential in situ transesterification process for fatty acid methyl ester quantification from microalgae. *Renewable Energy*, **68**, 560-569.

Kunjapur, A.M., Eldridge, R.B. 2010. Photobioreactor Design for Commercial Biofuel Production from Microalgae. *Industrial & Engineering Chemistry Research*, **49**(8), 3516-3526.

Kunst, L., Samuels, L. 2009. Plant cuticles shine: advances in wax biosynthesis and export. *Current Opinion in Plant Biology*, **12**(6), 721-727.

Kusdiana, D., Saka, S. 2001. Kinetics of transesterification in rapeseed oil to biodiesel fuel as treated in supercritical methanol. *Fuel*, **80**(5), 693-698.

Landels, A., Beacham, T.A., Evans, C.T., Carnovale, G., Raikova, S., Cole, I.S., Goddard, P., Chuck, C., Allen, M.J. 2019. Improving electrocoagulation floatation for harvesting microalgae. *Algal Research*, **39**, 101446.

Lee, S.Y., Cho, J.M., Chang, Y.K., Oh, Y.-K. 2017. Cell disruption and lipid extraction for microalgal biorefineries: A review. *Bioresource Technology*, **244**, 1317-1328.

Lee, Y.-H., Yeh, Y.-L. 2015. Reduction of oxygen inhibition effect for microalgal growth using fluoroalkylated methoxy polyethylene glycol-stabilized perfluorocarbon nano-oxygen carriers. *Process Biochemistry*, **50**(7), 1119-1127.

Li-Beisson, Y., Thelen, J.J., Fedosejevs, E., Harwood, J.L. 2019. The lipid biochemistry of eukaryotic algae. *Progress in Lipid Research*, **74**, 31-68.

Li, L., Dyer, P.W., Greenwell, H.C. 2018. Biodiesel Production via Trans-Esterification Using Pseudomonas cepacia Immobilized on Cellulosic Polyurethane. *Acs Omega*, **3**(6), 6804-6811.

Li, X., Hu, H.Y., Gan, K., Sun, Y.X. 2010. Effects of different nitrogen and phosphorus concentrations on the growth, nutrient uptake, and lipid accumulation of a freshwater microalga Scenedesmus sp. *Bioresource Technology*, **101**(14), 5494-5500.

Li, Z.R., Wakao, S., Fischer, B.B., Niyogi, K.K. 2009. Sensing and Responding to Excess Light. *Annual Review of Plant Biology*, **60**, 239-260.

Lloyd, N.D.H., Canvin, D.T., Culver, D.A. 1977. Photosynthesis and Photorespiration in Algae. *Plant Physiology*, **59**(5), 936-940.

Lu, S.H., Wang, J.X., Niu, Y.H., Yang, J., Zhou, J., Yuan, Y.J. 2012. Metabolic profiling reveals growth related FAME productivity and quality of Chlorella sorokiniana with different inoculum sizes. *Biotechnology and Bioengineering*, **109**(7), 1651-1662.

Ma, F., Hanna, M.A. 1999. Biodiesel production: a review. *Bioresource Technology*, **70**(1), 1-15.

Macedo, C., Abreu, F.R., Tavares, A.P., Alves, M.B., Zara, L.F., Rubim, J.C., Suarez, P.A. 2006. New heterogeneous metal-oxides based catalyst for vegetable oil trans-esterification. *Journal of the Brazilian Chemical Society*, **17**(7), 1291-1296.

Malek, A., Zullo, L.C., Daoutidis, P. 2016. Modeling and Dynamic Optimization of Microalgae Cultivation in Outdoor Open Ponds. *Industrial & Engineering Chemistry Research*, **55**(12), 3327-3337.

Mandotra, S.K., Kumar, P., Suseela, M.R., Nayaka, S., Ramteke, P.W. 2016. Evaluation of fatty acid profile and biodiesel properties of microalga Scenedesmus abundans under the influence of phosphorus, pH and light intensities. *Bioresource Technology*, **201**, 222-229.

Maraschin, F.D., Kulcheski, F.R., Segatto, A.L.A., Trenz, T.S., Barrientos-Diaz, O., Margis-Pinheiro, M., Margis, R., Turchetto-Zolet, A.C. 2019. Enzymes of glycerol-3-phosphate pathway in triacylglycerol synthesis in plants: Function, biotechnological application and evolution. *Progress in Lipid Research*, **73**, 46-64.

Maurino, V.G., Peterhansel, C. 2010. Photorespiration: current status and approaches for metabolic engineering. *Current Opinion in Plant Biology*, **13**(3), 249-256.

McHugh, D. 2003. A guide to the seaweed industry FAO Fisheries Technical Paper 441. *Food and Agriculture Organization of the United Nations, Rome*.

Merchuk, J.C., Gluz, M., Mukmenev, I. 2000. Comparison of photobioreactors for cultivation of the red microalga Porphyridium sp. *Journal of Chemical Technology and Biotechnology*, **75**(12), 1119-1126.

Miron, A.S., Camacho, F.G., Gomez, A.C., Grima, E.M., Chisti, Y. 2000. Bubble-column and airlift photobioreactors for algal culture. *AIChE Journal*, **46**(9), 1872-1887.

Miron, A.S., Garcia, M.C.C., Camacho, F.G., Grima, E.M., Chisti, Y. 2004. Mixing in bubble column and airlift reactors. *Chemical Engineering Research & Design*, **82**(A10), 1367-1374.

Mittelbach, M. 1996. Diesel fuel derived from vegetable oils .6. Specifications and quality control of biodiesel. *Bioresource Technology*, **56**(1), 7-11.

Momose, T., Ohkura, Y., Tomita, J. 1965. Determination of Urea in Blood and Urine with Diacetyl Monoxime-Glucuronolactone Reagent. *Clinical Chemistry*, **11**(2p1), 113-&.

Monyem, A., Van Gerpen, J.H., Canakci, M. 2001. The effect of timing and oxidation on emissions from biodiesel-fueled engines. *Transactions of the Asae*, **44**(1), 35-42.

Munkel, R., Schmid-Staiger, U., Werner, A., Hirth, T. 2013. Optimization of Outdoor Cultivation in Flat Panel Airlift Reactors for Lipid Production by Chlorella vulgaris. *Biotechnology and Bioengineering*, **110**(11), 2882-2893.

Murata, N., Takahashi, S., Nishiyama, Y., Allakhverdiev, S.I. 2007. Photoinhibition of photosystem II under environmental stress. *Biochimica Et Biophysica Acta-Bioenergetics*, **1767**(6), 414-421.

Mussgnug, J.H., Thomas-Hall, S., Rupprecht, J., Foo, A., Klassen, V., McDowall, A., Schenk, P.M., Kruse, O., Hankamer, B. 2007. Engineering photosynthetic light capture: impacts on improved solar energy to biomass conversion. *Plant Biotechnology Journal*, **5**(6), 802-814.

Mutanda, T., Ramesh, D., Karthikeyan, S., Kumari, S., Anandraj, A., Bux, F. 2011. Bioprospecting for hyper-lipid producing microalgal strains for sustainable biofuel production. *Bioresource Technology*, **102**(1), 57-70.

Muthuraj, M., Chandra, N., Palabhanvi, B., Kumar, V., Das, D. 2015. Process Engineering for High-Cell-Density Cultivation of Lipid Rich Microalgal Biomass of Chlorella sp FC2 IITG. *Bioenergy Research*, **8**(2), 726-739.

Muthuraj, M., Kumar, V., Palabhanvi, B., Das, D. 2014. Evaluation of indigenous microalgal isolate Chlorella sp FC2 IITG as a cell factory for biodiesel production and scale up in outdoor conditions. *Journal of Industrial Microbiology & Biotechnology*, **41**(3), 499-511.

Nagappan, S., Devendran, S., Tsai, P.-C., Dahms, H.-U., Ponnusamy, V.K. 2019. Potential of two-stage cultivation in microalgae biofuel production. *Fuel*, **252**, 339-349.

Norsker, N.-H., Barbosa, M.J., Vermuë, M.H., Wijffels, R.H. 2011. Microalgal production — A close look at the economics. *Biotechnology Advances*, **29**(1), 24-27.

Nunes, J.C., Nascimento, J.J.P., Peiter, A.S., Ferreira-Pinto, L., Soletti, J.I., de Carvalho, S.H.V., Alves, J.J.N., de Araujo, A.C.B. 2019. Experimental Data and Phase Equilibrium Modeling in Ternary and Pseudoquaternary Systems of Sunflower Oil for Biodiesel Production. *Journal of Chemical and Engineering Data*, **64**(2), 412-420.

Nwoba, E.G., Parlevliet, D.A., Laird, D.W., Alameh, K., Moheimani, N.R. 2019. Light management technologies for increasing algal photobioreactor efficiency. *Algal Research*, **39**, 101433.

Ogbonna, J.C., Tanaka, H. 1996. Night biomass loss and changes in biochemical composition of cells during light/dark cyclic culture of Chlorella pyrenoidosa. *Journal of Fermentation and Bioengineering*, **82**(6), 558-564.

Ogbonna, J.C., Yada, H., Tanaka, H. 1995. Light Supply Coefficient - a New Engineering Parameter for Photobioreactor Design. *Journal of Fermentation and Bioengineering*, **80**(4), 369-376.

Ong, H.C., Silitonga, A.S., Masjuki, H.H., Mahlia, T.M.I., Chong, W.T., Boosroh, M.H. 2013. Production and comparative fuel properties of biodiesel from non-edible oils: Jatropha curcas, Sterculia foetida and Ceiba pentandra. *Energy Conversion and Management*, **73**, 245-255.

Ouzounis, T., Rosenqvist, E., Ottosen, C.O. 2015. Spectral Effects of Artificial Light on Plant Physiology and Secondary Metabolism: A Review. *Hortscience*, **50**(8), 1128-1135.

Owen, N.A., Inderwildi, O.R., King, D.A. 2010. The status of conventional world oil reserves-Hype or cause for concern? *Energy Policy*, **38**(8), 4743-4749.

Pal, D., Khozin-Goldberg, I., Cohen, Z., Boussiba, S. 2011. The effect of light, salinity, and nitrogen availability on lipid production by Nannochloropsis sp. *Applied Microbiology and Biotechnology*, **90**(4), 1429-1441.

Palabhanvi, B., Muthuraj, M., Mukherjee, M., Kumar, V., Das, D. 2016. Process engineering strategy for high cell density-lipid rich cultivation of Chlorella sp FC2 IITG via model guided feeding recipe and substrate driven pH control. *Algal Research-Biomass Biofuels and Bioproducts*, **16**, 317-329.

Parmar, A., Singh, N.K., Pandey, A., Gnansounou, E., Madamwar, D. 2011. Cyanobacteria and microalgae: a positive prospect for biofuels. *Bioresource technology*, **102**(22), 10163-10172.

Pascher, A. 1931. *Systematische Übersicht über die mit Flagellaten in Zusammenhang stehenden Algenreihen und Versuch einer Einreihung dieser Algenstämme in die Stämme des Pflanzenreiches*. Verlag von C. Heinrich.

Patil, P.D., Gude, V.G., Mannarswamy, A., Cooke, P., Munson-McGee, S., Nirmalakhandan, N., Lammers, P., Deng, S. 2011. Optimization of microwave-assisted transesterification of dry algal biomass using response surface methodology. *Bioresource Technology*, **102**(2), 1399-1405.

Paul, A.A.L., Adewale, F.J. 2018. Data on optimization of production parameters on Persea Americana (Avocado) plant oil biodiesel yield and quality. *Data in Brief*, **20**, 855-863.

Philichi, T.L., Stenstrom, M.K. 1989. Effects of Dissolved-Oxygen Probe Lag on Oxygen-Transfer Parameter-Estimation. *Journal Water Pollution Control Federation*, **61**(1), 83-86.

Pierobon, S.C., Riordon, J., Nguyen, B., Sinton, D. 2016. Breathable waveguides for combined light and CO_2 delivery to microalgae. *Bioresource Technology*, **209**, 391-396.

Pires, J.C.M., Alvim-Ferraz, M.C.M., Martins, F.G. 2017. Photobioreactor design for microalgae production through computational fluid dynamics: A review. *Renewable & Sustainable Energy Reviews*, **79**, 248-254.

Pizarro, A.V.L., Park, E.Y. 2003. Lipase-catalyzed production of biodiesel fuel from vegetable oils contained in waste activated bleaching earth. *Process Biochemistry*, **38**(7), 1077-1082.

Pope, D.H. 1975. Effects of Light Intensity, Oxygen Concentration, and Carbon Dioxide Concentration on Photosynthesis in Algae. *Microbial Ecology*, **2**(1), 1-16.

Posten, C. 2009. Design principles of photo-bioreactors for cultivation of microalgae. *Engineering in Life Sciences*, **9**(3), 165-177.

Powles, S.B. 1984. Photoinhibition of Photosynthesis Induced by Visible Light. *Annual Review of Plant Physiology*, **35**(1), 15-44.

Pruvost, J., Van Vooren, G., Le Gouic, B., Couzinet-Mossion, A., Legrand, J. 2011. Systematic investigation of biomass and lipid productivity by microalgae in photobioreactors for biodiesel application. *Bioresource Technology*, **102**(1), 150-158.

Pulz, O., Scheibenbogen, K. 1998. Photobioreactors: Design and performance with respect to light energy input. In: Bioprocess and Algae Reactor Technology, Apoptosis. in: *Advances in Biochemical Engineering Biotechnology*, Vol. 59, Springer. Berlin, Heidelberg.

Rashid, U., Anwar, F. 2008. Production of biodiesel through optimized alkaline-catalyzed transesterification of rapeseed oil. *Fuel*, **87**(3), 265-273.

Raso, S., van Genugten, B., Vermuë, M., Wijffels, R.H. 2012. Effect of oxygen concentration on the growth of Nannochloropsis sp. at low light intensity. *Journal of applied phycology*, **24**(4), 863-871.

Rattanapoltee, P., Chulalaksananukul, W., James, A.E., Kaewkannetra, P. 2008. Comparison of autotrophic and heterotrophic cultivations of microalgae as a raw material for biodiesel production. *Journal of Biotechnology*, **136**, S412-S412.

Reiskind, J.B., Bowes, G. 1991. The Role of Phosphoenolpyruvate Carboxykinase in a Marine Macroalga with C4-Like Photosynthetic Characteristics. *Proceedings of the National Academy of Sciences of the United States of America*, **88**(7), 2883-2887.

Richmond, A., Boussiba, S., Vonshak, A., Kopel, R. 1993. A new tubular reactor for mass production of microalgae outdoors. *Journal of Applied Phycology*, **5**(3), 327-332.

Ritchie, R.J. 2006. Consistent sets of spectrophotometric chlorophyll equations for acetone, methanol and ethanol solvents. *Photosynthesis Research*, **89**(1), 27-41.

Rodolfi, L., Chini Zittelli, G., Bassi, N., Padovani, G., Biondi, N., Bonini, G., Tredici, M.R. 2009. Microalgae for oil: Strain selection, induction of lipid synthesis and outdoor mass cultivation in a low-cost photobioreactor. *Biotechnology and bioengineering*, **102**(1), 100-112.

Ryckebosch, E., Muylaert, K., Eeckhout, M., Ruyssen, T., Foubert, I. 2011. Influence of drying and storage on lipid and carotenoid stability of the microalga Phaeodactylum tricornutum. *J Agric Food Chem*, **59**(20), 11063-9.

Saad, M.G., Dosoky, N.S., Zoromba, M.S., Shafik, H.M. 2019. Algal Biofuels: Current Status and Key Challenges. *Energies*, **12**(10), 1920.

Sahoo, D., Seckbach, J. 2015. *The algae world*. Springer.

Sakarika, M., Kornaros, M. 2019. Chlorella vulgaris as a green biofuel factory: Comparison between biodiesel, biogas and combustible biomass production. *Bioresource Technology*, **273**, 237-243.

Saleh, M. 2018. Animal fat waste and cooking oil waste: A potential source for biodiesel. *Abstracts of Papers of the American Chemical Society*, **255**.

San Pedro, A., González-López, C.V., Acién, F.G., Molina-Grima, E. 2014. Outdoor pilot-scale production of Nannochloropsis gaditana: Influence of culture parameters and lipid production rates in tubular photobioreactors. *Bioresource Technology*, **169**, 667-676.

Sánchez Mirón, A., Cerón García, M.-C., García Camacho, F., Molina Grima, E., Chisti, Y. 2002. Growth and biochemical characterization of microalgal biomass produced in bubble column and airlift photobioreactors: studies in fed-batch culture. *Enzyme and Microbial Technology*, **31**(7), 1015-1023.

Sánchez Mirón, A., Contreras Gómez, A., García Camacho, F., Molina Grima, E., Chisti, Y. 1999. Comparative evaluation of compact photobioreactors for large-scale monoculture of microalgae. *Journal of Biotechnology*, **70**(1), 249-270.

Sánchez Mirón, A., García Camacho, F., Contreras Gómez, A., Grima, E.M., Chisti, Y. 2000. Bubble-column and airlift photobioreactors for algal culture. *AIChE Journal*, **46**(9), 1872-1887.

Saxena, P., Jawale, S., Joshipura, M.H. 2013. A Review on Prediction of Properties of Biodiesel and Blends of Biodiesel. *Procedia Engineering*, **51**, 395-402.

Scherholz, M.L., Curtis, W.R. 2013. Achieving pH control in microalgal cultures through fed-batch addition of stoichiometrically-balanced growth media. *Bmc Biotechnology*, **13**.

Schober, S., Mittelbach, M. 2007. Iodine value and biodiesel: Is limitation still appropriate? *Lipid Technology*, **19**(12), 281-284.

Scott, S.A., Davey, M.P., Dennis, J.S., Horst, I., Howe, C.J., Lea-Smith, D.J., Smith, A.G. 2010. Biodiesel from algae: challenges and prospects. *Current Opinion in Biotechnology*, **21**(3), 277-286.

Sforza, E., Simionato, D., Giacometti, G.M., Bertucco, A., Morosinotto, T. 2012. Adjusted Light and Dark Cycles Can Optimize Photosynthetic Efficiency in Algae Growing in Photobioreactors. *Plos One*, **7**(6).

Shafiei, S., Salim, R.A. 2014. Non-renewable and renewable energy consumption and CO_2 emissions in OECD countries: A comparative analysis. *Energy Policy*, **66**, 547-556.

Sharma, K.K., Schuhmann, H., Schenk, P.M. 2012. High lipid induction in microalgae for biodiesel production. *Energies*, **5**(5), 1532-1553.

Show, K.Y., Lee, D.J., Tay, J.H., Lee, T.M., Chang, J.S. 2015. Microalgal drying and cell disruption--recent advances. *Bioresour Technol*, **184**, 258-266.

Singh, B., Kaur, J., Singh, K. 2010. Production of biodiesel from used mustard oil and its performance analysis in internal combustion engine. *Journal of Energy Resources Technology*, **132**(3), 031001.

Singh, S.P., Singh, P. 2014. Effect of CO_2 concentration on algal growth: A review. *Renewable & Sustainable Energy Reviews*, **38**, 172-179.

Singh, S.P., Singh, P. 2015. Effect of temperature and light on the growth of algae species: A review. *Renewable & Sustainable Energy Reviews*, **50**, 431-444.

Slegers, P.M. 2014. Scenario studies for algae production, Wageningen University. Wageningen.

Slegers, P.M., van Beveren, P.J.M., Wijffels, R.H., van Straten, G., van Boxtel, A.J.B. 2013. Scenario analysis of large scale algae production in tubular photobioreactors. *Applied Energy*, **105**, 395-406.

Slegers, P.M., Wijffels, R.H., van Straten, G., van Boxtel, A.J.B. 2011. Design scenarios for flat panel photobioreactors. *Applied Energy*, **88**(10), 3342-3353.

Song, M., Pei, H., Hu, W., Ma, G. 2013. Evaluation of the potential of 10 microalgal strains for biodiesel production. *Bioresource Technology*, **141**, 245-251.

Su, C.-H., Chien, L.-J., Gomes, J., Lin, Y.-S., Yu, Y.-K., Liou, J.-S., Syu, R.-J. 2011. Factors affecting lipid accumulation by Nannochloropsis oculata in a two-stage cultivation process. *Journal of Applied Phycology*, **23**(5), 903-908.

Sun, J., Xiong, X.Q., Wang, M.D., Du, H., Li, J.T., Zhou, D.D., Zuo, J. 2019. Microalgae biodiesel production in China: A preliminary economic analysis. *Renewable & Sustainable Energy Reviews*, **104**, 296-306.

Sun, Y., Reddy, H.K., Muppaneni, T., Ponnusamy, S., Patil, P.D., Li, C., Jiang, L., Deng, S. 2014. A comparative study of direct transesterification of camelina oil under supercritical methanol, ethanol and 1-butanol conditions. *Fuel*, **135**, 530-536.

Sung, K.D., Lee, J.S., Shin, C.S., Park, S.C. 1999. Isolation of a new highly CO_2 tolerant fresh water microalga Chlorella sp. KR-1. *Renewable Energy*, **16**(1-4), 1019-1022.

Tan, S.X., Lim, S., Ong, H.C., Pang, Y.L. 2019. State of the art review on development of ultrasound-assisted catalytic transesterification process for biodiesel production. *Fuel*, **235**, 886-907.

Tang, D.H., Han, W., Li, P.L., Miao, X.L., Zhong, J.J. 2011. CO_2 biofixation and fatty acid composition of Scenedesmus obliquus and Chlorella pyrenoidosa in response to different CO_2 levels. *Bioresource Technology*, **102**(3), 3071-3076.

Tian-Yuan, Z., Yin-Hu, W., Jing-Han, W., Xiao-Xiong, W., Deantes-Espinosa, V.M., Guo-Hua, D., Xin, T., Hong-Ying, H. 2019. Heterotrophic cultivation of microalgae in straw lignocellulose hydrolysate for production of high-value biomass rich in polyunsaturated fatty acids (PUFA). *Chemical Engineering Journal*, **367**, 37-44.

Tikkanen, M., Mekala, N.R., Aro, E.M. 2014. Photosystem II photoinhibition-repair cycle protects Photosystem I from irreversible damage. *Biochimica Et Biophysica Acta-Bioenergetics*, **1837**(1), 210-215.

Tobar, M., Núñez, G.A. 2018. Supercritical transesterification of microalgae triglycerides for biodiesel production: Effect of alcohol type and co-solvent. *The Journal of Supercritical Fluids*, **137**, 50-56.

Tredici, M.R., Zittelli, G.C. 1998. Efficiency of sunlight utilization: Tubular versus flat photobioreactors. *Biotechnology and Bioengineering*, **57**(2), 187-197.

Ugwu, C.U., Aoyagi, H., Uchiyama, H. 2008. Photobioreactors for mass cultivation of algae. *Bioresource Technology*, **99**(10), 4021-4028.

Ugwu, C.U., Ogbonna, J.C., Tanaka, H. 2003. Design of static mixers for inclined tubular photobioreactors. *Journal of Applied Phycology*, **15**(2-3), 217-223.

Ugwu, C.U., Ogbonna, J.C., Tanaka, H. 2002. Improvement of mass transfer characteristics and productivities of inclined tubular photobioreactors by installation of internal static mixers. *Applied Microbiology and Biotechnology*, **58**(5), 600-607.

Um, B.H., Kim, Y.S. 2009. Review: A chance for Korea to advance algal-biodiesel technology. *Journal of Industrial and Engineering Chemistry*, **15**(1), 1-7.

Vasistha, S., Khanra, A., Rai, M.P. 2019. Progress and Challenges in Biodiesel Production from Microalgae Feedstock. in: *Microalgae Biotechnology for Development of Biofuel and Wastewater Treatment*, (Eds.) M.A. Alam, Z. Wang, Springer Singapore. Singapore, pp. 323-345.

Vega-Estrada, J., Montes-Horcasitas, M.C., Dominguez-Bocanegra, A.R., Canizares-Villanueva, R.O. 2005. Haematococcus pluvialis cultivation in split-cylinder internal-

loop airlift photobioreactor underaeration conditions avoiding cell damage. *Applied Microbiology and Biotechnology*, **68**(1), 31-35.

Vyas, A.P., Verma, J.L., Subrahmanyam, N. 2010. A review on FAME production processes. *Fuel*, **89**(1), 1-9.

Wang, B., Lan, C.Q., Horsman, M. 2012. Closed photobioreactors for production of microalgal biomasses. *Biotechnology Advances*, **30**(4), 904-912.

Wang, S.K., Stiles, A.R., Guo, C., Liu, C.Z. 2014. Microalgae cultivation in photobioreactors: An overview of light characteristics. *Engineering in Life Sciences*, **14**(6), 550-559.

Wang, Y.M., Seppanen-Laakso, T., Rischer, H., Wiebe, M.G. 2018a. Euglena gracilis growth and cell composition under different temperature, light and trophic conditions. *Plos One*, **13**(4).

Wang, Y.T., Fang, Z., Yang, X.X., Yang, Y.T., Luo, J., Xu, K., Bao, G.R. 2018b. One-step production of biodiesel from Jatropha oils with high acid value at low temperature by magnetic acid-base amphoteric nanoparticles. *Chemical Engineering Journal*, **348**, 929-939.

West, G. 1916. Algae (vol I) Botany handbooks. Cambridge, a treatise on the British fresh water algae, Cambridge University Press, London.

Widjaja, A., Chien, C.-C., Ju, Y.-H. 2009. Study of increasing lipid production from fresh water microalgae Chlorella vulgaris. *Journal of the Taiwan Institute of Chemical Engineers*, **40**(1), 13-20.

Williams, P.J.L., Laurens, L.M.L. 2010. Microalgae as biodiesel & biomass feedstocks: Review & analysis of the biochemistry, energetics & economics. *Energy & Environmental Science*, **3**(5), 554-590.

Wilson, D., Cooper, J.P. 1969. Effect of Light Intensity and CO_2 on Apparent Photosynthesis and Its Relationship with Leaf Anatomy in Genotypes of Lolium Perenne L. *New Phytologist*, **68**(3), 627-644.

Woo, K.C., Wong, S.C. 1983. Inhibition of CO_2 Assimilation by Supraoptimal CO_2 - Effect of Light and Temperature. *Australian Journal of Plant Physiology*, **10**(1), 75-85.

Xia, L., Ge, H., Zhou, X., Zhang, D., Hu, C. 2013. Photoautotrophic outdoor two-stage cultivation for oleaginous microalgae Scenedesmus obtusus XJ-15. *Bioresource Technology*, **144**, 261-267.

Xu, J.F., Fan, X., Zhang, X.W., Xu, D., Mou, S.L., Cao, S.N., Zheng, Z., Miao, J.L., Ye, N.H. 2012. Evidence of Coexistence of C-3 and C-4 Photosynthetic Pathways in a Green-Tide-Forming Alga, Ulva prolifera. *Plos One*, **7**(5).

Xu, L., Weathers, P.J., Xiong, X.R., Liu, C.Z. 2009. Microalgal bioreactors: challenges and opportunities. *Engineering in Life Sciences*, **9**(3), 178-189.

Yan, H., Guan, C.F., Jia, Y.C., Huang, X.X., Yang, W.M. 2018. Mixing characteristics, cell trajectories, pressure loss and shear stress of tubular photobioreactor with inserted self-rotating helical rotors. *Journal of Chemical Technology and Biotechnology*, **93**(5), 1261-1269.

Yeh, K.-L., Chang, J.-S. 2011. Nitrogen starvation strategies and photobioreactor design for enhancing lipid content and lipid production of a newly isolated microalga Chlorella vulgaris ESP-31: Implications for biofuels. *Biotechnology Journal*, **6**(11), 1358-1366.

Yen, H.-W., Hu, I.-C., Chen, C.-Y., Nagarajan, D., Chang, J.-S. 2019. Design of photobioreactors for algal cultivation. in: *Biofuels from algae*, Elsevier, pp. 225-256.

Zelitch, I. 1971. Dark Respiration and Photorespiration. in: *Photosynthesis, Photorespiration, and Plant Productivity*, Academic Press. New York, USA, pp. 127-171.

Zhu, L.D., Li, Z.H., Hiltunen, E. 2016. Strategies for Lipid Production Improvement in Microalgae as a Biodiesel Feedstock. *BioMed research international*, **2016**, 8792548-8792548.

Appendices

1. Calculation procedure of biodiesel properties

The standard FAME mix C4-C24 (Sigma Aldrich Chemicals, Bangalore) was analysed by GC according to the method described in section 3.9.6. For evaluation of resulted FAME composition in the produced biodiesel, the peak areas of known concentrations of individual FAMEs from C4-C24 were taken as reference. Based on the resulted peak areas of run samples, the unknown concentrations of individual FAMEs were calculated by extrapolating standard peak areas and presented in the Tables 5.1, 6.3, and 7.2. In addition to that, Table A1 (section 2, appendices) was constructed from the data analysis of GC. Consequently, the biodiesel properties were calculated by using the Eq. 3.6 – 3.16 (refer chapter 3). An example of the calculation procedure is given below.

For calculation of saponification value, the Eq. 3.6, $SV = \sum[(560 \times F_i)/M_i]$, was solved by substituting percentage of individual FAME (F_i) and molecular weight of individual FAME (M_i) of C12:0 – C20:0 FAMEs.

$$SV = \sum[(560 \times 0.57)/214] + \cdots + [(560 \times 10.60)]/268] + .. + [(560 \times 0.00)]/326]$$

$$SV = 191.71 \text{ mg KOH (g oil)}^{-1}$$

For calculation of iodine value, the Eq. 3.7, $IV = \sum[(254 \times F_i \times D_i)/M_i]$, was solved by substituting percentage of individual FAME (F_i), number of double bonds in individual FAME (D_i), and molecular weight of individual FAME (M_i) of C12:0 – C20:0 FAMEs.

$$IV = \sum[(254 \times 0.57 \times 0)/214] + \cdots + [(254 \times 10.60 \times 1)]/268] + .. + [(254 \times 0.00 \times 0)]/326]$$

$IV =$ 71.99 g I_2 (100 g oil)$^{-1}$

For calculation of cetane number, the Eq. 3.8, $CN = \left(46.3 + \frac{5458}{SV}\right) - (0.225 \times IV)$, was solved by substituting SV and IV obtained from the previous Eq. 3.6 and 3.7.

$$CN = \left(46.3 + \frac{5458}{191.71}\right) - (0.225 \times 71.99)$$

$$CN = 58.57$$

For calculation of degree of unsaturation, the Eq. 3.9, $DU = MUFA + (2 \times PUFA)$, was solved by substituting of MUFA and PUFA.

$$DU = 33.03 + (2 \times 20.04)$$

$$DU = 73.11$$

For calculation of higher heating value, the Eq. 3.10, $HHV = \sum[(F_i \times \delta_i)/100$, was solved by substituting of F_i and $\delta_i = 46.19 - \frac{1794}{M_i} - 0.21 \times D_i$.

Firstly, δ_i was calculated for all the FAMEs, i.e., C12:0 – C20:0.

E.g., $\delta_{C12:0} = 46.19 - \frac{1794}{214} - 0.21 \times 0$

= 37.81

$\delta_{C20:0} = 46.19 - \frac{1794}{326} - 0.21 \times 0$

= 40.69

$$HHV = \sum[(37.81 \times 0.57)/100] + \cdots + [(40.69 \times 0.00)] / 100]$$

$HHV = 38.36$ MJ kg^{-1}

For calculation of kinematic viscosity, the Eq. 3.11, $\nu = e^{\Sigma[F_i \times \ln(\nu_i)]/100}$, was solved by substituting of F_i and $\ln(\nu_i) = -12.503 - 0.178 * D_i + 2.496 \times \ln(M_i)$.

Firstly, $\ln(\nu_i)$ was calculated for all the FAMEs, i.e., C12:0 – C20:0.

E.g., $\ln(\nu_{C12:0}) = [-12.503 - (0.1780 \times 0) + 2.496 \times \ln(214)]$

= 0.89

$\ln(\nu_{C20:0}) = [-12.503 - (0.1780 \times 0) + 2.496 \times \ln(326)]$

= 1.94

$$\nu = e^{\Sigma\frac{[0.57\times0.89]}{100}+\cdots+\frac{[0\times1.94]}{100}}$$

$\nu = 1.396$ mm^2 s^{-1}

For calculation of density, the Eq. 3.12, $\rho = \sum[(\rho_i \times F_i)/100]$, was solved by substituting of F_i and $\rho_i = 0.8463 + \frac{4.9}{M_i} + 0.0118 \times D_i$.

Firstly, ρ_i was calculated for all the FAMEs, i.e., C12:0 – C20:0.

E.g., $\rho_{C12:0} = 0.8463 + \frac{4.9}{214} + 0.0118 \times 0$

= 0.869

$\rho_{C20:0} = 0.8463 + \frac{4.9}{326} + 0.0118 \times 0$

= 0.861

$$\rho = \sum[\frac{0.869 \times 0.57}{100} + \cdots + \frac{0.861 \times 0}{100}]$$

$\rho = 0.844$ g cm^{-3}

For calculation of flash point, the Eq. 3.13, $FP = 23.362 \times \sum[(N_i \times F_i)/100] + 4.854 \times \sum[(D_i \times F_i)/100]$, was solved by substituting of F_i, D_i, and N_i (no. of carbon atoms in respective FAME).

$$FP = \{23.362 \times \sum[(12 \times 0.57)/100] + \cdots + [(20 \times 0)/100]\} + \{4.854 \times \sum[(0 \times 0.57)/100] + \cdots . + [(0 \times 0)/100]\}$$

$FP = 389.7$ °C

For calculation of cloud point, the Eq. 3.14, $CP = (0.526 \times F_{C16:0}) - 4.992$ was solved by substituting $F_{C16:0}$.

$CP = (0.526 \times 13.18) - 4.992$

$CP = 1.94$ °C

For calculation of pour point, the Eq. 3.15, $PP = (0.571 \times F_{C16:0}) - 12.24$ was solved by substituting $F_{C16:0}$.

$PP = (0.571 \times 13.18) - 12.24$

$PP = -4.72$ °C

For calculation of cold filter plugging point, the Eq. 3.16, $CFPP = (0.511 \times F_{C16:0}) - 7.823$ was solved by substituting $F_{C16:0}$.

$CFPP = (0.511 \times 13.18) - 7.823$

$CFPP = -1.09$ °C.

2. Important tables

Table A1. Individual FAME composition of biodiesel sample (288 h) produced from FC2 biomass cultured in small-scale BC-PBR under simulated diurnal sunlight.

Name	M_i	D_i	W_i	F_i
C12:0	214	0	0.080	0.57
C13:0	228	0	0.076	0.54
C14:0	242	0	0.000	0.00
C15:3	250	3	0.478	3.40
C15:2	252	2	0.180	1.28
C15:1	254	1	0.210	1.50
C15:0	256	0	0.000	0.00
C16:3	264	3	0.280	1.99
C16:2	266	2	0.280	1.99
C16:1	268	1	1.488	10.60
C16:0	270	0	1.850	13.18
C17:2	280	2	0.370	2.64
C17:1	282	1	0.320	2.28
C17:0	284	0	0.520	3.70
C18:2 trans	294	2	0.000	0.00
C18:2 cis	294	2	1.226	8.73
C18:1 trans	296	1	0.000	0.00
C18:1 cis	296	1	2.620	18.66
C18:0	298	0	3.600	25.64
C18:3	292	3	0.000	0.00
C20:1	324	1	0.000	0.00
C20:0	326	0	0.000	0.00
Others			0.463	3.30
Total			14.041	100.00
SAT (% of TFC)			6.126	43.63

MUFA (% of TFC)	4.638	33.03
PUFA (% of TFC)	2.814	20.04

Table A2. Specifications of analytic instruments/equipment used in the study (refer chapter 3 for detailed setup and procedures).

Equipment	**Company/Model/Specifications**
Inverted microscope	Nikon Eclipse Ti8-E, Nikon Corporation, Japan
DC regulated power supply	Metravi Instruments Pvt. Ltd., India
Pulse width modulation adapter	Mouser electronics, USA
Lux meter	Sigma Instruments, India
Manual air/CO_2 flow meter	CM flowmeters Pvt. Ltd., India
Automatic air/CO_2 flow meter	Aalborg, USA
Process Control Unit	OPTO22, USA
I/O Units -20 to +20 mA, analog input -10 to +10 VDC, analog input +4 to +20 mA, analog output 0 to +10 VDC, analog output	 SNAP-AIMA-4 SNAP-AIV-4 SNAP-AOA-23 SNAP-AOV-25
dCO_2 probe assembly	Coleparmer India Pvt. Ltd.
DO probe assembly	Hoverlabs, India
Temperature probe assembly	Coleparmer India Pvt. Ltd.
pH probe assembly	Coultron electronics, India
Visible spectrophotometer	Model 2306, Electronics India, India
CP-Sil 8 CB column for GC	30 × 0.25 mm I.D, 0.20-µm film thickness, Agilent technologies, USA
Gas chromatograph	GC-FID, Varian, Netherlands
Flanged acrylic tubes	Sunacrylam Pvt. Ltd., India
Cool white LED cobs	50 W, 6500 K colour temperature, Ebay.in
Conventional bioreactor	Applikon Biotechnology B.V., Netherlands
Silicone tubing (for sparger)	Himedia Laboratories, India.

Table A3. Comparison of biomass production using various microalgal strains grown in bubble column/airlift/tubular photobioreactors operated photoautotrophically under natural sunlight. For data of current study, refer chapters 6 and 7.

Strain name	Type of photobioreactor & specifications	Biomass titer (growth period) ($g\ L^{-1}$)	Biomass productivity ($g\ L^{-1}\ day^{-1}$)	Maximum biomass productivity ($g\ L^{-1}\ day^{-1}$)	Temperature control	pH control	Reference
Chlorella sp. FC2 IITG	Bubble column (membrane sparging, without mixer), V-10 L, H-2.75 m AR-0.08 VVM, PL-0.075 m	9.0	0.86	1.13	No	No	Current study
Chlorella sp. FC2 IITG	Bubble column (membrane sparging, novel mixer), V-10 L, H-2.75 m AR-0.08 VVM, PL-0.075 m	8.6	0.86	1.46	No	No	Current study
Chlorella sp. FC2 IITG	Bubble column (membrane sparging, novel mixer), V-10 L, H-2.75 m AR-0.08 VVM, PL-0.075 m	4.2 (induction - phase started)	1.42	1.42	No	No	Current study
Chlorella vulgaris	Bubble column, V-8 L, H-1.014 m AR-0.4 VVM, PL-0.01 m	2.62	0.37	ND	No	No	(Guo et al., 2015)
Chlorella pyrenoidosa NCIM 2738	Bubble column (sintered disc sparger) V-1.25 L, H-1 m AR-0.2 VVM, PL-0.035 m	4.6	0.91	ND	No	No	(Singh et al., 2019)
Tetraselmis suecica	Annular column with perforated plastic tube, V-120 L, H-2 m, 0.23 VVM, PL-0.045 m	1.7	0.48	ND	Yes, 27 ºC	Yes 8.0	(Zittelli et al., 2006)
Haematococcus pluvialis	Horizontal tubular, airlift pumping, V-55 L, PL-0.03 m	7.0	0.41	0.55	Yes, 20 ºC	Yes 8.0	(Lopez et al., 2006)
Haematococcus pluvialis	Bubble column, V-55 L, H-2 m AR-1 VVM, PL-0.20 m	1.4	0.06	0.12	Yes, 20 ºC	Yes 8.0	(Lopez et al., 2006)

Chlorella sp. (FACHB-1748)	A photobioreactor (type is not mentioned), V-70 L, H-1.85 m PL-0.22 m	1.1 ± 0.1	0.154	ND	NM	NM	(Zhou et al., 2013)
Chlorella ellipsoidea	Plastic bag type bubble column (sparger-stainless steel sintered), V-200 L, H-1.6 m AR-0.1 VVM, PL-0.48 m	0.53	0.032	ND	ND	ND	(Wang et al., 2014a)
Phaeodactylum tricornutum UTEX 640	Bubble column, perforated pipe sparger, V-60 L, H-2 m PL-0.19 m	4.00	0.38	NM	Yes, 22 ºC	Yes 7.6	(Miron et al., 2002)
Phaeodactylum tricornutum UTEX 640	Draft-tube airlift, perforated pipe sparger, V-60 L, H-2 m PL-0.19 m	4.00	0.38	NM	Yes, 22 ºC	Yes 7.6	(Miron et al., 2002)
Phaeodactylum tricornutum UTEX 640	Split-cylinder airlift, perforated pipe sparger, V-60 L, H-2 m PL-0.19 m	4.00	0.38	NM	Yes, 22 ºC	Yes 7.6	(Miron et al., 2002)
Phaeodactylum tricornutum	Bubble-column, V-200 L, H-1.45 m, AR-0.25 VVM, PL-0.45 m	0.96	0.13	NM	No	No	(Branco-Vieira et al., 2018)
Heterosigma akashiwo	Bubble column, V- 35 L, H-2 m, AR-0.1 VVM, PL-0.150 m.	1.46	0.25	NM	No	No	(Fuentes-Grunewald et al., 2013)
Alexandrium minutum	Bubble column, V- 35 L, H-2 m, AR-0.1 VVM, PL-0.150 m.	1.20	0.35	NM	No	No	(Fuentes-Grunewald et al., 2013)
Karlodinium veneficum	Bubble column, V- 35 L, H-2 m, AR-0.1 VVM, PL-0.150 m.	1.06	0.22	NM	No	No	(Fuentes-Grunewald et al., 2013)

*ND – Not Defined, NM – Not Measured, V – Volume, AR – Aeration Rate, H – Height, and PL – Path Length.

Table A4. Comparison of biodiesel (in terms of FAME or lipid) production from various microalgal strains grown in bubble column/airlift/tubular photobioreactors operated photoautotrophically under natural sunlight.

Strain name	Induction strategy	Total FAME (% of DCW)	Overall FAME productivity (mg L^{-1} day^{-1})	FAME titer (g L^{-1})	Reference
Chlorella sp. FC2 IITG, w/o internal mixer	Single-stage	15.14	133	1.4	Present study (refer chapter 6)
Chlorella sp. FC2 IITG, w/o internal mixer	Two-stage, N-starvation	34.9	110	3.3	Present study (refer chapter 6)
Chlorella sp. FC2 IITG, internal mixer	Two-stage, N-starvation	15.91	133	1.4	Present study (refer chapter 7)
Chlorella sp. FC2 IITG, internal mixer*	Two-stage, N-starvation	48.9	521	3.6	Present study (refer chapter 7)
Chlorella pyrenoidosa	Two-stage, N-starvation	30.0	142	1.4	(Singh et al., 2019)
Tetraselmis suecica	Single-stage	31.0	150	0.53	(Zittelli et al., 2006)
Chlorella sp.(FACHB-1748)	Single-stage	21.3	33.7	0.23	(Zhou et al., 2013)
Chlorella ellipsoidea	Single-stage	7.4	2.45	0.039	(Wang et al., 2014a)
Phaeodactylum tricornutum	Single-stage	9.08	6.23	0.087	(Branco-Vieira et al., 2018)
Heterosigma akashiwo	Single-stage	23	56.1	0.25	(Fuentes-Grunewald et al., 2013)
Alexandrium minutum	Single-stage	22	80.7	0.25	(Fuentes-Grunewald et al., 2013)
Karlodinium veneficum	Single-stage	12	26.7	0.13	(Fuentes-Grunewald et al., 2013)

*Lipid induction with lower biomass

3. Important figures

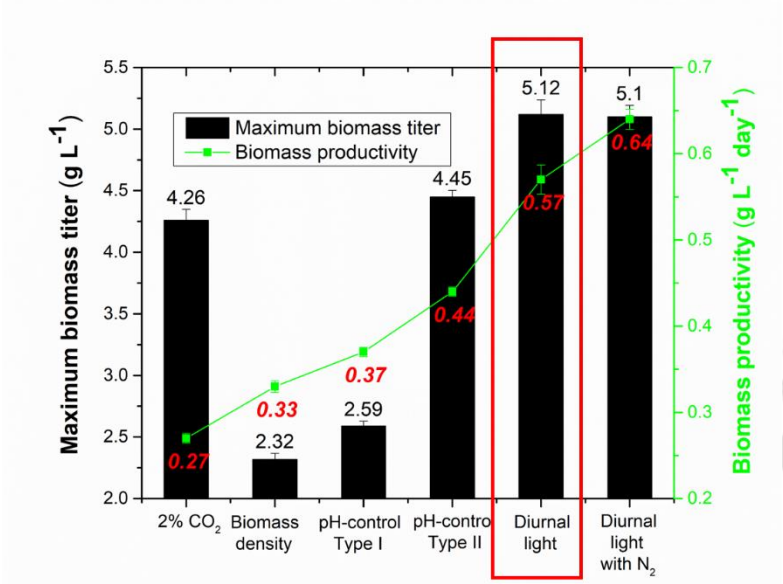

Fig. A1 Comparison of biomass titers and productivities of *Chlorella* sp. FC2 IITG grown in medium-scale BC-PBR using various CO_2 feed strategies under diurnal simulated sunlight (indoor). Refer chapter 6 for experiments.

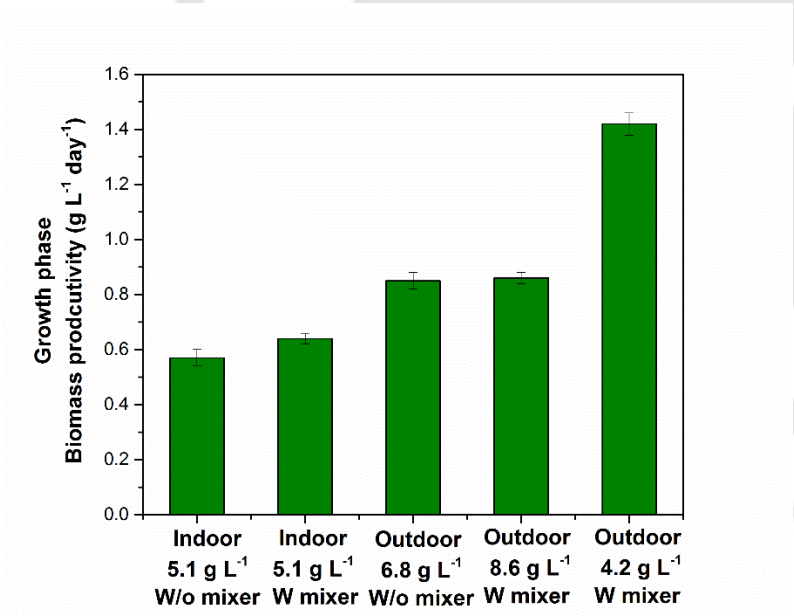

Fig. A2 Comparison of growth-phase biomass productivities of *Chlorella* sp. FC2 IITG grown in medium-scale BC-PBR with (W) and without (W/o) integration of mixer using real time light intensity based CO_2 feed strategy under diurnal simulated sunlight (indoor) and natural sunlight (outdoor) conditions. Refer chapter 6 and 7 for detailed experiments.

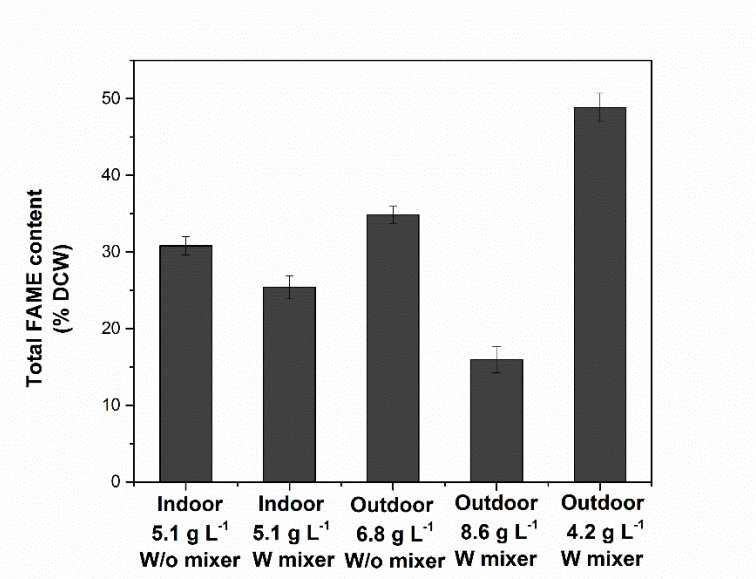

Fig. A3 Comparison of total FAME content (TFC) in biodiesel produced from *Chlorella* sp. FC2 IITG grown in medium-scale BC-PBR with (W) and without (W/o) integration of mixer using real time light intensity based CO_2 feed strategy under diurnal simulated sunlight (indoor) and natural sunlight (outdoor) conditions. Two-stage lipid induction strategy was used for the experiments. Refer chapter 6 and 7 for detailed experiments.

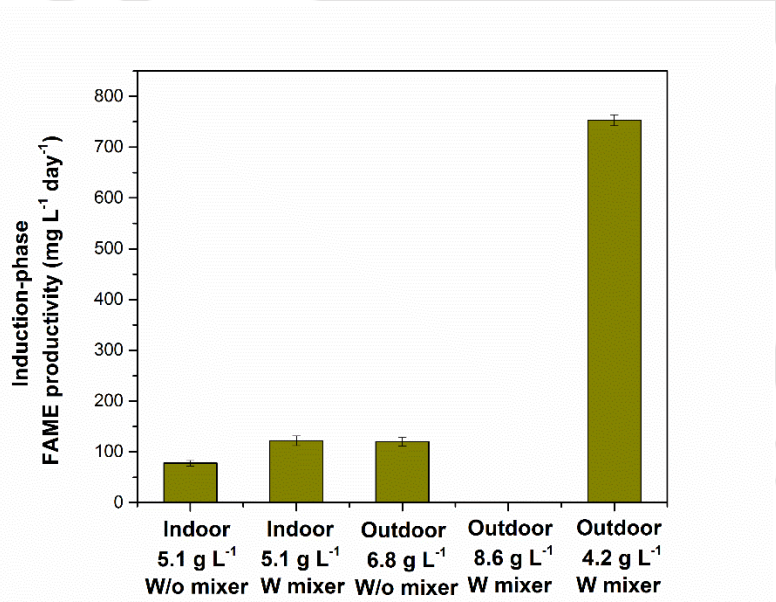

Fig. A4 Comparison of induction-phase FAME (biodiesel) productivities in medium-scale BC-PBR with (W) and without (W/o) integration of mixer using real time light intensity based CO_2 feed strategy under diurnal simulated sunlight (indoor) and natural sunlight (outdoor) conditions. Two-stage lipid induction strategy was used for the experiments. Refer chapter 6 and 7 for detailed experiments.

List of publications

First-authored publications

- **Naira, V.R.,** Das, D., Maiti, S.K. 2018. Designing a CO_2 supply strategy for microalgal biodiesel production under diurnal light in a cylindrical-membrane photobioreactor. *Bioresource Technology,* 250, 936-941
- **Naira, V.R.,** Das, D., Maiti, S.K. 2019. Real time light intensity based carbon dioxide feeding for high cell-density microalgae cultivation and biodiesel production in a bubble column photobioreactor under outdoor natural sunlight. *Bioresource Technology*, 284, 43-55.
- **Naira, V.R.,** Das, D., Maiti, S.K. 2020. A novel bubble-driven internal mixer for improving productivities of algal biomass and biodiesel in a bubble-column photobioreactor under natural sunlight. *Renewable Energy*, 157, 605-615.
- **Naira, V.R.,** Mahesh, R., Panda, S.K., Maiti, S.K. 2020. Biorefinery Approaches for the Production of Fuels and Chemicals from Lignocellulosic and Algal Feedstocks. in: Biorefinery of Alternative Resources: Targeting Green Fuels and Platform Chemicals, (Eds.) S. Nanda, D.-V. N. Vo, P.K. Sarangi, Springer Singapore. Singapore, pp. 141-170.

Second-authored publications

- Singh, N.K., **Naira, V.R.,** Maiti, S.K. 2019. Production of biodiesel by autotrophic *Chlorella pyrenoidosa* in a sintered disc lab scale bubble column photobioreactor under natural sunlight. *Preparative Biochemistry & Biotechnology*, 49(3), 255-269.
- Mahesh, R., **Naira, V.R.,** Maiti, S.K. 2019. Concomitant production of fatty acid methyl ester (biodiesel) and exopolysaccharides using efficient harvesting technology in flat panel photobioreactor with special sparging system via *Scenedesmus abundans*. *Bioresource Technology*, 278, 231-241.

Conferences/Workshops

- **Venkateswara Rao Naira** (2014). Participated in lecture series/workshop on "Recent trends in Mathematical and Computational Biology", jointly organized by the National Network for Mathematical and Computational Biology and the department of Molecular Biology and Biotechnology, Tezpur University, Tezpur.
- **Venkateswara Rao Naira**, Debasish Das and Soumen Kumar Maiti (2015). Current Scenario in design of photobioreactors for mass culturing of algae. Participated and presented a poster in the workshop "Frontier Energy Research with Industry Academia Partnership" organized by Centre for Energy, Indian Institute of Technology Guwahati.
- **Venkateswara Rao Naira**, Debasish Das and Soumen Kumar Maiti (2015). Actively participated in the "RESEARCH CONCLAVE '15" organized by the PhD Council of Students' Academic Board (SAB), Indian Institute of Technology Guwahati.
- **Venkateswara Rao Naira**, Debasish Das and Soumen Kumar Maiti (2015). Elucidation of Inhibitory effects by carbondioxide supply and light intensity on the growth of microalgae in perspective to photobioreactor design. Participated and presented a poster in "CHEMCON 2015, 68th Annual Session of Indian Institute of Chemical Engineers", held at Indian Institute of Technology Guwahati.
- Navodit Kumar Singh, **Venkateswara Rao Naira** and Soumen Kumar Maiti (2016). Effects of CO_2 and light intensity on the biomass production of *Chlorella* sp. under autotrophic condition in the photobioreactor for the production of biodiesel. Participated in poster presentation in the "RESEARCH CONCLAVE '16" organized Students' Academic Board (SAB), Indian Institute of Technology Guwahati.
- **Venkateswara Rao Naira**, Debasish Das and Soumen Kumar Maiti (2016). Growth characteristics of an indigenous biodiesel candidate, Chlorella sp. FC2 IITG in photobioreactors under various light intensities and CO_2 concentrations. Participated and presented a poster in 57th Annual Conference of AMI and International Symposium on "Microbes and Biosphere: What's New and What's Next", held at Gauhati University, Guwahati.

- **Venkateswara Rao Naira**, Debasish Das and Soumen Kumar Maiti (2017). Understanding the effects of inoculum size, CO_2 and light intensity on growth of an indigenous microalgae, Chlorella sp. FC2 IITG in perspective to outdoor mass culturing for biodiesel production. Participated and presented a poster in National Conference on Biodiversity, Biology and Biotechnology of Algae (NCBBBA-2017) organized by Centre for Advanced Studies in Botany, University of Madras, Chennai.
- **Venkateswara Rao Naira**, Debasish Das and Soumen Kumar Maiti (2017). Microalgal-Biodiesel production technology under diurnal LED lighting equivalent to outdoor sunlight intensity. Participated and given an oral presentation in "Bioprocessing India 2017" organized by IIT Guwahati, India.
- **Venkateswara Rao Naira**, Debasish Das and Soumen Kumar Maiti (2018). A novel and scalable process design for indigenous microalgae cultivation: Achieving high biomass and biodiesel productivities under diurnal light. Participated and given an oral presentation in "Indo-Japan Bilateral Symposium on Future perspective of Bioresource Utilization in North- Eastern region", organized jointly by IIT Guwahati, India and GIFU University, Japan.
- **Venkateswara Rao Naira**, Debasish Das and Soumen Kumar Maiti (2018). A novel diurnal light based CO_2 elevation for high biomass density of microalgae under photoautotrophic cultivation Participated and given a poster presentation in "ALGAEUROPE-2018 INTERNATIONAL CONFERENCE", organized jointly by European Algae Biomass Association (EABA) and DLG Benelux Company.

Vitae

The author was born on 27th June 1993 in Andhra Pradesh, India. He passed the Secondary School Examination conducted by the Central Board of Secondary Education, from Jawahar Navodaya Vidyalaya, Srikakulam, in 2008. He qualified the Higher Secondary School Examination conducted by Board of Intermediate Education from Sri Chaitanya Junior College, Andhra Pradesh, in 2010. He completed Bachelor of Engineering in Biotechnology from National Institute of Technology Warangal, Telangana, India in 2014.

Venkateswara Rao Naira joined his Ph.D. programme in July 2014 at Department of Biosciences and Bioengineering, Indian Institute of Technology Guwahati, Assam, India. He received junior and senior research fellowships under the scheme run by the Ministry of Human Resource and Development (MHRD), India. He successfully completed the course work with 8.33/10 Cumulative Point Index (CPI). He gave the Open (PhD Synopsis) Seminar on 26th July 2019 and presented his thesis work before the Doctoral Committee and his performance was satisfactory. He submitted the PhD thesis on 31st July 2019 for examination. He gave the Defence Seminar on 8th October 2020.